Developing Heterogeneous Catalysts for Biomass Conversion

A thesis submitted in accordance with the regulations of the University of Cardiff for the degree of Doctor of Philosophy

By

Maha Alreshidi

School of Chemistry

Cardiff University

July 2023

ACKNOWLEDGEMENT

First and foremost, all prayers and thanks are to Allah without whose help this work would have not been completed.

I would like to thank many people for their support and help throughout my PhD degree journey.

I would like to greatly thank my supervisor, Dr. Meenakshisundaram Sankar, for his invaluable support, guidance and encouragement throughout my PhD degree journey. I am very fortunate and proud to be a student in his group.

I would like also to thank all Professional Services Staff in the CCI for their unlimited help and the department Technical Staff in chemistry school. Additionally, I would like to thank all the CCI members in labs 1.88, 0.90 and room 0.74 for the nice time we spent together.

A special thank you goes to Caru Shanahan and George Summers for their continued guidance and support.

Of course, without funding, this research would not have been possible, and so I am incredibly grateful to Hail University, Saudi Arabia.

Big thanks are given to my friends specially Sahar and Nuha for all the amazing time that we spent together in Cardiff.

Finally, great thanks to my parents, sisters, brothers and especially my older brother Hamed and younger brother Faisal. Words are not enough to express my love and gratitude to my husband Nasser Alrashdi for his unlimited love, and prayers and patience during the PhD degree journey.

I would especially like to thank my children Ghalia, Nour, Ahmad and Faisal, also I would like to especially thank my daughter Ghada and my son Badr for their unlimited patience and sacrifices- without them, I do not think I would have completed this journey successfully.

Abstract

Hydrogenation, a prominent chemical process, finds extensive applications in both commercial and academic realms, particularly in the synthesis of valuable chemical intermediates, high-tonnage products, and important chemicals like agrochemicals and pharmaceuticals.

The hydrogenation of phenol has been investigated using Pd (palladium) and Pd-Ru (palladium-ruthenium) supported on Al_2O_3 catalysts, which were operated in the liquid phase. The optimization of reaction conditions, including the choice of catalyst supports and metal loading, has been pursued to attain ideal outcomes. Notably, the Pd-Ru/Al_2O_3 catalyst, has demonstrated remarkable efficacy in phenol hydrogenation, outperforming other investigated supports and preparation methods employing modified impregnation with $NaBH_4$ reduction.

Additionally, Pd, Au (gold), and Pd-Au catalysts supported on Al_2O_3 catalysts have been utilized for the N-alkylation of phenol with p-toluidine, both with and without H_2, at a temperature of 120 °C. A comprehensive investigation of various factors, including pressure, catalyst mass, support material, Au:Pd ratio, Pd loading, and solvent, has been undertaken to assess their influence on the reaction outcomes.

Furthermore, Pd and Pd-Ru catalysts were studied for auto transfer reaction (HAT) involving benzyl alcohol and nitrobenzene. In this context, the synthesis of imine and secondary amine was thoroughly explored using Pd-Ru/Al_2O_3 catalysts at room temperature. The research revealed the exceptional effectiveness of Pd-Ru/Al_2O_3 catalysts for the synthesis of secondary amines under conditions of room temperature and low-pressure nitrogen (1 bar). Moreover, an investigation of various reaction parameters, such as temperature, catalyst treatment methods, and metal loading, has been conducted to gain a comprehensive understanding of the reaction system.

The characteristics of catalysts are significantly influenced by the interaction between the metal and the support. Particularly, the electronic interaction between these components contributes to the enhancement of catalytic capabilities and stability. Building upon this crucial observation, researchers have opted to prepare Pd-Au and Pd-Ru catalysts utilizing Al_2O_3 as the support material. In-depth characterizations, including Inductively Coupled Plasma (ICP), X-ray Diffraction (XRD), Brunauer-Emmett-Teller (BET) surface area analysis, X-ray Photoelectron Spectroscopy (XPS), Scanning Electron Microscopy (SEM), and Transmission Electron Microscopy (TEM), have been employed to investigate the structural and electronic properties of the Pd-Au and Pd-Ru catalysts supported on Al_2O_3.

These investigations contribute valuable insights into the development and optimization of hydrogenation processes, paving the way for the efficient production of chemical intermediates, high-value products, and critical chemicals used in diverse industries. Moreover, the exploration of various catalyst compositions and support materials allows researchers to tailor catalytic systems for specific applications, leading to enhanced efficiency and stability in hydrogenation reactions.

Abbreviations and Symbol

Å	Angstrom (10^{-10} meters)
BET	Brauner, Emmet and Teller
cm	Centimetre
cm^{-1}	Reciprocal Centimetre
°C	Degrees Celsius
eV	Electron Volts
FID	Flame ionisation detector
SMSI	Strong metal support interaction
g	Gram
GC	Gas Chromatography
h	Hours
ICP-MS	Inductively Coupled Plasma Mass Spectroscopy
M	Molar
mg	Milligram (10^{-3} g)
mol	Moles
min	Minutes
nm	Nanometre (10^{-9} m)
XRD	X-ray diffraction
SEM	Scanning electron microscopy
XPS	X-ray photoelectron spectroscopy
wt. %	Weight percent
Conv.	Conversion
Sel.	Selectivity
CHT	Catalytic transfer hydrogenation
HAT	Auto transfer reaction
PH	Palladium hydride
Pd-XB	Catalyst preparing by modified impregnation method and reduction with sodium borohydride
RBF	Round bottomed flask
S_{im}	sol-immobilisation method
M_{im}	modified impregnation method

Table of Contents

Chapter 1: Introduction

This chapter presents the motivations, challenges, and approaches involved in producing chemicals from phenol, selected as a model compound of biomass feedstock. It explores alternative processes for the preparation of cyclohexanol and N-alkylated amines. Lastly, the coupling of nitrobenzene with benzyl alcohol, using the hydrogen auto-transfer reactions process, is briefly outlined.

1.1. Catalysis history

The term "catalysis" was first used by Berzelius in 1836 during the reaction of the combustion of oxygen and hydrogen over platinum[1]. Berzelius explained the effects of porous platinum on the combustion of hydrogen and oxygen at ambient temperatures and noted that certain compounds could accelerate the reaction rate without changing themselves. Faraday interpreted the acceleration in the reaction rate in 1825 when he examined platinum's effects on oxidation reactions, attributing the activity of platinum to the adsorption process[6]. However, the principle of catalysis was first explored by Fulhame in 1794, demonstrating how a small amount of water could significantly affect the oxidation of carbon monoxide without itself being chemically affected[7].

Green chemistry, which involves the development of chemical products and processes that reduce or eliminate harmful substances, heavily relies on catalysis. Catalysis is a fundamental cornerstone of green chemistry, playing a crucial role in environmental preservation and economic benefits[8]. The design and implementation of innovative catalysts and catalytic systems have allowed the achievement of environmental protection while simultaneously reaping economic benefits[8]. Furthermore, catalysis is integral to a wide range of products as it is a vital part of the manufacturing process, where approximately 90 % of chemical industry products depend on catalytic processes[9]. The importance of catalysts extends to both academic and industrial research[9,10].

1.1.1. Catalysis definitions

Catalysts are substances that increase the rate of a chemical reaction without enduring any permanent change to their chemical composition. They affect the kinetics of both the forward and reverse reactions (i.e., increasing the rate constants of the reaction k_1 and k_2) but not the thermodynamics of the reaction or the equilibrium position[11], as shown below:

$$A \underset{k_2}{\overset{k_1}{\rightleftharpoons}} B$$

Where the rate constants k_1 and k_2 can be defined by the Arrhenius **equation1.1**[12]**:**

$$k = I_o \exp\left(\frac{-E_a}{RT}\right) \qquad \textbf{Equation1.1}$$

where I is the collision frequency, E_a is the activation energy (KJ mol^{-1}), R is the gas constant (8.314 JK^{-1} mol^{-1}), and T is the temperature in K.

Catalysis reduces the energy required to form one or more transition states between the reactant and the product. As a result, the activation energy of the reaction decreases while the reaction thermodynamics and products remain unchanged[7,9]. Catalysts provide an alternate reaction pathway, accelerating the reaction rate by lowering the activation energy. **Figure 1.1** illustrates the difference between catalytic and non-catalytic reaction profiles.

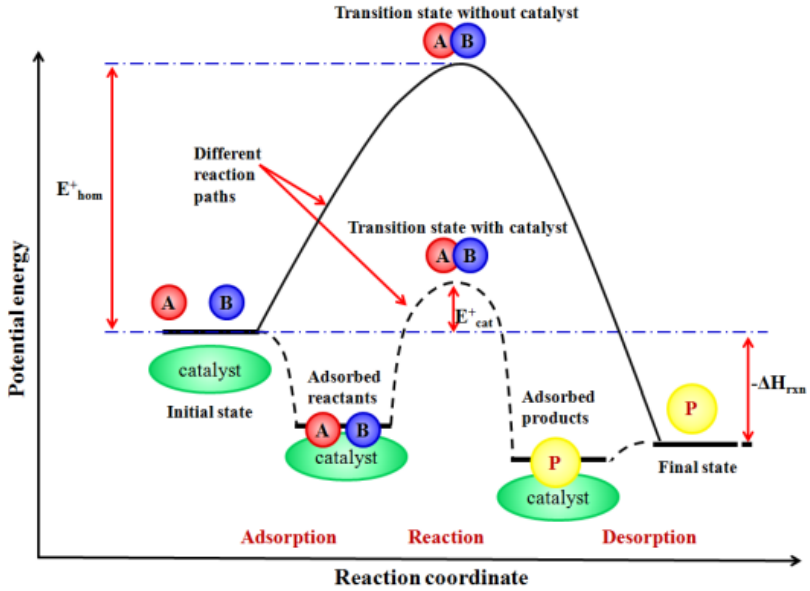

Figure 1.1: Schematic illustration of potential-energy diagram characterizing a simple chemical reaction in the presence or absence of a catalyst (A= reactant 1, B= reactant 2, and P= product). Reproduced from ref.[13].

1.2. Types of catalysis

Catalysis is categorised into bio-catalysis, homogeneous catalysis, and heterogeneous catalysis. Bio-catalysis involves natural catalysts, such as enzymes or bacteria, with reactions catalysed by fast, sensitive, and selective enzymes. Homogeneous catalysts operate in the same phase as the reactants and are commonly liquid, as mixing the catalyst with the reactants usually occurs in this state. Ideally, homogeneous catalysts are dissolved in a solvent with the substrates[14]. On the other hand, heterogeneous catalysts function in a phase different from that of the reactants. They are typically inorganic solids like metals, oxides, sulfides, or metal salts. However, heterogeneous catalysts can also be organic materials like organic hydroperoxides, ion exchangers, or enzymes.

1.2.1. Bio-catalysis

A biocatalyst is an enzyme, a naturally occurring complex protein that catalyses reactions within a living cell. Proteins comprise amino acids joined via peptide bonds, forming the enzyme's structure. An enzyme's active site is typically a cleft surrounded by an array of amino acid residues, as depicted in **Figure 1.2**[15]. The substrate is covalently linked to a specific location on the enzyme, known as the "active site". This is where the enzyme performs its catalytic function. A substrate can bind to an enzyme through four types of interactions: electrostatic contacts, hydrogen bonds, van der Waals interactions, and hydrophobic interactions. The enzyme-bound substrate undergoes a conformational shift, attaining a tense state from which it readily transitions to produce the product(s). The enzyme reduces the activation energy required to catalyse the reaction through this state of tension, or intermediate transition, of the substrate[16].

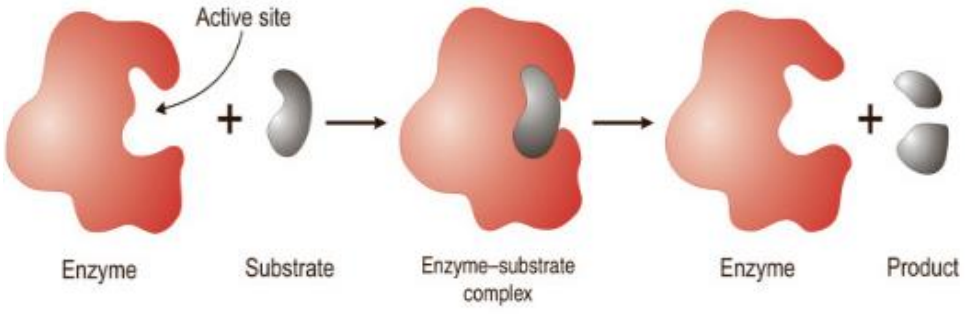

Figure 1.2: Schematic representation of an enzymatic reaction. Reproduced from ref.[16].

Selectivity is a crucial aspect of this type of organic synthesis, necessary to achieve a high yield of a specific product. A plethora of selective organic reactions is available for most synthetic needs[17].

1.2.2. Homogeneous catalysis

Homogeneous catalysts, typically metal complexes, function in the same phase as the reactants, usually liquid solvent[18]. Ligands in the metal complexes play an important role in homogeneous catalysis by determining the catalytic properties such as activity and selectivity. Consequently, selecting an appropriate metal and ligand is crucial for improving the activity and selectivity of the catalytic process[19]. Examples of homogeneously catalysed reactions include the oxidation of toluene to benzoic acid in the presence of Co and Mn benzoates and the hydroformylation of olefins to form the corresponding aldehydes catalysed by Co or Rh carbonyls[20]. However, homogeneous catalysis has several drawbacks, the most significant of which is the difficulty separating and recovering the catalyst since the catalyst and reaction mixture exist in the same phase.

1.2.3. Heterogeneous catalysis

Heterogeneous catalysis, common in the chemical industry, refers to a type of catalyst, typically in solid form[21], where the catalyst phase and reaction phase coexist in separate phases, such as gas/solid or gas/liquid/solid configurations[22]. Heterogeneous catalysis involves four steps: adsorption of the reactant onto the surface of the catalyst; activation of the adsorbed reactant; the reaction of the adsorbed reactant; and diffusion of the product from the surface into the gas or liquid phase (desorption). Adsorption is the first step in heterogeneous catalysis, where the adsorption of the reactants on the surface of the catalyst needs to be strong enough for the reactants to react, which can be physisorption (weak adsorption) or chemisorption (strong adsorption, which involves bond weakening or breaking in the reactant). Then, the rearrangement of electrons on the catalyst's surface occurs. The final stage is the desorption of products from the catalyst surface. However, very strong adsorption of the reactants can lead to difficulty in product desorption from the catalyst surface. The steps involved in heterogeneous catalytic reactions are illustrated in **Figure 1.3**.

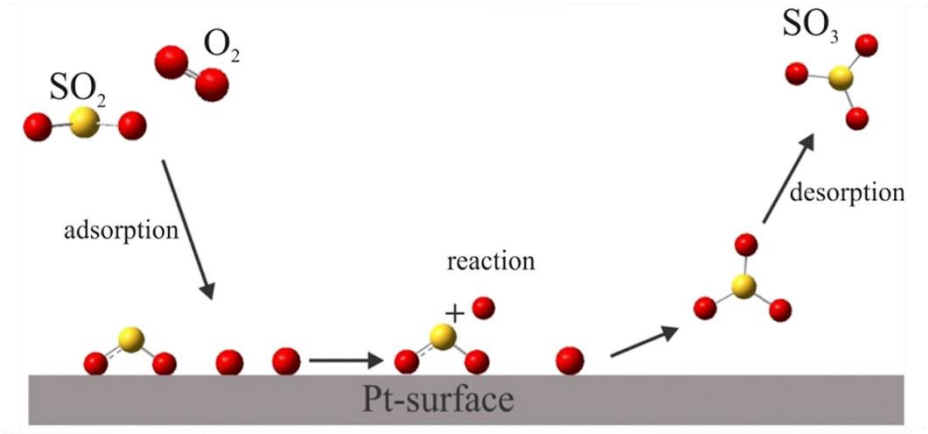

Figure 1.3: Steps of heterogeneous catalytic processes on a solid catalyst (The reaction cycle for the catalytic oxidation of SO_2). Reproduced from ref.[23].

Examples of heterogeneously catalysed reactions include ammonia synthesis from N_2 and H_2 over promoted iron catalysts in the gas phase[24] and Co supported on Mg–La mixed oxides as an efficient catalyst for ammonia synthesis in the liquid phase[25], these are examples of inorganic catalysis. Another example is the catalytic reaction cycle of SO_2 oxidation on the Pt surface, as depicted in **Figure 1.3**. A smaller proportion of sulfur trioxide is produced at higher temperatures, making the process less economical below this temperature range. This process, known as the contact process, occurs when the heated gases come into contact with the catalyst surface. However, platinum is sensitive to arsenic impurities in the sulfur feedstock, which can poison the catalyst. Therefore, additional precautions must be taken to remove sulfur and air contaminants. Nowadays, vanadium pentoxide (V_2O_5) is the predominant material used as a substitute for platinum in this process[23].

Compared to homogeneous catalysis, heterogeneous catalysis offers several advantages and is used in many industrial applications, such as the chemical, pharmaceutical, and petrochemical industries. For example, there is no difficulty in catalyst separation and reusability; heterogeneous catalysts can be reprocessed and used in the petrochemical industry[26]. Various classes of catalysis are reviewed in the following sections. Moreover, heterogeneous catalysis has also been utilised for new applications such as fuel cells and biotechnology. The differences between these two types of catalysts are presented in **Table 1.1**[27].

Table 1.1: Comparison between heterogeneous and homogenous catalysts:

Property	Heterogeneous	Homogenous
Catalyst phase	Generally solid	Metal complex
Selectivity	Variable	Usually High
Solvent	Required	Required
Recyclability	Easy	Difficult
Stability	Stable at high temperature	Decomposed
Application	Widespread	Limited

1.3. Biomass

The increasing industrialisation of the world in the past century has heavily relied on fossil fuels such as coal, natural gas, and oil as the primary sources of energy and organic matter[13,28,29]. However, the detrimental effects of greenhouse gas emissions and other forms of pollution from burning fossil fuels have prompted widespread efforts to transition to cleaner energy sources[29]. Despite significant solar and wind energy growth over the past decade[13,28], projections indicate that fossil fuels will remain the dominant energy source unless there are substantial changes in oil and gas prices. In addition to their use as transportation fuels, fossil fuels also serve as chemical feedstocks. Converting these feedstocks into valuable chemicals requires considerable energy proportional to their energy content[13]. The economic profitability of the chemical industry relies on the value of products derived from fossil fuels exceeding their energy content. While replacing fossil fuel-derived chemical feedstocks with renewable alternatives can offer environmental benefits, addressing these challenges on a larger scale requires significant changes in the energy and transportation sectors. Nonetheless, there is ongoing interest from academia and industry in developing processes that utilise non-fossil fuel feedstocks, driven by the potential for positive environmental impacts and economic advantages over conventional approaches[30,31]. Producing oxygenated or functionally complex molecules from biomass may present greater economic viability than hydrocarbons, leading to more sustainable processes.

Biomass is a renewable energy source containing a complex mix of carbon and is a significant contributor to meeting the world's energy demands[32,33]. Renewed attention began to be paid to biomass in the early 2000s due to concerns about the availability and cost of petroleum and the contribution of fossil fuels to the levels of greenhouse gases in the atmosphere. The sustainable development concept stimulated research

and development into biomass conversion for energy and chemical production. There is a wide range of biomass sources, conversion routes, and products in which catalysis is essential to provide clean and sustainable processes with high efficiency. On average, biomass energy accounts for one-third of total final energy consumption and approximately 75 % of the energy used in households[34]. Technically, additional benefits are associated with using renewable feedstocks to produce chemicals. Chemicals can be synthesised in fewer steps than alkanes, decreasing the overall waste generated[34–36]. In addition, bio-based products may offer favourable properties compared to hydrocarbon-derived products, such as biodegradability and biocompatibility[32,36].

The predominant constituents in terrestrial biomass are lignin, cellulose, and hemicellulose, rendering it lignocellulosic[29]. The composition of lignocellulosic biomass varies depending on its source, but typical ranges include 15-30 wt. % lignin, 30-50 wt. % cellulose, and 20-30 wt. % hemicellulose. Unlike cellulose, hemicellulose lacks a crystalline structure due to its irregular arrangement, making it more amenable to solubilisation and hydrolysis. Conversely, lignin is a complex and heterogeneous polymer composed of crosslinked aromatics, with paracoumaryl, coniferyl, and sinapyl alcohols as typical monomers[37,38] (**Figure 1.4)**.

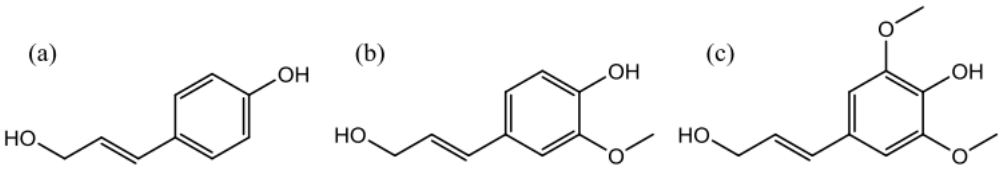

Figure 1.4: The three common monomers of lignin: (a) paracoumaryl, (b) coniferyl, and (c) sinapyl alcohols.

Polysaccharides, which are more abundant and accessible to convert into monomers than lignin, have traditionally received greater attention. However, recent advancements in lignin hydrogenolysis have sparked renewed interest in the depolymerisation products of lignin, leading to extensive research in various laboratories[39,40]. In reality, the current production of energy from dry biomass falls short of meeting the escalating energy demand, especially when compared to the energy generated from oil and natural gas, let alone the projected growth. For example, the United States alone used about 109 tonnes of oil and natural gas 2015. The specific energy density of desiccated biomass is roughly 35 % of that of oil and natural gas[28,41].

Consequently, even the anticipated annual biomass production cannot satisfy the existing energy demand associated with fossil fuels, not to mention the expected expansion. Nevertheless, it is worth noting that the United States has the potential to

produce around 109 tonnes of dry terrestrial lignocellulosic biomass annually without compromising agricultural productivity for food and animal feed. The farmgate price, which includes all costs except transportation, for such production capacity is estimated to range from $40 to $60 per dry tonne[41–43]. Based on the conclusions derived from reviewing the findings, it is evident that processes targeting high-value molecules, which do not necessitate extensive reduction and possess comparable functional complexity to monomers, show potential economic viability[29,44,45]. In the subsequent discussion, emphasis will be placed on specific products, such as phenol, carefully selected to align with the chemocatalytic chemistries studied in this research.

1.3.1. Catalytic conversion of biomass

The discovery and investigation of novel and efficient pathways for converting biomass into fuels and chemicals are among the significant challenges facing heterogeneous catalysis nowadays[46].

Many researchers are working to develop solid catalysts that can be easily recovered with simple purification stages and are resistant to deactivation[36,47]. Moreover, the cost of bioproducts is typically much higher than chemicals synthesised by traditional processes. This disparity is due to the higher price of the starting materials and the demand for food and biofuel in recent years, which has driven their price. However, the primary cause is the high cost of processing renewables. The processes used to synthesise chemicals from fossil fuels have been continuously enhanced for over a century, resulting in a very high degree of technical sophistication and cost optimisation.

Conversely, the processes used to obtain chemicals from biomass are still in a comparatively early stage, and their cost largely depends on the bioproducts' market price. Therefore, extensive research and development efforts in biotechnology, chemistry, and engineering are needed to increase the efficiency of biomass processing. In particular, new catalytic processes for the specific structure of oxygenated molecules must be designed. Furthermore, these new catalytic processes are needed to manage variations in feedstock availability and molecular structure.

Two processes are available to convert biomass derivatives into valuable bio-products through innovative catalytic routes: 1) The synthesis of chemicals through platform molecules, in which biomass is converted through biotechnological processes into platform molecules. These molecules can then be used as building blocks for chemical synthesis through catalytic routes; 2) The conversion of biomass

derivatives via one-pot processes, including one or several catalytic stages, into a mixture of chemicals of similar functionalities. These chemicals can then be used without separation in the formulation of end products[36].

1.4. Heterogeneous Catalysts

Heterogeneous catalysis is indispensable to many chemical processes, encompassing industrial applications and environmental systems. Separate phases of catalysts and reactants are exploited. Generally, the catalyst is solid, whereas the reactants may be gases or liquids. Interactions between the reactants and the active sites of the catalyst result in the formation of intermediate entities that play a crucial role in the chemical reaction. After the reaction, the products separate from the catalyst, preparing them for future cycles. Heterogeneous catalysts provide numerous advantages, including simple isolation from reaction mixtures, resistance to severe conditions such as high temperature and pressure, and high specificity for desired products. Numerous substances, including metals, metal oxides, carbides, and zeolites, can form heterogeneous catalysts.

1.4.1. Bimetallic Catalysts

Bimetallic catalytic systems are integral to the biomass conversion process, particularly for augmenting the value of triglyceride-derived glycerol and lignocellulose-derived foundational compounds like glucose, fructose, carboxylic acids (levulinic, itaconic acid, and lactic acid), furanic (furfural), and phenolic compounds[48,49]**.** Bimetallic catalysts have been researched extensively for their role in organic transformations including hydrogenation, hydrolysis (hydrodeoxygenation), oxidation, reductive amination, dehydration, and reductive depolymerisation. Adding a secondary metal to a primary metallic catalyst offers several advantages, such as curtailing side reactions, accelerating reaction speed, bolstering catalyst stability, modulating active metal size, and improving the electron attributes of the active metal. Furthermore, by tweaking the reactivity sites, bimetallic catalysts have demonstrated exceptional performance in various organic transformations[48]. For instance, in the hydrodeoxygenation-hydrogenation of methoxyphenols for cyclohexanol production, bimetallic catalysts like Co-Ni/-Al_2O_3 and Pd-Ru alloys have showcased a synergistic impact. Introducing Ru in Pd-Ru alloys facilitates the dispersion of Pd nanoparticles, revealing more active reaction sites and amplifying the activation of hydrogen or phenol. Similarly, Co-Ni/-Al_2O_3 catalysts have been devised for converting guaiacol to cyclohexanol, achieving a 71 % selectivity for cyclohexanol[50,51].

Typically, chosen catalysts for hydrogenation reactions are metal catalysts, with bimetallic catalysts containing Pd-Pt and Pd-Ru recognised as superior catalysts due to their exceptional catalytic activities compared to monometallic catalysts[52]. Pd-based bimetallic catalysts are commonly employed for the hydrogenation of alkynes to alkenes, alkadienes to alkenes, and nitriles to amines. Rh-based bimetallic catalysts are used for the hydrogenation of alkenes, while Pd-Pt supported on solid acids is utilised for the hydrogenation of aromatics[52–57]. In oil refineries, bimetallic or alloy catalysts that combine two metals have been developed to boost the octane number of gasoline and control the replacement of the harmful tetraethyl lead. These catalysts have shown improved performance and promise further utility in various applications within the petroleum industry[58].

Bimetallic catalysts, such as Pd-Ru and Pd-Au, often exhibit superior catalytic activity and selectivity compared to their monometallic counterparts, such as Pd, Au, and Ru. This enhanced performance is attributed to several pivotal factors:

1- Synergistic Effect: In bimetallic catalysts, the combined effect of two metals frequently outperforms each metal's catalytic activity or selectivity. This enhanced performance is attributed to the novel electronic or geometric structures in bimetallic catalysts, which can differ substantially from those in the monometallic systems. This synergistic effect may alter the catalytic reaction pathway, thereby improving the efficiency of the process.
2- Alloy Effect: Bimetallic catalysts can form nanoscale alloys, which often possess unique electronic structures and catalytic properties not found in their monometallic counterparts. Integrating a secondary metal can modulate the electronic structure of the primary metal, altering its adsorption characteristics and, thus, its catalytic behaviour. This alteration can lead to novel reaction pathways and improved catalytic efficiency.
3- Redistribution of Active Sites: Bimetallic catalysts can also provide a more optimal distribution of active sites, which is crucial for efficient catalysis. Introducing a secondary metal can influence the dispersion of the primary metal on the support, resulting in a more uniform distribution of active sites and thereby enhancing catalytic activity.

Hydrogenation of phenol to cyclohexanol: The bimetallic catalyst can provide dual active sites for enhanced reactivity. One metal in the bimetallic complex could primarily facilitate the activation of the hydrogen molecule, while the other could efficiently activate the phenol molecule, thereby promoting the overall reaction rate.

N-alkylation of p-toluidine with phenol: The presence of dual active sites in the bimetallic catalyst could allow simultaneous activation of the amine and phenol. Furthermore, the synergistic effect between two different metals might improve the selectivity of the reaction, leading to a higher yield of the desired product.
Coupling of nitrobenzene with benzyl alcohol: In this reaction, the secondary metal in the bimetallic catalyst could activate the nitro group in nitrobenzene, while the primary metal could activate the alcohol group in benzyl alcohol. This bifunctional activation could enhance the reaction efficiency and product selectivity.

1.5. Hydrogenation of phenol

Alkylcyclohexanone and alkylcyclohexanol are derived from the catalytic hydrogenation of alkyl-substituted phenols in the liquid phase using supported palladium and nickel catalysts (< 0.02 mm)[59].

Various catalysts, support, and reaction parameters regulate selectivity, an essential process from an ecological standpoint[58]. In addition to the hydrogenation of alkylphenols; the phenol hydrogenation process generates cyclohexanone and cyclohexanol as intermediates. Cyclohexanone and cyclohexanol are typically produced by phenol hydrogenation. Cyclohexanone is an important intermediate in producing nylon 6, nylon 66, and polyamide resins[60–62]. In the meantime, cyclohexanol is extensively used in the perfume industry and the field of fine chemistry.
Some studies have also reported the presence of other compounds, such as benzene and cyclohexane[60]. The production of these two compounds depends on the catalyst and solvent employed. In some studies, benzene was used as a solvent, and it was argued that phenol hydrogenation would be "predominant".

1.5.1. Selection of Phenol as the Model Compound

Studying various cyclohexanol synthesis pathways utilising a basic phenol molecule allows researchers to focus on the reaction kinetics and reduce substituent complexity. This method aids in explaining hydrogenation mechanisms and can be used to construct and optimise hydrogenation methods for aromatic molecules that are becoming increasingly complex. Because its hydrogenation can be applied to other aromatic compounds, phenol is used as a model chemical for alternative cyclohexanol synthesis. Field research validates this theory. Raspdli Galletti et al.[63] (2008) investigated the catalytic hydrogenation of phenol to cyclohexanone utilising Ru nanocolloids and supported Ru/Al_2O_3 nanocatalysts. Yu and Wang et al.[64], An improved Method for the reactivity and selectivity of heterogeneous catalytic hydrogenation of aromatic compounds at an atmospheric hydrogen pressure in 2013.

Phenol is an essential model component for a variety of purposes. Important is phenol, a straightforward aromatic molecule with a benzene ring and hydroxyl group. Phenol hydrogenation's kinetics, mechanism, and catalyst behaviour can be applied to similar aromatic compounds. Phenol was selected as a model ingredient for developing more effective and environmentally friendly aromatic compound conversion processes that produce valuable chemical products. Aromatic molecules are required for pharmaceuticals, plastics, and speciality compounds. Conventional conversion techniques involve harsh conditions, energy-intensive procedures, and catalysts that are harmful to the environment. Researchers are investigating the processes and kinetics of phenol hydrogenation in order to identify the parameters that influence reaction selectivity, conversion, and catalyst deactivation. One can enhance catalytic systems and reaction conditions by refining phenol hydrogenation and applying their findings to other aromatic compounds. Green chemistry and sustainable industrial practices aim to reduce waste, energy consumption, and the environmental impact of aromatic chemical conversions. A. Corma and H. Garcia[65] (2006) investigate silica-bound homogeneous catalysts as recoverable and reusable catalysts in organic synthesis, emphasising the need for environmentally friendly processes. In conclusion, phenol was chosen as a paradigm for hydrogenation because its behaviour applies to other aromatic compounds. Studies on catalytic hydrogenation and kinetic modelling support this concept. Scientists optimise catalytic systems, reaction conditions, and process efficacy to develop environmentally and economically viable aromatic chemical conversion methods. Researchers contribute to the global greening of industrial practices by employing a sustainable strategy. Alternative methods of cyclohexanol synthesis have been investigated. Hydration and oxidation of cyclohexane are common procedures[66]. These procedures necessitate stringent conditions and generate large amounts of by-products. Hydrogenation of phenol may resolve these issues. Phenol hydrogenation is more benign and selective than competing reactions[67]. This makes it a promising subject for research. Phenol is supported as a model molecule for various cyclohexanol production methods. Phenol, a simple benzene ring with a hydroxyl group, is an excellent starting point for several reasons[68]. First, the simplicity of phenol enables a focused and methodical analysis of the hydrogenation process, thereby enhancing our understanding of the reaction mechanism and kinetics. This is necessary for the development of efficient and selective catalysts.

Using a straightforward phenol instead of one with functional groups simplifies the mechanism of the reaction. Reducing variables facilitates the identification and comprehension of hydrogenation reaction fundamentals. This methodology offers a solid scientific foundation for future optimisations the scientific rationale for selecting

phenol as the model chemical is based on its realism. Hydrogenation of phenol may disclose the behaviour and reactivity of aromatic compounds with similar structures. Phenol hydrogenation can be applied to aromatic molecules other than cyclohexanol synthesis[69].

Due to its simplicity, representativeness, and potential for greater selectivity under milder reaction conditions, phenol serves as the model chemical for alternative cyclohexanol synthesis techniques. Phenol hydrogenation may contribute to developing more efficient, selective, and sustainable cyclohexanol production methods[70]. Experimentation and theory have uncovered the phenol hydrogenation procedure. This transition requires noble metal catalysts such as palladium (Pd), platinum (Pt), and ruthenium (Ru). These catalysts absorb and activate hydrogen gas and phenol. By understanding the reaction mechanism, researchers can comprehend the critical processes and parameters that influence the efficiency and selectivity of phenol hydrogenation. This knowledge is required to develop and optimise procedures for the hydrogenation of phenol and aromatic compounds. By studying reaction kinetics and identifying rate-limiting phases, researchers can target catalyst characteristics such as surface composition, geometry, and active site accessibility to enhance hydrogenation efficiency[71]. Understanding the reaction process also permits the investigation of reaction conditions and parameters that improve product selectivity and yield. The reaction mechanism can optimise temperature, pressure, the ratio of hydrogen to phenol, and the solvent. Studying the chemical mechanism of phenol hydrogenation can aid in developing novel processes and catalysts. By discovering hydrogenation reaction success criteria, researchers can create new catalysts, investigate new reaction routes, and develop more sustainable and efficient cyclohexanol synthesis methods. This supports the scientific objective of greening chemical reactions and enhancing catalytic processes.

1.5.1.1. Catalysts

When considering alternative processes for cyclohexanol synthesis, assessing the pros and cons of competing processes is essential. Two commonly used competing processes are the oxidation of cyclohexane and the hydration of cyclohexene. However, these processes have certain limitations that make them less favourable compared to the hydrogenation of phenol. For example, the oxidation of cyclohexane involves harsh conditions and often leads to the formation of significant amounts of by-products. This not only complicates the purification process but also decreases the overall yield and selectivity of cyclohexanol. Moreover, cyclohexane oxidation requires expensive catalysts and poses challenges regarding process scalability and environmental impact[72].

Similarly, the hydration of cyclohexene suffers from its own set of drawbacks. This process typically necessitates using concentrated acids as catalysts, such as sulfuric or phosphoric acid. These acids can be corrosive and hazardous, posing safety concerns and requiring careful handling. Additionally, the hydration of cyclohexene is prone to side reactions, leading to the formation of undesirable by-products[72]. In contrast to these competing processes, the hydrogenation of phenol offers several advantages. First, phenol can be readily obtained from various sources, including petroleum refining and biomass conversion[73,74]. The hydrogenation of phenol has the potential to be conducted under milder conditions, such as moderate temperatures and pressures, making it more energy-efficient and economically viable.

Moreover, the selectivity of the phenol hydrogenation process can be enhanced through catalyst design and optimisation, leading to higher yields of cyclohexanol with minimal by-product formation[68]. The choice of a simple phenol, as opposed to a substituted phenol, for the model compound in alternative cyclohexanol synthesis processes was driven by several factors. First and foremost, simple phenol provides a fundamental understanding of the reaction mechanism and catalytic properties. It allows researchers to investigate the key factors influencing the hydrogenation process without the added complexities introduced by substituents. By focusing on simple phenol, it becomes easier to isolate and analyse the effects of different catalysts, reaction conditions, and process variables on the selectivity and efficiency of cyclohexanol production[75] .

Furthermore, studying the hydrogenation of simple phenol provides a robust scientific foundation for subsequent studies on substituted phenols. Once the basic principles of phenol hydrogenation are established, researchers can explore how different substituents on the phenol ring affect the reaction kinetics, catalyst performance, and product selectivity. This stepwise approach allows for a more systematic and informed development of alternative processes for cyclohexanol synthesis. In summary, the hydrogenation of phenol offers a compelling alternative to competing processes for cyclohexanol production. Its milder reaction conditions, enhanced selectivity, and potential for optimisation make it an attractive choice for industrial applications. By focusing on simple phenol as the model compound, researchers can gain valuable insights into the fundamental aspects of the hydrogenation process, paving the way for developing more efficient, selective, and sustainable processes for cyclohexanol synthesis.

Ni, Co, Ru, Pt or Rh nanocatalysts are commonly used to produce cyclohexanol. These include the nature of the NPs (size, shape, density of electronic states, and structure of metals) as well as the qualities of the support material (acidity or alkalinity)[76]. Because of its exceptional capacity to absorb and activate hydrogen and

phenol against cyclohexanone, Pd is one of the platinum group metals most researched for phenol hydrogenation toward cyclohexanone[77].

Ru is one of the less expensive noble metals for practical use; however, it is challenging to catalyse the phenol hydrogenation to cyclohexanone from cyclohexanol. To achieve phenol hydrogenation toward cyclohexanone, logically constructing the microenvironment around Ru sites is required. Compared with other noble metals such as Pd and Pt metals, the low-cost noble metal Ru has sparked much interest in the hydrogenation of phenol[77]. Based on the theory that low temperatures delay the transfer and aggregation of Pd NPs, Pd/Al_2O_3 prepared catalysts that contain various particle sizes of Pd NPs to control the reduction temperature.

The catalyst prepared with Pd of particle size of 3 nm (reduced by $NaBH_4$ at 273 K) revealed a selectivity of cyclohexanone of 98 % with the conversion of phenol > 99 %. This excellent performance of the catalyst was attributed to the interaction between the hydroxyl group of phenol and the hydroxyl group of catalysts and that between the aromatic ring of phenol and Pd NPs[2,78]. This study examined the effect of particle size of ZrO_2-supported Pd and of alloying with Ag for the hydrogenation of phenol in the aqueous phase. Their findings indicated that the liquid-phase hydrogenation of phenol was a structure-sensitive reaction on Pd/ZrO_2[79]. In a study by Raut et al.[80], the catalyst was used for the hydrogenation of phenol under mild conditions. The catalyst activity was checked by varying factors such as the temperature of the reaction, time, H_2 partial pressure, metal loading and the amount of catalyst[81]. The catalyst was recovered from the product and reused four times without significant loss in its catalytic activity. After a reaction time of 1 h, the Ru/Al_2O_3 nanocatalyst exhibited high reactivity (82 % conversion) and selectivity to cyclohexanone (67 %) at 80 °C and 20 bar hydrogen pressure. In addition to the conventional reduction methods, Raspolli Galletti et al. used the microwave-assisted solvothermal method to reduce Ru/Al_2O_3. The prepared catalyst with small particle size (2.23 nm) and narrow size distribution achieved 87 % cyclohexanone selectivity with ChemNanoMat phenol conversion exceeding 81 %[82]. A non-noble metal Co to reduce phenol has been used, marking the first use of Co metal for phenol hydrogenation, and the main product was cyclohexanol instead of cyclohexanone.

1.5.1.2. Supports

Hydrogen is introduced to the aromatic ring via a spill-over mechanism during phenol hydrogenation. As shown in **Figure 1.5**, Neri et al.[83] first proposed the two-site model. On the one hand, phenol is adsorbed on co-planar acid sites, which is conducive to

the formation of cyclohexanol due to the intense adsorption between the aromatic ring and the support. The other model has non-planar adsorption, formed on basic or neutral sites such as silica. This form has a weaker interaction between the benzene ring and surface which tends to produce cyclohexanone selectively[54,84].

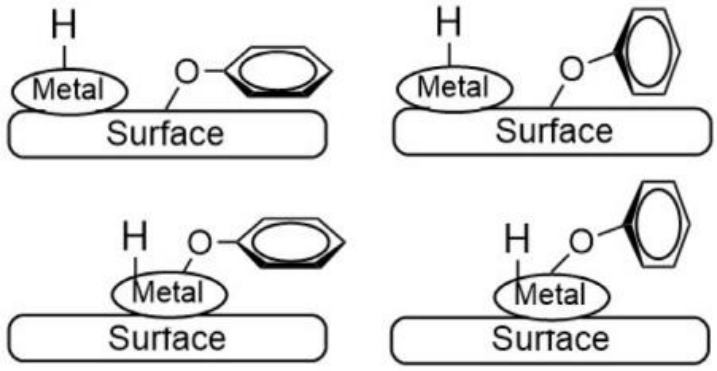

Figure 1.5: Adsorption of phenol on surface via: (a) co-planar mode (two-site model), (b) non-planar mode (two-site model), (c) co-planar mode (one-site model), (d) non-planar mode (one-site model). Reproduced from ref.[54,85].

The selection of support materials for phenol hydrogenation catalysts is crucial, as they play a significant role in determining the activity and selectivity of the catalysts. Various support materials, including oxides and carbon materials, have been investigated for their suitability in the liquid-phase hydrogenation of phenol. Oxides such as Al_2O_3, MgO, TiO_2, CeO_2, and ZrO_2 are commonly used as supports due to their mechanical and chemical stabilities, adjustable surface properties, tunable hydrophilicity and acid-base properties[86,87]. For example, Al_2O_3 supports are widely employed in gas-phase and liquid-phase phenol hydrogenation processes due to their adjustable pore structure, shape-selective catalytic properties, and acid-base performance. Hydrotalcite (HT) has also demonstrated promise as a support for phenol hydrogenation due to its basic sites that promote phenol adsorption. Carbon materials, such as mesoporous and nitrogen-doped carbon, have been used to support transition metals in phenol hydrogenation. These carbon supports offer advantages such as a high specific surface area, large pore volume, thermal conductivity, and low manufacturing cost. In addition, nitrogen-doped carbon materials have shown enhanced catalytic reactivity compared to nitrogen-free carbons[86,88].

The choice of support materials and their properties significantly influence the adsorption behaviour of phenol and subsequent hydrogenation reactions. For instance, acidic supports like silica-alumina favour coplanar adsorption, leading to strong adsorption and the formation of cyclohexanol and cyclohexane. On the other

hand, basic or neutral supports like silica result in non-planar adsorption (**Figuer1.6**)[89].

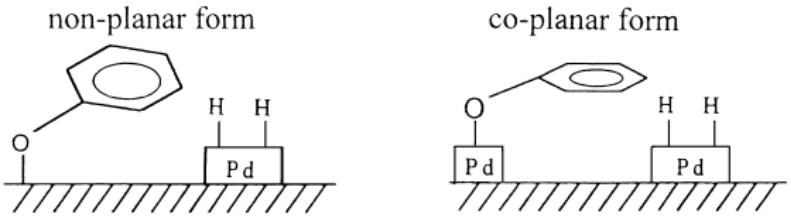

Figure1.6: Non-planar and coplanar adsorption mode of phenol on the supports. Reproduced from ref.[90].

1.5.1.3. Reaction environment

In liquid-phase reactions, solvents wield significant influence over the reaction's equilibrium. Their impact extends to the reaction rate and mechanism, affecting factors such as solubility, mass transfer, the sorption functions of reactants, and interactions with catalysts. Water (H_2O) has emerged as a favoured solvent for phenol hydrogenation, courtesy of its ability to amplify catalyst activity and optimise the selectivity towards cyclohexanone. Through DFT electronic-structure calculations, Yoon et al. discerned that the presence of the liquid phase diminishes the work function of the metal. They expounded that introducing a hydrogen (H) adatom promotes neutral hydrogen transfer in both gas and liquid phases, thereby minimally impacting water on the energy barriers of phenol hydrogenation[58]. Their revelations suggested that the liquid environment influences the energy of charged surface-bounding intermediates, thus encouraging the preferential formation of cyclohexanone during the phenol hydrogenation process. Supercritical carbon dioxide ($scCO_2$) represents another frequently utilised solvent system. Its edge lies in enhancing the reaction rate, thanks to the infinite miscibility of hydrogen (H_2) with carbon dioxide (CO_2), which mitigates transfer resistance at the gas-liquid interface. Rode et al. embarked on an exploration of a variety of charcoal-supported catalysts for phenol hydrogenation and examined the reaction mechanism under deuterium oxide conditions. They discovered that phenol could be robustly adsorbed by rhodium nanoparticles (NPs) with low electron density, facilitated by electron transfer from rhodium to CO_2. This resulted in a comparably high turnover number (TON) for rhodium-based catalysts. Conversely, palladium nanoparticles exhibited a stronger affinity for CO_2 than other metals, and the competing adsorption between CO_2 and phenol on the palladium NP surface led to reduced catalytic activity compared to rhodium- and ruthenium-based catalysts. Regarding selectivity, experiments

demonstrated that diluting CO_2 with hydrogen (H_2) under high CO_2 pressure curtailed the likelihood of hydrogenating phenol to cyclohexanol[86,91,92].

As for solvent choice, there are two strategies to attain cyclohexanol: direct conversion of phenol and hydrogenation of cyclohexanone. Fujita et al. postulated that CO_2 presence obstructs the second path (hydrogenation of cyclohexanone) without impacting the first path (direct phenol conversion). This occurs because CO_2 engages with cyclohexanone rather than phenol, causing a slowdown in the hydrogenation process[93].

An intriguing observation was shared by Han et al., who probed the synergistic effect between palladium-based catalysts and Lewis acids such as $AlCl_3$, $SnCl_2$, and $ZnCl_2$. This amalgamation manifested excellent catalytic performance for phenol hydrogenation under comparatively mild conditions. In these dual catalyst systems, activating the benzene ring of phenol on Lewis acid coordination and the activation of H_2 on palladium NPs expedited the swift generation of cyclohexanone. Concurrently, the acid-base interaction between the Lewis acid and cyclohexanone thwarted further hydrogenation of cyclohexanone to cyclohexanol[94].

The reaction mechanism of phenol hydrogenation has been thoroughly scrutinised in the empirical literature, particularly in acidic and basic solutions, using a blend of experiments and DFT calculations. It has been noted that activity decreases in basic solutions due to the creation of phenolate, which materialises through the combination of phenol with hydroxide (-OH) ions. This phenolate formation hinders the subsequent hydrogenation reaction[86,94].

1.6. Cross-coupling reaction

In recent years, heterogeneous catalysis has been used for simple cross-coupling reactions based on metal leaching to facilitate the desired reaction. However, a drawback of this approach is that the leached metal must be re-adsorbed to eliminate contamination in the final product, following a "release-and-catch" strategy. This reliance on re-adsorption is not ideal from the perspective of product use or reproducibility. Additionally, achieving high selectivity in heterogeneously catalysed reactions is not straightforward. Nevertheless, the development of cross-coupling chemistry has revolutionised modern synthetic organic chemistry. Transition-metal-catalysed carbon-carbon and carbon-heteroatom bond-forming reactions have significantly impacted the synthesis of pharmaceuticals, agrochemicals, and natural products. Pd-catalysed cross-coupling reactions represent one of the essential classes of synthetic transformations in modern organic chemistry. These reactions have significantly advanced the field of homogeneous catalysis, which has experienced rapid growth in recent years, as evidenced by the increasing number of

publications in this area. Transition metal-catalysed reactions are vital in producing many industrially essential chemicals, where homogeneous catalysis is rapidly expanding. The field of cross-coupling is predominantly driven by homogeneous catalysis and has gained recognition among synthetic chemists in academia and industry, irrespective of their prominence[95–97]. . In some instances, metals such as copper or nickel are used instead of Pd to perform these cross-couplings, although the catalytic activity of these metals is generally lower compared to Pd[96].

1.6.1. N-Alkylation phenols with amines

N-Alkylation of phenols with amines is a well-studied reaction in organic chemistry. Phenols are aromatic compounds that contain a hydroxyl group (-OH) attached to an aromatic ring. On the other hand, amines are organic compounds that contain a nitrogen atom with a lone pair of electrons. When phenols are reacted with amines under appropriate conditions, the hydroxyl group of the phenol can be replaced by an alkyl group from the amine, forming an N-alkylated product. This reaction is commonly used to modify phenolic compounds and has various applications in fields such as pharmaceuticals, polymers, and materials science[98]. Lignin, on the other hand, is a complex and highly heterogeneous polymer derived from the plant cell wall[99]. It comprises various phenolic monomers, such as p-coumaryl, coniferyl, and sinapyl alcohols, which are connected through different linkages. Lignin is a mixture of different phenolic units, and its structure is highly complex and irregular[99,100]. Due to lignin's complexity and heterogeneity, studying lignin's direct alkylation with amines is challenging. Various phenolic units and the complexity of the lignin structure make it difficult to control the reaction and obtain specific products.

Additionally, lignin often contains other functional groups, such as methoxyl ($-OCH_3$) and carboxyl (-COOH), which can also react with amines, leading to side reactions and product mixtures. Therefore, phenol is often used as a model compound to simplify the study of N-alkylation reactions. Furthermore, phenol represents a simple aromatic compound with a single hydroxyl group, allowing for easier control of the reaction and product analysis. By using phenol as a model compound, researchers can gain insights into the fundamental aspects of the N-alkylation reaction, such as the reaction conditions, reactivity, and selectivity. Once the fundamental aspects of the N-alkylation reaction are understood using phenol as a model, researchers can then apply this knowledge to lignin and develop strategies for the selective modification of lignin. However, it is important to note that lignin is a complex mixture, and the reactions that occur in lignin may differ from those observed with phenol. Therefore, while the insights gained from phenol studies are valuable, further

investigations are needed to develop efficient and selective methods for the N-alkylation of lignin.

The most common synthesis processes of secondary amines include coupling amines with alkyl halides (**Scheme 1.1**, route I)[101], alcohols (**Scheme 1.1**, route II)[102], [103], and carbonyl compounds (**Scheme 1.1**, route III)[104]. However, toxic and unstable agents such as alkyl halides, aldehydes and phosphine ligands are widely utilised in traditional syntheses, which always result in environmental problems[105,106].

Beller et al.[107] reported a simple catalytic method for the N-alkylation of amine-reducing agents such as carboxylic acids and silanes by developing a new process for the synthesis of alkylamines, amination via N-arylation by Buchwald–Hartwig (**Scheme 1.1**, route IV)[108], [109]. The reaction between anilines and phenolic provides a new non-fossil approach to cyclohexylamine derivatives, which are extensively investigated structural units in the pharmaceutical industry (**Scheme 1.1**, route V)[110].

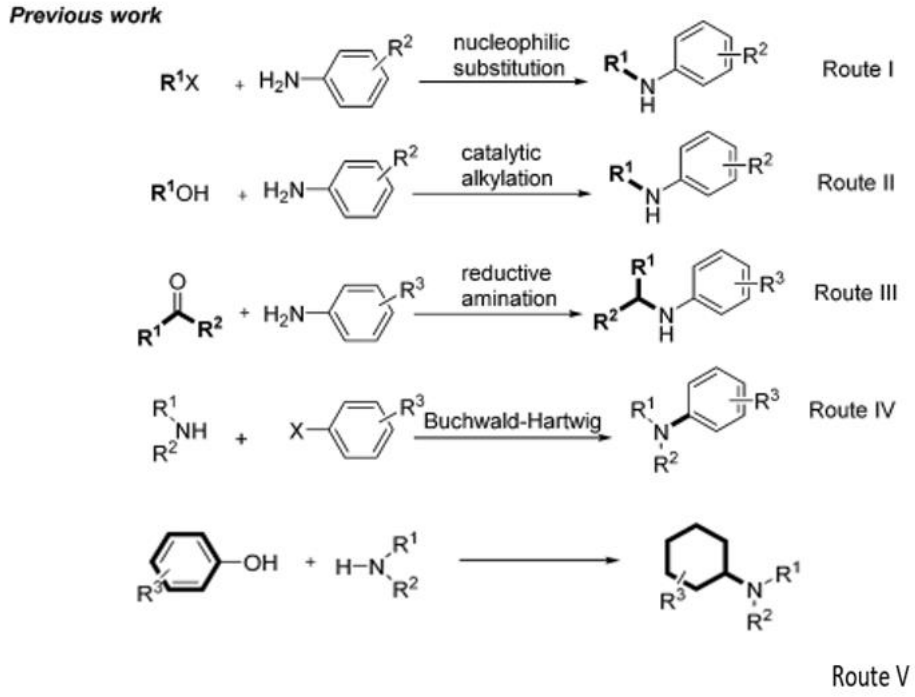

Scheme 1.1: Methods for direct amine alkylation. Reproduced from ref.[110].

1.6.1.1. Amination phenol with P-Toluidine

1.6.1.1.1. Amination using hydrogen gas

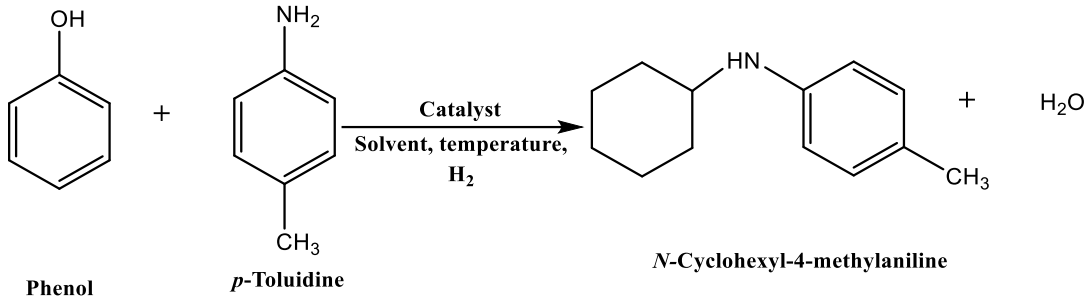

Scheme 1.2: N-alkylation of ρ-toluidine with phenol.

Chen et al. reported a highly efficient palladium-catalysed reaction between anilines and phenolic lignin model monomers and analogues for developing novel conversion methods[110]. This transformation signifies a new catalytic strategy for promoting the cleavage of a C–O bond[111]. Additionally, secondary amine compounds are crucial in pharmaceuticals, agrochemicals, and materials. Therefore, the synthesis of secondary amines has been extensively studied at laboratory and industrial scales. Furthermore, a new non-fossil approach to cyclohexylamine derivatives, widely explored structural units in the pharmaceutical industry, has been introduced[112].

Phenols are directly converted into secondary amines in significant yields through hydrogenation and amination tandem reactions over the Al_2O_3 supported palladium hydride catalyst[113]. However, phenols possess a highly reactive hydroxy group and a C-O bond with a high dissociation energy due to p–π conjugation. In recent years, substantial progress has been made in developing coupling reactions of phenols by catalytic C-O bond cleavage, transforming them into more active derivatives[114]. The model reaction used in this process was N-alkylation of ρ-toluidine with phenol (**Scheme 1.2)**.

1.6.1.1.2. Amination using catalytic transfer hydrogenation (CTH) pathway

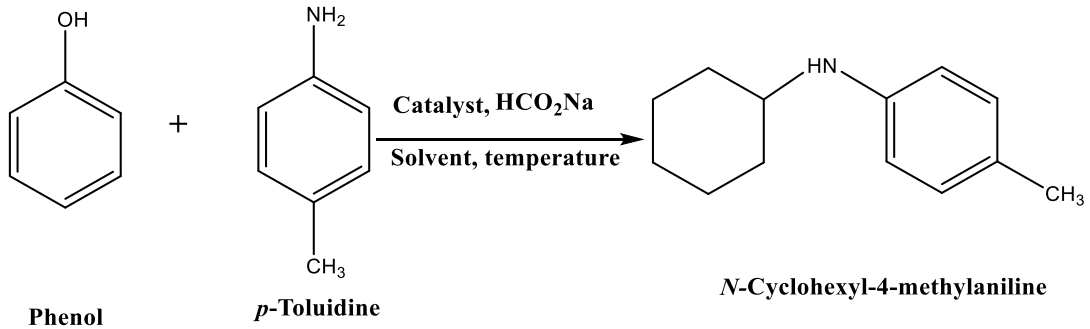

Scheme 1.3: Direct amine of phenol with p-toluene by Catalytic transfer hydrogenation method.

Organic molecules such as alcohols, acids and acid salts can act as hydrogen donors in hydrogenation reactions integrated with catalysts via a pathway known as catalytic transfer hydrogenation (CTH). The process of high-pressure, flammable hydrogen gas treatment can be avoided and the solubility of hydrogen donors can be enhanced using the CTH method. Moreover, the lower hydrogenating capability of most organic hydrogen donors can effectively control product selectivity when partially hydrogenated molecules are targeted, compared to molecular H_2. This theory is applied to the selective hydrogenation of phenol[115,116]. Xiang et al.[117] demonstrated that hydrogen formed from the APR of methanol or ethanol over the Raney Ni or Pd/Al_2O_3 catalyst could be used in situ for the hydrogenation of phenol and its derivatives (phenol, o-cresol and p-tert-butylphenol) to produce cyclohexanone with higher cyclohexanone selectivity than H_2 gas. Zhang et al.[118] compared the catalytic performance of several Pd-based catalysts in different conditions. Their findings revealed that when using a molecular H_2 hydrogen source, the catalyst activities followed the trend: Pd/MIL-101>Pd/TiO_2 -AC>Pd/AC>Pd/C commercial> Pd/Al_2O_3 >Pd/TiO_2. In contrast, activity changed to the following order: Pd/AC>Pd/C-commercial>Pd/TiO_2-AC>P d/MIL-101>Pd/TiO_2> Pd/Al_2O_3 when formic acid was employed as a hydrogen donor. Given that both the decomposition of formic acid and hydrogenation of phenol occurs in the CTH system, these two reactions may influence each other, affecting the overall reaction rates. The authors determined that the optimum catalyst for in situ hydrogenation reactions should enable all reactants to approach the active sites. Pd/AC exhibited the highest activity in the CHT process, possibly due to its specific adsorption ability for phenol and formic acid[118]. The model reaction used in this process was N-alkylation of ρ-toluidine with phenol, in which hydrogen was replaced by nitrogen when the catalytic transfer hydrogenation (CTH) pathway was used for hydrogenation reactions (**Scheme 1.3)**.

1.7. Hydrogen auto-transfer reactions

The hydrogen auto-transfer process, or borrowing hydrogen (BH) or a self-supplying system for active hydrogen, combines a transfer hydrogenation process with a concurrent reaction on the in situ generated reactive intermediate[105,119,120]. This reaction is a part of the hydrogen transfer reaction fields used and typically begins with the abstraction of a hydrogen atom from the starting reagent (R1-H) via the corresponding catalyst to produce a new reagent (R1). Finally, the abstracted hydrogen is returned and incorporated into the final product, hence the reaction name. **Figure 1.7** illustrates a generalisation of the (HAT) process.

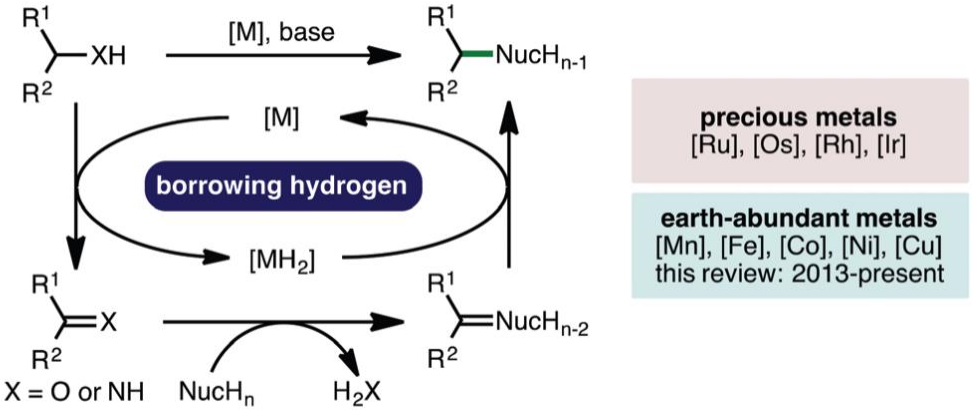

Figure1.7: Generalisation of the HAT approach. Reproduced from ref.[119].

This reduction reaction sequence has garnered much attention due to its inherent high atom economy, permitting alcohols or amines to be employed as alkylating agents and generating water or ammonia as the only by-products, respectively.

Hydrogen auto-transfer reaction techniques have traditionally utilised valuable second and third-row transition metal catalysts (based on Ru, Os, Rh, and Ir) to facilitate hydrogen transfer[119]. However, the development of heterogeneous catalysts for green chemical synthesis represents a growing area in catalysis and green-sustainable chemistry.

Shimizua reviewed recent examples of hydrogen transfer-type reactions using supported transition metal catalysts. The most notable reactions included: (1) transfer hydrogenation of carbonyl compounds; (2) transfer dehydrogenation of alcohols; (3) N-alkylation of amines or NH_3 with alcohols; (4) alkylation of acidic CH_2 or CH_3 groups with alcohols; (5) self- and cross-alkylation of alcohols; (6) N-or C3- alkylation of indoles with alcohols; (7) synthesis of quinolines from nitroarenes and alcohols; (8) synthesis of thioethers from thiols and alcohols; and (9) cross-alkylation of amines with various amines[121]. In addition, the typical reaction mechanistic features were discussed, such as a domino dehydrogenation–condensation–hydrogenation sequence of alcohols (or amines) and nucleophiles.

The reported that heterogeneously catalysed direct C–C, C–N, and C–S bond formation reactions borrow the hydrogen methodology and can offer practical and atom-efficient routes to valuable chemicals from alcohols (or amines) under neutral conditions. They also found that, in contrast to Ru- and Ir-based organometallic catalysis, various metals, including non-noble metals, are available in the heterogeneous catalytic system. The organometallic systems generally require additives (ligand, acid, or base) in the solution, decreasing economy and atom economy, whereas most state-of-the-art heterogeneous systems operate under additive-free conditions[121]. Furthermore, this study reported that the key concept in

the catalyst design in some systems is the multi-functionality of the metal-loaded acidic and/or basic metal oxides. In these systems, the acid and/or base sites on the support selectively catalyse the condensation reactions, and the metal site catalyses the transfer dehydrogenation of alcohol (or amines) and transfer hydrogenation of condensation products as intermediates. Many studies have shown that the catalyst was developed empirically, and a good combination of a metal with a suitable oxidation state and size and support has been determined by screening studies[121].

Rhodium(I) complexes have been examined as catalysts for the hydrogen-borrowing reactions of amines and alcohols. Bidentate carbene-triazole ligands were readily synthesised by 'click' reactions, allowing various ligand backbones to be obtained. This study confirmed that catalytic transformations are highly efficient, can reach completion in approximately six hours and promote C−N bond formation across a range of primary alcohol and amine substrates. In addition, site-selective catalysis can be obtained using substrates with more than one reactive site. According to the author, this study was the first to report a heterogeneous rhodium catalyst used for hydrogen borrowing[122].

In a study by Huang et al., pyridyl triazole gold(I) complexes were synthesised, revealing that the triazole part coordinated with gold(I). Furthermore, the study reported that pyridyl triazole gold(I) complexes proved to be an efficient pre-catalyst for the most challenging gold-catalysed hydrogen auto transfer reaction and the dehydrogenation of alcohols and amines compared to the $Ph_3PAuCl/AgOTf$ catalyst. This is because they provided an efficient method to selectively synthesise imines, substituted amines, and functionalised ketones in excellent yields with high chemo-selectivity. This finding suggested that triazole ligands are helpful in forming gold nanoparticles and delaying agglomeration in these reactions[123].

Zhaojun et al.[124] demonstrated that a BINAP-Cu system supported by hydrotalcite offers a highly efficient catalyst for the atom-efficient and green hydrogen auto-transfer reaction and dehydrogenative cyclisation. Furthermore, this BINAP-Cu complex supported by hydrotalcite is highly air-stable and can be recycled at least five times under solvent-free conditions.

1.7.1. The coupling of nitrobenzene with benzyl alcohol

The oxygen-rich biomass feedstock can be converted to hydrocarbons using the hydrodeoxygenation strategy. Hydrogen auto transfer is an interesting method whereby hydrogen from a dehydrogenation reaction is effectively used in the hydrogenation or hydrodeoxygenation reactions in situ. One of the hydrogen auto transfer (HAT) reactions is the synthesis of imines, secondary amines, and tertiary

amines from benzyl alcohol and nitrobenzene directly, without using any external hydrogen[125].

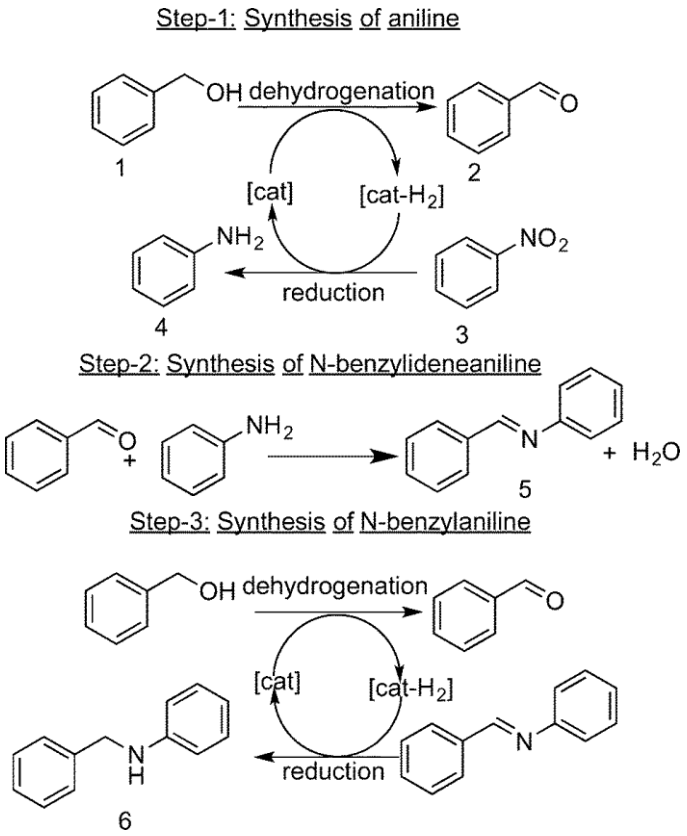

Scheme 1.4: HAT reaction steps to produce (5) N-benzylideneaniline and (6)N-benzylaniline from (1) benzyl alcohol and (3) nitrobenzene. (2) is benzaldehyde and (4) is aniline. Reproduced from ref.[126].

A HAT strategy was utilised to investigate the activity of all the monometallic and bimetallic catalysts via the direct synthesis of amines and imines from benzyl alcohol and nitrobenzene without using any external hydrogen or a hydrogen donor. The HAT reaction involves three steps to synthesise an amine from benzyl alcohol and nitrobenzene (see **Scheme 1.4**)[126].

1.8. Objectives and aims of this thesis

The selective hydrogenation of phenol is a promising and challenging topic in heterogeneous metal catalysis. The hydrogenation of phenol will be studied using supported metal catalysts under a green reduction system.

Firstly, using Al_2O_3 as a support for Pd and Ru-Pd nanoparticulate catalysts for the hydrogenation of phenol selectively to cyclohexanol, will be examined under mild conditions. The optimisation of the reaction conditions, such as the metal loading and

support, and choice of metal, will also be considered. Secondly, the thesis will investigate whether the functional groups of phenols (OH) and amines (NH_2) can be coupled to secondary amines under mild conditions. The impact of the mono and bimetallic system (palladium and palladium X, (X=Au, Ru, Cu, Fe, and Ni) on the amination of phenol will also be examined. In addition, different pathways will be used for the hydrogen source in the amination of phenol, either by having organic molecules act as hydrogen donors as catalytic transfer hydrogenation (CTH) or by using hydrogen gas. The benefit of using the CTH method is that the solubility of hydrogen donors avoids high- pressure and flammable hydrogen gas.

Moreover, the CTH method can control product selectivity when partially hydrogenated molecules are targeted, compared to molecular H_2. Furthermore, the hydrogen auto-transfer (HAT) is another pathway to coupling benzyl alcohol with nitrobenzene. This protocol is also known as either (HAT) a self-supplying system for active hydrogen. (HAT) approach combines a transfer hydrogenation process with a concurrent reaction on the in situ generated reactive intermediate. In addition, the influence of the metallic ratio and loading and the temperature will be monitored to support the influence of hydrogenation and, therefore, the choice of metal.

1.9. Thesis outline

Chapter 1: Introduction

The initial chapter of this thesis serves as a gateway to the subject matter, sketching out the background, relevance, and objectives of the study. It encapsulates a panoramic view of the general knowledge in the domain, pinpoints lacunae in the existing literature, and crafts the research queries that the thesis aims to unravel.

Chapter 2: Experimental

Chapter two zeros in on the experimental blueprints and procedures wielded in the investigation. It furnishes an in-depth account of the materials, apparatus, and methods harnessed in the research. Details on sample preparation, reaction conditions, data acquisition techniques, and analytical approaches for characterising catalysts and end products may be found in this chapter.

Chapter 3: Catalysts Characterisation

The third chapter is devoted to the comprehensive examination of the catalysts employed in the study. It thoroughly analyses the catalysts' physical and chemical attributes, such as surface area, pore size distribution, elemental composition, and crystalline structure. A host of characterisation techniques, including X-ray diffraction (XRD), scanning electron microscopy (SEM), transmission electron microscopy (TEM), and spectroscopic methods, may be utilised for this purpose.

Chapter 4: Phenol Hydrogenation

Chapter four hones in on the exploration of phenol hydrogenation. It unfurls the experimental outcomes and analyses related to phenol hydrogenation, encompassing reaction conditions, catalytic activity, selectivity, and reaction mechanisms. The chapter might also explore the impact of various factors, including catalyst composition, reaction temperature, pressure, and solvent on the phenol hydrogenation process.

Chapter 5: N-Alkylation Phenols with Amines

Chapter five investigates the N-alkylation of phenols with amines. It discusses the experimental revelations and analysis of the interaction between phenols and amines, emphasising the catalytic systems employed, reaction conditions, product selectivity, and reaction mechanisms. This chapter might also address the optimisation of reaction parameters and the identification of the most efficacious catalysts for achieving the intended results.

Chapter 6: Hydrogen Auto Transfer Reactions

Chapter six plunges into the examination of hydrogen auto-transfer reactions. It scrutinises the experimental probes and analyses of reactions that involve the transfer of hydrogen atoms between diverse reactant molecules. This chapter may encompass the catalytic systems employed, reaction conditions, mechanistic insights, and the sway of reaction parameters on hydrogen auto transfer reactions.

Chapter 7: Conclusion

The concluding chapter of the thesis encapsulates the research's primary discoveries, inferences, and implications. It underscores the contributions made by the study, deliberates the limitations and potential future trajectories, and proffers recommendations for subsequent research. This chapter brings the thesis full circle and reasserts its importance in the larger scheme of the research field.

1.10. References

1 J. J. Berzelius, *Edinburgh New Philosophical Journal 1836,* XXI., 1836.

2 K. A. Resende, C. E. Hori, F. B. Noronha, H. Shi, O. Y. Gutierrez, D. M. Camaioni and J. A. Lercher, *Appl. Catal. A Gen.*, 2017, **548**, 128–135.

3 M. Barbato and C. Bruno, *Mol. Phys. Hypersonic Flows*, , DOI:10.1007/978-94-009-0267-1.

4 R. M. A. Roque-Malherbe and S. Use, *INglomayor*, 2019, **16**, 51–71.

5 S. K. Vishwakarma, , DOI:10.13140/RG.2.2.25613.46568.

6 W. C. MCC. L., *Nature*, 1920, 104, 463–464.

7 C. B. Lindström, L.J. Pettersson, 2003, **7**, 130–138.

8 P. T. Anastas, M. M. Kirchhoff and T. C. Williamson, *Appl. Catal. A Gen.*, 2001,

221, 3–13.

9 J. W. N. I. Chorkendorff, *Concepts of Modern Catalysis and*, 2005, vol. 12 Suppl 1.

10 J. C. Berg and H. Alper, 1989, **67**, 3–4.

11 Michael Bowker, *ZENECA*, 1998, 1–90.

12 M. Schwaab and J. C. Pinto, *Chem. Eng. Sci.*, 2007, **62**, 2750–2764.

13 L. Hussein, .

14 A. Behr, S. Reyer, Y. Brunsch and V. Manz, *Synthesis (Stuttg).*, 2012, **44**, 575–578.

15 A. Tathe, A. P. G. Nikalje and M. Ghodke, .

16 A. Blanco and G. Blanco, *Med. Biochem.*, 2017, 153–175.

17 J. Song, Z. F. Huang, L. Pan, K. Li, X. Zhang, L. Wang and J. J. Zou, *Appl. Catal. B Environ.*, 2018, **227**, 386–408.

18 C. G. W, J. Wiley and N. York, 1980, 179–180.

19 L. Fanfoni, A. Meduri, E. Zangrando, S. Castillon, F. Felluga and B. Milani, *Molecules*, 2011, **16**, 1804–1824.

20 A. Gizli, G. Aytimur, E. Alpay and S. Atalay, *Chem. Eng. Technol.*, 2008, **31**, 409–416.

21 O. Deutschmann, H. Knözinger, K. Kochloefl and T. Turek, *Ullmann's Encycl. Ind. Chem.*, , DOI:10.1002/14356007.O05_O03.

22 F. Zaera, *Chem. Soc. Rev.*, 2013, **42**, 2746–2762.

23 K. Kakaei, M. D. Esrafili and A. Ehsani, *Interface Sci. Technol.*, 2019, **27**, 1–21.

24 M. Kitano, S. Kanbara, Y. Inoue, N. Kuganathan, P. V. Sushko, T. Yokoyama, M. Hara and H. Hosono, *Nat. Commun.*, 2015, **6**, 1–9.

25 H. Ronduda, M. Zybert, W. Patkowski, A. Ostrowski, P. Jodłowski, D. Szymański and W. Raróg-Pilecka, *Int. J. Hydrogen Energy*, 2022, **47**, 35689–35700.

26 G. Rothenberg, *Catalysis: Concepts and Green Applications,* WILEY-VCH GmbH & Co. KGaA, 2008.

27 W. A. eds. Cornils, B. and Herrmann, *Aqueous-phase organometallic catalysis: concepts and applications*, 2004.

28 B. Surveys, S. Team and U. S. Eia, .

29 G. W. Huber, S. Iborra and A. Corma, *Chem. Rev.*, 2006, **106**, 4044–4098.

30 J. S. Guest, S. J. Skerlos, J. L. Barnard, M. B. Beck, G. T. Daigger, H. Hilger, S. J. Jackson, K. Karvazy, L. Kelly, L. Macpherson, J. R. Mihelcic, A. Pramanik, L. Raskin, M. C. M. Van Loosdrecht, D. Yeh and N. G. Love, *Environ. Sci. Technol.*, 2009, **43**, 6126–6130.

31 M. Dusselier, P. Van Wouwe, A. Dewaele, E. Makshina and B. F. Sels, *Energy Environ. Sci.*, 2013, **6**, 1415–1442.
32 R. Fang, H. Liu, R. Luque and Y. Li, *Green Chem.*, 2015, **17**, 4183–4188.
33 G. Morales, J. Iglesias and J. A. Melero, 2020, 4–7.
34 I. E. Agency, *World Energy Outlook 1998*, 1998.
35 Y. Nakagawa and K. Tomishige, *Catal. Surv. from Asia*, 2011, **15**, 111–116.
36 P. Gallezot, *ChemSusChem*, 2008, **1**, 734–737.
37 A. E. Ashley, A. L. Thompson and D. O 'hare, , DOI:10.1002/anie.200.
38 J. S. Lupoi, S. Singh, R. Parthasarathi, B. A. Simmons and R. J. Henry, *Renew. Sustain. Energy Rev.*, 2015, **49**, 871–906.
39 S. Van Den Bosch, W. Schutyser, S. F. Koelewijn, T. Renders, C. M. Courtin and B. F. Sels, *Chem. Commun. (Camb).*, 2015, **51**, 13158–13161.
40 J. Zhang, J. Teo, X. Chen, H. Asakura, T. Tanaka, K. Teramura and N. Yan, *ACS Catal.*, 2014, **4**, 1574–1583.
41 B. Saulsbury, *US Department of Energy US Department of Energy Publications Biomass Energy Data Book , Volume 1*, 2015, vol. 1.
42 A. Corma Canos, S. Iborra and A. Velty, *Chem. Rev.*, 2007, **107**, 2411–2502.
43 G. W. Huber, S. Iborra and A. Corma, *Chem. Rev.*, 2006, **106**, 4044–4098.
44 M. Dusselier, M. Mascal and B. F. Sels, *Top. Curr. Chem.*, 2014, **353**, 1–40.
45 J. E. Holladay, J. F. White, J. J. Bozell and D. Johnson, , DOI:10.2172/921839.
46 T. Zhang, *Adv. Oxid. Process. - Appl. Trends, Prospect.*, , DOI:10.5772/INTECHOPEN.90393.
47 W. Ouyang, A. Yepez, A. A. Romero and R. Luque, *Catal. Today*, 2018, **308**, 32–37.
48 D. M. Alonso, S. G. Wettstein and J. A. Dumesic, *Chem. Soc. Rev.*, 2012, **41**, 8075–8098.
49 S. N. H. Md Dostagir, M. K. Awasthi, A. Kumar, K. Gupta, S. Behrens, A. Shrotri and S. K. Singh, *ACS Sustain. Chem. Eng.*, 2019, **7**, 9352–9359.
50 M. Zhou, J. Ye, P. Liu, J. Xu and J. Jiang, *ACS Sustain. Chem. Eng.*, 2017, **5**, 8824–8835.
51 C. Huang, X. Yang, H. Yang, P. Huang, H. Song and S. Liao, *Appl. Surf. Sci.*, 2014, **315**, 138–143.
52 R. P. A.M. Ruppert, K. Weinberg, *Angewandte Chemie International*, 2012, vol. 51.
53 S. Narayanan and K. Krishna, *Catal. Today*, 1999, **49**, 57–63.
54 Y. Wang, J. Yao, H. Li, D. Su and M. Antonietti, *J. Am. Chem. Soc.*, 2011, **133**, 2362–2365.
55 G. Busca, *Structural, Surface, and Catalytic Properties of Aluminas*, Elsevier

Inc., 1st edn., 2014, vol. 57.

56 N. Mahata, K. V. Raghavan and V. Vishwanathan, *Appl. Catal. A Gen.*, 1999, **182**, 183–187.

57 S. Narayanan and K. Krishna, *Appl. Catal. A Gen.*, 1996, **147**, 253–258.

58 Y. Yoon, R. Rousseau, R. S. Weber, D. Mei and J. A. Lercher, *J. Am. Chem. Soc.*, 2014, **136**, 10287–10298.

59 J. Tobicik and L. Cerveny, *J. Mol. Catal. A-Chemical*, 2003, **194**, 249–254.

60 E. J. Shin and M. A. Keane, *Ind. Eng. Chem. Res.*, 2000, **39**, 883–892.

61 E. J. Shin and M. A. Keane, *J. Catal.*, 1998, **173**, 450–459.

62 Y. Pérez, M. Fajardo and A. Corma, *Catal. Commun.*, 2011, **12**, 1071–1074.

63 A. M. Raspolli Galletti, C. Antonetti, I. Longo, G. Capannelli and A. M. Venezia, *Appl. Catal. A Gen.*, 2008, **350**, 46–52.

64 T. Yu, J. Wang, X. Li, X. Cao and H. Gu, *ChemCatChem*, 2013, **5**, 2852–2855.

65 A. Corma and H. Garcia, *Adv. Synth. Catal.*, 2006, **348**, 1391–1412.

66 W. Yao, Y. Chen, L. Min, H. Fang, Z. Yan, H. Wang and J. Wang, *J. Mol. Catal. A Chem.*, 2006, **246**, 162–166.

67 A. Li, K. Shen, J. Chen, Z. Li and Y. Li, *Chem. Eng. Sci.*, 2017, **166**, 66–76.

68 X. Liu, W. Jia, G. Xu, Y. Zhang and Y. Fu, *ACS Sustain. Chem. Eng.*, 2017, **5**, 8594–8601.

69 G. Porwal, S. Gupta, S. Sreedhala, J. Elizabeth, T. S. Khan, M. A. Haider and C. P. Vinod, *ACS Sustain. Chem. Eng.*, 2019, **7**, 17126–17136.

70 Y. Qin, R. Li, W. Mi, W. Shi, B. Lu and X. Tong, *Diam. Relat. Mater.*, 2021, **111**, 108163.

71 A. Bjelić, M. Grilc, M. Huš and B. Likozar, *Chem. Eng. J.*, 2019, **359**, 305–320.

72 Y. Hong, D. Sun and Y. Fang, *Chem. Cent. J.*, 2018, **12**, 1–9.

73 E. Field, F. H. Dempster and G. E. Tilson, *Ind. Eng. Chem.*, 1940, **32**, 489–496.

74 Q. Bu, H. Lei, S. Ren, L. Wang, J. Holladay, Q. Zhang, J. Tang and R. Ruan, *Bioresour. Technol.*, 2011, **102**, 7004–7007.

75 M. A. Ali and A. Abutaleb, *Catal. Letters*, 2022, **152**, 1555–1581.

76 G. Xue, L. Yin, S. Shao and G. Li, *Nanotechnology*, 2021, **33**, 072003.

77 Y. Zhu, G. Yu, J. Yang, M. Yuan, D. Xu and Z. Dong, *J. Colloid Interface Sci.*, 2019, **533**, 259–267.

78 F. Zhang, S. Chen, H. Li, X. M. Zhang and H. Yang, *RSC Adv.*, 2015, **5**, 102811–102817.

79 K. A. Resende, C. E. Hori, F. B. Noronha, H. Shi, O. Y. Gutierrez, D. M. Camaioni and J. A. Lercher, *Appl. Catal. A Gen.*, 2017, **548**, 128–135.

80 A. N. Raut, S. U. Nandanwar, Y. R. Suryawanshi, M. Chakraborty, S. Jauhari,

S. Mukhopadhyay, K. T. Shenoy and H. C. Bajaj, *Kinet. Catal.*, 2016, **57**, 39–46.

81 A. N. Raut, S. U. Nandanwar, Y. R. Suryawanshi, M. Chakraborty, S. Jauhari, S. Mukhopadhyay, K. T. Shenoy and H. C. Bajaj, *Кинетика И Катализ*, 2016, **57**, 42–48.

82 A. M. R. Galletti, C. Antonetti, A. M. Venezia and G. Giambastiani, *Appl. Catal. A Gen.*, 2010, **386**, 124–131.

83 H. Chen and J. Sun, *J. Ind. Eng. Chem.*, 2021, **94**, 78–91.

84 H. Li, J. Liu, S. Xie, M. Qiao, W. Dai, Y. Lu and H. Li, *Adv. Funct. Mater.*, 2008, **18**, 3235–3241.

85 Y. Z. Chen, C. W. Liaw and L. I. Lee, *Appl. Catal. A Gen.*, 1999, **177**, 1–8.

86 X. Kong, Y. Gong, S. Mao and Y. Wang, *ChemNanoMat*, 2018, **4**, 432–450.

87 M. M. Najafpour, G. Renger, M. Hołyńska, A. N. Moghaddam, E. M. Aro, R. Carpentier, H. Nishihara, J. J. Eaton-Rye, J. R. Shen and S. I. Allakhverdiev, *Chem. Rev.*, 2016, **116**, 2886–2936.

88 K. R. Reddy, K. V. Karthik, S. B. B. Prasad, S. K. Soni, H. M. Jeong and A. V. Raghu, *Polyhedron*, 2016, **120**, 169–174.

89 L. L. R. Vono, C. Broicher, K. Philippot and L. M. Rossi, *Catal. Today*, 2021, **381**, 126–132.

90 G. Neri, A. M. Visco, A. Donato, C. Milone, M. Malentacchi and G. Gubitosa, *Appl. Catal. A Gen.*, 1994, **110**, 49–59.

91 C. V. Rode, U. D. Joshi, O. Sato and M. Shirai, *Chem. Commun.*, 2003, **3**, 1960–1961.

92 H. Wang, F. Zhao, S. ichiro Fujita and M. Arai, *Catal. Commun.*, 2008, **9**, 362–368.

93 S. I. Fujita, T. Yamada, Y. Akiyama, H. Cheng, F. Zhao and M. Arai, *J. Supercrit. Fluids*, 2010, **54**, 190–201.

94 M. Li, Y. Li, L. Jia and Y. Wang, *Catal. Commun.*, 2018, **103**, 88–91.

95 C. C. C. Johansson Seechurn, A. Deangelis and T. J. Colacot, *RSC Catal. Ser.*, 2015, **2015**-**Janua**, 1–19.

96 R. Greco, W. Goessler, D. Cantillo and C. O. Kappe, *ACS Catal.*, 2015, **5**, 1303–1312.

97 H. Zeng, Z. Qiu, A. Domínguez-Huerta, Z. Hearne, Z. Chen and C. J. Li, *ACS Catal.*, 2017, **7**, 510–519.

98 G. Boucher, *Crit. Sociol.*, 2011, **37**, 493–497.

99 M. Stöcker, *Angew. Chemie Int. Ed.*, 2008, **47**, 9200–9211.

100 J. Zakzeski, P. C. A. Bruijnincx, A. L. Jongerius and B. M. Weckhuysen, *Chem. Rev.*, 2010, **110**, 3552–3599.

101 R. N. Salvatore, C. H. Yoon and K. W. Jung, *Tetrahedron*, 2001, **57**, 7785–7811.

102 R. Kawahara, K. I. Fujita and R. Yamaguchi, *Adv. Synth. Catal.*, 2011, **353**, 1161–1168.

103 S. Bähn, S. Imm, L. Neubert, M. Zhang, H. Neumann and M. Beller, *ChemCatChem*, 2011, **3**, 1853–1864.

104 P. K. Verma, U. Sharma, N. Kumar, M. Bala, V. Kumar and B. Singh, *Catal. Letters*, 2012, **142**, 907–913.

105 G. Guillena, D. J. Ramón and M. Yus, *Chem. Rev.*, 2010, **110**, 1611–1641.

106 M. Zhang, H. Yang, Y. Zhang, C. Zhu, W. Li, Y. Cheng and H. Hu, *Chem. Commun.*, 2011, **47**, 6605–6607.

107 I. Sorribes, K. Junge and M. Beller, *J. Am. Chem. Soc.*, 2014, **136**, 14314–14319.

108 D. S. Surry and S. L. Buchwald, *Angew. Chem. Int. Ed. Engl.*, 2008, **47**, 6338–6361.

109 J. F. Hartwig, *Acc. Chem. Res.*, 2008, **41**, 1534–1544.

110 Z. Chen, H. Zeng, H. Gong, H. Wang and C. J. Li, *Chem. Sci.*, 2015, **6**, 4174–4178.

111 J. Cornella, C. Zarate and R. Martin, *Chem. Soc. Rev.*, 2014, **43**, 8081–8097.

112 R. Skouta, S. J. Dixon, J. Wang, D. E. Dunn, M. Orman, K. Shimada, P. A. Rosenberg, D. C. Lo, J. M. Weinberg, A. Linkermann and B. R. Stockwell, *J. Am. Chem. Soc.*, 2014, **136**, 4551–4556.

113 L. Yan, X. X. Liu and Y. Fu, *RSC Adv.*, 2016, **6**, 109702–109705.

114 M. Tobisu and N. Chatani, *Acc. Chem. Res.*, 2015, **48**, 1717–1726.

115 M. J. Gilkey and B. Xu, *ACS Catal.*, 2016, **6**, 1420–1436.

116 J. Zhang, *Green Energy Environ.*, 2018, **3**, 328–334.

117 Y. Xiang, X. Li, C. Lu, L. Ma, J. Yuan and F. Feng, *Ind. Eng. Chem. Res.*, 2011, **50**, 3139–3144.

118 A. M. Ruppert, N. Keller, A. S. Dumon, C. Michel, P. Sautet and J. Grams, 2015, 2–7.

119 B. G. Reed-Berendt, K. Polidano and L. C. Morrill, *Org. Biomol. Chem.*, 2019, **17**, 1595–1607.

120 T. Irrgang and R. Kempe, *Chem. Rev.*, 2019, **119**, 2524–2549.

121 K. I. Shimizu, *Catal. Sci. Technol.*, 2015, **5**, 1412–1427.

122 C. M. Wong, M. B. Peterson, I. Pernik, R. T. McBurney and B. A. Messerle, *Inorg. Chem.*, 2017, **56**, 14682–14687.

123 R. Huang, Y. Yang, D. S. Wang, L. Zhang and D. Wang, *Org. Chem. Front.*, 2018, **5**, 203–209.

124 Z. Xu, X. Yu, X. Sang and D. Wang, *Green Chem.*, 2018, **20**, 2571–2577.

125 M. H. S. A. Hamid, P. A. Slatford and J. M. J. Williams, *Adv. Synth. Catal.*, 2007, **349**, 1555–1575.

126 M. Sankar, Q. He, S. Dawson, E. Nowicka, L. Lu, P. C. A. Bruijnincx, A. M. Beale, C. J. Kiely and B. M. Weckhuysen, *Catal. Sci. Technol.*, 2016, **6**, 5473–5482.

Chapter 2: Experimental

2.1. Materials

The chemical materials used in this experimental work are listed in **Tables 2.1** and **2.2**.

Table 2.1: List of chemicals used for catalyst preparation:

Materials for catalyst preparation	
Material	**Supplier**
Active carbon (G-60, decolourising)	Sigma Aldrich
Cerium (IV) oxide (CeO_2) of ≥ 99.0 %	Aldrich
MgO, 97 %	Aldrich
Sodium borohydride powder $NaBH_4$ (≥ 98 %)	Aldrich
Polyvinyl alcohol (PVA)	Sigma Aldrich
Zeolite Y hydrogen , S.A.730 m/g, 5.1:1 molar ratio SiO_2:Al_2O_3 (25 g), 98 %	Alfa Aesar
TiO_2 (P25), 99 %	Degussa
Al_2O_3 (nanopowder,13 nm primary particle size TEM),(99,8 % trace metals basis)	Aldrich
Chloroauric acid, $HAuCl_4$	Johnson Matthey, 99.9%
$PbCl_2$ (99.999 %)	Aldrich
NaOH	Fisher
Ethanol absolute	VWR
$FeCl_2$ (assay:98 %)	Sigma Aldrich
$NiCl_2$, 98 %	Sigma Aldrich
$CuCl_2.2H_2O$, Cu content 37.274 %	Sigma Aldrich
Sodium formate, reagent grade, 97 %	Sigma Aldrich
Hexane anhydrous, 95 %	Sigma Aldrich
$RuCl_3$, Ru content 45-55 %	Aldrich
Mesitylene,98 %	Sigma Aldrich
Toluene, ≥ 99.5 %	Sigma Aldrich
Isopropanol (IPA) ≥ 98 %	Sigma Aldrich

Table 2.2: Chemicals used for catalytic testing:

Materials of reactants and products	
Material	**Supplier**
Phenol (C_6H_5OH), 99.0-100.5 %	Sigma Aldrich
Cyclohexanone, ≥ 99.0 %	Sigma Aldrich
Cyclohexanol, ≥ 99.0 %	Sigma Aldrich
Para-toluidine (p-$CH_3C_6H_4NH$), 99.7 %	Aldrich
N-Cyclohexyl-4-methyl aniline	Sigma Aldrich
4-Methyl-N-(4-methyl cyclohexyl) aniline	Sigma Aldrich
4-Methylcyclohexanone, 99 %	Sigma Aldrich
Benzyl alcohol ,99.0 %	Sigma Aldrich
Nitrobenzene, ≥ 99.0 %	Sigma Aldrich
Benzaldehyde, ≥ 99 %	Sigma Aldrich
Aniline, ≥ 99.5 %	Sigma Aldrich
N-Benzylideneaniline(99 %)	Aldrich
N-Benzylaniline (≥ 99 %)	Aldrich

2.2. Catalyst preparation method

Several supported metal catalysts were prepared and tested for different reactions discussed in this thesis in the following three chapters. This chapter provides a comprehensive overview of the preparation methods and procedures employed for synthesizing various catalysts reported in this work. The metal loading on the support is expressed as the weight percentage of the metal relative to the support.

2.2.1. Sol-immobilisation method

Supported 5 wt.% Pd and Au bimetallic catalysts (2 g) were prepared using the sol-immobilization method reported elsewhere [1]. The preparation method is as follows: the required amount of $HAuCl_4.3H_2O$ (Sigma Aldrich) with a concentration of 8.9

mg/mL, $PdCl_2$ (Sigma Aldrich) with a Pd concentration of 6 mg/mL dissolved in 0.58 M HCl, and $RuCl_3$ (Sigma Aldrich) with a Ru concentration of 6 mg/mL were added to 800 mL of deionized water under continuous stirring. Freshly prepared polyvinyl alcohol (1wt % solution, MW = 10,000, 80% hydrolysed) was added (PVA/Au (by wt.) = 0.65) to protect and stabilize the Au nanoparticles. The mixture was stirred for another 15 minutes, and then a freshly prepared $NaBH_4$ solution (0.2 M, $NaBH_4$/Au (mol/mol) = 5) was added to form a dark-brown sol. The mixture was stirred for an additional 30 minutes while adjusting the pH to 2 by dropwise addition of concentrated H_2SO_4 (with TiO_2, Al_2O_3) (Addition of concentrated H_2SO_4, to firmly attach metal ions to the support's surface). Approximately 1.98 g of the support was added to the colloid mixture and stirred for 2 hours. The catalyst was filtered, washed using deionized water (2 L), and then dried at 110 °C in an oven for 16 hours prior to use. The addition of acid during preparation modifies the size of metal nanoparticles intended for immobilisation on supports, thereby enhancing the catalytic activity of the final catalyst for direct product synthesis and subsequent degradation[2].

2.2.2. Modified impregnation method

In this thesis, a modified impregnation method was adopted to prepare all of the catalysts, followed by reductive treatment in the furnace, unless other methods were specified. The entire bimetallic and monometallic catalysts were prepared using the recently reported modified impregnation method[3,4].

The typical catalyst synthesis procedure consisted of charging the required amount of precursor solutions [$HAuCl_4.3H_2O$ (Sigma Aldrich) with concentration of 8.9 mg/mL, $PdCl_2$ (Sigma Aldrich) with a Pd concentration of 6 mg/mL dissolved in 0.58 M HCl, $RuCl_3$ (Sigma Aldrich) with a Ru concentration of 6 mg/mL] wt. ((1:1) by weight) into a clean 50 ml round bottomed flask (RBF) fitted with a magnetic stirrer.

The solution volume was adjusted to a total volume of 16 ml using deionised water. This RBF was then submerged into a controlled temperature silicone oil bath using a hot plate stirrer 800 rpm at 30 °C. The temperature of the oil bath was raised from 30 °C to 60 °C over a period of 10 minutes. The required amount of support (TiO_2 (Degussa Evonik P25), CeO_2 with a particle size < 5 µm, Sigma Aldrich), active carbon (G-60) (Sigma Aldrich), Magnesium (II) oxide (MgO), and aluminium oxide (Al_2O_3) was then gradually added with homogeneous stirring at 60 °C over a period of 8-10 minutes.

Once the entire amount of support had been added, the slurry was stirred at 60 °C for another 15 minutes. The oil bath was then heated to 95 °C, and the slurry was stirred for a further 16 hours to evaporate the water, resulting in a dry solid powder. The solid powder was collected and ground thoroughly using a mortar and pestle to

form a uniform mixture. The ground catalyst was transferred and spread out over a glass calcination boat. The dried material was further subjected to high-temperature reduction treatment at 450 °C by passing a dilute gas mixture of 5 % H_2 in Ar under constant flow and a heating rate of 2 K/minute for 4 hours. Catalysts were prepared with a total of 1 wt. % with a 1:1 weight ratio of the two metals on a 2 g scale at room temperature. Pre-prepared catalysts using this process were labelled as M_{Im}. The reduction process was performed using a furnace under a steady flow of 5% H_2 in Ar. This was true for all catalysts except mono PdHx and bimetallic PdHx-M (M=Au, Ru, Ni, Fe and Cu) support catalysts, which were reduced by $NaBH_4$. NaOH solution was added dropwise to the mixture of dried powder with 10 mL of deionized water until the pH value reached 12. Stirring of the alkaline solution in an ultrasound bath continued for 20 minutes, and then 2 mL (19.3 g/l) $NaBH_4$ aqueous solution (10 equiv. to $PdCl_2$) was added dropwise to reduce the release of gas. Stirring in the ultrasound bath continued for another 30 minutes after adding $NaBH_4$. To ensure complete reduction of Pd^{2+} cations, the mixture was filtered and washed with deionized water three times. The wet powders were dried in an oven at 80 °C for a period of 12 hours in the final step[5,6].

2.2.3. Catalysts preparation

2.2.3.1. Preparation of Pd/support

Various Pd/X catalysts (X= (TiO_2 (Degussa Evonik P25), CeO_2 of particle size < 5 µm, Sigma Aldrich), active carbon (G-60) (Sigma Aldrich), Magnesium (II) oxide (MgO), and gamma aluminium oxide (Al_2O_3)) were prepared using a modified impregnation method. The synthesis procedure for obtaining 1 g of Pd/support followed the methodology previously reported by Sankar et al.[3]. The specific catalyst was prepared by dissolving the required amount of $PdCl_2$ (Sigma Aldrich) with a Pd concentration of 6 mg/mL in 0.58 M HCl, and then adding it to deionized water. The solution was mixed with the appropriate amount of support (MgO, CeO_2, active carbon (G-60), TiO_2, Al_2O_3) under continuous stirring at 60 °C. After adding all the support, the mixture was heated at 95 °C to facilitate water evaporation. The resulting dry material underwent high-temperature treatment through gas-phase reduction using a 5 % diluted stream of H_2 at 450 °C, with a heating rate of 2 K/minute for 4 hours. These catalysts were designated as Pd/Al_2O_3.

2.2.3.2. Preparation of PdH/support

These catalysts, designated as PdH/Al_2O_3, were prepared using the modified impregnation method following the procedure outlined in Section 2.2.2, with one exception: the treatment step. Instead of the previous treatment, the dried material

underwent reduction using $NaBH_4$ aqueous solution. Subsequently, the mixture was filtered and washed with deionized water three times. Finally, the wet powders were dried in an oven at 80 °C for 12 hours to obtain the PdH/Al_2O_3 catalysts.

2.2.3.3. Preparation of Pd-Au/support on TiO_2 or Al_2O_3

Bimetallic Pd-X catalysts were also prepared using the modified impregnation method. The total metal loadings of the Pd-X catalysts varied, with two specific ratios used: 2.5:2.5 and 1:1.

Pd-Au catalysts supported on TiO_2 (Degussa Evonik P25) and gamma aluminium oxide (Al_2O_3) were synthesized using the modified impregnation method. The dried material was subsequently subjected to high-temperature treatment with gas phase reduction under a 5 % diluted stream of H_2 at 450 °C, employing a heating rate of 2 K/minute for 4 hours[4,7]. The bimetallic catalysts containing Pd and Au were designated as 2.5%Pd-2.5%Au/TiO_2 and 2.5%Pd-2.5%Au/Al_2O_3, respectively.

2.2.3.4. Preparation of Pd-XH/Al_2O_3 (where X = Au, Ru, Cu, Fe and Ni)

Bimetallic catalysts, identified as Pd-X, were synthesized by employing a refined impregnation approach. The proportion of metal constituents within the Pd-X catalysts varied. For each bimetallic compound, the metal ratios were configured at 2.5:2.5, with the exception of the Pd-Ru variant. This specific catalyst used three different metal configurations: 0.5:0.5, 2.5:2.5, and 1:1.

The Pd-X catalysts, underpinned by gamma-aluminium oxide (Al_2O_3), were generated using the adapted impregnation technique. Following a drying process, the compound was reduced using a sodium borohydride ($NaBH_4$) aqueous solution. Different bimetallic catalysts that include Pd and X elements were labelled accordingly: 2.5%Pd-2.5%AuH/TiO_2, 2.5%Pd-2.5%AuH/Al_2O_3, 2.5%Pd-2.5%RuH/Al_2O_3, 2.5%Pd-2.5%FeH/Al_2O_3, 2.5%Pd-2.5%CuH/Al_2O_3 and 2.5%Pd-2.5%NiH/Al_2O_3, respectively.

2.3. Catalyst testing

The reaction was conducted using the Radleys reactor, which was equipped with a magnetic stirrer (refer to **Figure 2.1**). The flow of gas and pressure were regulated using a press flow gas controller. The catalyst weight used for the reactions varied between 30mg and 40mg. Isopropyl alcohol (IPA), toluene, hexane, and water were employed as solvents, with a total volume of 5 ml. The system was adjusted to the desired temperature and pressure, with the reaction temperature ranging from 30 °C to 50 °C, and a constant hydrogen pressure of 1 bar maintained for all reactions. The stirrer was set at 1000 rpm. Conversion and selectivity were determined by analysing

the data obtained from GC analysis, with mesitylene serving as an internal standard for calculation purposes.

Figure 2.1: Catalyst testing using a Radleys reactor.

2.3.1. Phenol hydrogenation

The hydrogenation of phenol served as the model reaction (refer to **Scheme 2.1**) for the catalyst evaluation process. The procedure was carried out in a 50 mL Radleys reactor (detailed in **Figure 2.1**). Initially, the reactor was filled with a total of 5 mL solution, made up of 0.2 mmol of phenol, dissolved in water to yield a 0.1 M concentration. Subsequently, roughly 40 mg (7 mmol) of the catalyst was introduced into the reactor.

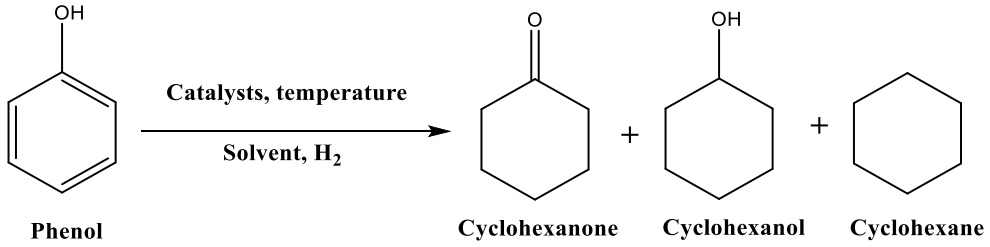

Scheme 2.1: phenol hydrogenation.

The Radleys glass reactor was subsequently sealed, followed by purging with hydrogen gas thrice, before its pressurization to 1 bar using hydrogen. This pressure was maintained throughout the experiment, with a constant supply of hydrogen to compensate for the consumption during the reaction. The standard reaction temperature was set at 50 °C, and the solution was persistently agitated using a magnetic stirrer at a speed of 1000 rpm.

Upon the reaction's completion, the reactor was cooled using an ice bath for a duration of 10 minutes, followed by separation of the reaction mixture and the solid catalyst via centrifugation. For analytical purposes, 1 mL of the reaction mixture was combined with 0.1 mL of 2-propanol (an external standard). A gas chromatographic (GC) method was utilized for the data analysis. In this reaction, both 5 wt. % of PdH/Al_2O_3 and RuH/Al_2O_3 monometallic catalysts were employed. Furthermore, bimetallic catalysts consisting of 1:1 5 wt. % of $2.5\%Au\text{-}2.5\%PdH/Al_2O_3$, $2.5\%Ru\text{-}2.5\%PdH/Al_2O_3$, $2.5\%Cu\text{-}2.5\%PdH/Al_2O_3$, $2.5\%Ni\text{-}2.5\%PdH/Al_2O_3$ and $2.5\%Fe\text{-}2.5\%PdH/Al_2O_3$ were also incorporated in this procedure.

2.3.2. N-Alkylation of phenol with p-toluidine

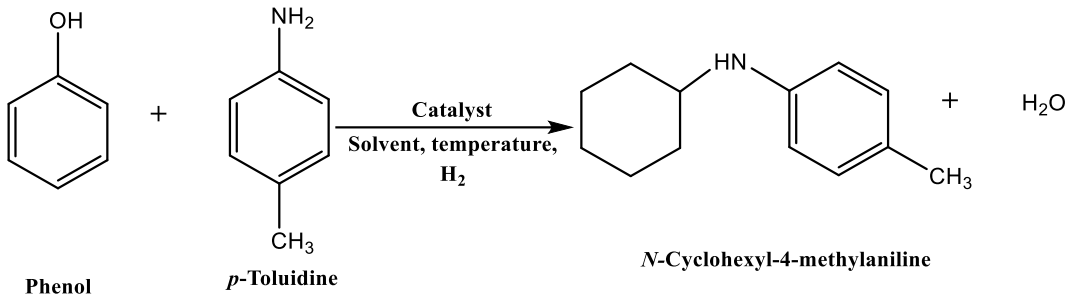

Scheme 2.2: N-alkylation of ρ-toluidine with phenol.

In this process, the model reaction used was the N-alkylation of p-toluidine with phenol (as illustrated in **Scheme 2.2**). Both phenol (0.2 mmol, 18.8 mg) and p-toluidine (0.4 mmol, 42.8 mg) were introduced into a Radleys reactor (see **Figure 2.1**), equipped with a stirrer operating at a speed of 1000 rpm. Pd supported catalysts (5 % mol, 40 mg) were incorporated into the mix, followed by the addition of 2 ml of solvent. This mixture was heated to the desired temperature of 50 °C, using an oil bath under a 1 bar H_2 atmosphere. When utilizing the catalytic transfer hydrogenation (CTH) pathway for hydrogenation reactions, hydrogen was substituted with nitrogen. The resultant products were purified by Thin Layer Chromatography (TLC) and identified through Gas Chromatography-Mass Spectrometry (GC-MS) and both 1H and 13C Nuclear Magnetic Resonance (NMR) spectrometry. Conversions and yields of products were evaluated using a gas chromatograph (Agilent Technologies 7820A), fitted with a CP-WAX 57-CB column and a Flame Ionization Detector (FID), with mesitylene serving

as the internal standard. For GC analysis, 1 ml of the reaction mixture was combined with 0.1 ml of an external standard.

Various catalysts were used in this reaction. Monometallic catalysts employed included 10 wt.% of Pd/C and 5%Pd/CeO_2, 5%Pd/MgO, 5%Pd/Al_2O_3, 5%Pd/TiO_2, 5%Pd/C, 5%PdH/Al_2O_3 and 5%PdH/TiO_2). In addition, toluene functioned as the solvent, while hexane and ethyl acetate were used for silica gel of 230-400 mesh size in column chromatography. The gas mixtures used were He-N_2-H_2, and the external standard for GC analysis was mesitylene. Apart from the monometallic catalysts, bimetallic catalysts in a 1:1 ratio such as 2.5%Au-2.5%Pd/TiO_2, 2.5%Au-2.5%Pd/Al_2O_3, 2.5%Au-2.5%PdH/TiO_2 and 2.5%Au-2.5%PdH/Al_2O_3 were also utilised in this reaction.

2.3.3. Auto transfer reaction benzyl alcohol with nitrobenzene

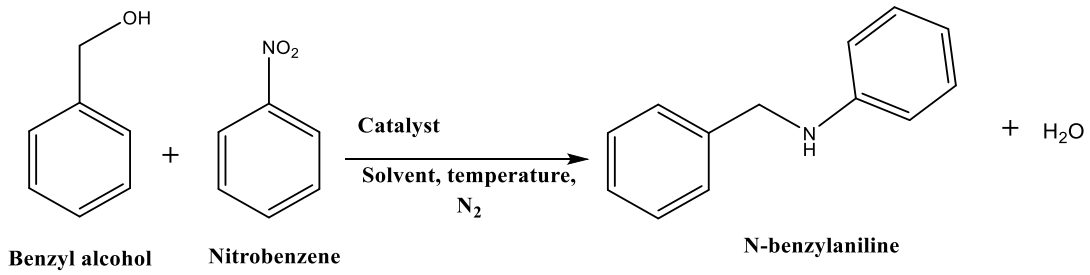

Scheme 2.3: HAT reaction of benzyl alcohol with nitrobenzene.

Direct synthesis of amines and imines from nitrobenzene and benzyl alcohol (**Scheme 2.3**), The hydrogen auto-transfer reactions were conducted either in a stainless steel high-pressure tinyclave reactor (Buchi AG) fitted with a stirrer operating at a speed of 1000 rpm (**Figure 2.2**) or in a Radleys reactor (**Figure 2.1**). In a typical reaction, the reactor was charged with the appropriate quantities of all compounds, including Benzyl alcohol [Sigma Aldrich, 99-100.5 %] (4.866 g), nitrobenzene [Sigma Aldrich, ACS reagent, 99.0 %] (0.56 g), catalyst (30 mg), and mesitylene [Sigma Aldrich, 98 %] (5 ml). The reactor was then purged three times with 1 bar of N_2 before being sealed with 1 bar of He or N_2. The reaction was initiated when the temperature of the reaction mixture reached the specified value (120 °C). The reaction time ranged from 30 minutes to 3 hours. At the end of the reaction, the reaction vessel was cooled using an ice bath to approximately 10 °C, and the pressure was released through the exhaust system. The reaction mixture was subsequently pipetted out and filtered using filter paper, and the catalyst was washed multiple times with acetone. The reaction mixture was analysed using a gas chromatograph (GC) (Agilent Technologies 7820A) equipped with a CP-WAX 57-CB column and an FID detector.

Approximately 1 ml of the reaction mixture was mixed with 0.1 ml of an external standard (n-dodecane) and injected into the GC.

For the preparation of monometallic catalysts, 5 wt. % of PdH/Al_2O_3 and 5 wt. % of RuH/Al_2O_3 were utilized. Additionally, bimetallic catalysts with a 1:1 weight ratio were used, including 5wt.% of 2.5%Au-2.5%PdH/Al_2O_3, 2.5%Ru-2.5%PdH/Al_2O_3, 2.5%Cu-2.5%PdH/Al_2O_3, 2.5%Ni-2.5%PdH/Al_2O_3 and 2.5%Fe-2.5%PdH/Al_2O_3. Furthermore, bimetallic catalysts with a 1:1 weight ratio, such as 1wt.% of 0.5%Au-0.5%Pd/TiO_2, 0.5%Ru-0.5%Pd/TiO_2, 0.5%Ru-0.5%Pd/Mo2C, 0.5%Ru-0.5%Pd/CeO_2, 0.5%Au-0.5%Pd/CeO_2, and bimetallic catalyst Ru-$PdHAl_2O_3$, were employed with varying loadings (5wt.%, 1wt.%, 0.5wt.%, and 0.2wt.%).

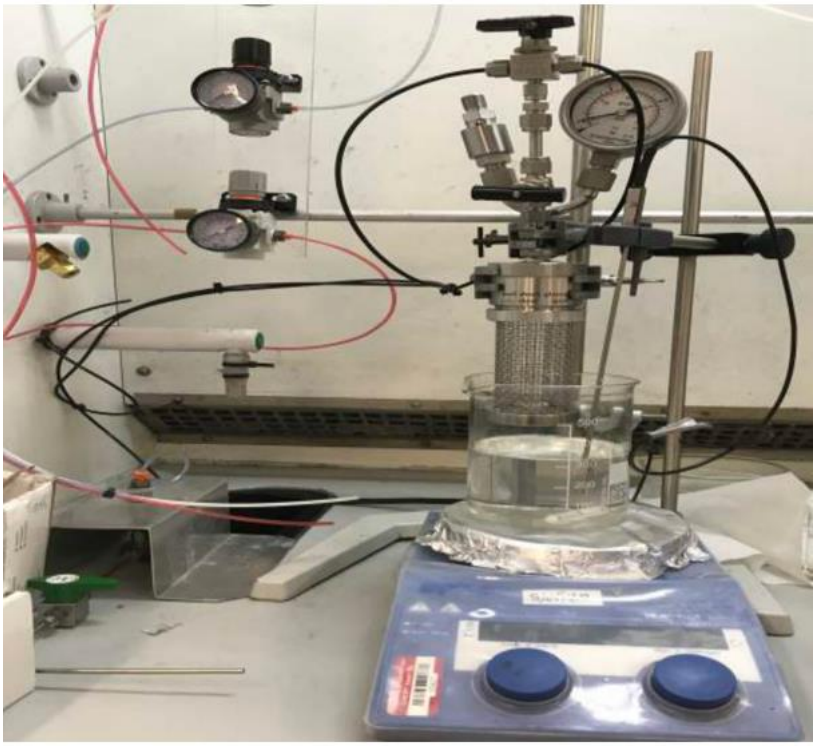

Figure 2.2: Catalyst testing using a Buchi reactor.

2.4. Quantitative and Qualitative Analysis

For both quantitative and qualitative evaluations of the reaction mixtures, techniques such as Gas Chromatography (GC), Gas Chromatography-Mass Spectrometry (GC-MS), and Nuclear Magnetic Resonance (NMR) spectrometry were utilised. Detailed descriptions of these methodologies are provided in this section.

2.4.1. Gas chromatography (GC)

Chromatographic methods are extensively utilised to separate liquid mixtures into their individual components. The fundamental principle of this technique involves contacting a liquid sample with a solid, or stationary phase. Subsequently, a mobile phase, either gas or liquid, is introduced to elute the sample along the stationary

phase. This allows the mixture to be separated due to differing levels of interaction (both physical and chemical) between the sample components and the stationary phase.

Gas Chromatography (GC) is an analytical procedure that requires the sample to be vaporized at high temperatures prior to its injection into a capillary column housed within an oven. This ensures that the vaporized species are retained in the gaseous phase. Often, a temperature gradient is used to promote the separation of compounds based on their respective boiling points. The vapours are transported through the column, and the resulting outputs at the column's end are analysed by a Flame Ionization Detector (FID) (refer to **Figure 2.3**).

The FID operates by combusting the eluted organic molecules in a hydrogen flame, resulting in ion formation. These ions are detected by a set of electrodes, and the signal generated is directly proportional to the number of ions formed and detected. Consequently, this facilitates the extraction of quantitative results upon calibration of the instrument. Although this technique is particularly effective for detecting and quantifying volatile hydrocarbons, it is not applicable for the study of inorganic molecules.

For this study, an Agilent Technologies 7820A GC system equipped with a CP-wax52 column (capillary column, 25 m, 0.35 mm ID, 0.2 microns) was used, coupled with a FID detector. The system utilized helium as the carrier gas. The data analysis was performed using the flame ionization detector.

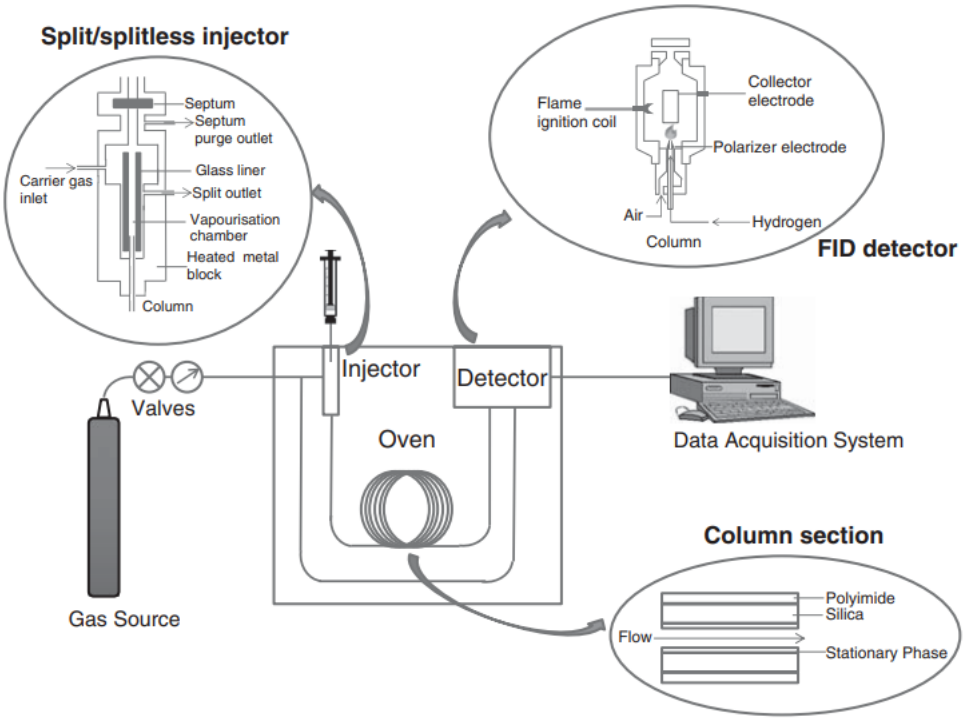

Figure 2.3: Scheme of a GC-FID equipment. Reproduced from ref.[8].

The sample, with a volume of 0.2 µL, was injected at a temperature of 300 °C into a split ratio of 10:1, with an average column velo city of 5.92 cm/sec, using helium as the carrier gas. Initially, the oven temperature was maintained at 50 °C for a duration of 2 minutes. Subsequently, the temperature was programmed to increase at a rate of 10 °C/minute until it reached 220 °C, which was then held for 5 minutes. Finally, the analysis was completed by ramping the temperature up to 250 °C at a rate of 75 °C/minute, and this final temperature was maintained for 2 minutes. (Refer to **Figure 2.4** for the phenol hydrogenation setup.)

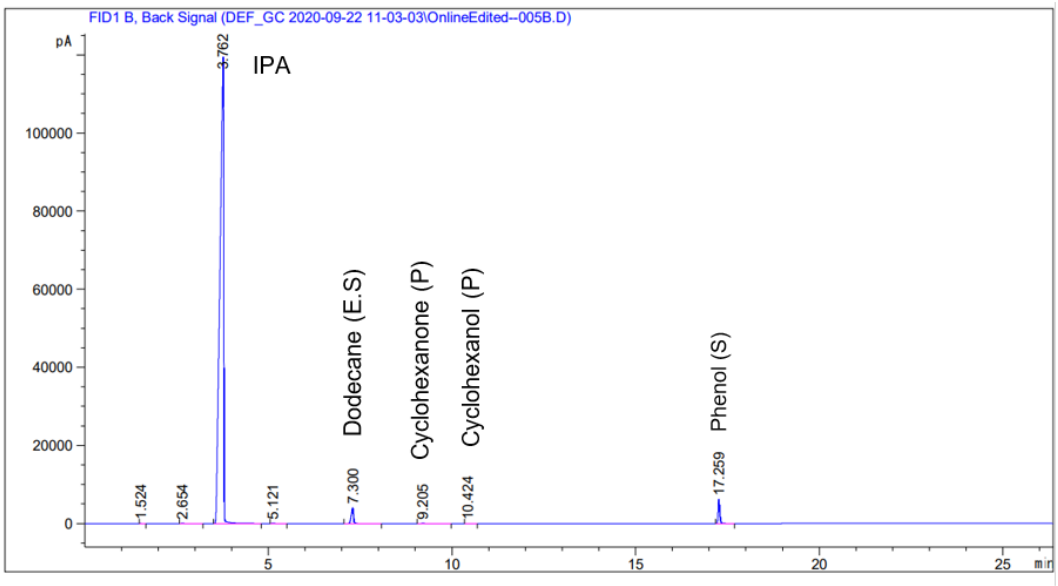

Figure 2.4: Gas chromatogram of the product of a typical phenol hydrogenation (where, S = Substrate, P = Product and E.S. = External Standard).

Phenol conversion was quantified as the percentage of phenol moles converted relative to the initial quantity of phenol moles. On the other hand, selectivity was determined as the percentage of cyclohexanol moles compared to the moles of hydrogenated products. Conversion, selectivity and carbon balance were calculated using the following **equations(2.1, 2.2 and 2.3):**

$$Conversion\ of\ R\% = \frac{[R]_o - [R]_{o1}}{[R]_o}\ x100 \quad \textbf{Equation 2.1}$$

Where, R is the reactant, $[R]_o$ is the initial concentration of reactant, and $[R]_{o1}$ is the final concentration of reactant determined by GC analysis.

$$Selectivity\ to\ o\ P_i\% = \frac{[P]_i}{[P]_o}\ x\ 100. \quad \textbf{Equation 2.2}$$

Where, P is the product, $[P]_i$ is the concentration of P_i which can be determined through GC analysis, $[P]_o$ is the total concentration of all products determined by GC.

$$SCarbon\ balance\ \% = \frac{[C]_i}{[C]_o}\ x\ 100. \quad \textbf{Equation 2.3}$$

Where, $[C]_o$ is the carbon concentration of reactants, and $[C]_1$ is the carbon concentration of residual reactants and products measured by GC.

Each experiment was repeated at least twice to ensure satisfactory reproducibility. The error margin for phenol conversion was typically around ± 4%. Carbon balance was consistently within the range of 100 ± 5%.

The catalytic hydrogenation of phenol was monitored using GC, and the disappearance of the substrate and formation of products were quantified using an external calibration method. To create the calibration curve, five aqueous solutions of each known compound with known concentrations were prepared and mixed with a known mass of dodecane (used as an external standard). These solutions were then injected into the GC, and the peak areas were normalized to the area of the standard to construct the calibration plot. An example of the calibration curve for phenol is provided below **Figure 2.5**.

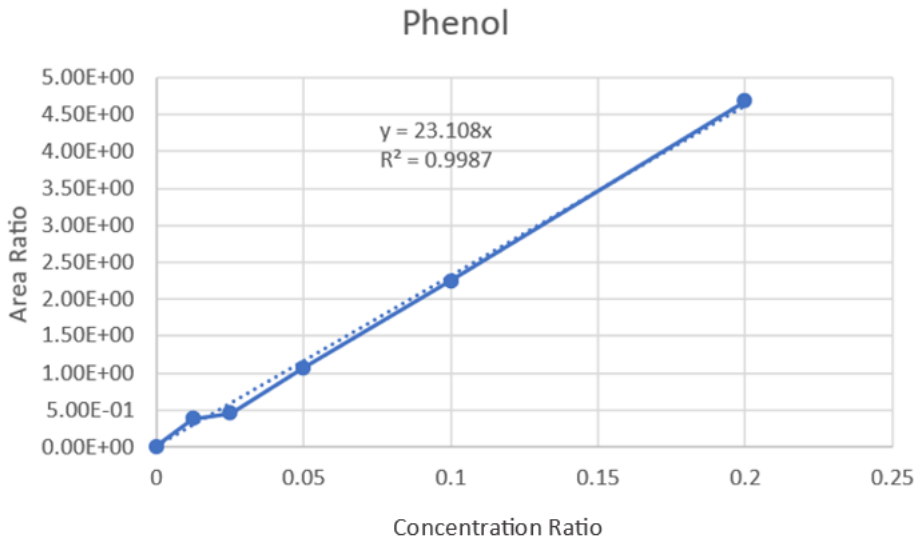

Figure 2.5: Calibration curve of phenol at different concentrations.

The slope of the calibration curve is referred to as the response factor, and it can be utilised to quantify a known compound in a post-reaction solution. Response factors for all the reaction components were determined using the same method, and they are presented in **Table 2.3** Specifically, the response factors for phenol, cyclohexanone, and cyclohexanol were found to be 23.11, 19.45, and 22.51, respectively.

Table 2.3: Response factor of phenol, cyclohexanone and cyclohexanol:

Chemicals	Response factor
Phenol	23.11
Cyclohexanone	19.45
Cyclohexanol	22.51

2.4.2. Gas chromatography-mass spectrometry (GC-MS)

Gas Chromatography-Mass Spectrometry (GC-MS) is a widely used method for identifying compounds within a reaction mixture. It delivers quantitative information concerning the quantity and chemical structure of the compounds under analysis. GC-MS is a versatile analytical instrument, with numerous applications in the chemical industry. It comprises a gas chromatograph, an interface, a mass spectrometer, and an interconnected data-control system. By integrating these elements, GC-MS can separate mixtures into their individual components and provide both qualitative and quantitative characterizations based on their volume and chemical structure. The analytical process begins with the injection of a volatile sample into a heated inlet port, where it is vaporized and transported through the column by a mobile phase, typically helium. The analytes within the sample interact with the stationary phase in the column, effecting their separation. As these separated compounds exit the column, they undergo ionization, usually via electron ionization in the case of the GCT Premier system, within the mass spectrometer source under vacuum conditions. The resultant ion beam is then directed through a Time of Flight (TOF) tube, where ions are segregated based on their mass-to-charge ratio (with lower mass ions moving faster than higher mass ions). Ultimately, the ion beam reaches a detector (mass analyser), where mass spectra are generated[9]. All GC-MS analyses were carried out and scrutinized by Dr. Simon Waller at Cardiff University's GC-MS facility. The system employed for this study was a Walters GCT Premier connected to a HP 6890N mass spectrometer, specifically for the identification of phenol hydrogenation products[10].

2.4.3. Nuclear magnetic resonance spectroscopy (NMR)

NMR is one of the most commonly used techniques in analytical chemistry and is a form of spectroscopy. This technique provides valuable insights into the physical, chemical, and biological properties of compounds. NMR is particularly useful for samples containing nuclei with spin. It is sensitive to specific isotopes of elements

based on the differences in nuclear spins.[11]. In organic chemistry, the chemical environment of ^{1}H and ^{13}C nuclei is of great interest as it provides valuable information for deducing the structures of organic compounds. NMR spectroscopy can be employed to analyse molecular conformation in solution and investigate physical features at the molecular level, such as solubility and conformational exchange. For this experiment, a Bruker 500 MHz NMR instrument with version 3.2 TopSpin software was used to record the ^{1}H NMR spectra. The results were reported in ppm along with the corresponding number of protons, multiplicity, and assignment. The chemical shifts within the ^{1}H NMR spectrum were measured in deuterated chloroform ($CDCl_3$). In order to determine the structure of N-cyclohexyl-4-methylaniline, which was formed through the N-alkylation of ρ-toluidine with phenol, NMR spectroscopy was employed (discussed in Chapter Five).

2.4.4. X-ray powder diffraction (XRD)

XRD is a commonly utilized analytical method for identifying the bulk phase of crystalline materials and the dimensions of their unit cells. [12]. When a concentrated X-ray beam encounters a crystalline sample, it scatters, resulting in constructive interference when the dispersed X-rays align in phase with each other (see **Figure 2.6**). This phenomenon leads to the creation of a diffraction pattern.

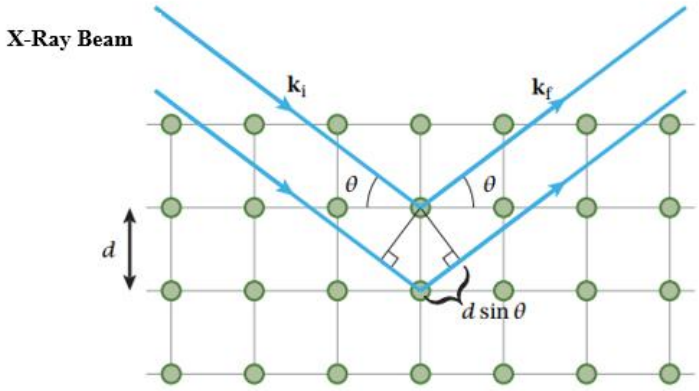

Figure 2.6: X-ray interaction with a crystalline surface. Reproduced from ref.[13].

The distances between planes can be calculated using Bragg's **equation 2.4**:

$$n\lambda = 2dsin\theta \qquad \textbf{Equation 2.4}$$

In this context, n represents an integer, λ denotes the X-ray's wavelength, d refers to the distance between two lattice planes, and θ symbolizes the diffraction angle.

The XRD pattern of a pure powder sample effectively serves as a fingerprint of the material's morphology, with each substance presenting a unique diffraction pattern. As depicted in **Figure 2.7**, the X-ray equipment comprises an X-ray source, a rotating sample stage, and a detector that collects diffracted X-rays.

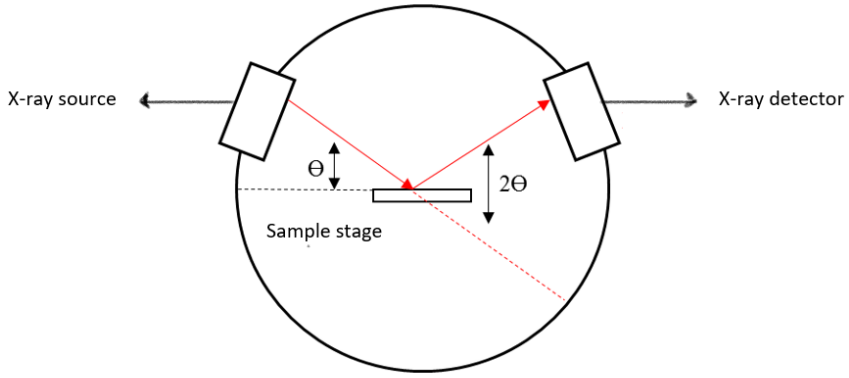

Figure 2.7: Basic setup of a X-ray diffractometer. Reproduced from ref.[14].

In order to achieve a satisfactory response that complies with Bragg's law, the production and utilisation of monochromatic X-ray beams are required. The use of target materials is advantageous for generating such beams. Copper is the most commonly used target material for single-crystal diffraction, providing Cu Kα radiation with a wavelength of 1.5418 Å. By varying the incident angle of the X-ray beam while keeping the wavelength constant, a range of diffracted rays can be detected, measured, and processed to obtain a diffractogram. The diffraction peaks can be converted into d-spacing values, allowing for the identification of the crystal and elemental structure by comparing these values with standard reference patterns. Various data can be extracted through XRD analysis. The composition, purity, crystalline structure, and unit cell dimensions of a powder sample can be determined by comparing the diffractogram with reference standards and literature data. Additionally, the average particle size (L) of crystallites can be estimated based on the diffraction line broadening (β) corresponding to the diffraction angle (θ) using constant wavelength radiation (λ), as per the Scherrer equation (**Equation 2.5**)[15,16]. Please note that long-range crystal order is essential to generate diffraction signals. Hence, nanoparticles can be challenging to detect if their size is less than approximately 5 nm.

$$L = \frac{K\lambda}{\beta cos\theta} \quad \textbf{Equation 2.5}$$

Where K is the constant, typically close to unity, λ is the radiation wavelength, β is the full width at half maximum of the reflection, and θ is the diffraction angle of the line maximum. The XRD analysis was performed using a PANalytical X'Pert PRO MPD instrument equipped with a Cu Kα X-ray source. The catalyst sample (0.5 g) was powdered, placed on a sample disc, and flattened. The discs were then inserted into the XRD apparatus after being placed on a sample holder. A typical scan was conducted in the range of diffraction angle (2θ) from 10° to 80° with a step size of 0.02°. The XRD measurements were performed at a voltage of 40 kV and a current of 40 m A, using an X'Celerator detector. The obtained XRD patterns were analysed by comparing them to the patterns available in the JCPDS database. The XRD analytical technique was used to determine the crystalline phase of various substances, including Al_2O_3 , 5%PdH/Al_2O_3, 5%Pd/Al_2O_3, 5%PdH/TiO_2, 2.5%Pd-2.5%AuH/Al_2O_3, 2.5%Pd-2.5%Au/Al_2O_3, 2.5%Pd-2.5%RuH/Al_2O_3 and 0.5%Pd-0.5%RuH/Al_2O_3, as further explained in detail in chapter three.

2.4.5. Brunauer Emmett Teller (BET) surface area analysis

The Brunauer Emmett Teller (BET) method[17] is the most commonly adopted technique for determining the surface area of finely ground and porous substances. The surface areas of the samples, as assessed by the BET technique, were measured using a Quadrasorb Automated Surface Area & Pore Size Analyzer. The underlying principle of this approach is encapsulated in the BET equation (**Equation 2.6**).

$$\frac{p}{v(p_o-p)} = \frac{1}{v_m c} + \frac{(c-1)}{v_m c p_0} \quad \textbf{Equation 2.6}$$

C = BET constant

V = Volume of the adsorbed gas

V_m = Volume of the monolayer of adsorbed gas

P = Equilibrium pressure

P^o = Saturation pressure of adsorbates at the temperature of adsorption.

The relationship obtained from the $\frac{p}{v(p_o-p)}$ with $^{p}/_{p_o}$ should be a straight line, where $1/v_m c$ is the intercept and the slope is $\frac{(c-1)}{v_m c}$. The sample surface area can be determined using **equation 2.7**:

$$S = (V_m).(N_a).(A) \quad \textbf{Equation 2.7}$$

Where, S is the specific surface area, Na is the Avogadro's number and A is the cross sectional area of adsorbent gas.

The basic BET (Brunauer-Emmett-Teller) approach is used to estimate or determine the surface area of a gas-adsorbed surface based on the amount of gas adsorbed. In BET surface area estimation, N_2 gas is commonly used as the adsorptive gas at a constant temperature (77 K). The total amount of gas adsorbed at a specific pressure is used to calculate the amount of gas molecules required to form a monolayer on the sample's surface. The surface area can then be determined based on the size of the adsorbed N_2 molecules. For nitrogen physisorption analysis, a Micromeritics Gemini 2360 analyser was used. Approximately 0.1 g of catalyst samples was placed in a sample tube, which was then degassed for 50 minutes at 120 °C to remove moisture and other surface contaminants. After the tube had cooled to ambient temperature, it was connected in parallel to an empty reference tube and both tubes were immersed in liquid nitrogen in a Dewar. The configuration was first run without a sample, followed by a run with the material for nitrogen physisorption analysis using liquid nitrogen (-196 °C) as the gas intake.

A five-point analysis was typically employed to determine the surface area, and the BET equation was used to compute the surface area. The BET analysis was performed to determine the surface area of fresh and reduced nanoparticles of 5%P/Al_2O_3 and 2.5%Pd-2.5%Au/Al_2O_3, as further discussed in chapter three.

2.4.6. Scanning electron microscopy (SEM)

SEM techniques involve the use of an electron microscope, which uses electrons instead of light to generate high-magnification, three-dimensional images. In comparison to optical microscopy, SEM provides a greater depth of focus for the images. **Figure 2.8** shows the typical SEM, where an electron beam is generated by an electron gun. The beam passes through the microscope column, guided by electromagnetic lenses that focus and direct it towards the sample. When the electron beam interacts with the sample, two types of electrons are generated: secondary electrons and backscattered electrons. Secondary electrons are produced when the high-energy electron beam displaces loosely held surface electrons. These secondary electrons are detected using a secondary electron detector to generate an image of the sample's surface.

The detection of secondary electrons is based on the surface area at the specific intersection point of the electron beam, making it relevant for topographic features. On the other hand, backscattered electrons are high-energy electrons that are

scattered back out of the sample by the atomic nuclei. The intensity of the backscattered signal depends on the atomic number of the area of interaction. The backscattered electron image displays contrast in chemical composition, providing information about the surface topography and average atomic number in the scanned area. Both secondary and backscattered electrons are collected by a detector, which converts them into a signal and sends it to a viewing screen to create the sample image[18,19].

For this study, the analysis was conducted using a Tescan MAIA3 field emission gun scanning electron microscope (FEG-SEM) operating at 15 kV. The backscattered electron detector was used to acquire images. The samples were dispersed as powder onto 300 mesh copper grids coated with a holey carbon film. The SEM techniques revealed a better dispersion of the Pd phase and the alloyed phase in the 5%PdH/Al_2O_3 sample as well as a better dispersion of the Pd phase and the Au-Pd alloy phase in the 2.5%Pd-2.5%AuH/Al_2O_3 sample (Chapter three).

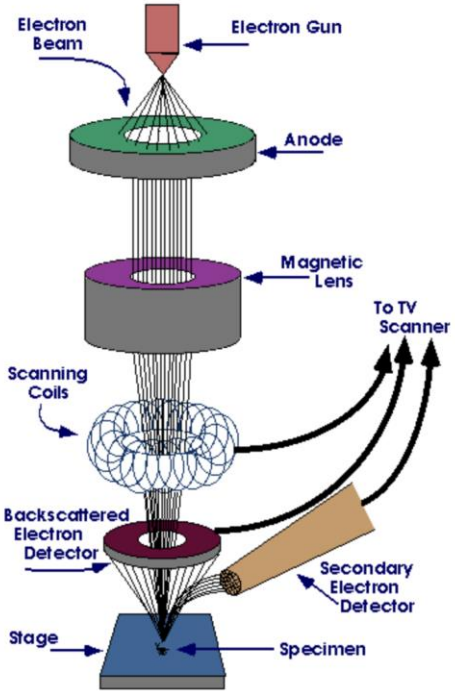

Figure 2.8: Schematic diagram of SEM. Reproduced from ref.[20].

2.4.7. Transmission Electron Microscopy (TEM)

Transmission Electron Microscopy (TEM), depicted in **Figure 2.9**, is an advanced imaging technique that utilizes both transmitted and diffracted electrons. Bright field images, which are two-dimensional projections of the transmitted electrons, depend on the distribution of mass, the density of the sample, and its thickness.

Contrastingly, dark field images depict diffracted electrons that are slightly angled differently from the electrons in the transmitted beam. The differential images generated are due to the attenuation of the electron beam, a function of the density and thickness of the sample, and also due to diffraction and interference phenomena. Compared to Scanning Electron Microscopy (SEM), TEM offers superior magnification and resolution capabilities, making it invaluable in catalysis to determine particle dispersion, size, morphology, and to study interactions between metal and support[21].

In this work, TEM and Scanning Transmission Electron Microscopy (STEM) were performed utilizing a JEOL JEM-2100 microscope, as shown in **Figure 2.10**, operating at 200 kV. Energy dispersive X-ray analysis (EDX) was conducted using an Oxford Instruments XMax^N 80 detector. The ImageJ software package was employed to analyse the collected data. Sample preparation involved dispersion in ethanol via sonication, followed by deposition on 300 mesh copper grids coated with a holey carbon film.

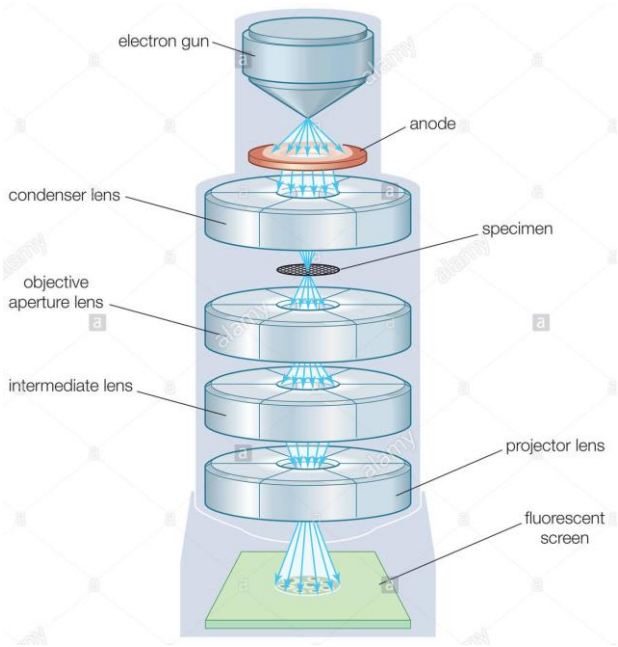

Figure 2.9: Schematic representation of the electron beam detector used in TEM. Reproduced from ref.[22].

Figure 2.10: JEOL JEM2100 TEM**.**

2.4.8. Inductively coupled plasma mass spectrometry (ICP-MS)

ICP-MS is an extremely effective technique for determining metal concentrations in a solution, and it is also highly sensitive to a variety of elements. The ionization process is summarized as follows: specimen introduction, ICP torch, interfaces, and mass spectrometry. Curves resulting from linear calibrations can be observed across multiple orders of intensity[23]. The ICP-MS analysis was conducted by Dr. Simon Waller at Cardiff University's ICP-MS service using the Agilent 7900 ICP-MS instrument. The torch used was made of quartz, and the plasma was generated by a combination of the RF coil and argon gas. This resulted in the formation of a superheated gas or plasma consisting of free electrons and ions. When the sample entered the plasma through the nebulizer and spray chamber, it was dried, and any molecules present were desiccated. As a result, the electrons were removed, forming ions that could be detected by a mass analyser. Argon gas was used for the plasma, while helium was utilized in the collision/reaction cell. The RF coil wrapped around the torch initiated and maintained the plasma.

ICP-MS is known for its high speed, precision, and sensitivity, and it is a sequential technique used for analysing multiple elements, unlike atomic absorption techniques. The calibration was performed from 0 PPM to 1 PPM with five calibration points.

The standards used for calibration match the matrix of the samples. If the samples are diluted, the matrix is also diluted consistently. To calculate the metal loading based on the ICP data, 250 mg of the M sample was digested in an aqua regia mixture (three parts HCl and one part HNO_3) and diluted to a total volume of 25 ml. After the ICP-MS analysis, the result for M is given in ppm (n ppm). The dilution factor can be calculated as the volume makeup in ml divided by the weight of the sample. The actual

concentration of the M sample can then be determined by multiplying the ICP-MS result (n ppm) with the dilution factor, resulting in ppm.

2.4.9. X-ray photoelectron spectroscopy (XPS)

XPS (X-ray photoelectron spectroscopy) is a widely utilized surface-sensitive technique in catalytic research for determining the elemental composition, elemental oxidation state, and metal dispersion[24]. Additionally, it can be utilised to investigate the dispersion of supported catalysts[25]. This technique is based on the photoelectronic effect. When X-ray photons (E = hυ) collide with the sample, they interact with the inner shell electrons whereby an atom absorbs an energy photon (hυ) and ejects a photoelectron with a kinetic energy specified by Einstein's equation (**Equation 2.8**):

$$Ek = h\upsilon - Eb - \varphi \qquad \textbf{Equation 2.8}$$

Where E_k is the kinetic energy of the ejected photoelectron, $h\upsilon$ is the energy of the incident X-ray photon, E_b is the binding energy of the photoelectron with respect to the fermi level, and φ is the work function of the spectrometer.

The kinetic energy determined by XPS is used to calculate the binding energy of the photoelectron, which is unique to each element and its associated orbitals. The binding energy is characteristic of the elemental orbital from which the photoelectron was expelled. It is altered by changes in the initial chemical state of the emitting atom, enabling the extraction of valuable chemical information.

X-ray Photoelectron Spectroscopy (XPS) is a versatile technique, proving highly useful in discerning the oxidation state of an atom, as the binding energy (E_b) of an electron in an atom is influenced by its chemical bonding. Each element boasts unique binding energy values linked to all core atomic orbitals, and the concentration of the element in question is proportional to the intensity of the corresponding peak. The core components of an XPS instrument include an X-ray source, a sample stage, an energy analyser dedicated to photoelectrons, and an electron detector. These elements work in concert to deliver insightful data regarding the elemental composition and chemical state of the materials under investigation. The XPS analysis data presented in this work were obtained by Dr. David Morgan using the Kratos Axis Ultra DLD system. The system utilized a monochromatic Al Kα X-ray source operating at 140 W (see **Figure 2.11**). XPS spectra were collected in the hybrid mode of operation, employing a combination of electrostatic and magnetic

lenses. High-resolution spectra were acquired at a pass energy of 40 eV, while survey spectra were obtained at a pass energy of 160 eV. Charge neutralization was achieved using low-energy electrons, and all spectra were subsequently calibrated to the C (1s) signal of adventitious carbon, assumed to have a binding energy of 284.8 eV. The experimental binding energies are reported with an uncertainty of ±0.2 eV.

Figure 2.11: Kratos Axis Ultra DLD X-ray photoelectron spectrometer used in the current study.

2.5. References

1 H. Alshammari, P. J. Miedziak, D. W. Knight, D. J. Willock and G. J. Hutchings, *Catal. Sci. Technol.*, 2013, **3**, 1531–1539.

2 C. B. Paris, A. G. Howe, R. J. Lewis, D. Hewes, D. J. Morgan, Q. He and J. K. Edwards, *ACS Catal.*, 2022, **12**, 4440–4454.

3 M. Sankar, N. Dimitratos, P. J. Miedziak, P. P. Wells, C. J. Kiely and G. J. Hutchings, *Chem. Soc. Rev.*, 2012, **41**, 8099–8139.

4 M. Sankar, Q. He, M. Morad, J. Pritchard, S. J. Freakley, J. K. Edwards, S. H. Taylor, D. J. Morgan, A. F. Carley, D. W. Knight, C. J. Kiely and G. J. Hutchings, *ACS Nano*, 2012, **6**, 6600–6613.

5 L. Yan, X. X. Liu and Y. Fu, *RSC Adv.*, 2016, **6**, 109702–109705.

6 P. V. Markov, G. O. Bragina, G. N. Baeva, A. V. Rassolov, I. S. Mashkovsky and A. Y. Stakheev, *Kinet. Catal.*, 2018, **59**, 601–609.

7 E. Nowicka and M. Sankar, *J. Zhejiang Univ. Sci. A*, 2018, **19**, 5–20.

8 A. C. Soria, S. Rodríguez-Sánchez, J. Sanz and I. Martínez-Castro, *Food*

Oligosaccharides Prod. Anal. Bioactivity, 2014, **9781118426494**, 370–398.

9 O. D. Sparkman, *J. Am. Soc. Mass Spectrom.*, 2011, **19**, R1–R5.

10 C. N. M. F.G. Kitson, B.S. Larsen, *Gas chromatography and mass spectrometry: a practical guide, Academic Press, 1996*, 1996.

11 H. Frieblin, *WILEY-VCH Verlag GmbH Co. KGaA, Weinheim*.

12 D. Macquarrie, *Appl. Organomet. Chem.*, 2005, **19**, 696–696.

13 P. J. Ray, K. Lefmann and L. Udby, *Master's Thesis, Univ. Copenhagen*.

14 G. Vourlias, *Coatings*, 2020, **10**, 1–14.

15 A. L. Patterson, *Phys. Rev.*, 1939, **56**, 978.

16 U. Holzwarth and N. Gibson, *Nat. Nanotechnol. 2011 69*, 2011, **6**, 534–534.

17 S. Brunauer, P. H. Emmett and E. Teller, *J. Am. Chem. Soc.*, 1938, **60**, 309–319.

18 E. Stach, S. Kim, D. Zakharov, Y. Zvinevich, F. Riberio, L. Miller, R. Colby, N. Salmon and B. Kabius, *Microsc. Microanal.*, 2010, **16**, 294–295.

19 X. Zhou, T. Li, Y. Cui, Y. Fu, Y. Liu and L. Zhu, *ACS Appl. Mater. Interfaces*, 2019, **11**, 1733–1738.

20 C. Temiz and C. Temiz, *Electron Microsc.*, , DOI:10.5772/INTECHOPEN.103956.

21 J. C. Yang, M. W. Small, R. V. Grieshaber and R. G. Nuzzo, *Chem. Soc. Rev.*, 2012, **41**, 8179–8194.

22 B. Shi, *Young Sci. Journal; Canterbury*, 2016, **2009**, 33–35.

23 H. Nasirian, Z. Nasirian and S. M. T. Sadeghi, *Int. J. Entomol. Res.*, 2014, **2**, 47–57.

24 J. W. Niemantsverdriet, *Spectrosc. Catal.*, 2007, I–XVIII.

25 M. H. Engelhard, T. C. Droubay and Y. Du, *Encycl. Spectrosc. Spectrom.*, 2017, 716–724.

Chapter 3: Catalyst characterisation

3.1. Introduction

The catalysts utilized in this study were manufactured using sol-immobilisation and modified impregnation[1], thoroughly detailed in Chapter 2 (Sections 2.2.1 and 2.2.2). Various nanoparticle metal catalysts supported on gamma-alumina, such as 5%Pd/Al_2O_3, 5%PdH/Al_2O_3, 5%Pd/TiO_2, and others are addressed in this chapter. Catalysts developed through modified impregnation and $NaBH_4$ reduction are distinguished with an 'H' in their symbol, like 5%PdH/Al_2O_3. Sol immobilization involves creating a (sol) of the metal precursor and depositing it on a support, enhancing distribution of metal nanoparticles and active site availability. Nonetheless, the metal precursor may not be fully reduced, potentially limiting catalyst activity. This issue can be mitigated with a reducing agent like $NaBH_4$. The reduction of the metal precursor ensures its active, reduced state, enhancing catalytic activity as the metal is already in the required oxidation state. However, challenges in achieving a good metal dispersion on the support can arise if reduction is done before immobilization. This can lead to metal particle agglomeration, reducing the number of active sites and thus catalytic activity. Improved performance of $NaBH_4$ reduced catalysts compared to those where metal is reduced before support addition could be attributed to the balance struck between achieving a reduced active metal phase and maintaining good metal dispersion. A potential mechanism might involve the formation of metal nanoparticles directly on the support post metal precursor immobilization, leading to uniform distribution and high active site count. Conversely, pre-reduction might induce nanoparticle agglomeration, leading to lower dispersion and fewer active sites. In summary, catalyst preparation should balance between a fully reduced, active metal phase and a high dispersion of metal nanoparticles on the support.

Supplementary catalyst characterization, such as TEM for nanoparticle properties, XPS for surface composition, and BET for surface area, provides an enhanced understanding of their influence on catalytic performance, thereby guiding further catalyst synthesis optimization. As discussed in Chapter Three, XPS, TEM, and BET collectively offer comprehensive catalyst analysis. XPS offers crucial insights into the catalyst's surface chemical composition, particularly elemental oxidation states and surface chemistry. This is vital as the catalyst surface houses the catalytic reactions, and alterations in surface chemistry can affect activity and selectivity. TEM delivers morphological and structural data, offering detailed information about nanoparticle size, morphology, dispersion, and crystalline phases of the catalysts, all critical factors influencing catalyst activity and stability. BET analysis determines the catalyst's

specific surface area, a critical parameter because a larger surface area correlates with increased activity due to the availability of more active sites for reaction. In your research, these techniques synergistically provide an in-depth understanding of catalyst structure and composition. XPS details the catalyst's surface's chemical state, revealing any changes that occurred during preparation, such as oxidation. TEM supplements this by presenting the catalyst's physical structure, offering data on particle size and distribution. Finally, BET indicates the collective influence of these factors on the overall surface area, a key determinant of catalytic performance. Without the specific data from these analyses, linking them to catalytic performance becomes challenging. However, these techniques combined can elucidate how the catalyst's structure, morphology, surface chemistry, and surface area might influence its activity and stability. Depending on the findings, the catalyst preparation method can be optimized to enhance its performance. Should discrepancies arise between expected and actual catalyst properties, additional measurements can be conducted using techniques such as X-ray diffraction (XRD) for phase identification, or inductively coupled plasma mass spectrometry (ICP-MS) for elemental analysis. These techniques could offer further insight into the catalyst's structure, composition, and function, aiding in the verification or refinement of hypotheses developed from initial XPS, TEM, and BET analyses.

3.2. Supports

In this study, commercial gamma-alumina Al_2O_3 was used as a support alongside other metal oxide supports (TiO_2, CeO_2, and zeolite Y hydrogen), enabling comparison of their activities to the most used support Al_2O_3[2], a well-established support material, has a competitive edge due to its high specific surface area, uniform pore size distribution, adaptable pore size, and exceptional hydrothermal, thermal, and chemical stability. Widely utilized for its thermal stability and high surface area[3], Al_2O_3 finds prominent applications in dehydrogenation processes such as phenol hydrogenation in catalytic converters. It has demonstrated high activity for complex reactions, including methanethiol synthesis and alcohol dehydration[4,5].

3.2.1. Al_2O_3 support

The gamma-alumina oxide, nano powder trace metal basis Al_2O_3, used in this study sourced from Aldrich. Structural characterization of the commercial Al_2O_3 was conducted via XRD, TEM, and adsorption[6,7] . The primary particle size of Al_2O_3, as procured commercially, is 13 nm (according to TEM) with a surface area ranging from 85 to 115 m^2 / g (as per BET). The XRD patterns of Al_2O_3, depicted in **Figure 3.1**[8] show diffraction peaks at 2θ = 19.5°, 31.9°, 37.6°, 39.5°, 45.9°, 60.9°, and 67.0°.

These correspond to the reflections from the (1 1 1), (2 2 0), (3 1 1), (2 2 2), (4 0 0), (5 1 1), and (4 4 0) planes of Al_2O_3, respectively (JCPDS No.:10–0425)[9] .

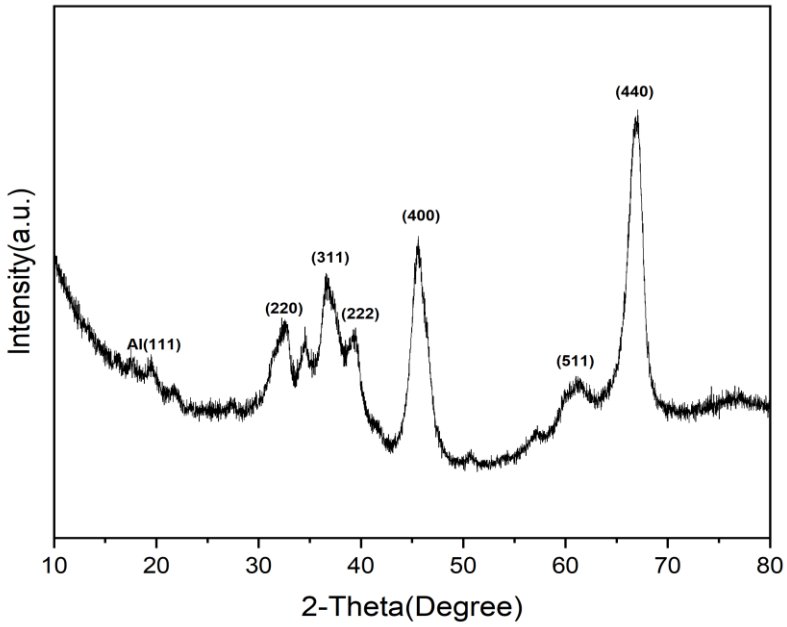

Figure 3.1: XRD profile of commercial gamma-alumina Al_2O_3 support.

3.3. Monometallic Catalysts

3.3.1. Monometallic 5%PdH/Al_2O_3 and 5%Pd/Al_2O_3 catalysts

The Pd and PdH catalysts supported on Al_2O_3 were synthesized using methods outlined in Chapter 2 (Sections 2.2.3.1 and 2.2.3.2), emphasizing the dispersion of active sites and the metal-support interaction. The catalytic activity of Pd hinges significantly on the active phase's distribution and site proportion. Thus, Pd shape regulation is crucial for high-activity catalyst production. Several techniques, including modified impregnation (M_{im}) and sol-immobilisation (S_{im}) (discussed in Chapter 2, Sections 2.2.2 and 2.2.1), have been developed to enhance Pd catalysts' activity. However, the catalyst preparation conditions, particularly reduction by heat treatment or sodium borohydride ($NaBH_4$), play a vital role as they affect the catalyst structure and capabilities. In this experiment, commercial nanopowder Al_2O_3, as detailed in Section 3.2, was used as a support. The catalyst exhibited impressive stability and coke resistance in hydrogenation, cross-coupling, and auto-transfer reactions, as elaborated in Chapters 4, 5, and 6. The produced PdH catalyst displayed desirable physical, chemical, and catalytic characteristics, standing out even among transition metal hydrides, primarily due to the success of the 'proton gas' model and palladium's superior hydrogen disruption resistance[10]. Consequently, surface stabilization

warrants further consideration when designing metal-hydrogen reservoirs to prevent material degradation[11]. Divalent palladium (Pd^{2+}) was impregnated onto the aluminium oxide surface using the M_{im} method. It was then prepared and reduced in two ways. The first method involved $NaBH_4$ reduction at room temperature, followed by purification, washing, and drying at 80 °C to produce the 5%PdH/Al_2O_3 catalyst. The second method involved heat treatment reduction at 450 °C under 5%H_2/Ar, resulting in the 5%Pd/Al_2O_3 catalyst. These were tested in a hydrogenation reaction. During the catalyst screening, the 5%PdH/Al_2O_3 catalyst was the only one to display notable catalytic activity. Additionally, these Pd catalysts were tested for phenol hydrogenation, demonstrating satisfactory and similar performance levels. The limited catalytic activity of Pd catalysts in reductive amination was attributed to p-toluidine's poisoning effects. However, they performed well in the auto transfer reaction of benzyl alcohol with nitrobenzene. These results were confirmed using XRD, SEM, TEM–EDX, and XPS techniques.

Chemical composition and crystal structure of the catalysts 5%PdH/Al_2O_3, 5%Pd/Al_2O_3, and their supporting material were analysed using powder X-ray diffraction (XRD), with patterns exhibited in **Figure 3.2.** Upon comparison, the density of peaks for the catalysts was found to be less than the solid support material (**Figure 3.1**). In the case of PdO, expected reflection peaks would be at 2θ = 32.83°, 42.29°, and 61.25°, corresponding to (002), (110) and (200) planes of the tetragonal PdO structure (JCPDS No: 01–085–0713) respectively[12–14]. validating the PdO phase's existence (red line). This observation concurs with prior research, highlighting that basic sites on the Al_2O_3 surface can enhance palladium dispersion during impregnation, causing the lack of prominent diffraction patterns for fresh Pd/Al_2O_3. Upon reduction, the catalysts exhibited high crystallinity. The Al_2O_3 substrate showed broad peaks at 2θ = 37.6°, 45.9°, and 67.12° (green line), likely a result of significant palladium content. A broad peak of palladium oxide at 32.83° was also discerned (see **Figure 3.2**). The PdO peaks diminished as Pd/Al_2O_3 underwent reduction, resulting in an increase in Pd^0 peaks. Specific diffraction peaks at 2θ = 40.2°, 46.78°, and 68.31° were found to correspond to the (111), (200) and (220) planes of the cubic Pd phase (JCPDS No. 01-087-0639) respectively (blue line)[15,16]. The palladium deposition on the alumina support did not alter the support's structure, indicating that the noble metal remained finely dispersed post-deposition[17]. Interestingly, a new peak at a lower angle (2θ = 39.5°) was observed from PdH species in the 5%PdH/Al_2O_3 catalyst, indicating a shift from the broad peak of metallic palladium from Pd0 at 2θ = 40.0°, attributed to peak convolution with the (101) palladium hydride peak[18]. The diffraction peaks at 2θ = 32.5°, 39.5°, and 78.5° corresponded to the (100), (101) and (121) planes of the tetragonal PdH phase (JCPDS No. 01-073-0004) respectively

(black line). This lower angle shift in the nanocatalyst's characteristic peaks compared to the Pd0 blue line, as well as the negative shift of the diffraction peaks, suggests Pd nanocrystal expansion, which aligns with the XPS and TEM results. Thus, these findings confirm the successful production of the proposed PdH nanocatalyst under the given synthetic condition[19].

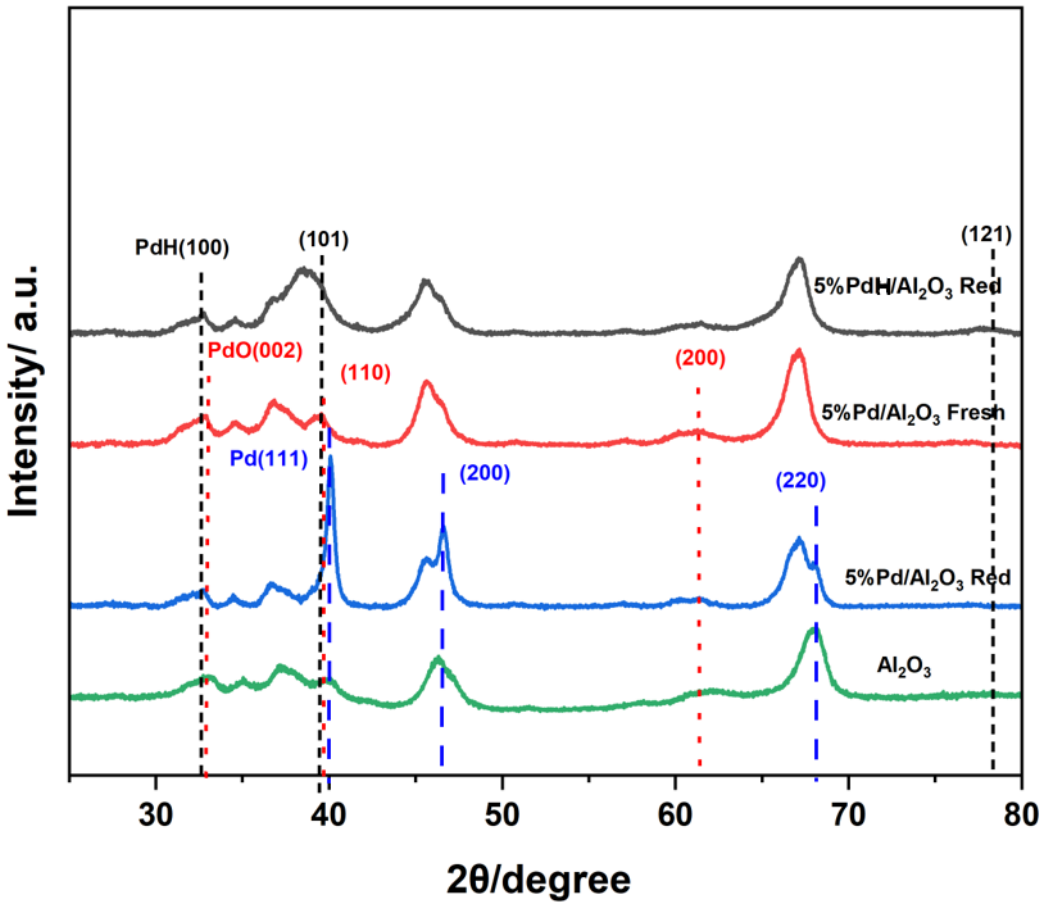

Figure 3.2: XRD patterns for 5%PdH/Al_2O_3 (Catalysts reduction with $NaBH_4$ (black)) , 5%Pd/Al_2O_3 (Catalysts before treatment, fresh (red line)), 5%Pd/Al_2O_3 Red (Catalyst reduction by heat treatment (blue line)), and the Al_2O_3 substrate (green line).

Hydrogen absorption into Pd typically results in two separate phases: the α-phase (at low H concentrations, with negligible XRD peak shift) and the β-phase (at high H concentrations, exhibiting lower angle shifts in XRD peaks). The BET surface area's alterations can also illustrate this phenomenon[20].

BET surface area measurements of the samples were conducted using nitrogen physisorption (-196 °C) via a Quadrasorb Automated Surface Area and Pore Size Analyser, as detailed in Chapter 2, Section 2.5.2. Each measurement utilised approximately 0.1 g of catalyst, with the specific surface area determined via the BET method. The BET surface area was found to be 53 m^2/g before reduction and

escalated to 122 m^2/g after reduction (refer to **Table 3.1**). Specific BET surface area was calculated as 85-115 m^2/g for Al_2O_3 and 53 m^2/g for the fresh 5%Pd/Al_2O_3 catalyst. The decrease in BET surface area for the 5%Pd/Al_2O_3 nanocatalyst suggests Pd NPs attachment to the Al_2O_3 surface, corroborated by recent studies[21]. Conversely, an increase in BET surface area of the reduced 5%PdH/Al_2O_3 catalyst suggests a superior dispersion of Pd NPs on the Al_2O_3 surface, consistent with findings from other contemporary research. In summary, the hydrogen absorption phases and BET surface area changes collectively provide critical insights into the catalyst's transformation during the reduction process. Such observations further underscore the importance of these catalyst attributes and their roles in influencing the catalyst's efficacy in various applications[22].

Table 3.1: Surface area of 5%PdH/Al_2O_3 fresh and reduced nanoparticles:

Catalyst	**Surface area $m^2 g^{-1}$**
5%Pd/Al_2O_3 fresh	53
5%PdH/Al_2O_3 reduced	122

The reduction in BET surface field of the fresh 5%Pd/Al_2O_3 nanocatalyst suggests Pd nanoparticle binding on the Al_2O_3 surface. Upon loading Pd metal onto the Al_2O_3 support, which exhibits a crystalline structure, a diffraction peak of 40.2° corresponding to the Pd(111) surface is observed (JCPDS No. 01-087-0639) (**Figure 3.2**), signifying the maintenance of the crystalline structure of the Al_2O_3 support.

X-ray photoelectron spectroscopy (XPS) analyses were conducted to uncover the oxidation stages of the Pd metal in the created 5%Pd/Al_2O_3 and 5%PdH/Al_2O_3 catalysts (**Figure 3.3 and Figure 3.4**, respectively). These investigations aimed to evaluate the oxidation state of the metals. The deconvolution of the spectra suggested that two forms of palladium existed on both samples' surfaces: the oxidised state (PdO) with binding energy E_b ($Pd3d_{5/2}$) ~ 337–338 eV and the reduced state (Pd^0) with E_b ($Pd3d_{5/2}$) ~ 335–336 eV.

According to existing literature, palladium supported on Al_2O_3 can exist as Pd^0, PdO or PdO_2 or a combination of these[23]. The binding energies of the Pd3d line in these compounds are in narrow ranges equal to E_b ($Pd3d_{5/2}$) = 335.1–335.4 eV for Pd^0[24] , E_b ($Pd3d_{5/2}$) = 336.8–337.2 eV [35,53,55] or 336.3–336.8 eV[25] , for PdO and E_b ($Pd3d_{5/2}$) = 337.8–339.3 eV for PdO_2[26] , similar to the findings in this study (Lee & Kim, 2020). An E_b ($Pd3d_{5/2}$) = 336.1 eV was observed for reduced palladium between Pd^0

and PdO. XPS characterisation of synthesised 5%Pd/Al_2O_3 and 5%PdH/Al_2O_3 catalysts (**Figures 3.3 and 3.4**) was conducted to investigate the Pd element's valence state and content on the catalyst surface. The XPS spectra exhibited two pairs of peaks and one set of solid double peaks in both prepared catalysts, attributed to the Pd^0 and oxidised Pd^{2+}species. This suggests that the majority of Pd atoms on the Al_2O_3 supports were in the metallic state, although a considerable amount of Pd^{2+} was also found, likely generated from Pd particle attachment to the oxygen of Al_2O_3 or re-oxidation of Pd metal by O_2 in the air[27].

In the 5%Pd/Al_2O_3 sample, the XPS-derived atomic ratios showed a Pd^{2+}/ Pd^0 ratio of 0.5, whereas in the 5%PdH/Al_2O_3 sample it was 0.2 (**Figures 3.3 and 3.4**). This lower ratio in the 5%PdH/Al_2O_3 catalyst suggests a larger presence of Pd^0, indicative of a strong interaction between palladium and alumina, and the formation of more metallic palladium species in the 5%PdH/Al_2O_3 catalyst due to the addition of H_2 gas and the creation of PdH species during reduction with $NaBH_4$. These findings are corroborated by the high catalytic activity of the reactions selected to test the catalyst's efficacy (Chapters 4, 5 and 6). Lastly, a shift of 0.28 eV to a higher binding energy in the Pd peak on PdH/Al_2O_3 compared to Pd/Al_2O_3 aligns with empirical literature findings[19,20]

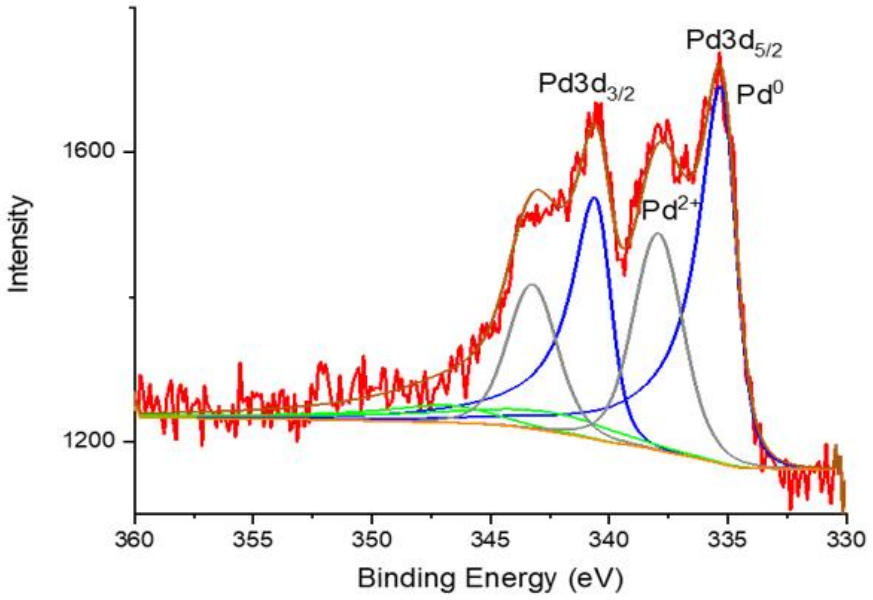

Figure 3.3: Pd 3d XPS spectra of Pd/Al_2O_3 catalyst

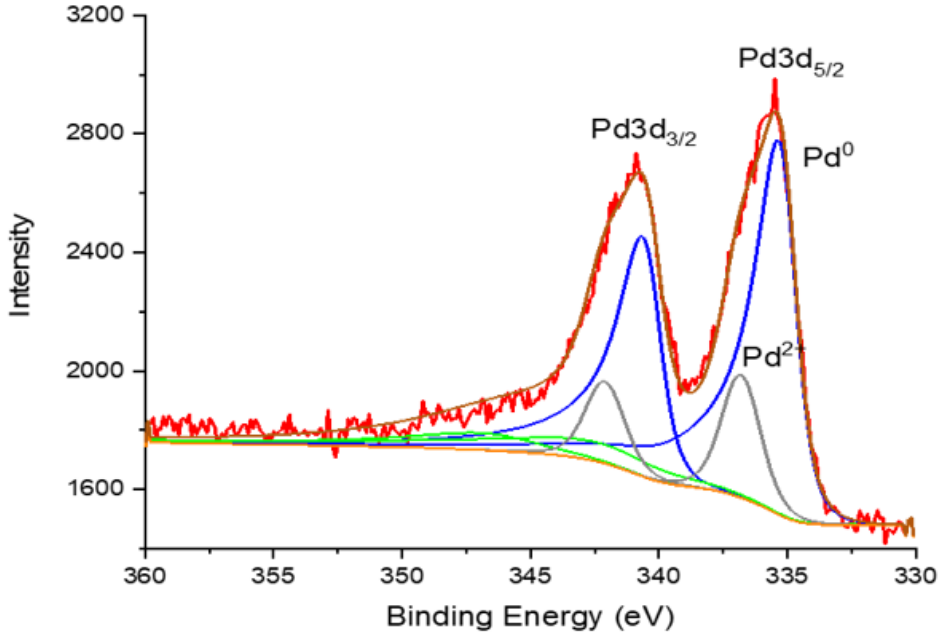

Figure 3.4: Pd 3d XPS spectra of PdH/Al_2O_3 catalyst

The shift in peaks in both the XRD and XPS characterizations indicate the successful formation of PdH species, in alignment with previous studies. From these results, we can conclude that PdH/Al_2O_3 has been successfully prepared[19,20].

Scanning Electron Microscopy (SEM) imaging of the catalysts prepared by the modified impregnation of palladium metal with reduction by $NaBH_4$ revealed the presence of small metal particles (see **Figure 3.5.A**). The surface morphologies of the $5\%PdH/Al_2O_3$ catalyst vary significantly, as evidenced by the SEM images. Energy Dispersive X-ray (EDX) spectroscopy analysis of the catalyst, presented in **Figure 3.5.C**, revealed the extent of metal loading for the catalysts. However, in similar studies, it's been found that an increase in Pd loading generally results in a reduction in dispersion[28]. In the case of the $5\%PdH/Al_2O_3$ sample, the SEM image data suggests a superior dispersion of the Pd phase and the alloyed phase (see **Figure 3.5.B**). Thus, it's inferred that the preparation method used has led to effective dispersion of Pd, an important factor influencing the performance of such catalysts.

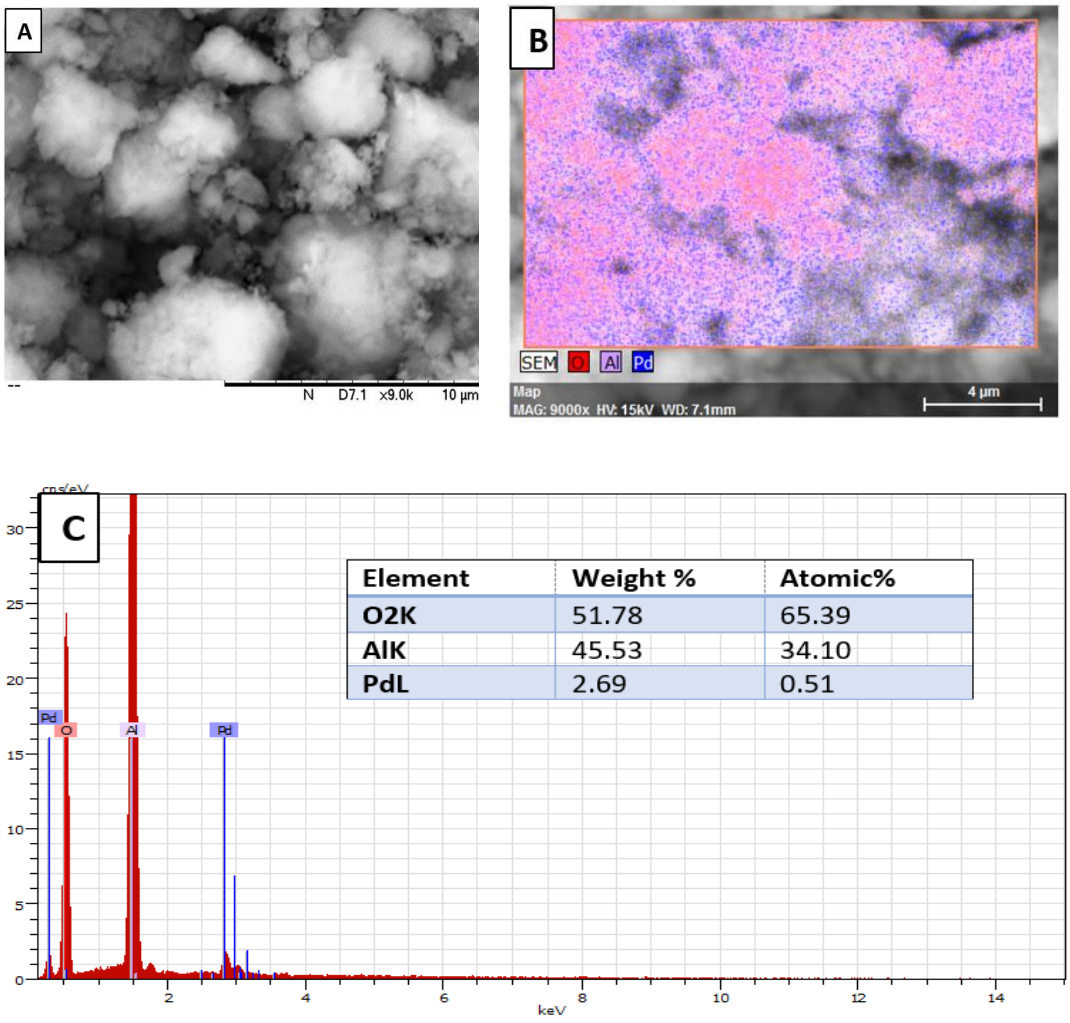

Figure 3.5: A SEM image of 5%PdH/Al_2O_3 (A), map of 5%PdH/Al_2O_3 (B) and EDX spectrum of 5%PdH/Al_2O_3 (C)

Transmission Electron Microscopy (TEM) and TEM-Energy Dispersive X-ray (TEM-EDX) analyses were performed to further elucidate the microstructure of the as-prepared catalysts, specifically the 5%PdH/Al_2O_3 catalyst. These analyses aimed to determine the average particle size, morphology, and crystal structure of the catalyst. The TEM images, as presented in **Figure 3.6 A**, confirmed the presence of well-dispersed Pd nanoparticles on the Al_2O_3 support material surface. The particle size distribution histogram obtained from the TEM image revealed sizes ranging between 2 nm and 8 nm, with an average particle size of 3.52 nm (See **Figure 3.6 A**). The TEM-EDX spectrum depicted in **Figure 3.6 B** was generated from multiple images taken from various regions of the TEM. This spectrum affirmed the presence of Pd, Al, and O atoms within the analysed regions. The existence of these elements is indicative of the successful loading of Pd onto the Al_2O_3 support material[29]. Highly dispersed catalysts with small Pd particle sizes can often result in exceptional catalytic activity, as suggested by previous research. The TEM results thus not only confirm

the successful preparation of the 5%PdH/Al_2O_3 catalyst but also suggest its potential for excellent catalytic performance due to the small size and high dispersion of Pd particles.

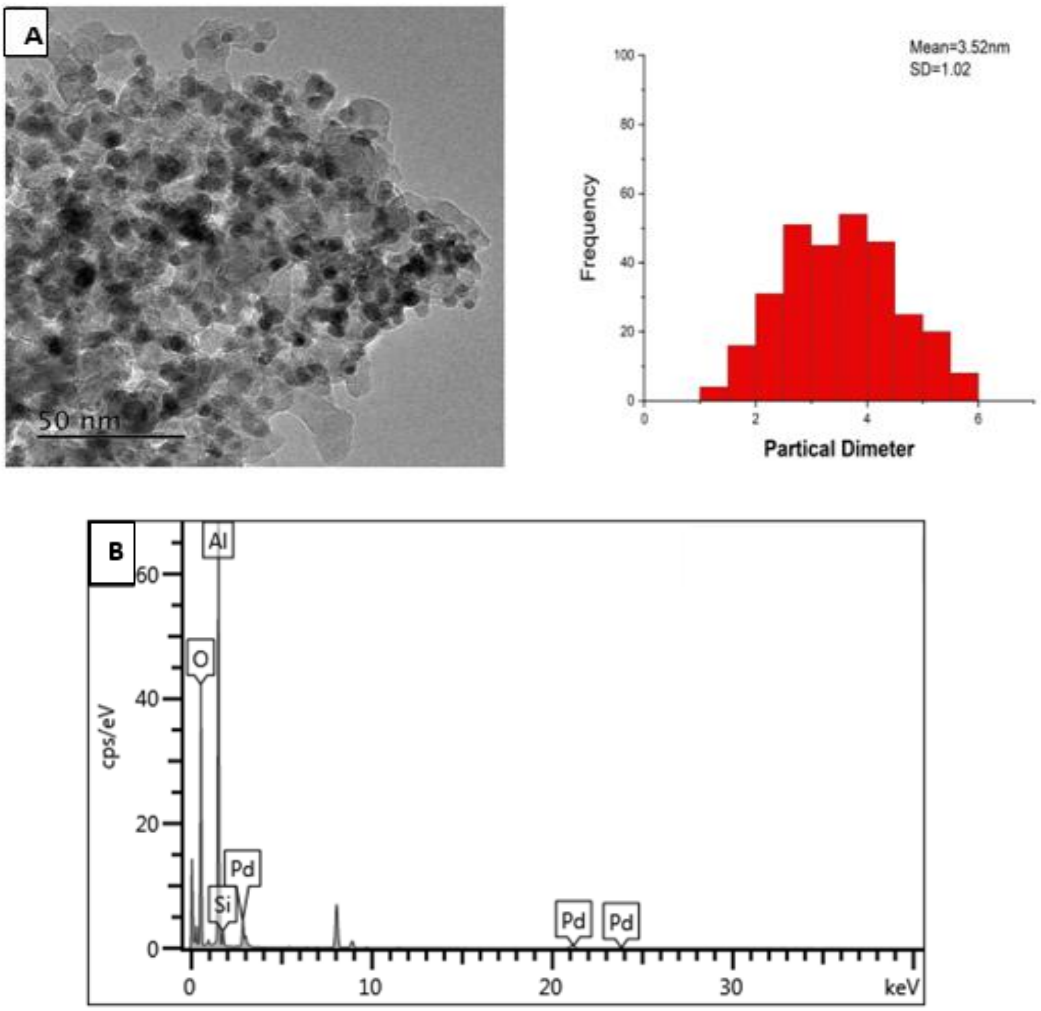

Figure 3.6: TEM picture of 5%PdH/Al_2O_3; (A) TEM image with size distribution histograms of the Pd nanoparticles and (B) TEM–EDX spectrum

3.3.2. Monometallic catalyst 5%Pd supported on TiO_2

X-Ray Diffraction (XRD) patterns were generated for both the 5%PdH/TiO_2 catalyst and pure TiO_2 support, as depicted in **Figure 3.7**. These XRD patterns help validate the formation of the catalysts by comparing the experimental data with known patterns from the Joint Committee on Powder Diffraction Standards (JCPDS) reference database. Reflection peaks from the anatase TiO_2 phase were observed at 2θ = 25° and 48°. These peaks correspond to the (101) and (200) crystal planes of TiO_2 in the anatase phase (JCPDS No. -84-1286)[30,31]. The presence of these reflection peaks confirms the existence of the TiO_2 phase in the sample. Upon examination of the 5%PdH/TiO_2 catalyst using XRD, three additional peaks were observed at 2θ = 42.27°, 44.17°, and 64.35°. These peaks correspond to the (101), (110), and (112)

crystal planes of metal PdH (JCPDS No. 01-073-0004), respectively. This observation not only verifies the presence of the palladium hydride (PdH) state in the loaded PdH particles, but it also shows the stability of the PdH crystals in the sample. This could potentially enhance the performance of the catalyst. Interestingly, no characteristic diffraction patterns of the PdO phase were found in the 5%PdH/TiO_2 catalyst, suggesting that these sites are likely below the visibility threshold of X-ray analysis. Moreover, the typical reflections of palladium metal were not observed except at 2θ = 46.78°, suggesting that Pd species are uniformly dispersed within the TiO_2 support, and the majority of the formed palladium species are PdH species. The change in nanocrystal structure could be attributed to the shape-directing capabilities of hydrogen evolution during reduction, which manifests as a visible peak shift in the XRD spectra[16]. The formation of PdH species and their uniform dispersion within the TiO_2 support material could be key factors in enhancing the catalyst's performance.

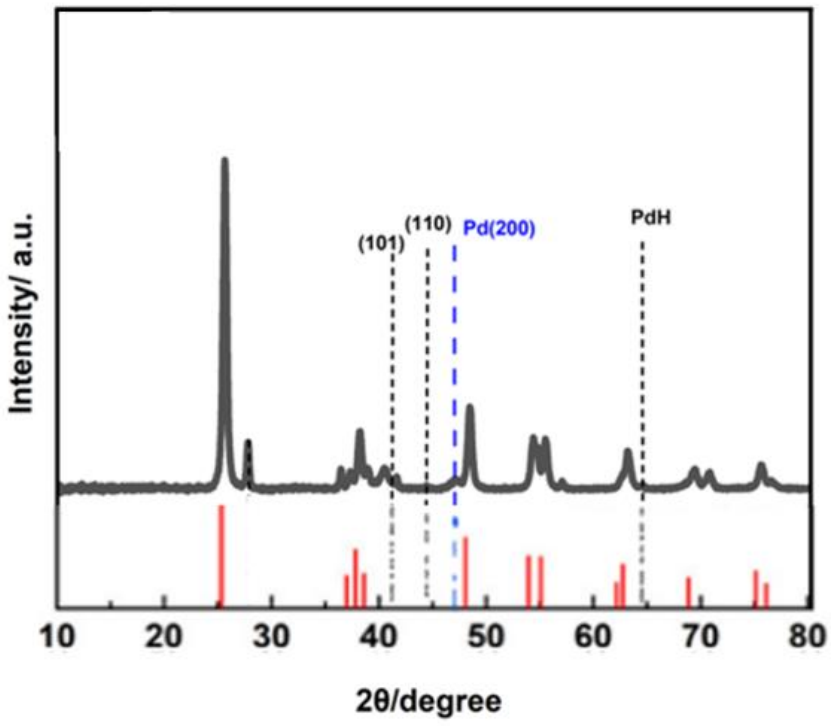

Figure 3.7: Indexed XRD patterns of TiO_2 intermediate (JCPDS -84-1286) and 5%PdH/TiO_2 sample

The Pd/TiO_2 catalysts and TiO_2 were systematically characterized using X-ray diffraction (XRD). The diffraction peak at 38°, 54°, and 63° represent the crystalline phase of Pd corresponding to Pd^0. The strong diffraction peaks at 25.4° and 48° indicate the anatase phase of TiO_2[22] (The reference codes are 04–002-8296). However, the absence of Pd-related peaks suggests that Pd atoms are highly dispersed on the TiO_2 surface, a finding in line with previous studies The XRD patterns

of Pd/TiO_2, exhibit the typical diffraction peaks of TiO_2. These diffraction peaks associated with TiO_2 are unaffected by the addition of Pd NPs. However, no Pd NPs peak was observed, suggesting that Pd NPs may be evenly distributed on TiO_2 nanowires[32].

Comparisons between the XRD diffraction patterns of $5\%PdH/Al_2O_3$ (see **Figure 3.2**) and $5\%PdH/TiO_2$ (see **Figure 3.7**) provide further insights into the structure and . The $5\%PdH/Al_2O_3$ XRD pattern has a peak at 39.5°, likely due to peak convolution with the (101) palladium hydride peak, which appears to have shifted to the lower-angle side (the β-phase) of the broad peak from Pd0 at 2θ = 40.0° (the (111) plane). In contrast, the $5\%PdH/TiO_2$ XRD data show that palladium hydride peaks cause a slight shift in the fitted palladium phase peaks from their indexed positions. For example, the (111) palladium fitted peak at 40.2° is shifted to the right of the indexed reference peak position at 42.27°, likely due to peak convolution with the (101) palladium hydride peak (the α-phase) [33]. The presence of palladium hydride in $5\%PdH/TiO_2$ might be due to palladium's ability to store hydrogen gas within its crystal lattice, combined with the properties of the support and Pd metal dispersion.

To further confirm the formation of PdH, X-ray photoelectron spectroscopy (XPS) was employed to study the catalyst's valence band structure. The results from this analysis are presented in **Figures 3.8 and 3.9.** X-ray photoelectron spectroscopy (XPS) data shows atomic ratios of Pd^{2+}/ Pd^0 in the $5\%Pd/TiO_2$ and $5\%PdH/TiO_2$ samples to be 0.5 and 0.2, respectively. This means that the ratio of Pd^{2+} to Pd^0 is lower in the $5\%PdH/TiO_2$ catalyst, suggesting that both catalysts contain Pd^0 and Pd^{2+} components, with the Pd^0 acting as the active species in the tested reactions. A larger presence of Pd^0 could indicate a strong interaction between palladium and alumina.

Additionally, the $5\%PdH/TiO_2$ catalyst could form more metal palladium species due to the addition of H_2 gas which forms PdH species during reduction with $NaBH_4$. High catalytic activity in the selected test reactions supports this theory, as outlined in Chapters 4, 5 and 6.

The deconvoluted Pd 3d signal (**Figures 3.8**) provides insight into the different oxidation states of Pd on the surface of the photocatalysts. For example, in the Pd/TiO_2 sample, Pd $3d_{5/2}$ peaks with binding energies around 335.0 eV, 336.0 eV and 337.2 eV are indicative of metallic Pd (Pd^0), Pd^{2+} and Pd^{4+} species, respectively. Here, metallic Pd was the dominant species, making up 51.1 % of the sample[34].

In the PdH/TiO_2 sample, the XPS analysis (**Figures 3.9**) assigns peaks at 335.0 eV and 340.3 eV to Pd^0 $3d_{5/2}$ and Pd^0 $3d_{3/2}$, respectively. A weak peak at 341.1 eV is

attributed to Pd^{2+} $3d_{3/2}$, while a peak at 336.0 eV corresponds to Pd^{2+} $3d_{5/2}$. The presence of Pd^{2+} could be due to the surface Pd naturally oxidizing in the air[35,36].

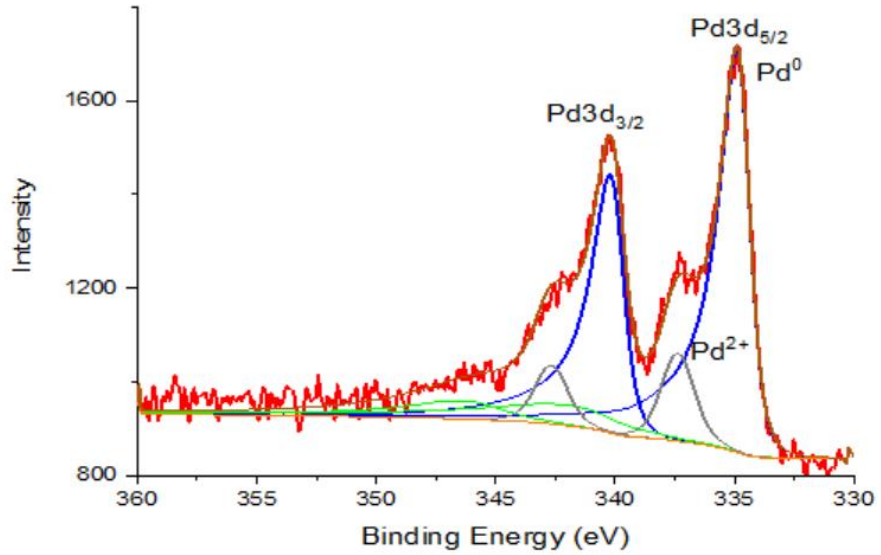

Figure 3.8: Pd 3d XPS spectra of Pd/TiO_2 catalyst

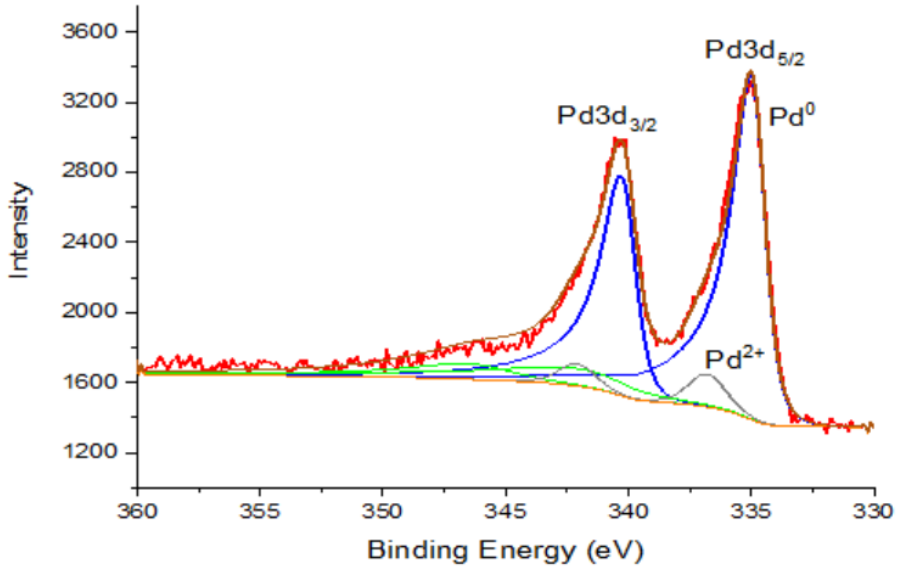

Figure 3.9: Pd 3d XPS spectra of PdH/TiO_2 catalyst

3.4. Bimetallic Catalysts

3.4.1. Bimetallic 2.5%Pd-2.5%AuH/Al_2O_3 and 2.5%Pd-2.5%Au/Al_2O_3 catalysts

Catalytic performance is significantly influenced by the preparation conditions, which directly affect the surface properties of catalysts. A bimetallic Pd and Au supported on Al_2O_3 catalyst was fabricated employing documented procedures (refer to Section 2.2.3.3). This study investigated the catalytic activity of the 2.5%Pd-2.5%AuH/Al_2O_3 catalyst by applying two preparation methods: modified impregnation and sol-immobilisation (refer to Sections 2.2.2 and 2.2.1, respectively). The reduction conditions of the catalyst prepared via modified impregnation, namely reduction through heat treatment or sodium borohydride $NaBH_4$, were specifically considered. A high-surface-area nanopowder Al_2O_3 (115 m^2/g) with a particle size of 13 nm served as the catalyst support. This catalyst exhibited impressive stability and activity in the hydrogenation and cross-coupling reactions discussed in Chapters 4 and 5, respectively. Bimetallic Pd-Au supported on Al_2O_3 has been the subject of considerable research.

BET analysis was utilized to determine the surface areas of the 2.5%Pd-2.5%AuH/Al_2O_3 catalyst. Notably, reduced catalysts had larger surface areas compared to the fresh ones. The nitrogen physisorption BET analysis results (**Table 3.2**) indicated a surface area increment for the reduced catalyst, suggestive of a good dispersion of Pd and Au nanoparticles within the support pores. This analysis was repeated, yielding a maximum error of no more than 1 m^2g^{-1}. Increased research on supported bimetallic catalysts, especially Pd-Au on Al_2O_3, would further elucidate the synergistic effects on catalytic performance. This may lead to more optimized preparation methods for high-activity catalysts, particularly for reactions like hydrogenation and cross-coupling. Additionally, further investigation into the impact of reduction methods and conditions on catalysts' surface properties is warranted to deepen our understanding of the mechanisms underlying these phenomena.

Table 3.2: Surface area of 2.5%Pd-2.5%Au/Al_2O_3 fresh and reduced nanoparticles

Catalyst	**Surface area $m^2 g^{-1}$**
2.5%Pd-2.5%Au/Al_2O_3 fresh	94
2.5%Pd-2.5%AuH/Al_2O_3 reduced	120

XRD analysis of the 2.5%Pd-2.5%AuH/Al_2O_3 catalysts affirmed the dispersion of metallic Au and Pd across all catalysts' supports. Characteristic reflections for Au were anticipated at 2θ = 38° (111), 44° (200), 64° (220), and 77° (311), while for Pd, they were expected at 2θ = 40° (111), 46° (200), and 68° (220). Additional reflections originated from the catalyst support. Corresponding to the (100), (101), and (121) planes of the tetragonal phase of PdH (JCPDS No. 01-073-0004), diffraction peaks were seen at 2θ = 32.5°, 39.5°, and 78.5°.

The XRD patterns of the fresh and reduced catalysts were investigated to monitor the presence of Pd-Au alloy and Pd phases. **Figure 3.10** depicts the XRD patterns of the fresh 2.5%Pd-2.5%Au/Al_2O_3 and the reduced 2.5%Pd-2.5%Au/Al_2O_3 and 2.5%Pd-2.5%AuH/Al_2O_3 catalysts, prepared by modified impregnation, along with the reflections of the Al_2O_3 support. The fresh sample's XRD pattern (blue line) revealed a characteristic peak of Au at 2θ = 38° (111), intensifying after thermal treatment in the reduced 2.5%Pd-2.5%Au/Al_2O_3 sample (red line). The absence of a discernible Pd peak could be due to a small crystallite size (< 5 nm) under the XRD detection limit or high metal dispersion on the Al_2O_3 support, corroborated by TEM (see **Figure 3.12**) and SEM data (see **Figure 3.11**). The peak at 78.5° in the 2.5%Pd-2.5%AuH/Al_2O_3 catalyst (green line) corresponded to the (121) plane of PdH species. The expanded region in **Figure 3.10** highlights the (111) cubic metal phase reflection in reduced samples, suggesting the presence of Au or Au-Pd alloy peaks, though Pd species remained undetected, likely due to the limitations of the XRD. The absence of diffraction peaks for the deposited metals (Au, Pd) in the 2.5%Pd-2.5%AuH/Al_2O_3 XRD spectra could also be attributed to XRD's detectability constraints. The TEM data revealed a mean particle size of 4.38 nm for the metal catalyst, reinforcing this interpretation.

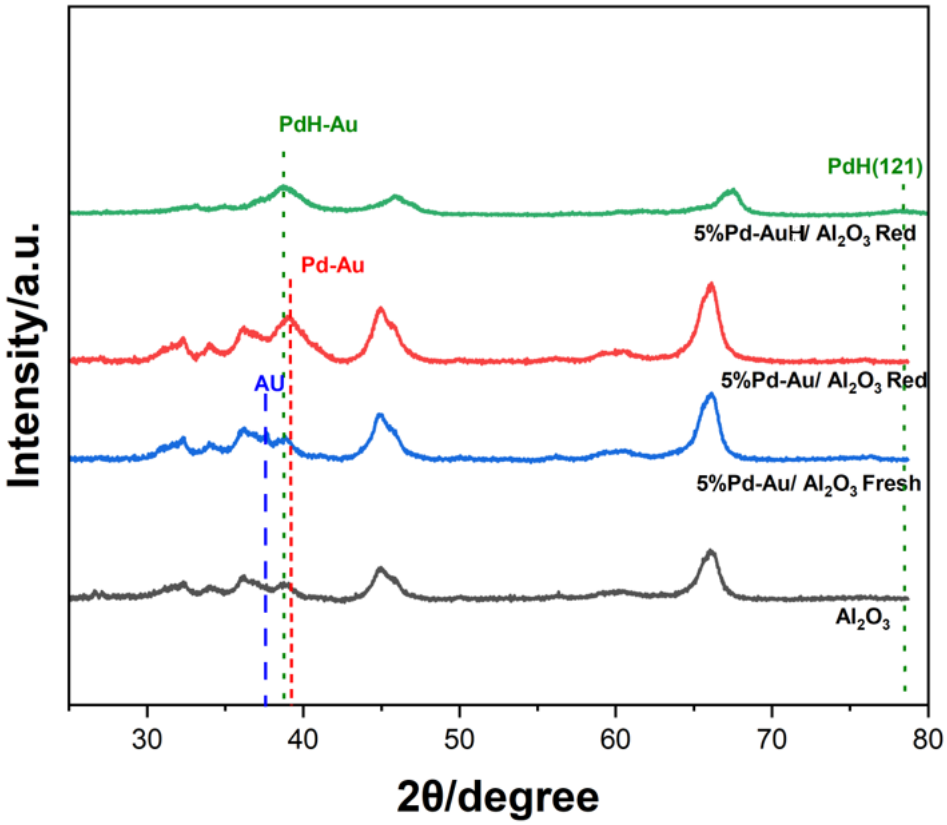

Figure 3.10: XRD patterns for 2.5%Pd-2.5%AuH/Al_2O_3 (green line) and 2.5%Pd-2.5%Au/Al_2O_3 (fresh (blue line) and reduction (red line)) catalysts, and the Al_2O_3 substrate (black line).

In summary, these results emphasize the importance of employing complementary techniques to characterize nanoscale catalysts thoroughly. The observed inconsistencies between XRD, SEM, and TEM data underpin the complex nature of these catalytic systems, and necessitate further investigation to clarify the formation and behaviour of the bimetallic particles.

The SEM results for the 2.5%Pd-2.5%AuH/Al_2O_3 sample demonstrate enhanced dispersion of the Pd phase and the Au-Pd alloy phase, as shown in **Figure 3.11 B**. Furthermore, the EDX analysis, depicted in **Figure 3.11 C**, verifies the metal loadings for the catalysts.

TEM imaging, presented in **Figure 3.12**, revealed observable particles in the reduced 2.5%Pd-2.5%AuH/Al_2O_3 sample, boasting a diameter of 4.38 nm. In comparison, the 2.5%Pd-2.5%AuH/Al_2O_3 reused sample showed slightly larger particles with a diameter of 4.42 nm, as evident from the TEM images in **Figure 3.13**. Consistently sized particles of Pd and Pd-Au alloy, with diameters of 4.38 nm and 4.42 nm, respectively, were observable across both samples.

Taken together, these SEM and TEM results affirm the successful preparation of the PdH and Pd-AuH nanoparticles. Despite the marginal increase in particle size after reuse, this discrepancy is minimal and potentially attributable to the interactions during the reaction process. Future work could explore this further, investigating how these nanoparticles evolve with reuse and their potential impact on catalytic performance.

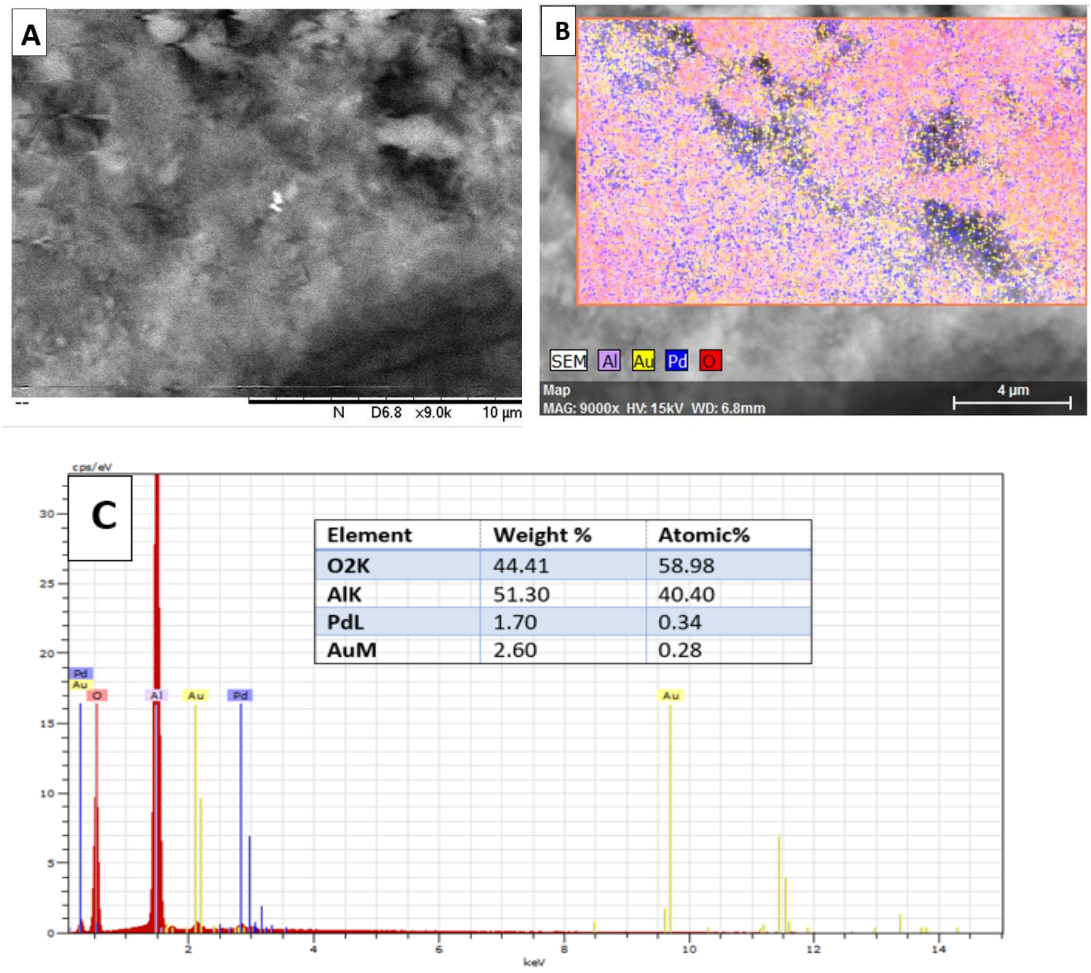

Figure 3.11: SEM image of 2.5%Pd-2.5%AuH/Al_2O_3 (A), the map of 2.5%Pd-2.5%AuH/Al_2O_3 (B) and EDX spectrum (C)

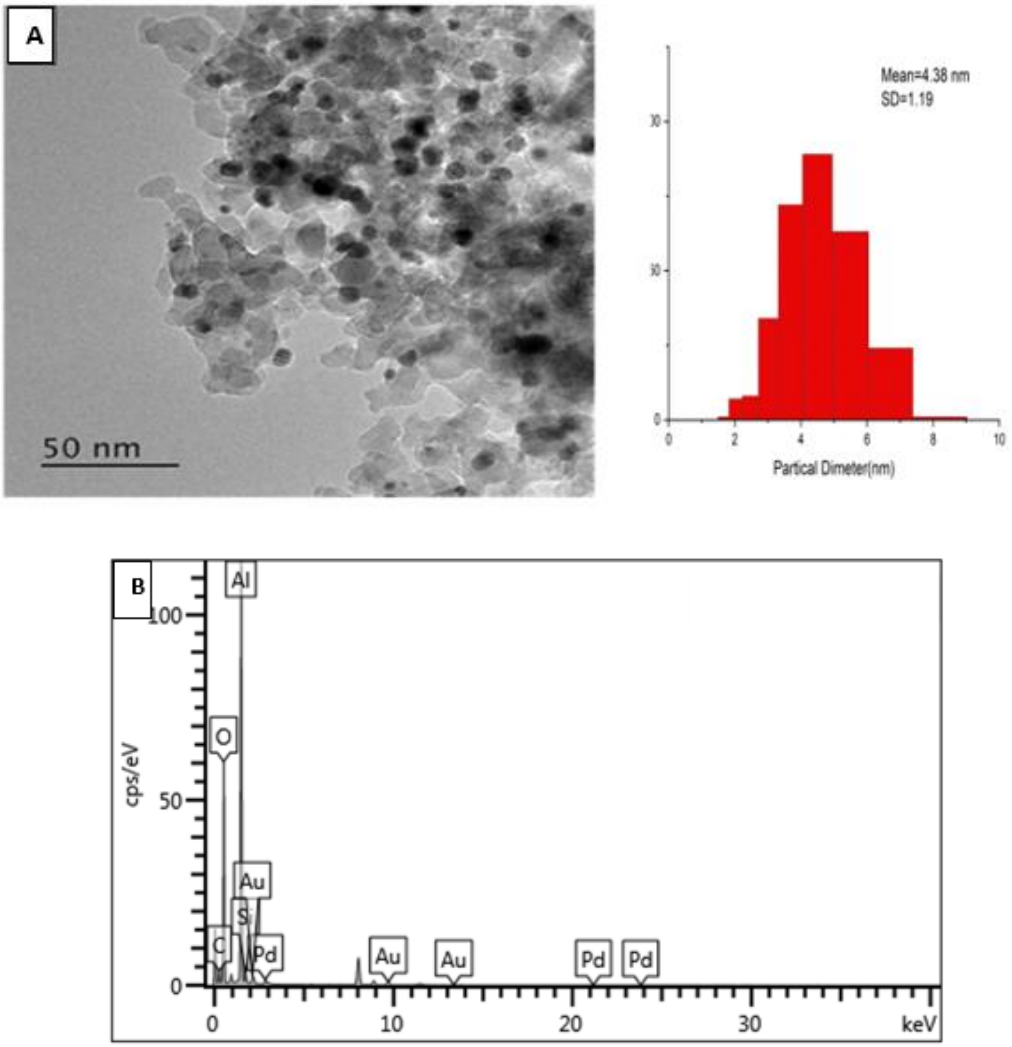

Figure 3.12: TEM picture of 2.5%Pd-2.5%AuH/Al_2O_3, (A) TEM image with size distribution histograms of the Pd-Au nanoparticles and (B) TEM–EDX spectrum

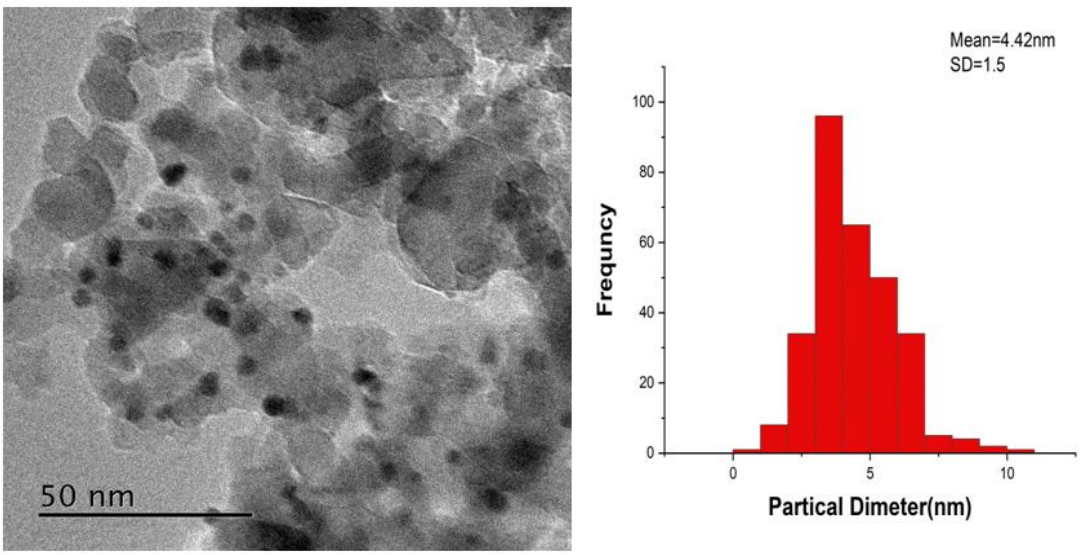

Figure 3.13: TEM picture of 2.5%Pd-2.5%AuH/Al_2O_3 reused

The catalytic activity of the PdH species was investigated by preparing a bimetallic Pd-Au catalyst on an alumina support using two distinct methods: modified impregnation and sol-immobilisation, with the details described in Chapter 2 (Sections 2.2.2 and 2.2.1, respectively). Sodium borohydride ($NaBH_4$) was employed as the reducing agent for both methods.

Previously, the preparation of 2.5%Pd-2.5%AuH/Al_2O_3 using modified impregnation was discussed in detail, with analysis based on TEM and XPS data. The 2.5%Pd-2.5%Au/Al_2O_3 catalyst prepared using sol-immobilisation was further investigated, with corresponding TEM and XPS data displayed in **Figures 3.14 and 3.15** respectively.

From the TEM images, both the fresh and reused catalyst samples indicated the presence of similarly sized Pd and Pd-Au alloy particles, having diameters of 3.27 nm and 3.53 nm, respectively. These findings corroborate the successful preparation of Pd and Pd-Au nanoparticles. Despite a slight increase in particle size upon reuse, the variance is marginal and could be attributed to interactions occurring during the reaction process. Future work can delve deeper into the influence of these particle size changes on catalyst activity over time.

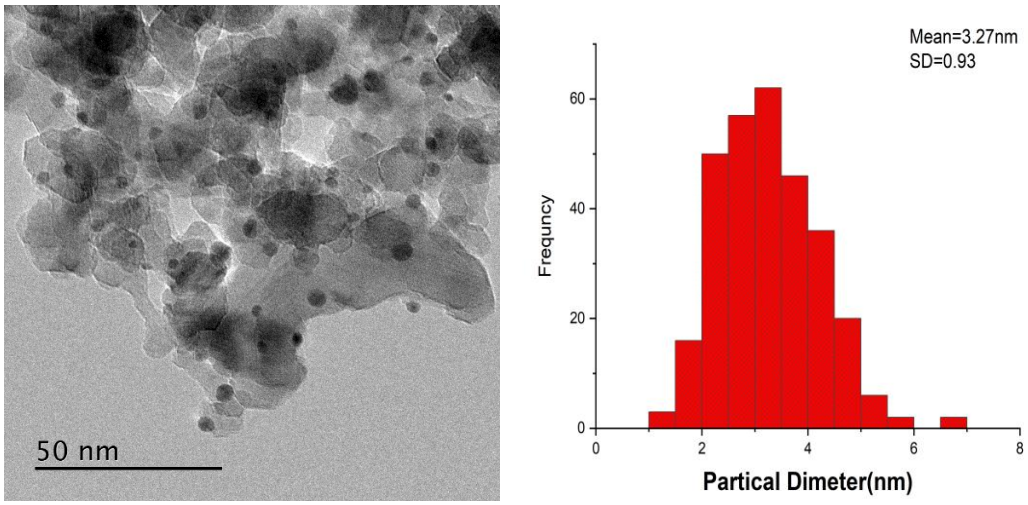

Figure 3.14: TEM picture of 2.5%Pd-2.5%Au/Al_2O_3 with the size distribution histogram

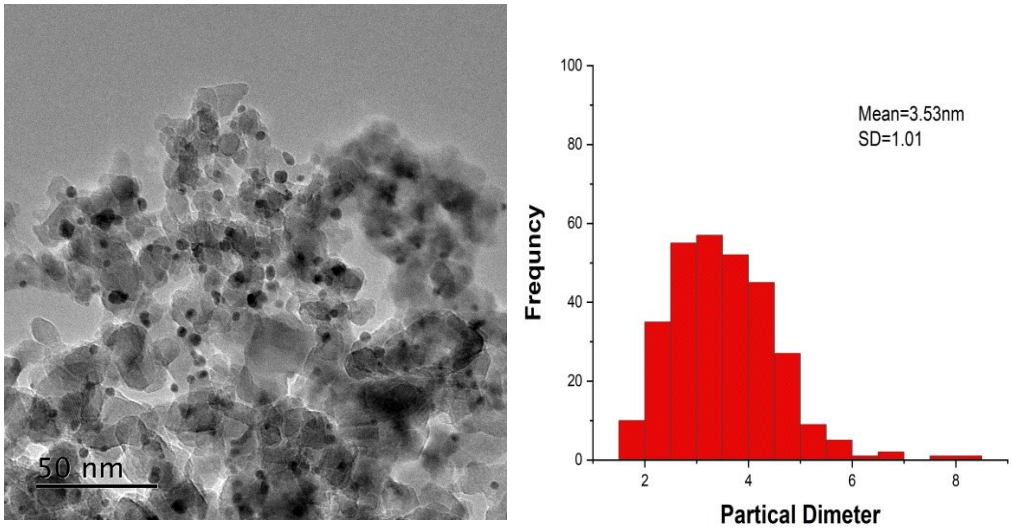

Figure 3.15: TEM picture of 2.5%Pd-2.5%Au/Al_2O_3 reused with the size distribution histogram

The oxidation state of the metals in the samples was examined using X-ray photoelectron spectroscopy (XPS). **Figure 3.16** presents the XPS spectra of Au and Pd from the 2.5%Pd-2.5%AuH/Al_2O_3 support catalyst, prepared via modified impregnation and reduced with $NaBH_4$. Characteristic spin-orbit components, such as the Au $4f_{7/2}$ peak at 83.8 eV and the $4f_{5/2}$ signal at 87.45 eV with a separation of 3.65 eV[37], were identified in the Au 4f region of the XPS spectra. Simultaneously, the Pd region XPS spectra exhibited two slightly asymmetric peaks where the $3d_{5/2}$ photoelectron peak is centred at 334.9 eV, revealing a secondary spin-orbit component, $3d_{3/2}$, at a distance of 5.25 eV, standing at 340.15 eV[38,39].

As depicted in **Figure 3.16**, the XPS spectra reveal that the binding energies of $Pd3d_{5/2}$ and $Pd3d_{3/2}$ peaks are situated at 335.66 eV and 340.96 eV, respectively, which are slightly offset towards higher binding energies. In contrast, the Au $4f_{7/2}$ and Au $4f_{5/2}$ peaks of Pd-Au clearly shifted towards lower binding energy levels, with Au $4f_{7/2}$ and $4f_{5/2}$ peaks present at lower binding energies of 83.38 and 87.0 eV, respectively. This tendency suggests that Au atoms received electrons from Pd atoms via alloying interaction, corroborating alloy formation[40,41]. According to the charge compensation concept, Pd atoms in Pd-Au might exhibit poor electronic states, which could be crucial in augmenting the reaction pathway of cross-coupling, thereby leading to heightened activity.

Binding energies centered at 335.66 eV ($Pd3d_{5/2}$) and 340.96 eV ($Pd3d_{3/2}$) are attributed to the characteristic signature of metallic Pd (see **Figure 3.16**). A positive shift (0.76 eV) in the $Pd3d_{5/2}$ peak relative to the pure Pd peak (334.9 eV) is observed in the core-shell NPs[42].

Considering the TEM results, this energy may signify possible particle-size effects, whereby Pd core-hole screening during photoemission results in a higher binding energy for small particles[43]. Based on XPS data, the presence of Cl^- 2p at 198.68 eV with %At Conc. 0.14 is confirmed, whether this Cl is adsorbed on the Pd itself or neighbouring sites. This latter point echoes the findings of Shen et al.[44], who reported analogous Pd binding energies for Cl^- containing catalysts, suggesting that Pd maintains a more positive valency, resulting in a more stable Pd surface structure than the corresponding halide-free system. Notably, a slight variance was observed when comparing the XPS data of the fresh 2.5%Pd-2.5%AuH/Al_2O_3 (see **Figure 3.16 a & b**) with the reused catalyst (see **Figure 3.16 c & d**) and the corresponding TEM **Figures (3.14 and 3.15)**. Nevertheless, the Pd-Au bimetallic catalyst demonstrated an ability to be easily recovered and reused in the amination of phenol (cross-coupling reaction) (see Chapter 5) up to three times without any discernible efficiency loss[45].

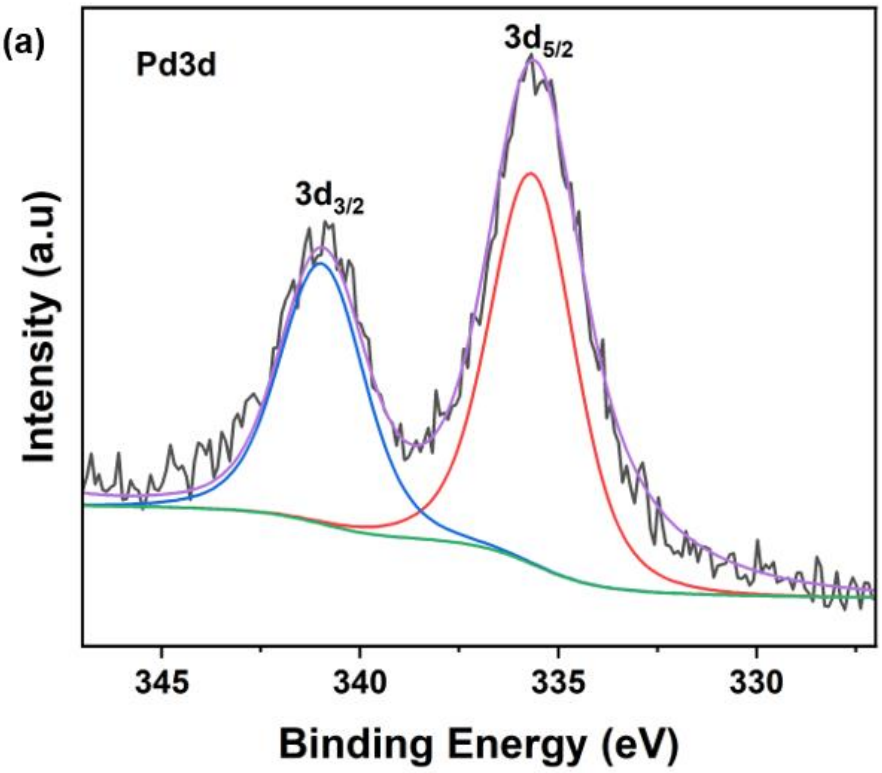

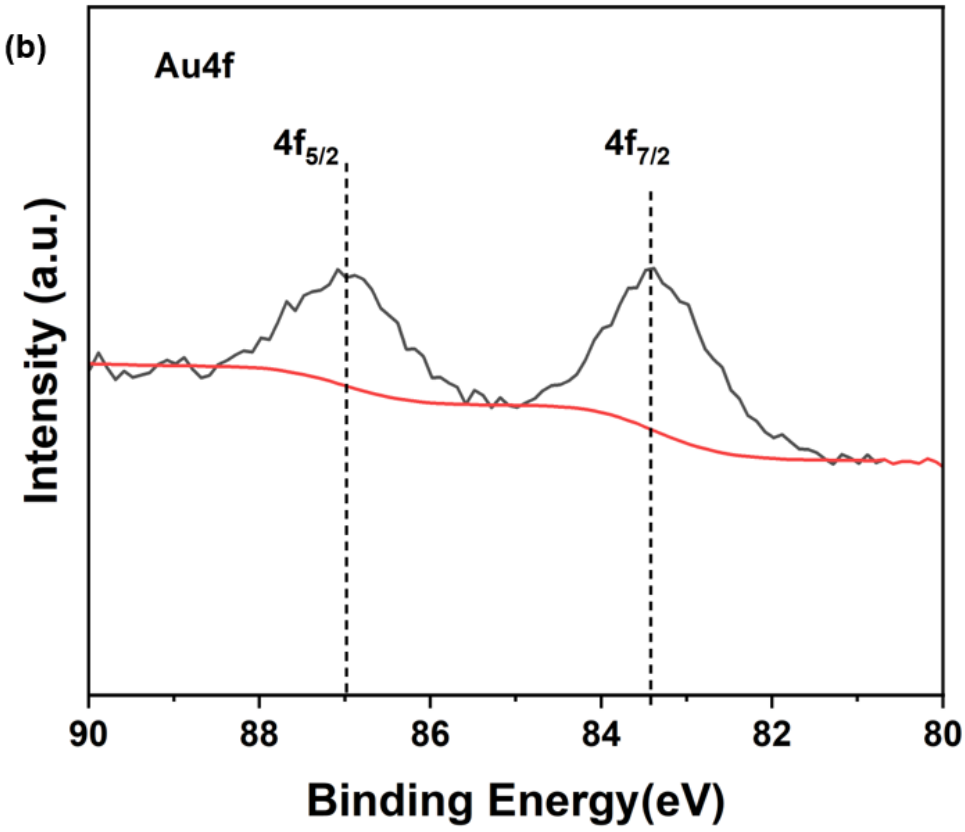
(b)
Au4f
4f5/2
4f7/2
Intensity (a.u.)
90
88
86
84
82
80
Binding Energy(eV)

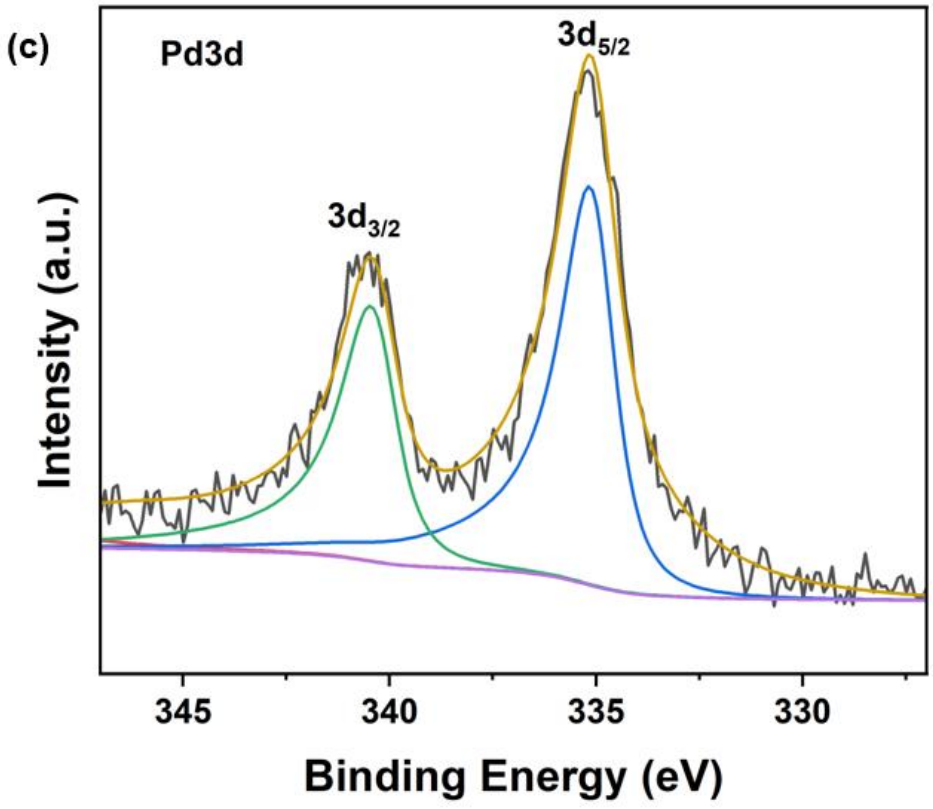
(c)
Pd3d
3d5/2
3d3/2
Intensity (a.u.)
345
340
335
330
Binding Energy (eV)

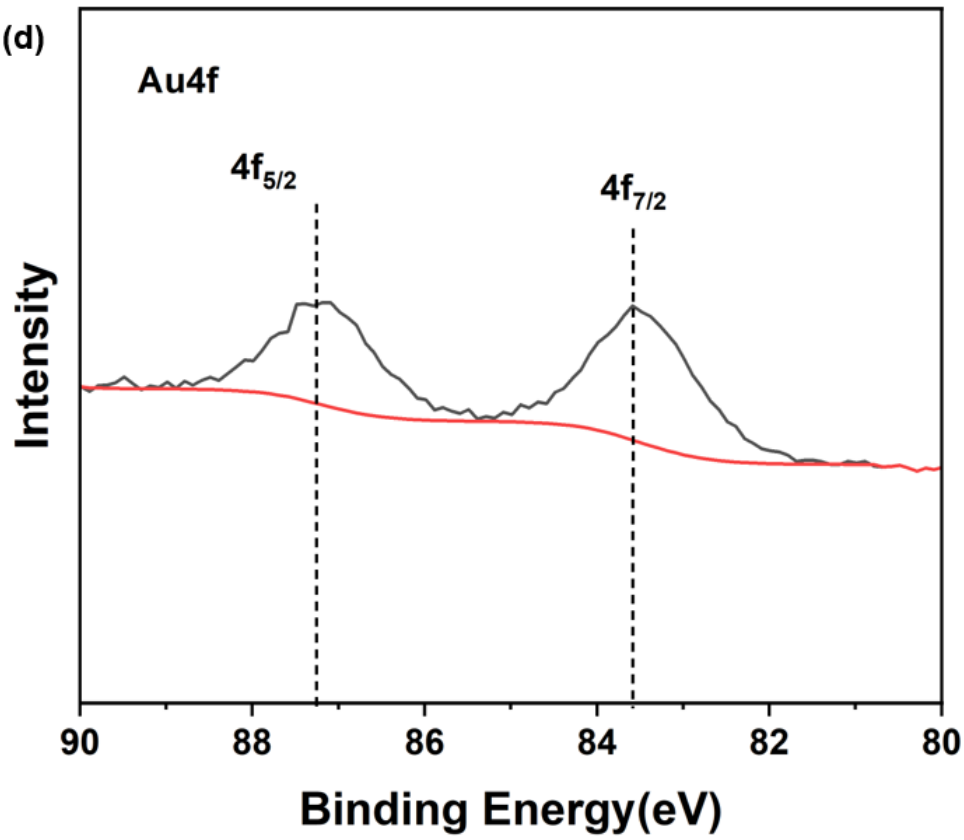

Figure 3.16: Pd 3d and Au 4f XPS spectra of 2.5%Pd-2.5%AuH/Al_2O_3 catalyst (a & b), reused 2.5%Pd-2.5%AuH/Al_2O_3 catalyst (c & d)

The XPS spectra, depicted in **Figure 3.17 a & c**, reveals the binding energies of $Pd3d_{5/2}$ and $Pd3d_{3/2}$ peaks are situated at 335.74 eV and 341.04 eV respectively, which signifies a shift to 0.84 eV on the higher side in binding energy. Interestingly, the Au $4f_{7/2}$ and Au $4f_{5/2}$ peaks of Pd-Au (displayed in **Figure 3.17 b & d**) do not demonstrate a shift in binding energy, with Au $4f_{7/2}$ and Au $4f_{5/2}$ peaks existing at binding energies of 83.81 eV and 87.01 eV, respectively. Notably, for the catalyst prepared using the sol-immobilisation method, no peak associated with Cl^- is observed. **Tables 3.3 and 3.4** provide insight into the constituents of the 2.5%Pd-2.5%Au/Al_2O_3 S_{im} and 2.5%Pd-2.5%AuH/Al_2O_3 M_{im} catalysts, which were prepared using both the modified impregnation (2.5%Pd-2.5%AuH/Al_2O_3 M_{im}) and sol-immobilisation (2.5%Pd-2.5%Au/Al_2O_3 S_{im}) techniques. Based on the XPS data presented in **Tables 3.3 and 3.4**, the composition of Pd-Au alloys was assessed, and the Pd/Au molar ratio for 2.5%Pd-2.5%Au/Al_2O_3 S_{im} was found to be 1.7, which changed to 3.2 after the catalyst was reused. Conversely, the Pd/Au molar ratio for the 2.5%Pd-2.5%AuH/Al_2O_3 M_{im} catalyst showed a slight change from 2.1 before use to 2.6 after reuse. In both catalysts, excess Au was noted as the Au metal peak.

These results indicate that the Pd/Au molar ratio changes in both catalysts upon reuse, suggesting that the reusability of these catalysts impacts the Pd-Au alloy's

composition. This could have significant implications on the catalyst's performance and stability, thus warranting further investigation. The absence of Cl^- in the catalyst prepared using sol-immobilisation suggests different reaction environments and potential catalyst behaviours between the two preparation methods. This difference further emphasises the importance of catalyst preparation techniques and their influence on the final properties and performance of the catalyst.

Table 3.3: XPS data of 2.5%Pd-2.5%Au/Al_2O_3 S_{im} and 2.5%Pd-2.5%AuH/Al_2O_3 M_{im} catalysts:

Sample Identifier	**Name**	**Position**	**%At Conc.**	**Sample Identifier**	**Name**	**Position**	**%At Conc.**
2.5%Pd-2.5%Au/Al_2O_3 **S_{im}**	Pd 3d	335.74	0.06	2.5%Pd-2.5%AuH/Al_2O_3 **M_{im}**	Pd 3d	335.66	0.10
	Pd 3d	341.04	0.04		Pd 3d	340.96	0.07
	Au 4f	83.81	0.06		Au 4f	83.38	0.08
	Al 2p	74.61	15.97		Al2p	74.28	17.13
	O 1s	531.51	27.08		O 1s	531.08	27.78
	C 1s	284,81	6.98		C 1s	284.68	5.03
	O 1s	531.01	27.71		O 1s	530.68	29.02
	C 1s	285.01	6.66		C 1s	284.68	3.98
	S 2p	169.01	0.19		Cl 2p	198.68	0.14
	Al 2p	74.01	15.16		S 2p	161.68	0.08
	Pd 3d	335.01	0.14		Al 2p	73.68	16.34
	Au 4f	83.01	0.04		Pd 3d	334.68	0.21
					Au 4f	82.68	0.06
	Ratios				**Ratios**		
	Pd/Au	1.7			Pd/Au	2.1	
	O/Al	1.7			O/Al	1.6	

Table 3.4: XPS data of 2.5%Pd-2.5%Au/Al_2O_3 S_{im} and 2.5%Pd-2.5%AuH/Al_2O_3 M_{im} reused catalysts:

Sample Identifier	**Name**	**Position**	**%At Conc.**	**Sample Identifier**	**Name**	**Position**	**%At Conc.**
2.5%Pd-2.5%Au/Al_2O_3 **S_{im}**	Pd 3d	335.13	0.08	2.5%Pd-2.5%AuH/Al_2O_3 **M_{im}**	Pd 3d	335.11	0.13
	Pd 3d	340.43	0.05		Pd 3d	340.41	0.08
	Au 4f	83.22	0.05		Au 4f	83.59	0.1
	Al 2p	74.42	19.01		Al 2p	74.39	22.25
	O 1s (Al2O3)	531.1	26.09		O 1s (Al2O3)	531.05	33.76
	O 1s (OH/Organic)	532.21	22.25		O 1s (OH/Organic)	532.18	21.08
	C 1s	284.7	22.27		C 1s	284.66	13.54
	C 1s	286.09	6.52		C 1s	285.87	6.12
	C 1s	288.53	3.65		C 1s	288.52	2.73
					Cl 2p	198.49	0.17
	Ratios				**Ratios**		
	Pd/Au	3.2			Pd/Au	2.6	
	O/Al	1.4			O/Al	1.5	

The intricate relationship between chloride ions and gold nanoparticles is indeed a significant area of research. As you mentioned, chloride ions are known to promote the mobility and agglomeration of gold species after heat treatment, often leading to a decrease in the catalytic activity of supported gold-based catalysts. Thus, numerous studies have attempted to eliminate chloride ions to enhance the activity of these catalysts[46]. On the other hand, some researchers have employed excess chloride ions to decrease the particle size of supported noble metal nanoparticle-based catalysts, resulting in potentially higher catalytic activities due to an increased surface area. Your current research demonstrates a similar approach, wherein excess Cl^- ions are utilized to synthesize highly active and stable supported gold-palladium nanoparticle-based catalysts from their precursors ($HAuCl_4$ and $PdCl_2$).

In the aqueous medium, the presence of both Au(III) and Pd(II) metal ions enables the formation of a more homogeneous mixture, which leads to improved dispersion during the impregnation step[47]. This is reflected in the higher percentage At Conc. for Pd and Au in the catalyst prepared via modified impregnation as compared to sol-immobilisation, as evident in the tables.

The presence of Cl^- ions seems to be crucial in maintaining the metal's distribution and its interaction with the support, leading to enhanced catalytic activity. This is visible in the XPS data, where the Cl^- ion remains present for catalysts prepared by modified impregnation. In contrast, the XPS results for catalysts prepared via sol-immobilisation, which lack excess chloride ions, demonstrate decreased activity. Furthermore, the increase in the Pd/Au ratio in the reused samples could potentially indicate the production of Pd^{2+}, which could contribute to the reduced activity of the sol-immobilisation catalyst. Despite having smaller particle sizes (as indicated by TEM data), which usually leads to increased activity, the sol-immobilisation catalyst's activity has declined, which underscores the importance of chloride ions in this system.

In conclusion, while chloride ions have been seen as detrimental in some scenarios, they appear to play a beneficial role in the preparation of your gold-palladium nanoparticle-based catalysts. This complex role of chloride ions presents an interesting avenue for further research and potential optimizations in the preparation and application of these catalysts.

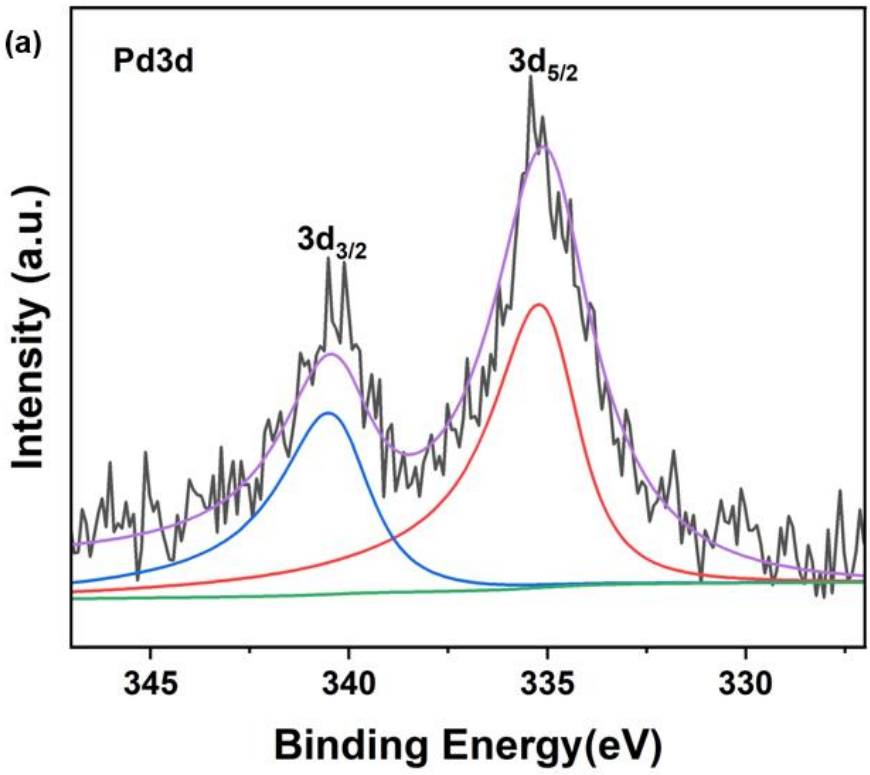

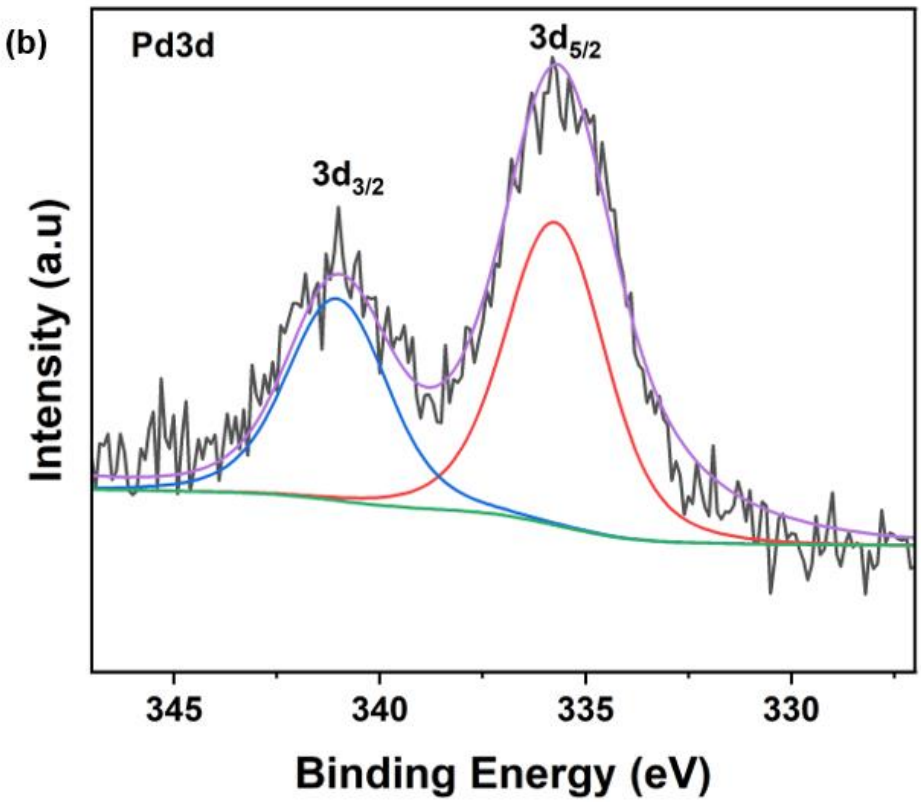
(b)
Pd3d
3d5/2
3d3/2
Intensity (a.u)
345
340
335
330
Binding Energy (eV)

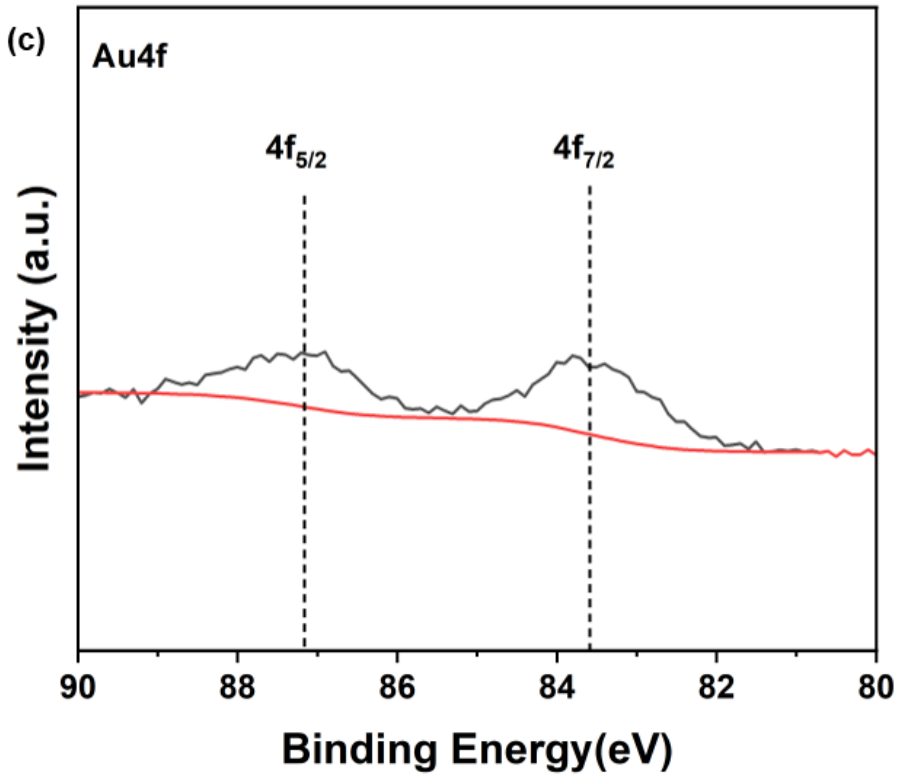
(c)
Au4f
4f5/2
4f7/2
Intensity (a.u.)
90
88
86
84
82
80
Binding Energy(eV)

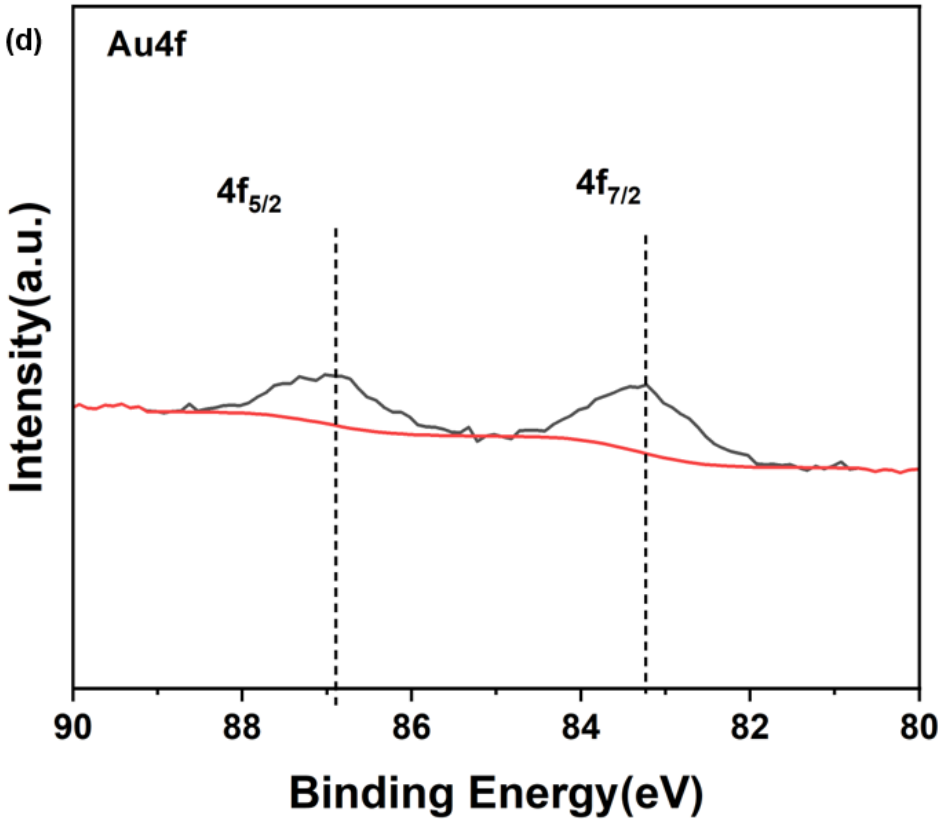

Figure 3.17: Pd 3d and Au 4f XPS spectra of 2.5%Pd-2.5%Au/Al_2O_3 catalyst (a & b), reused 2.5%Pd-2.5%Au/Al_2O_3 catalyst (c & d)

3.4.2. Bimetallic 2.5%Pd-2.5%Au/TiO_2 catalyst

The 2.5%Pd-2.5%Au/TiO_2 catalyst, renowned for its superior catalytic performance, benefits from the unique synergy of gold and palladium atoms, particle size, and nature of the active sites. Bimetallic catalysts such as Au-Pd frequently have their active sites situated at the interface of the two metals. The nanoparticle size significantly affects the catalyst's performance due to the increased surface-to-volume ratio. Two main preparation methods, sol-immobilisation and impregnation, can alter the catalyst properties. Typically, sol-immobilisation leads to better nanoparticle dispersion on the support, thereby enhancing the catalyst's activity. Conversely, impregnation may result in larger particles or agglomerates, diminishing the catalyst's performance, yet allows superior control over metal loading[48]. Post-preparation treatments such as calcination and reduction can significantly modify the catalyst. Calcination eliminates organic matter and alters the metal's oxidation state. Reduction reverts the metal to its active oxidation state. Both these processes can impact the dispersion, active sites, and overall catalyst performance. Support choice, like TiO_2, a popular choice due to its high surface area, thermal stability, and distinctive redox properties, profoundly impacts these factors. The metal-support interaction affects the

metal nanoparticle dispersion, catalyst stability, and the nature of the active sites[36]. For uncharacterized catalysts, researchers can refer to similar literature to infer properties. For instance, if a specific 2.5%Pd-2.5%Au/TiO_2 catalyst's particle size was not measured, researchers could draw upon analogous studies to gain understanding.

Techniques like Transmission Electron Microscopy (TEM), X-Ray Photoelectron Spectroscopy (XPS), and Brunauer-Emmett-Teller (BET) surface area measurement provide insights into catalysts' physicochemical properties. This understanding allows researchers to interpret catalytic data effectively and design more potent catalysts. Therefore, a detailed understanding of catalyst preparation, treatment, and characterization methods, along with support choice, is pivotal in optimizing the catalyst's design and performance for specific applications.

The XRD patterns of the bare TiO_2 and Au-Pd/TiO_2 samples (**Figure 3.18)**, obtained via sol-immobilisation, revealed eight distinct peaks. Located at 2θ values of 25.3°, 36.9°, 37.8°, 38.6°, 48.0°, 53.9°, 55.2° , and 62.7°, these peaks correspond to (1 0 1), (1 0 3), (0 0 4), (1 12), (2 0 0), (1 0 5), (2 1 1), and (2 0 4) anatase TiO_2 crystal facets (PDF No.21-1272), respectively[36,48]. These findings suggest that the Au-Pd nanoparticles are well-dispersed on the TiO_2 support, retaining the anatase structure of TiO_2, which is beneficial to the photocatalytic performance of the bimetallic catalyst. It is generally recognized that anatase TiO_2 provides a high specific surface area, contributing to the adsorption capacity and the photocatalytic activity of the catalyst. The accurate indexing of these facets further provides insights into the crystalline nature of the support, which is crucial for understanding the photocatalytic processes at the atomic scale. This characterization is essential as it directly relates to the overall performance and stability of the catalyst system.

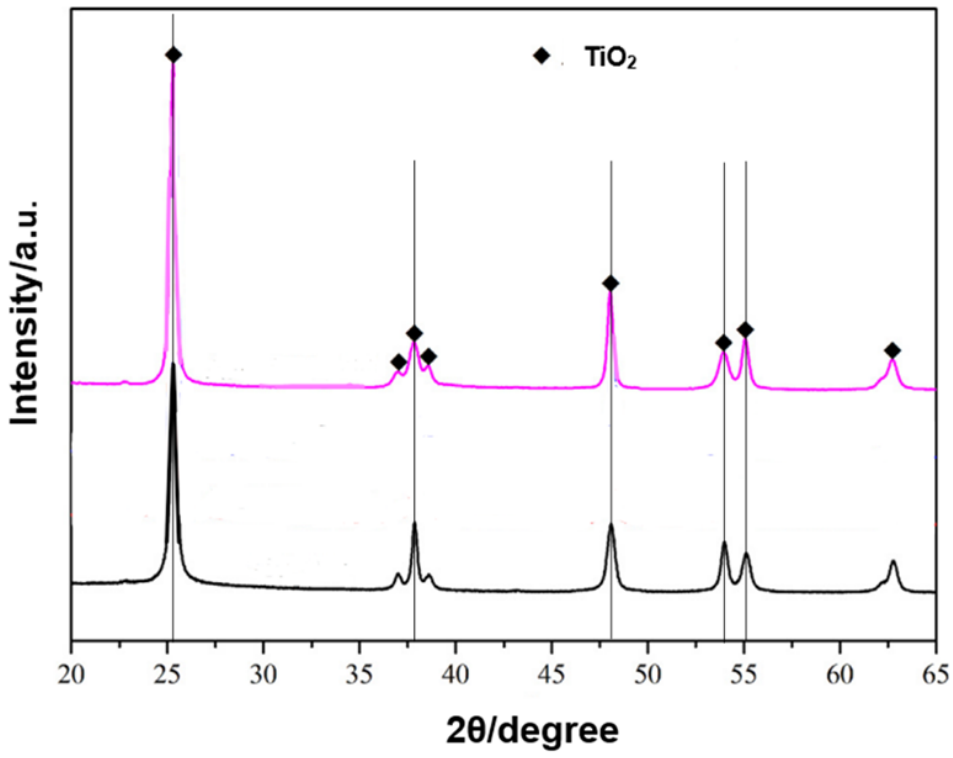

Figure 3.18: XRD patterns of series of TiO_2 and their corresponding 2.5%Pd-2.5%Au/TiO_2 catalyst

X-ray photoelectron spectroscopy (XPS) analysis was employed to ascertain the chemical states of Au, Pd, Ti, and O within the Au-Pd/TiO_2, as demonstrated in **Figure 3.19 (a, b).**The Au 4f spectra revealed two distinctive peaks for Au $4f_{5/2}$ and $4f_{7/2}$, positioned at 87.2 eV and 83.5 eV respectively, compared to the conventional spin-orbit split peaks for metallic Au, found at 87.7 eV and 84.0 eV. This 0.5 eV shift towards lower binding energy might suggest a charge transfer from Pd to Au, given that Au is more electronegative than Pd. Regarding Pd 3d, we observed two characteristic peaks at 340.9 eV and 335.6 eV, corresponding to $3d_{3/2}$ and $3d_{5/2}$, signifying that Pd^0 was integrated into the Au-Pd alloy rather than forming Pd(II) species. In previous research, metallic Pd's 3d region was reported to have peaks at 340.4 eV and 335 eV. However, in our study, a shift of approximately 0.5 eV to higher binding energy was detected, providing further evidence of the electronic interaction between Au and Pd. Consequently, the XPS results propose an alloying of Au and Pd[48].

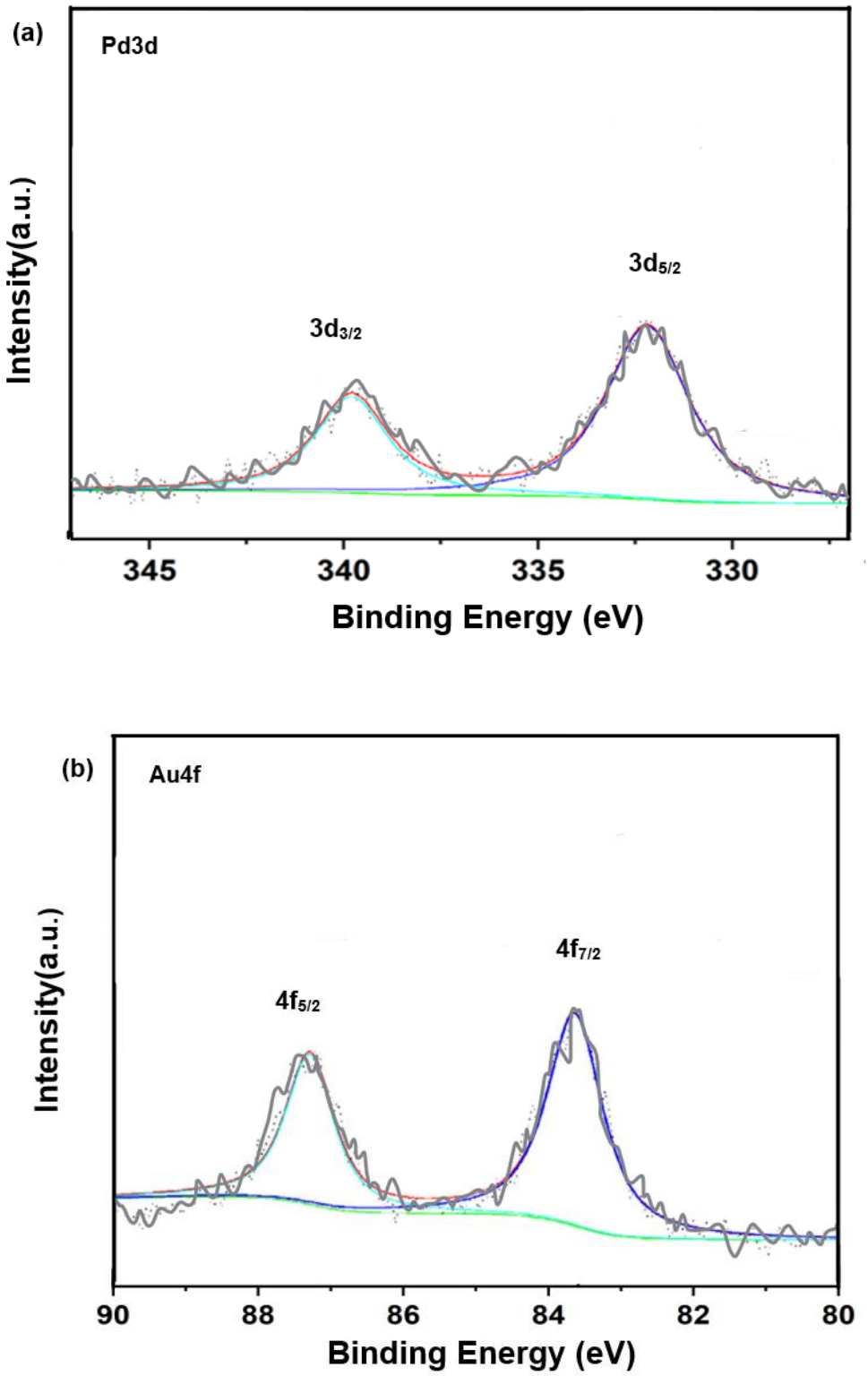

Figure 3.19: XPS spectra of Au 4f (a) and Pd 3d (b) for 2.5%Pd-2.5%Au/TiO_2 catalyst.

Transmission electron microscopy (TEM) was used to assess the particle size distribution of Au-Pd nanoparticles (NPs) on the 2.5%Pd-2.5%Au/TiO_2 catalyst. **Figure 3.20** reveals that the Au-Pd NPs were markedly dispersed over the TiO_2

supports. Measurements from 150 individual nanoparticles taken from the TEM images revealed a consistent particle size distribution for the 2.5%Pd-2.5%Au/TiO_2 catalyst, with an average Au-Pd particle size of 3.3 nm. This observation is in line with previous studies suggesting that particle size significantly influences catalytic performance[1]. Consequently, maintaining such uniformity in particle size could enhance catalytic efficiency.

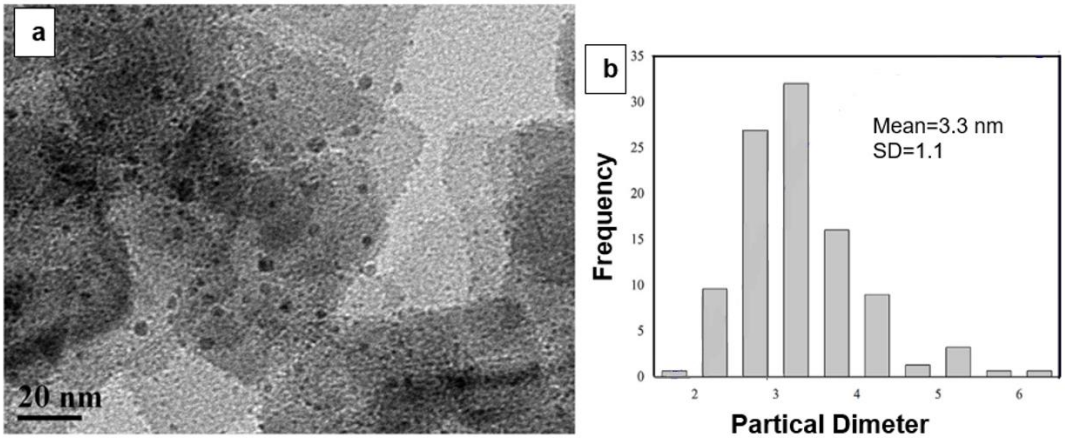

Figure 3.20: (a) TEM images and (b) Au-Pd particle size distribution histograms of 2.5%Pd-2.5%Au/TiO_2 catalyst

XPS analysis was utilised to verify the presence or lack of Cl^- in the fresh 2.5%Pd-2.5%AuH/TiO_2 catalyst (**Table 3.5:)** prepared by modified impregnation . Interestingly, neither the fresh nor the spent catalyst showed traces of Cl^-, implying it was below the detection limit of XPS (approximately 0.1 atom %)[49].

Table 3.5: XPS of 2.5%Pd-2.5%AuH/TiO_2 catalyst:

Sample Identifier	**Name**	**Position**	**%At Conc.**
2.5%Pd-2.5%AuH/TiO_2	Pd 3d	334.8	0.07
	Au 4f	83.3	0.03
	Ti 2p	459.1	14.73
	O 1s	531.01	35.32
	C 1s	285.01	49.48
	C 1s	284,81	6.98
	Ratios		
	Pd/Au	2.3	
	O/Ti	2.4	

Notably, post-reaction, the catalyst showed no visible metal particles in the 1−2 nm range[50].

The highest stability of the 2.5%Pd-2.5%AuH/TiO_2catalyst can be attributed to its reduced gold content and the minimal presence of Cl^-, coupled with moderate Au content. This suggests that the Cl^- content and the ratio of Pd to Au are important parameters in defining the catalyst's stability, highlighting the need for more focused research on tuning these variables for optimal catalytic performance.

3.4.3. Bimetallic 2.5%Pd-2.5%RuH/Al_2O_3 and 0.5%Pd-0.5%RuH/Al_2O_3

Ruthenium, another metal that can synergize with palladium, forms an active bimetallic Pd-RuH catalyst on an alumina support, proficient in the selective hydrogenation of phenol to cyclohexanol[51]. While monometallic palladium exhibits high activity for selective hydrogenation of phenol to cyclohexanone, adding ruthenium alters its behaviour, promoting the selective hydrogenation of phenol to cyclohexanol[50]. This phenomenon was elaborated in Chapter 4, where Pd-RuH/Al_2O_3 was prepared via modified impregnation and reduced using $NaBH_4$ to form the active catalyst. Notably, two different loadings of Pd-RuH/Al_2O_3 (5 % and 1 %) were evaluated for their efficiency in phenol hydrogenation and auto-transfer reaction for nitrobenzene with benzyl alcohol (see Chapter 6).

For 2.5%Pd-2.5%RuH/Al_2O_3 and 0.5%Pd-0.5%RuH/Al_2O_3, XRD, TEM, and XPS investigations were carried out to better understand the catalyst stability and activity[52–54].

TEM analysis showed in **Figures 3.21, 3.22** and **3.23**, that particles in both catalysts adopted a sphere-like morphology, likely attributed to surface energy minimization. The fewer particles observable per image hint at low loading and high dispersion, particularly in the 0.5%Pd-0.5%RuH/Al_2O_3 samples. The average particle size for the 2.5%Pd-2.5%RuH/Al_2O_3 catalyst was around 3.2 nm, whereas the 0.5%Pd-0.5%RuH/Al_2O_3 catalyst exhibited a smaller particle size of 2.17 nm, possibly owing to increased surface mobility of Ru during the preparation process[54]. Furthermore, TEM-EDX analysis (**Figure 3.21, 3.22** and **3.23**) confirmed the distribution of Pd and Ru in the bimetallic system, complementing XPS data obtained later. For reused 0.5%Pd-0.5%RuH/Al_2O_3 samples, the average particle size was 3 nm, similar to their monometallic counterparts, but slightly smaller than the 2.5%Pd-2.5%RuH/Al_2O_3 catalyst. These observations suggest a geometric effect between Pd and Ru and indicate that excessive Ru loading may induce metal particle aggregation.

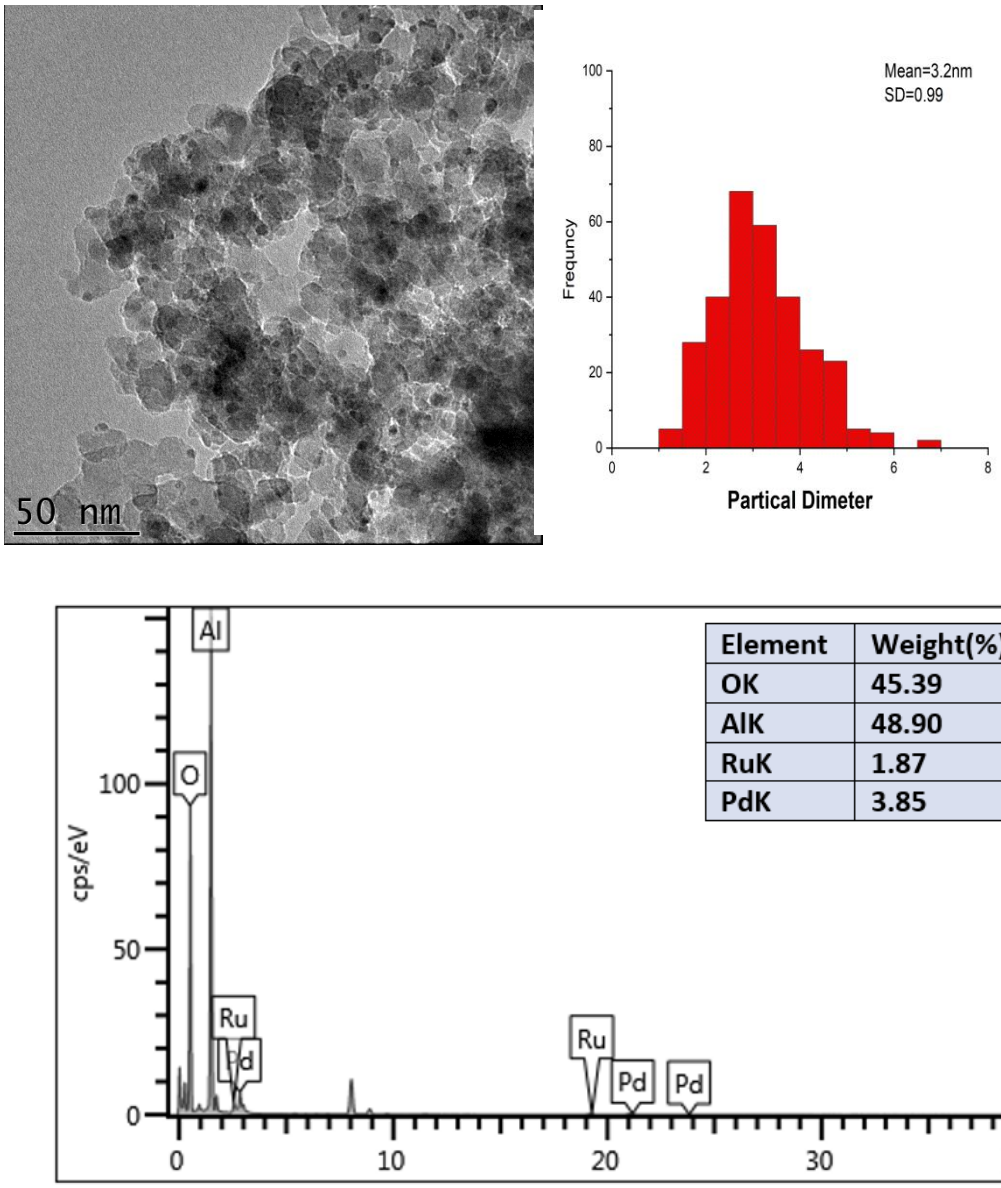

Figure 3.21: TEM of 2.5%Pd-2.5%RuH/Al_2O_3, TEM image with size distribution histograms of the Pd-RuH nanoparticles and TEM–EDX spectrum

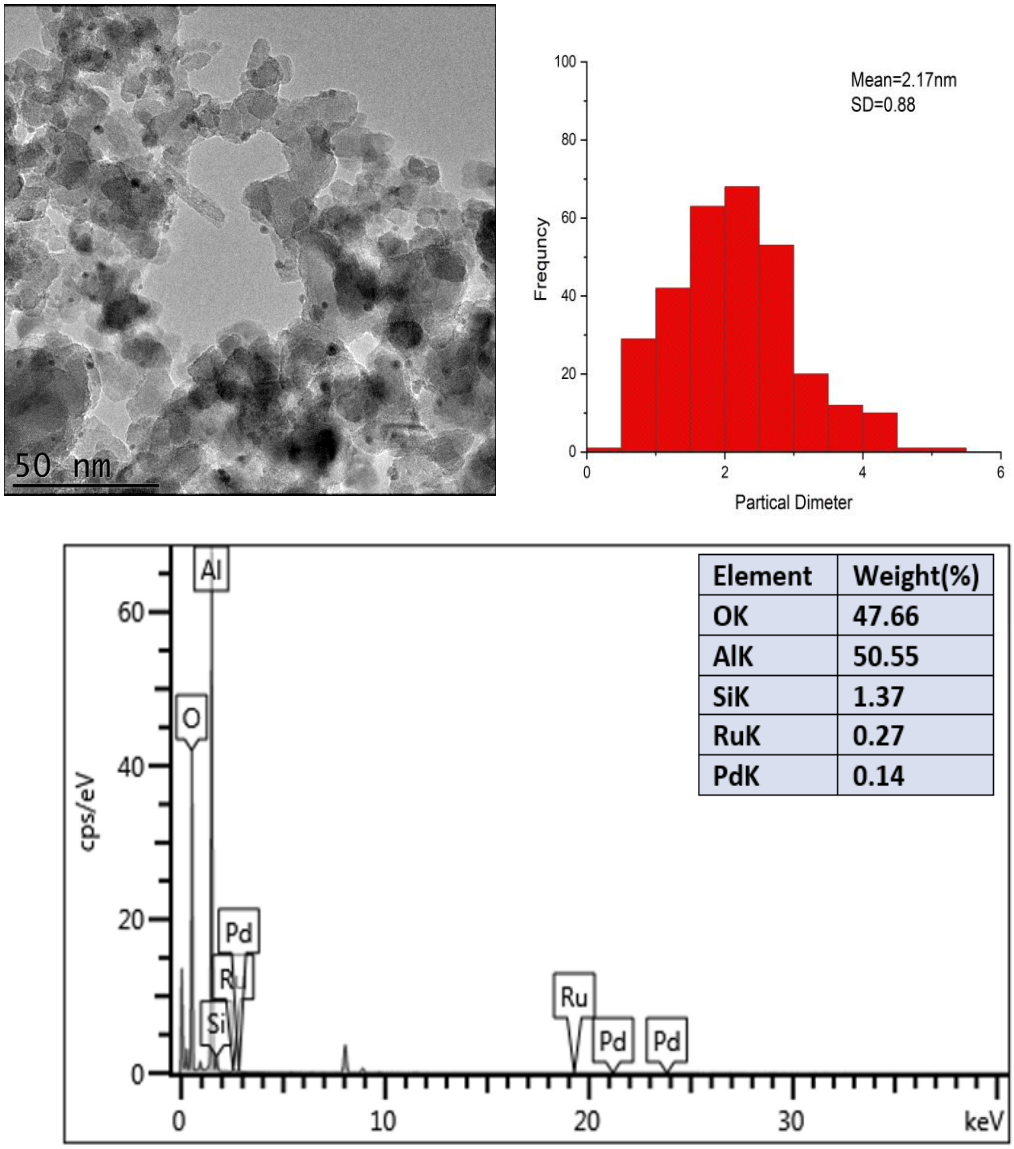

Figure 3.22: TEM of 0.5%Pd-0.5%RuH/Al_2O_3 TEM image with size distribution histograms of the Pd-RuH nanoparticles, TEM–EDX spectrum

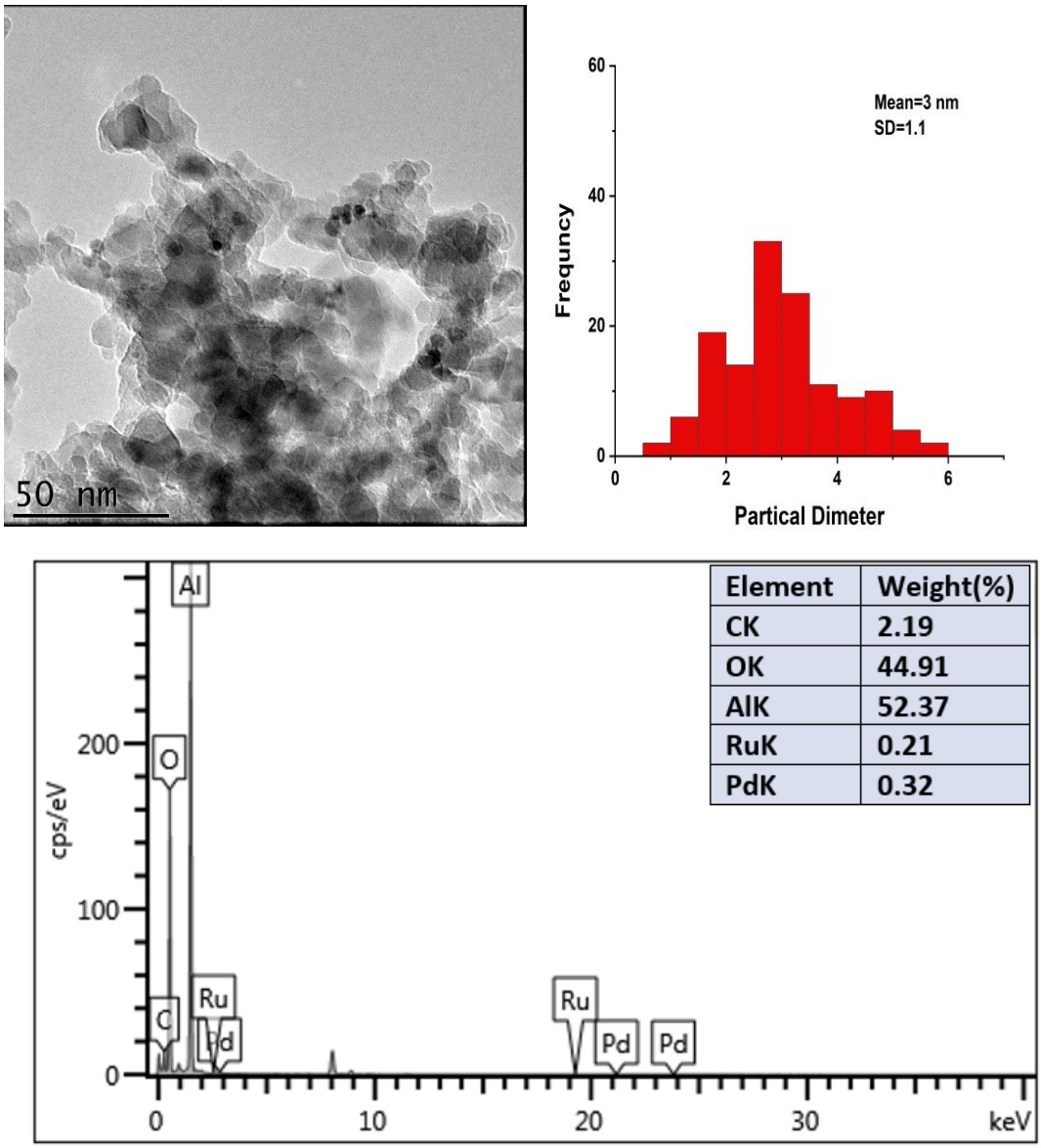

Figure 3.23: TEM of 0.5%Pd-0.5%RuH/Al_2O_3 reused TEM image with size distribution histograms of the Pd-RuH nanoparticles, TEM–EDX spectrum

XPS examinations offered key insights into the Ru-Pd interactions and the valence states of the surface metal species in these samples[55]. Specifically, the Pd $3d_{5/2}$ and Ru $3d_{5/2}$ spectra of the 2.5%Pd-2.5%RuH/Al_2O_3 catalyst is shown in **Figure 3.24(c & d)** compared with XPS for mono metallic Pd (see **Figure 3.24 b**) and Ru (see **Figure 3.24 a**) catalyst exhibited noticeable shifts. The Pd core-level binding energy bifurcated into two peak pairs associated with the higher Pd $3d_{5/2}$ energy value of PdO (~ 336.18 eV) the lower energy of metallic Pd^0 (~334.9 eV). On further inspection **(Figure 3.24 d)** , the Pd^0 and Pd^{2+} peaks of the 2.5%Pd-2.5%RuH/Al_2O_3 catalyst showed slight shifts (335.64 eV and 337.19 eV, respectively), (positive shift (0.74–0.79 eV)), indicative of an alteration in the electronic properties of Pd when alloyed with Ru, substantiated by the binding energy shift of Ru. Concurrently, the Ru $3d_{3/2}$

and Ru $3d_{5/2}$ peaks overlapped with the C 1s. The Ru $3d_{5/2}$ XPS signal revealed the chemical state of Ru (**Figure 3.24 c),** , with the binding energies of Ru $3d_{5/2}$ in the catalyst (280.82) being credited to Ru^0. The 0.82 -eV shift of Ru peaks suggests a strong charge-transfer interaction between the Ru and Pd atoms in the bimetallic catalyst, with Ru mainly existing in the Ru^0 state.

To gain a deeper understanding of the XPS results, the valence states of the surface Pd and Ru species were derived using the peak-fitting method. The XPS-derived oxidized and reduced metal states ratio for Pd was Pd^{2+}/ Pd^0 =1.2. Such alterations in the electronic state of Pd and Ru in bimetallic Pd-Ru samples have been documented in prior research affirming the significant interactions between Pd and Ru in the bimetallic catalysts[56].

This study aligns with the recent surge in interest in bimetallic catalysts, primarily due to their distinctive properties that can be tuned by varying the metal combinations and the atomic ratios, allowing the optimisation of catalytic activity and selectivity. Further investigation into the Ru-Pd alloy could elucidate the charge-transfer dynamics and pave the way for future catalyst design.

(a) RuH/Al_2O_3

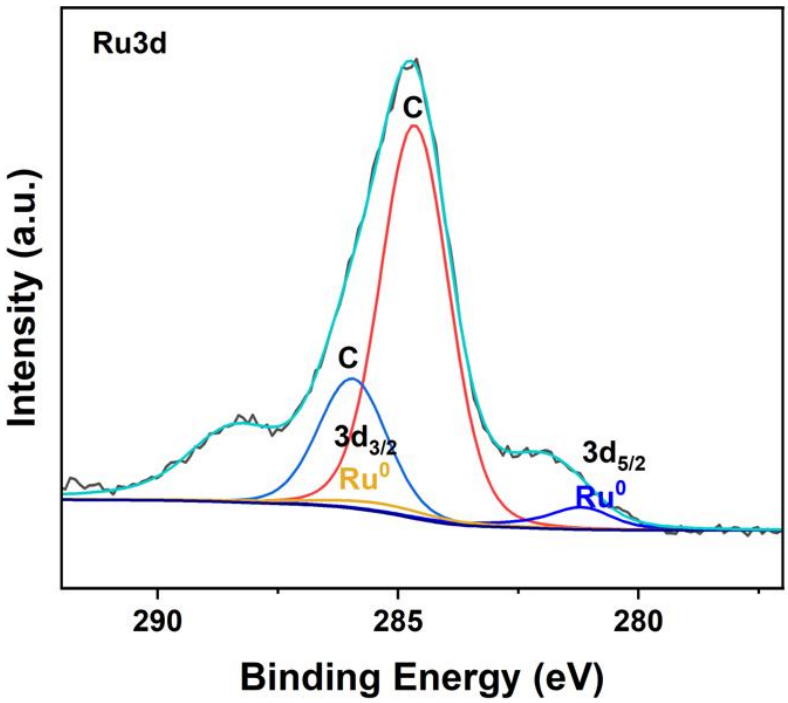

(b) PdH/Al_2O_3

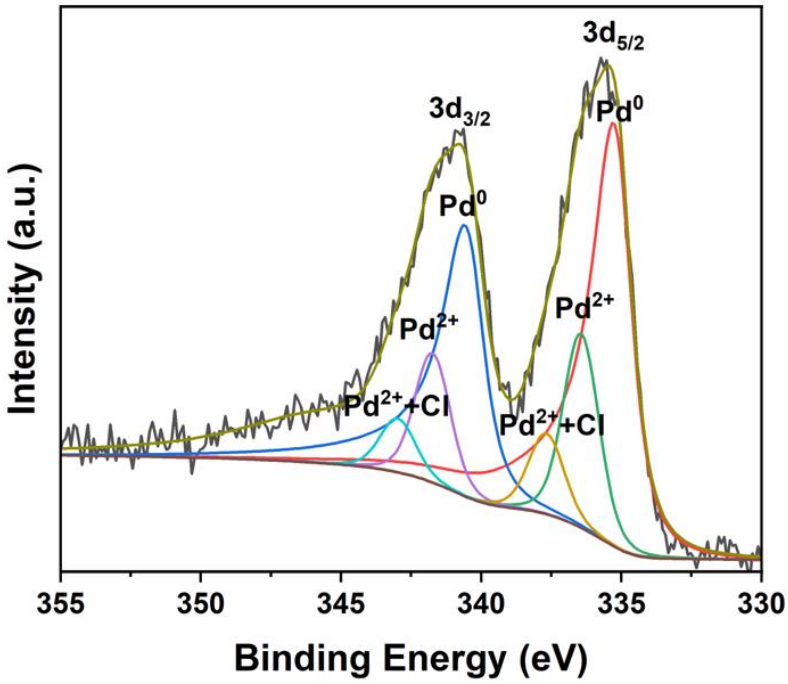

(c) $2.5\%Pd\text{-}2.5\%RuH/Al_2O_3$

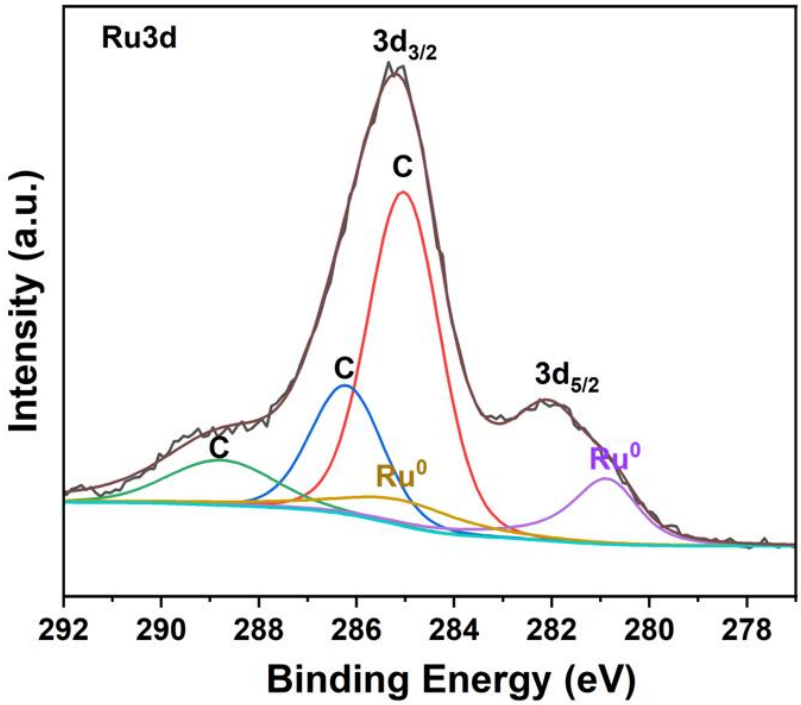

(d) 2.5%Pd-2.5%RuH/Al_2O_3

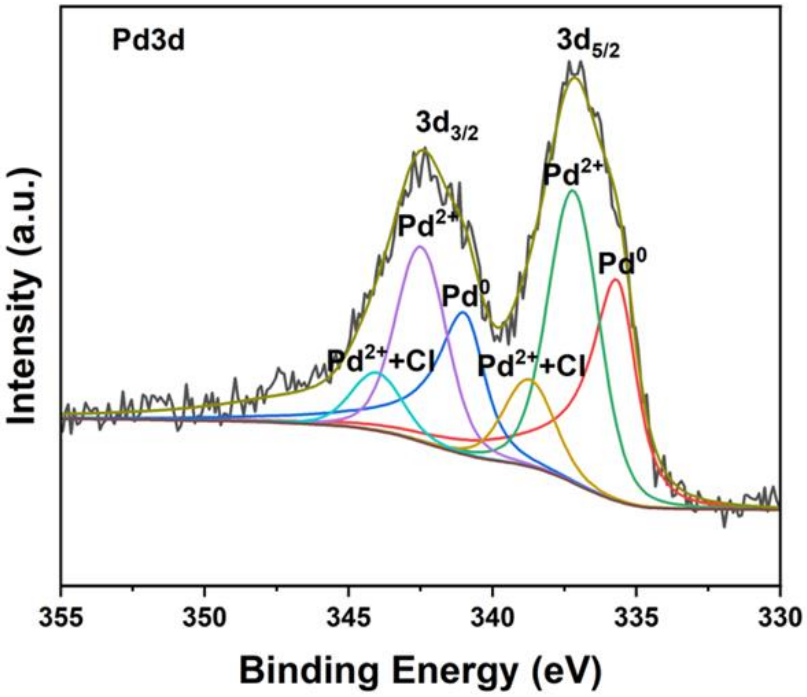

Figure 3.24: Pd 3d and Ru 3d XPS spectra of monometallic 5%RuH/Al_2O_3 (a) and 5%PdH/Al_2O_3 (b), and bimetallic 2.5%Pd-2.5%RuH/Al_2O_3 catalyst (c & d)

The influence of metal loading on the synthesis of the Pd-Ru bimetallic catalyst was assessed by analysing the electronic structure of the low-loading 0.5%Pd-0.5%RuH/Al_2O_3 catalyst (**Figure 3.25)** and reused samples using XPS. XPS allows the elucidation of surface elemental composition and oxidation state, providing key insights into the catalyst's structure (see **Table 3.6** The XPS data revealed distinct peaks related to Pd metal and Pd^{2+}, with the Pd^{2+}/Pd^0 molar ratio being 0.6 and 0.3 for the 0.5%Pd-0.5%RuH/Al_2O_3 and reused catalyst respectively. A singular peak corresponding to Ru^0 was also observed, positioned at 279.91 and 280.75 for the fresh and reused samples, respectively[52,56]. Interestingly, no Pd peaks were observed, a phenomenon likely due to the small particle size of the catalysts. This observation aligns with TEM data, which previously reported mean particle sizes of 2.17 nm and 3 nm, both of which are less than 5 nm and are thus too small to be detected by XPS, which typically measures up to approximately 5 nm from the sample surface. The presence of Pd in the prepared samples was confirmed exclusively via the TEM–EDX spectrum, reinforcing the sensitivity and complementary nature of these techniques in characterizing nanoscale catalysts.

These findings underscore the crucial role of metal loading in determining the catalyst's electronic structure and surface composition, providing valuable insights for the optimisation of bimetallic catalyst synthesis.

(a) 0.5%Pd-0.5%RuH/Al_2O_3

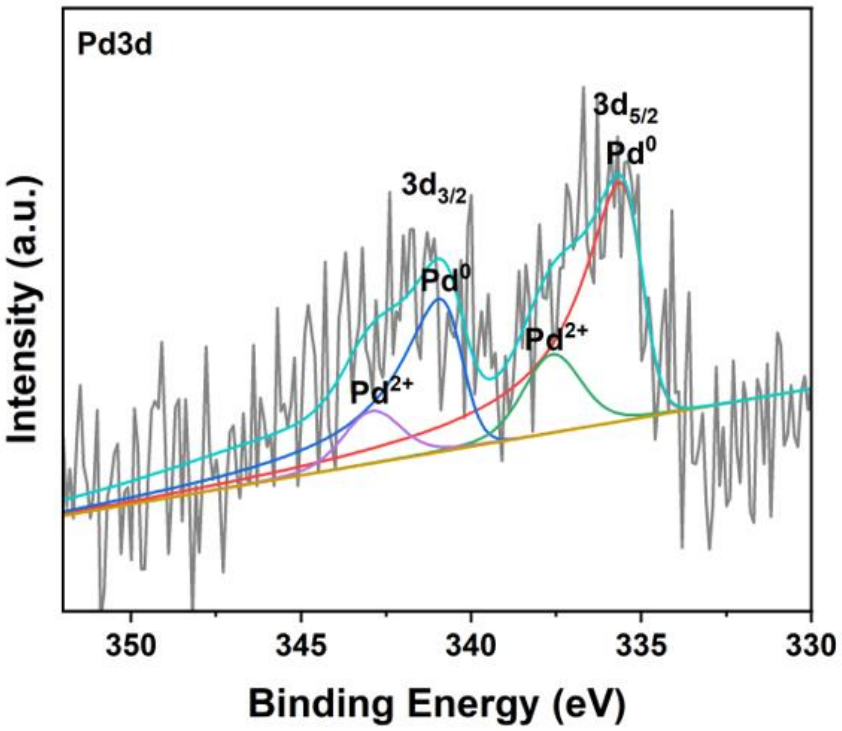

(b) 0.5%Pd-0.5%RuH/Al_2O_3

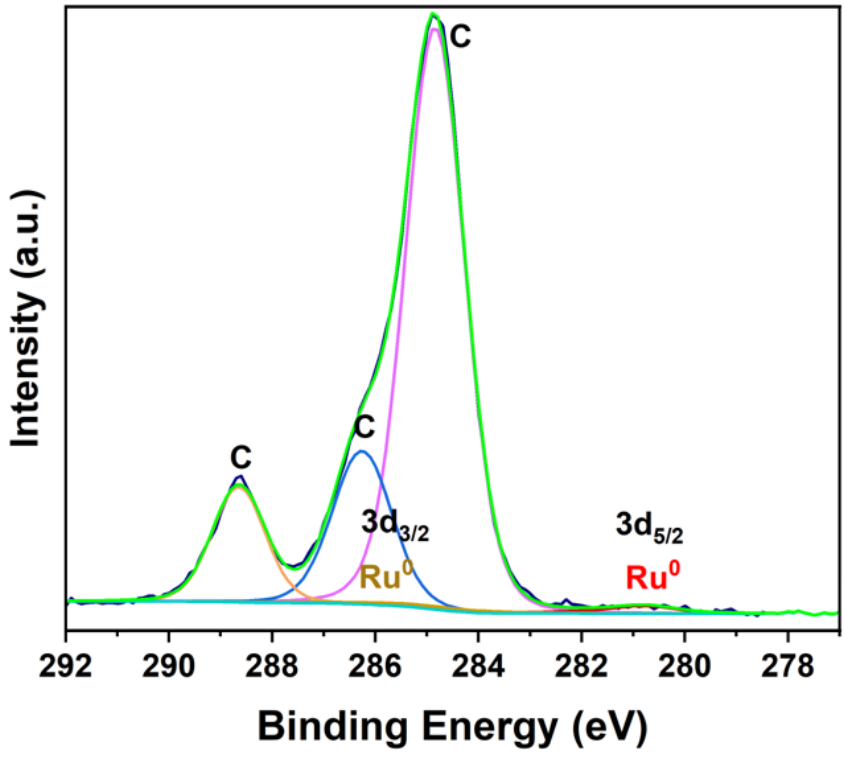

Figure 3.25: Pd 3d (a) and Ru 3d (b) XPS spectra of 0.5%Pd-0.5%RuH/Al_2O_3 catalyst.

Table 3.6: XPS data of 0.5%Pd-0.5%RuH/Al_2O_3 and reused 0.5%Pd-0.5%RuH/Al_2O_3catalysts

Compound	Pd^0 Position/ %At Conc.	Pd^{2+}3d Position/ %At Conc.	Cl^-2p Position/ %At Conc.	$Ru^0$3d Position/ %At Conc.	C1s Position/ %At Conc.
0.5%Pd-0.5%RuH/Al_2O_3	335.31/0.55	336.34/0.33	198.99/0.7	279.91/0.22	284.96/22.98
0.5%Pd-0.5%RuH/Al_2O_3 Reused	335.41/0.06	337.62/0.02	199.4/0.35	280.75/0.05	284.84/31.92

The X-ray diffraction (XRD) patterns of Al_2O_3 and 2.5%Pd-2.5%RuH/Al_2O_3 catalysts were compared with bimetallic catalysts pairing Pd with various noble and non-noble metals (Ru, Au, Ni, Fe, and Cu) supported on Al_2O_3, as well as with monometallic Pd and Ru. All catalysts were synthesized through a modified impregnation method and reduced with $NaBH_4$ (refer to Chapter 2, Section 2.2.2 and **Figure 3.26**). The minor changes in the XRD patterns when compared to pure Al_2O_3 indicate that the mesoporous structure of Al_2O_3 is largely preserved upon metal addition. Distinct peaks at 2θ values of 38.4°, 42.2°, 44.0°, 69.4°, and 78.4° match the (100), (002), (101), (110), and (103) planes of Ru metal (as per JCPDS Card no. 06-0663). Absence of Pd characteristic peaks, as seen in **Figure 3.26**, could be attributed to its low loading or potential overlap with Al_2O_3's broad, high-intensity peaks[54]. An interesting variation in XRD diffraction patterns related to the 2.5%Pd-2.5%RuH/Al_2O_3 catalyst was observed, which has been detailed in the preceding section.

These findings highlight the structural stability of Al_2O_3 support and indicate the successful incorporation of Ru and Pd into the bimetallic catalysts, even though Pd detection proves challenging due to low loading or peak overlap issues.

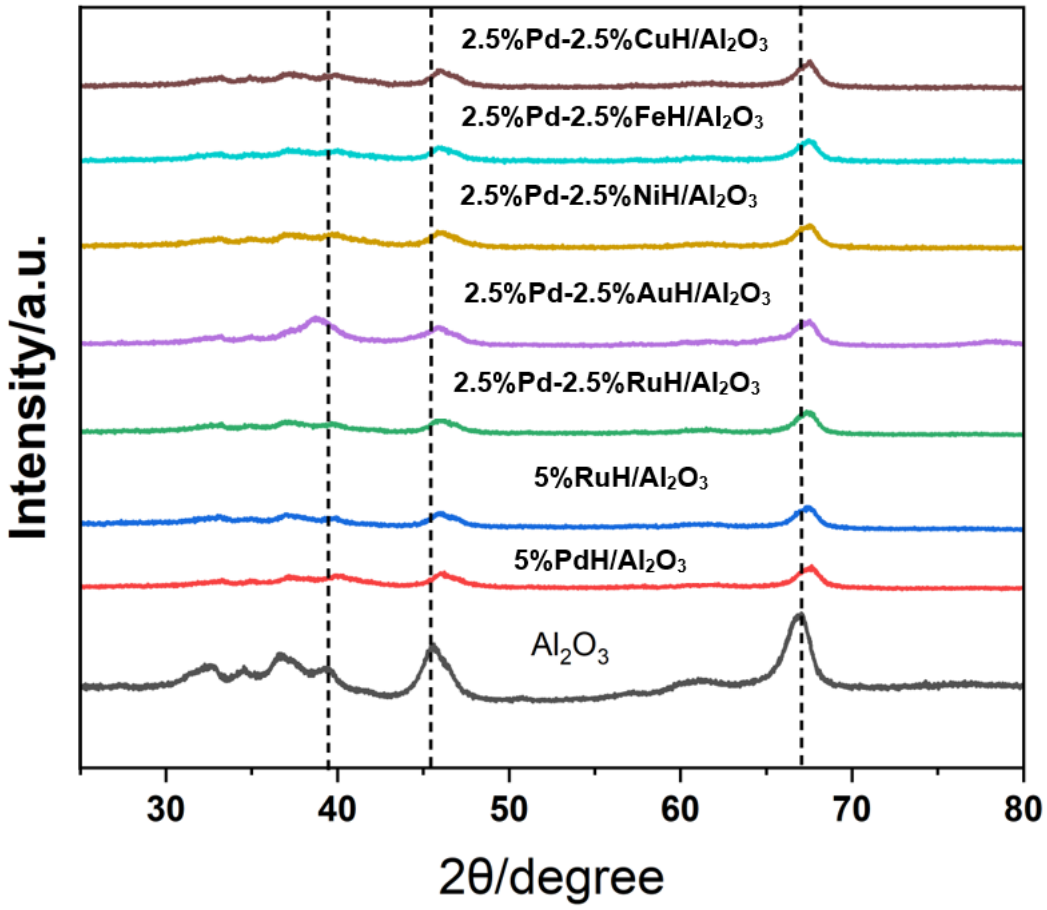

Figure 3.26: XRD Al_2O_3 patterns for monometallic Pd and Ru compared with bimetallic Pd with Ru, Au, Ni, Fe and Cu catalysts

X-ray photoelectron spectroscopy (XPS) was employed to shed light on the interactions between Pd and various metal elements M (where M includes Ru, Au, Ni, Cu, and Fe) in monometallic Pd, Ru and bimetallic catalysts. Additionally, the valence states of the surface metal species for these samples were examined, with findings compiled in **Table 3.7.** As per the table, $Pd^{2+}3d+Cl^-$ was a common observation across all bimetallic catalysts, with the sole exception being 2.5%Pd-2.5%AuH/Al_2O_3.

This indicates the complex interactions taking place between Pd and other elements in the catalysts. It highlights the unique behaviour of the Pd-Au combination, which deviates from the others and warrants further investigation. These findings contribute to a better understanding of the behaviour of Pd-based catalysts when combined with different metals, which could help in the optimization of their performance.

Table 3.7: XPS data for monometallic Pd and Ru compared with bimetallic Pd-M (M= Ru, Au, Ni, Fe and Cu) catalysts

Compound	Pd^0 Position/ %At Conc.	$Pd^{2+}3d$ Position/ %At Conc.	$Pd^{2+}3d+Cl^-$ Position/ %At Conc.	Cl^-2p Position/ %At Conc.	M=(Ru, Au, Ni, Cu and Fe) Position/ %At Conc.	Ru3d O_x Position/ %At Conc.	C1s Position/ %At Conc.
5%PdH	335.22/0.73	336.44/0.18	337.67/0.07	198.73/0.64	------	------	------
5%RuH	------	------	------	198.92/1.71	**$Ru^0$3d** (281.31/0.08)	281.85/0.26	284.66/15.04
2.5%Pd-2.5%RuH	335.64/0.29	337.19/0.27	338.72/0.16	199.64/0.52	**$Ru^0$3d** (280.82/0.2)	281.9/0.37	285.03/11.23
2.5%Pd-2.5%AuH	335.21/0.31	336.62/0.05	------	198.75/0.56	**$Au^0$4f** (83.75/0.18)	------	------
2.5%Pd-2.5%NiH	335.31/0.55	336.34/0.33	337.68/0.12	198.99/0.7	**Ni 2p** (856.49/0.83)	------	------
2.5%Pd-2.5%CuH	335.45/0.49	336.93/0.25	338.42/0.05	199.22/0.84	**$Cu2p_{3/2}$ (**933.22/1.44)	------	------
2.5%Pd-2.5%FeH	335.36/0.72	336.24/0.15	337.72/0.05	198.38/0.63	**Fe2p** (710.98/1.33)	------	------

The provided table presents XPS data for different compounds, including monometallic Pd and Ru, as well as bimetallic Pd-M catalysts where M represents Ru, Au, Ni, Cu, and Fe. The data includes the position and relative atomic concentration of Pd0, Pd2+3d, Pd2+3d+Cl-, Cl-2p, M (Ru, Au, Ni, Cu, and Fe), Ru3d Ox, and C1s.

Based on the literature review, the XPS data in the table can provide insights into the surface chemistry and valence states of the metal species in the catalysts. For example, in the case of 5%PdH, the presence of Pd^0 at 335.22 eV indicates the metallic state of palladium, while the Pd^{2+}3d peak at 336.44 eV suggests the existence of oxidized palladium species. The absence of a $Pd^{2+}3d+Cl^-$ peak implies the absence of chloride species. Additionally, the Cl^-2p peak at 198.73 eV indicates the presence of chlorine. These observations are in line with previous studies on Pd-based catalysts. For the 5%RuH compound, the absence of Pd peaks suggests that only ruthenium is present. The Ru3d Ox peak at 281.31 eV indicates the oxidation state of ruthenium, while the C1s peak at 284.66 eV suggests the presence of carbonaceous species. These findings are consistent with the characteristics of monometallic Ru

catalysts. In the case of 2.5%Pd-2.5%RuH, the Pd^{2+}3d peak at 337.19 eV and the presence of Ru3d Ox peak at 280.82 eV indicate the coexistence of oxidized Pd and Ru species. This suggests an interaction between Pd and Ru in the bimetallic catalyst, leading to modified electronic properties compared to monometallic counterparts. The XPS data for 2.5%Pd-2.5%AuH shows Pd^0 at 335.21 eV, indicating metallic Pd, while the Au^0 4f peak at 83.75 eV indicates the presence of gold species. The absence of Pd^{2+}3d+Cl^- suggests the absence of chloride species in this bimetallic catalyst. The interaction between Pd and Au in the catalyst can be inferred from the presence of both elements. Similarly, for 2.5%Pd-2.5%NiH, the presence of Pd^{2+}3d at 336.34 eV and Ni 2p peak at 856.49 eV suggests the coexistence of oxidized Pd and Ni species. This indicates the formation of a bimetallic catalyst with potential synergistic effects. For 2.5%Pd-2.5%CuH, the presence of Pd^{2+}3d and $Cu2p_{3/2}$ peaks indicates the coexistence of oxidized Pd and Cu species. The relatively high intensity of the $Cu2p_{3/2}$ peak suggests a higher concentration of copper in the bimetallic catalyst. Lastly, for 2.5%Pd-2.5%FeH, the presence of Pd^0 and Fe 2p peaks suggests the presence of metallic Pd and Fe species. The Fe2p peak at 710.98 eV indicates the oxidation state of iron. This indicates the formation of a bimetallic catalyst with Pd and Fe. In summary, the XPS data presented in the table provide valuable information about the surface chemistry and valence states of different metal species in the catalysts. These findings contribute to understanding the composition and electronic properties of the catalysts, which are crucial factors influencing their catalytic performance.

The XRD analysis of the low loading sample 0.5%Pd-0.5%RuH/Al_2O_3 does not provide significant information about the catalyst. When compared to catalysts with the same metals supported on different metal oxides (TiO_2, CeO_2, and zeolite Y hydrogen), the XRD technique does not offer any additional insights. **Figure 3.27** demonstrates that the limited information obtained for the high loading 2.5%Pd-2.5%RuH/Al_2O_3 catalyst also applies to the low loading sample. The XRD diffraction signals primarily correspond to the metal oxide support, rather than the specific composition of the catalyst. This finding is consistent with previous studies on similar catalyst systems[23,29,57,58].

In summary, the XRD analysis of the low loading 0.5%Pd-0.5%RuH/Al_2O_3 catalyst does not provide significant information about its composition and structure. The signals observed in the XRD pattern primarily originate from the metal oxide support, limiting the insights that can be gained from this technique.

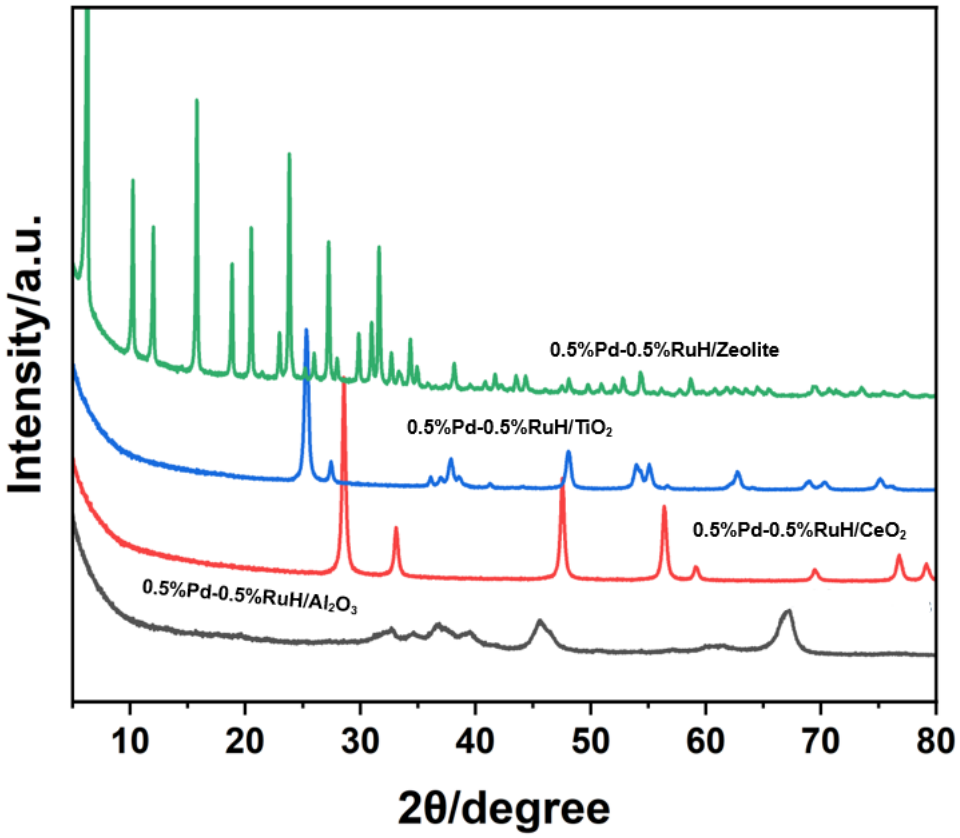

Figure 3.27: XRD patterns for 0.5%Pd-0.5%RuH/Al_2O_3, 0.5%Pd-0.5%RuH/CeO_2, 0.5%Pd-0.5%RuH/TiO_2 and 0.5%Pd-0.5%RuH/zeolite Y hydrogen

To provide further characterization of the catalysts, XPS analysis was conducted on the 0.5%Pd-0.5%RuH/Al_2O_3, 0.5%Pd-0.5%RuH/CeO_2, 0.5%Pd-0.5%RuH/TiO_2, and 0.5%Pd-0.5%RuH/zeolite Y hydrogen catalysts. The XPS results are presented in **Table 3.8.** From the table, it can be observed that only the 0.5%Pd-0.5%RuH/zeolite Y hydrogen catalyst exhibits the presence of Pd and Ru metals and their oxide states in the presence of chloride (Cl^-). In contrast, the 0.5%Pd-0.5%RuH/TiO_2 catalyst shows the presence of Pd and Ru metals and their oxide states in the absence of chloride. For the 0.5%Pd-0.5%RuH/CeO_2 catalyst, no peaks corresponding to Pd metal or chloride are observed. Interestingly, the 0.5%Pd-0.5%RuH/Al_2O_3 catalyst shows no peaks related to the Ru oxide state, suggesting the absence of Ru oxide species in this catalyst.

Table 3.8: XPS data for bimetallic 0.5%Pd-0.5%Ru catalyst supported on deferent metal oxide

Compound	Pd^0 Position/ %At Conc.	$Pd^{2+}3d$ Position/ %At Conc.	Cl^-2p Position/ %At Conc.	$Ru^0 3d$ Position/ %At Conc.	Ru3d O_x Position/ %At Conc.	C1s Position/ %At Conc.
0.5%Pd-0.5%RuH/Zeolite Y hydrogen	334.94/0.45	336.98/0.13	198.05/0.21	279.91/0.22	280.76/0.35	284.8/11.78
0.5%Pd-0.5%RuH/TiO_2	335.18/0.27	337.36/0.2	------	280.61/0.32	281.38/0.17	284.8/18.77
0.5%Pd-0.5%RuH/CeO_2	------	337.83/0.73	------	281.23/0.55	281.93/0.28	284.8/21
0.5%Pd-0.5%RuH/Al_2O_3	335.31/0.55	336.34/0.33	198.99/0.7	279.91/0.22	------	284.96/22.98

Table 3.8 presents the XPS data for the bimetallic 0.5%Pd-0.5%Ru catalyst supported on different metal oxides, including zeolite Y hydrogen, TiO_2, CeO_2, and Al_2O_3. The table provides information on the positions and relative atomic concentrations of Pd^0, $Pd^{2+}3d$, Cl^-2p, Ru^0 3d, Ru 3d Ox, and C1s.

For the 0.5%Pd-0.5%RuH/Zeolite Y hydrogen catalyst, the presence of Pd^0 at 334.94 eV and $Pd^{2+}3d$ at 336.98 eV suggests the coexistence of metallic and oxidized palladium species. The Cl^-2p peak at 198.05 eV indicates the presence of chloride. In terms of ruthenium, the Ru^0 3d peak at 279.91 eV and Ru 3d Ox peak at 280.76 eV indicate the presence of ruthenium in different oxidation states. The C1s peak at 284.8 eV suggests the presence of carbonaceous species. In the case of the 0.5%Pd-0.5%RuH/TiO_2 catalyst, the presence of Pd^0 at 335.18 eV and $Pd^{2+}3d$ at 337.36 eV indicates the coexistence of metallic and oxidized palladium species. The absence of a Cl^-2p peak suggests the absence of chloride in this catalyst. The Ru^0 3d peak at 280.61 eV and Ru 3d Ox peak at 281.38 eV indicate the presence of ruthenium in different oxidation states. The C1s peak at 284.8 eV indicates the presence of carbonaceous species. For the 0.5%Pd-0.5%RuH/CeO_2 catalyst, no peak corresponding to Pd^0 is observed. However, the presence of $Pd^{2+}3d$ at 337.83 eV suggests the existence of oxidized palladium species. The absence of a Cl^-2p peak suggests the absence of chloride in this catalyst. The Ru^0 3d peak at 281.23 eV and Ru 3d Ox peak at 281.93 eV indicate the presence of ruthenium in different oxidation states. The C1s peak at 284.8 eV suggests the presence of carbonaceous species. In the case of the 0.5%Pd-0.5%RuH/Al_2O_3 catalyst, the presence of Pd^0 at 335.31 eV

and Pd^{2+}3d at 336.34 eV indicates the coexistence of metallic and oxidized palladium species. The Cl^{-}2p peak at 198.99 eV indicates the presence of chloride. However, no peaks related to the Ru3d Ox state are observed, suggesting the absence of ruthenium oxide species in this catalyst. The C1s peak at 284.96 eV suggests the presence of carbonaceous species.

Overall, the XPS results provide insights into the presence and oxidation states of Pd and Ru metals in the different catalysts, as well as the role of chloride in their formation. The variations in the XPS spectra highlight the importance of the catalyst support and composition on the surface chemistry of the catalysts.

3.5. References

1 M. Sankar, Q. He, M. Morad, J. Pritchard, S. J. Freakley, J. K. Edwards, S. H. Taylor, D. J. Morgan, A. F. Carley, D. W. Knight, C. J. Kiely and G. J. Hutchings, *ACS Nano*, 2012, **6**, 6600–6613.

2 S. Yue, Z. Yin, X. Zou, X. Zou, X. Lu and X. Wang, *ChemistrySelect*, , DOI:10.1002/SLCT.202103743.

3 M. Trueba and S. P. Trasatti, *Eur. J. Inorg. Chem.*, 2005, **2005**, 3393–3403.

4 S. Roy, G. Mpourmpakis, D. Y. Hong, D. G. Vlachos, A. Bhan and R. J. Gorte, *ACS Catal.*, 2012, **2**, 1846–1853.

5 M. Weber-Stockbauer, O. Y. Gutiérrez, R. Bermejo-Deval and J. A. Lercher, *Catal. Sci. Technol.*, 2019, **9**, 509–516.

6 V. González-Pea, I. Díaz, C. Márquez-Alvarez, E. Sastre and J. Pérez-Pariente, *Microporous Mesoporous Mater.*, 2001, **44**–**45**, 203–210.

7 S. Badoga, R. V. Sharma, A. K. Dalai and J. Adjaye, *Appl. Catal. A Gen.*, 2015, **489**, 86–97.

8 G. Paglia, C. E. Buckley, T. J. Udovic, A. L. Rohl, F. Jones, C. F. Maitland and J. Connolly, , DOI:10.1021/cm035193e.

9 J. Jiang and Y. Ding, *Inorganica Chim. Acta*, 2022, **534**, 120830.

10 F. A. Lewis, *Platin. Met. Rev*, 1960, **4**, 132–137.

11 P. D. Cobden, B. E. Nieuwenhuys, V. V. Gorodetskii and V. N. Parmon, *Platinum Metals Review* (1998) **42**(4) 141-144 .

12 M. D. Obradović, Z. M. Stančić, U. Lačnjevac, V. V. Radmilović, A. Gavrilović-Wohlmuther, V. R. Radmilović and S. L. Gojković, *Appl. Catal. B Environ.*,

2016, **189**, 110–118.

13 T. Pham Huu, S. Gil, P. Da Costa, A. Giroir-Fendler and A. Khacef, *Catal. Today*, 2015, **257**, 86–92.

14 S. Agarwal, M. J. Ahemad, S. Kumar, D. Van Dung, P. Rai, M. Kumar, K. Awasthi and Y. T. Yu, *J. Alloys Compd.*, 2022, **900**, 163545.

15 S. J. Lee, Y. Yu, H. J. Jung, S. S. Naik, S. Yeon and M. Y. Choi, *Chemosphere*, 2021, **262**, 128358.

16 A. N. Mitropoulos, F. J. Burpo, C. K. Nguyen, E. A. Nagelli, M. Y. Ryu, J. Wang, R. K. Sims, K. Woronowicz and J. K. Wickiser, *Materials (Basel).*, , DOI:10.3390/MA12060894.

17 A. S. Ivanova, E. M. Slavinskaya, R. V. Gulyaev, V. I. Zaikovskii, O. A. Stonkus, I. G. Danilova, L. M. Plyasova, I. A. Polukhina and A. I. Boronin, *Appl. Catal. B Environ.*, 2010, **97**, 57–71.

18 L. Yan, X. X. Liu and Y. Fu, *RSC Adv.*, 2016, **6**, 109702–109705.

19 J. Zhang, M. Chen, H. Li, Y. Li, J. Ye, Z. Cao, M. Fang, Q. Kuang, J. Zheng and Z. Xie, *Nano Energy*, 2018, **44**, 127–134.

20 Z. Zhao, X. Huang, M. Li, G. Wang, C. Lee, E. Zhu, X. Duan and Y. Huang, *J. Am. Chem. Soc.*, 2015, **137**, 15672–15675.

21 A. P. Kumar, D. Bilehal, A. Tadesse and D. Kumar, *RSC Adv.*, 2021, **11**, 6396–6406.

22 S. Ntshibongo, M. Maumela and N. Bingwa, *Inorg. Chem. Commun.*, , DOI:10.1016/j.inoche.2022.110101.

23 L. S. F. Feio, C. E. Hori, S. Damyanova, F. B. Noronha, W. H. Cassinelli, C. M. P. Marques and J. M. C. Bueno, *Appl. Catal. A Gen.*, 2007, **316**, 107–116.

24 M. Brun, A. Berthet and J. C. Bertolini, *J. Electron Spectros. Relat. Phenomena*, 1999, **104**, 55–60.

25 V. A. de la Peña O'Shea, M. C. Alvarez-Galvan, J. Requies, V. L. Barrio, P. L. Arias, J. F. Cambra, M. B. Güemez and J. L. G. Fierro, *Catal. Commun.*, 2007, **8**, 1287–1292.

26 L. S. Kibis, A. I. Titkov, A. I. Stadnichenko, S. V. Koscheev and A. I. Boronin, *Appl. Surf. Sci.*, 2009, **255**, 9248–9254.

27 Z. Chen, M. Zhang, J. Hua, M. Yang, Y. Dong and H. Cheng, *Int. J. Hydrogen*

Energy, 2021, **46**, 9718–9729.

28 P. Cañizares, A. De Lucas, F. Dorado, A. Durán and I. Asencio, *Appl. Catal. A Gen.*, 1998, **169**, 137–150.

29 İ. Gözeten and M. Tunç, *J. Nanoparticle Res. 2022 241*, 2022, **24**, 1–20.

30 K. Thamaphat, P. Limsuwan and B. Ngotawornchai, *Nat. Sci.)*, 2008, **42**, 357–361.

31 N. Hurley, L. Li, C. Koenigsmann and S. S. Wong, *Molecules*, , DOI:10.3390/MOLECULES26040909.

32 M. Du, G. Zeng, C. Ye, H. Jin, J. Huang, D. Sun, Q. Li, B. Chen and X. Li, *Mol. Catal.*, 2020, **483**, 110771.

33 L. L. Jewell and B. H. Davis, *Appl. Catal. A Gen.*, 2006, **310**, 1–15.

34 Y. Chen, L. Soler, M. Armengol-Profitós, C. Xie, D. Crespo and J. Llorca, *Appl. Catal. B Environ.*, , DOI:10.1016/j.apcatb.2022.121275.

35 J. B. Zhong, Y. Lu, W. D. Jiang, Q. M. Meng, X. Y. He, J. Z. Li and Y. Q. Chen, *J. Hazard. Mater.*, 2009, **168**, 1632–1635.

36 S. Pearton, *Nanoscale*, 2010, **2**, 1057.

37 M. P. Casaletto, A. Longo, A. Martorana, A. Prestianni and A. M. Venezia, *Surf. Interface Anal.*, 2006, **38**, 215–218.

38 D. Teschner, A. Pestryakov, E. Kleimenov, M. Hävecker, H. Bluhm, H. Sauer, A. Knop-Gericke and R. Schlögl, *J. Catal.*, 2005, **230**, 186–194.

39 J. Moulder, W. Stickle, W. Sobol and K. D. Bomben, *Physics* **1992**.

40 R. Liu, Y. Yu, K. Yoshida, G. Li, H. Jiang, M. Zhang, F. Zhao, S. ichiro Fujita and M. Arai, *J. Catal.*, 2010, **269**, 191–200.

41 X. Yang, D. Chen, S. Liao, H. Song, Y. Li, Z. Fu and Y. Su, *J. Catal.*, 2012, **291**, 36–43.

42 J. Guo, M. Zhang, J. Xu, J. Fang, S. Luo and C. Yang, *RSC Adv.*, 2022, **12**, 2246.

43 V. E. Viola, T. D. Thomas and G. T. Seaborg, *Torbjijrn Sikk. Phys. Hev*, 1958, **46**, 16.

44 Y. Shen, S. Wang and K. Huang, *Appl. Catal.*, 1990, **57**, 55–70.

45 N. A. Nemygina, L. Z. Nikoshvili, I. Y. Tiamina, A. V. Bykov, I. S. Smirnov, T.

Lagrange, Z. Kaszkur, V. G. Matveeva, E. M. Sulman and L. Kiwi-Minsker, *Org. Process Res. Dev.*, 2018, **22**, 1606–1613.

46 M. C. Kung, R. J. Davis and H. H. Kung, *J. Phys. Chem. C*, 2007, **111**, 11767–11775.

47 C. R. Adhikari, D. Parajuli, K. Inoue, K. Ohto, H. Kawakita and H. Harada, *New J. Chem.*, 2008, **32**, 1634–1641.

48 Z. Wang, J. Feng, X. Li, R. Oh, D. Shi, O. Akdim, M. Xia, L. Zhao, X. Huang and G. Zhang, *J. Colloid Interface Sci.*, 2021, **588**, 787–794.

49 N. Al-Rifai, P. J. Miedziak, M. Morad, M. Sankar, C. Waldron, S. Cattaneo, E. Cao, S. Pattisson, D. Morgan, D. Bethell, G. J. Hutchings and A. Gavriilidis, *Ind. Eng. Chem. Res.*, 2017, **56**, 12984–12993.

50 L. L. R. Vono, C. Broicher, K. Philippot and L. M. Rossi, *Catal. Today*, 2021, **381**, 126–132.

51 X. Kong, Y. Gong, S. Mao and Y. Wang, *ChemNanoMat*, 2018, **4**, 432–450.

52 X. Kang, K. Miao, Z. Guo, J. Zou, Z. Shi, Z. Lin, J. Huang and S. Chen, *J. Catal.*, 2018, **364**, 183–191.

53 L. Yu, D. Jiang, J. Xu, L. Ma and X. Li, *China Pet. Process. Petrochemical Technol.*, 2012, **14**, 83–89.

54 J. Zhang, K. Gao, S. Wang, W. Li and Y. Han, *RSC Adv.*, 2017, **7**, 6447–6456.

55 Y. V. Larichev, B. L. Moroz and V. I. Bukhtiyarov, *Appl. Surf. Sci.*, 2011, **258**, 1541–1550.

56 T. Zhu, M. Yang, X. Chen, Y. Dong, Z. Zhang and H. Cheng, *J. Catal.*, 2019, **378**, 382–391.

57 M. Sajjadi, M. Nasrollahzadeh, H. Ghafuri, T. Baran, Y. Orooji, N. Y. Baran and M. Shokouhimehr, *Int. J. Biol. Macromol.*, , DOI:10.1016/J.IJBIOMAC.2022.04.075.

58 K. Yamaguchi, T. Koike, J. W. Kim, Y. Ogasawara and N. Mizuno, *Chem. - A Eur. J.*, 2008, **14**, 11480–11487.

Chapter 4: High-performance and stable Ru-Pd nanoparticles catalyst supported on AL_2O_3 for selective hydrogenation of phenol

4.1. Introduction

Phenols are recognized as some of the most resilient yet relatively widespread compounds in bio-oil, and their direct hydrogenation and hydrolysis bear considerable importance for the progress of sustainable chemistry[1,2]. Frequently, the hydrogenation processes of phenol yield cyclohexanone, a semi-hydrogenated product, and cyclohexanol, a fully hydrogenated by-product.

Cyclohexanol holds substantial value in the chemical industry, acting as a pivotal stage in the production of hexamethylene diamine, caprolactam for nylon 6, and adipic acid for nylon 66[3,4]. Interestingly, phenol hydrogenation is favoured due to its lower required temperatures and pressures, even though the oxidation of cyclohexane leads to a lower conversion rate and generates more undesirable by-products[5]. Additionally, cyclohexanol can be generated through the hydrogenation of phenol - a method deemed as environmentally friendly and efficient due to its enhanced atomic economy and energy-saving properties[6]. This has piqued the curiosity of researchers, particularly in the domain of liquid-phase phenol hydrogenation[7].

The conversion of phenol into cyclohexanol through hydrogenation can be achieved via a one-step or two-step process. In the one-step process, Ni, Co, or Pd catalysts can convert phenol directly to cyclohexanol. In contrast, the two-step process requires an initial partial hydrogenation of phenol to an unstable intermediate cyclohexenol, which is then easily isomerized to cyclohexanone by Ru or Rh catalysts before a subsequent hydrogenation into cyclohexanol, or alternatively, the intermediate cyclohexenol may be directly hydrogenated into cyclohexanol [8,9] (**Scheme 4.1**).

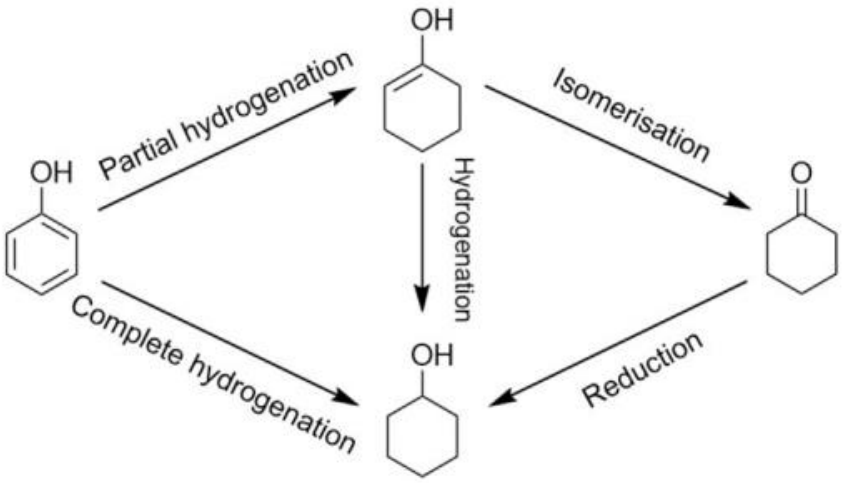

Scheme 4.1: Reaction mechanism for cyclohexanol formation. Reproduced from ref[10].

Due to their exceptional hydrogenation properties, noble metal catalysts such as Ru[11] and Pt[12], supported composite materials have superseded traditional catalysts in numerous procedures. However, these methods necessitate extreme conditions (exceeding 100 °C and/or 15 bar H_2), leading to high energy consumption, which is detrimental to sustainable development[13–15]. For example, Tan et al.[4] evaluated Pd/NaY catalysts at 235 °C and 5 MPa H_2 for the hydrogenation of phenol in ethanol, yielding a phenol conversion of 78.2 % with a selectivity of 92.3 % for cyclohexanol. Moreover, the ring hydrogenation of methoxyphenols in an aqueous medium exhibits high selectivity (74 %) for the production of methoxycyclohexanols through a Pd/Al_2O_3 based catalyst with a conversion rate of 57 %[16]. Conversely, using a less acidic carbon black support (Ru/CB), methoxycyclohexanol was produced with 60 % selectivity from guaiacol in the n-decane medium, achieving a complete conversion (100 %)[17]. It has been discovered that supported Ru-based catalysts offer greater cost-effectiveness and efficiency in comparison to other noble metal catalysts[18]. Vinokurov et al.[19] synthesized core/shell ruthenium-halloysite (a tubular nanoclay) nanocomposites, which, when applied in an aqueous 3 MPa H_2 solution at 80 °C, successfully converted phenol to cyclohexanol entirely. Supported Ru-based catalysts have proven to be more cost-effective than other noble metal catalysts[18]. Phenol's adsorption onto the support can occur in two distinct manners depending on the support's nature. For acidic supports like silica-alumina, a co-planar adsorbed state is induced, which results in robust adsorption, paving the way for the formation of cyclohexanol and cyclohexane. Conversely, a non-planar adsorption state emerges on basic or neutral sites such as silica, where there exists a weaker interaction between the benzene ring and the surface, favouring cyclohexanone selectivity[20,21]. Consequently, a fresh phenol molecule promptly substitutes cyclohexanone to circumvent excessive hydrogenation, leading to the generation of cyclohexanol. To

achieve high reactivity, it is typical to use bifunctional catalysts with two distinct sites: one for hydrogenation at the metal site and the other for dehydration and hydrolysis at the acid site[22].

The two-site concept, as demonstrated in **Figure 4.1,** was first proposed[23] . When co-planar adsorption occurs on acid sites, phenol produces cyclohexanol due to the strong co-adsorption between the aromatic ring and the support[24]. However, when phenol is adsorbed on base sites in a non-planar fashion, cyclohexanone is formed.

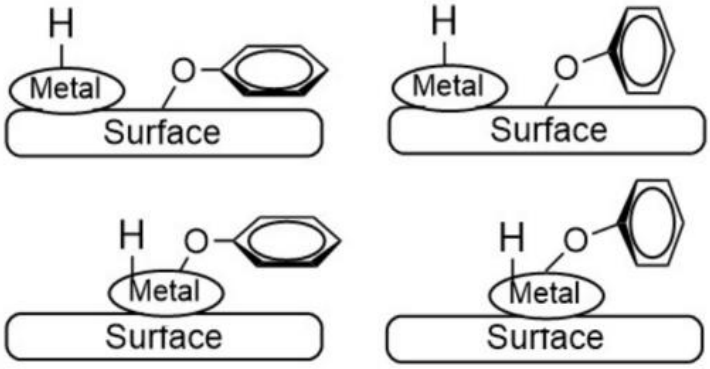

Figure 4.1: Adsorption of phenol on surface via: (a) co-planar mode (two-site model), (b) non-planar mode (two-site model), (c) co-planar mode (one-site model), (d) non-planar mode (one-site model). Reproduced from ref.[23].

Xiang et al.[25] demonstrated that the hydrophilic/hydrophobic properties of the catalysts Pd supported on CNTs highly affects the catalytic performance in phenol in situ hydrogenation. Such an effect on the adsorption/desorption behaviours of phenol on the catalysts. In the hydrophobic catalysts the adsorption of phenol is mainly at only the Pd sites, which leads to the major product being cyclohexanol. The solubility of methoxyphenols in hexadecane notably favours the use of Ni catalysts over others for the conversion process towards cyclohexanol[26,27]. A Cobalt-Nickel alloy nanoparticle (NP) was synthesized and embedded in Nitrogen-doped carbon layers to expedite the selective hydrogenation of phenol to cyclohexanol. Given that cyclohexanone was not detected, the proposed one-step hydrogenation of phenol presented a direct synthesis route for cyclohexanol15. Previously, it was observed by Liao et al. that a Pd-Ru/MSN catalyst exhibited an activity five times greater than that of Pd/MSN for the liquid-phase hydrogenation of phenol under milder conditions (50 ºC, 1.0 MPa P H_2, m (Pd) / m (phenol) = 1:500, reaction for 60 min.), achieving 72 % conversion and selectivity for all products, namely Cyclohexanone at 63 %, Cyclohexanol at 26 %, and Cyclohexane at 11 %[28]. The improved catalytic activity was attributed to enhanced Pd dispersion and the electrical interaction between Pd and Ru facilitated by the addition of Ru.

The creation of a highly efficient and operative catalyst for one-step selective hydrogenation necessitates a catalyst that can regulate hydrogenation selectivity, an attribute that is more environmentally friendly and preferred in catalyst design[29,30]. The high activity and good cyclohexanol selectivity of the Pd-Ru/MSN catalyst make it an appealing choice for both foundational research and practical applications.

A first-principles examination of phenol hydrogenation was conducted by Yoon et al.[31], in which they manipulated various quantities of water (H_2O) volumes to create vapor and liquid conditions. Giraldo et al.[32,33], probed into the vapor phase hydrogenation of phenol, employing solvents such as cyclohexane, benzene, toluene, and ethanol over an Rh/SiO_2 catalyst. Their results revealed that cyclohexane yielded a higher phenol conversion rate, while the solvent type, whether cyclohexane, benzene, or toluene, did not alter the selectivity towards cyclohexanone. They also found that ethanol decreased the phenol conversion due to its inhibitory effect on the hydrogenation of aromatic compounds, a tendency that becomes more pronounced with dwindling catalytic activity[34]. They also noted that the use of alcohols for phenol hydrogenation was not favoured due to the possibility of phenol alkylation yielding corresponding alkylphenols[35]. In liquid-phase reactions, solvents significantly influence reaction equilibrium. They affect the mechanism and reaction rate by modifying the solubility, mass transfer, and sorption functions of reactants, and they also interact with catalysts. Recently, H_2O has emerged as a preferred solvent for phenol hydrogenation as it aids in improving catalyst activity and cyclohexanol selectivity[36]. The strength of adsorption of reactants and products on the catalyst surface could be influenced by the solvent. For instance, the hydrogenation of phenol to cyclohexanone, which due to its water immiscibility, might not readily desorb from the catalyst surface. On the contrary, cyclohexanone might easily desorb in other solvents due to its better solubility, thereby avoiding further hydrogenation to cyclohexanol[37].

Zhang et al.[38], . documented the fabrication of a multi-component mesoporous core-shell structured nano-catalyst through the encapsulation of a hydrophobic mesoporous carbon with amino-functionalised mesoporous silica, followed by coordination of Pd precursors and subsequently reduced with a $NaBH_4$ reagent. The resulting $Pd/MCN@MS\text{-}NH_2$ catalyst demonstrated good dispersion in the aqueous medium owing to the inherent hydrophilic properties of the mesoporous silica shell. Oxides are another class of support frequently used in the liquid-phase hydrogenation of phenol due to their robust mechanical, chemical stabilities, and adjustable surface properties[39]. Alumina (Al_2O_3), traditionally used in the gas-phase hydrogenation of phenol, is also extensively employed for liquid-phase hydrogenation of phenol, given its tuneable pore structure and significant shape-selective catalytic property acid-base

properties. Furthermore, TiO_2, CeO_2, and ZrO_2 have been reported as competent supports for phenol hydrogenation due to their capability of modulating hydrophilicity and acid-base properties[40,41]. Cheng et al.[42], Catalysts with 3 nm Pd NPs demonstrated high activity and favoured the selective formation of cyclohexanone under an atmospheric pressure of hydrogen in aqueous media with no additives. Exceptional selectivity (> 99 %) and conversion of 99 % were achieved within 3 hours at 333 K. This was ascribed to the optimal interaction between the hydroxyl group of phenol and the hydroxyl group of catalysts, and between the aromatic ring of phenol and Pd NPs.

In a subsequent study by Resende et al.[41], the particle sizes of Pd/ZrO_2 catalysts were examined using transmission electron microscopy (TEM), revealing that the liquid-phase hydrogenation of phenol was a structure-sensitive reaction on Pd/ZrO_2. Pd/ZrO_2 with higher Pd dispersion was characterized by lower turnover frequencies (TOF). The researchers also reported a decline in activation energies as coverage increased with the decrease in particle size, thereby suggesting the possibility of unfavourable entropy with small particle sizes in the case of Pd (1-2 nm). Furthermore, a study by Raut et al. reported that Ru served as an effective metal component for phenol hydrogenation in the liquid phase[35]. The Ru/Al_2O_3 catalyst, prepared via the traditional hydrogen reduction process with Ru NPs sizes between 10 nm and 50 nm, demonstrated 82 % conversion of phenol with 67 % selectivity of cyclohexanone under mild conditions (After a reaction time of 1 hour, at 80 °C and 20 bar hydrogen pressure).

The aim of this study is investigating the effectiveness of supported bimetallic catalysts over monometallic catalysts for the hydrogenation of phenol. The selective hydrogenation of phenol over commercial gamma-alumina is used in the current study. A comparison was made using bimetallic catalysts that alloy an active Pd noble metal with noble metals (Au and Ru) and non-noble metals (Ni, Fe and Cu) under mild conditions.

4.2. Experimental work

4.2.1. Catalysts preparation

All catalysts mentioned in the study were prepared using the modified impregnation method (M_{im}) and subsequently reduced with sodium borohydride ($NaBH_4$). This preparation method was utilized for the synthesis of Pd/Al_2O_3 monometallic catalysts, as well as bimetallic catalysts denoted as Pd-X (where X represents Au, Ru, Ni, Fe, and Cu). Detailed procedures for the synthesis of these catalysts can be found in

Chapter 2 of the study, specifically in Sections 2.2.3.2 and 2.2.3.4, respectively. To distinguish the catalysts prepared via the modified impregnation method and $NaBH_4$ reduction from those prepared using the normal impregnation method and heat treatment reduction, a letter "H" was added to the names of the former set of catalysts. This labelling system allows for clear differentiation and facilitates accurate referencing of the catalysts throughout the research.

The utilization of the modified impregnation method and $NaBH_4$ reduction offers several advantages, including enhanced control over the catalyst's composition and structure. Additionally, this method may lead to improved catalytic activity and selectivity, which is essential for the successful implementation of these catalysts in various hydrogenation reactions. By investigating various monometallic and bimetallic catalyst compositions prepared through this approach, the study aims to shed light on the influence of different metals and their interactions on the catalyst's performance and efficiency.

It is worth noting that this systematic approach to catalyst preparation and labelling ensures that the catalysts' properties and performances can be accurately compared and analysed, providing valuable insights into the design of effective hydrogenation catalysts for diverse industrial applications.

4.2.2. Catalyst testing

In the present study, the performance of Pd monometallic catalysts and bimetallic Pd-X (where X represents Au, Ru, Ni, Fe, and Cu) catalysts supported on gamma-alumina was evaluated through the hydrogenation of phenol, which served as the model reaction (for more details, refer to Chapter 2, sections 2.3.1.).

The hydrogenation of phenol was chosen as the model reaction because it provides a well-defined and commonly used benchmark for evaluating the catalytic activity and selectivity of hydrogenation catalysts. Phenol hydrogenation is a valuable test reaction to assess the efficiency of catalysts in promoting the addition of hydrogen to the aromatic ring of phenol, resulting in the formation of cyclohexanone or cyclohexanol, depending on the reaction conditions and catalyst properties.

To analyse the performance of the catalysts during the hydrogenation process, a gas chromatographic (GC) method was employed for data analysis. Gas chromatography is a widely used technique in catalysis research to quantify reactant conversion and product selectivity. The GC method allows researchers to monitor the changes in the reactant and product concentrations over time, enabling the determination of reaction rates and product distributions.

By utilizing the hydrogenation of phenol as the model reaction and employing GC for data analysis, the study aims to comprehensively evaluate the catalytic activity and

selectivity of both Pd monometallic and bimetallic Pd-X catalysts supported on gamma-alumina. This evaluation is crucial for understanding the influence of different metal compositions on the catalyst's performance and exploring potential synergistic effects between Pd and other metals in the hydrogenation process. The findings from this research can contribute to the design and optimization of efficient catalysts for various hydrogenation reactions, with implications for industrial applications in the production of valuable chemicals and intermediates.

4.3. Results and discussion

4.3.1. Different noble and non-noble bimetallic systems (Pd-X) (X=Au, Cu, Ni and Ru) catalyst testing

In this study, the noble metals chosen were Au, Pd and Ru, whereas Ni, Fe and Cu were the non-noble metals. Experimentally, bimetallic catalysts were used because they provide a synergistic effect. Pd was used as one of the two metals in all five bimetallic catalysts because of its proven high activity for phenol hydrogenation. Au, Ru, Ni, Cu and Fe were used as pairs Pd in bimetallic catalysts with loading of 5 % wt. The ratio of the metal was 1:1 by weight. Commercial gamma-alumina was used as a support for all catalysts.

For comparison, **Table 4.1** summarises the results from the catalytic test reaction regarding phenol conversion and product selectivity (cyclohexanone and cyclohexanol) using the bimetallic catalysts previously mentioned supported on Al_2O_3. After a reaction time of 3 h, the reaction was performed under the same conditions and two catalysts (Pd-Cu and Pd-Fe) showed low conversion ≥ 10 of phenol. The Pd-Ru and Pd-Ni catalysts were the only ones to approximately reach 99 % selectivity towards cyclohexanol with 100 % and 48 % conversions respectively. However, the Pd-Ni catalyst appears to have lower conversion of 48 % than Pd-Ru 100 % conversion. Meanwhile, the Pd-Au catalyst had high selectivity towards cyclohexanone, 95 % selectivity with low conversion 25 %. In addition, when Pd-Ru catalyst using beside the cyclohexanol, the cyclohexane appeared as another product with 1 % selectivity. These results confirm that during the hydrogenation of phenol, the second metal Ru plays a key role in product selectivity and conversion as well.

Moreover, the selective hydrogenation of phenol and phenol conversion were affected by the composition of the metal pair with palladium metal when prepare bimetallic catalyst. This is clear from the results shown in **Table 4.1.**

Table 4.1: Hydrogenation of phenol using a supported bimetallic catalyst under the same conditions:

Catalysts	Conv. (%) phenol	Sel. (%)		Mass balance (%)
		Cyclohexanone	Cyclohexanol	
2.5%Pd-2.5%RuH/Al_2O_3	**100**	**0**	**99**	**98**
2.5%Pd-2.5%AuH/Al_2O_3	**25**	**95**	**5**	**96**
2.5%Pd-2.5%CuH/Al_2O_3	**12**	**57**	**43**	**94**
2.5%Pd-2.5%NiH/Al_2O_3	**48**	**1**	**99**	**95**
2.5%Pd-2.5%FeH/Al_2O_3	**10**	**77**	**23**	**97**

Reaction conditions: Phenol 0.5 mmol, catalyst 30 mg, isopropanol (IPA) used as a solvent, temperature 50 ºC, 3 hours. 1 bar H_2 gas, all samples analysed by the GC using dodecane as an internal standard.

4.3.2. Time online studies for bimetallic catalysts

To gain deeper insight into the catalytic behaviour of the bimetallic catalysts, reaction conditions were modified by extending the reaction time in online studies. These studies lasted for 180 minutes and results are represented in **(Figures 4.2, 4.3, 4.4, 4.5 and 4.6).** A notable increase in selectivity towards cyclohexanol was observed for the Pd-Ru and Pd-Ni catalysts. Compared to the other catalysts, the selectivity towards cyclohexanone and cyclohexanol (0 % and 99 %, 1 % and 99 %, Pd-Ru and Pd-Ni respectively) appears similar for both catalysts. Nevertheless, the Pd-Ru catalyst demonstrates higher activity than the Pd-Ni catalyst for phenol conversion, registering conversion rates of 100 % and 48 % respectively. Detailed studies of the phenol hydrogenation reaction over the 2.5%Pd-2.5%RuH/Al_2O_3 catalyst are presented in **Figure 4.2.** The conversion of phenol significantly increased with extended reaction time, reaching 100 % at 30 minutes. Furthermore, the selectivity of cyclohexanol surpassed 99 % within the initial 30 minutes of the reaction. While a diminished selectivity for cyclohexanone is observed, this is potentially due to the immediate hydrogenation of cyclohexanone into cyclohexanol once it starts to form. Transmission electron microscopy (TEM) analysis was conducted to investigate the morphological features and average particle size of Pd-Ru in the 2.5%Pd-2.5%RuH/Al_2O_3 catalyst. As per the TEM analysis results discussed in chapter 3,

section 3.6 (**Figure 3.16**), the average particle size was approximately 3.2 nm. Comparatively, the particle size of the 5%PdH/Al_2O_3 catalyst varied between 2 nm and 8 nm, with an average particle size of 3.52 nm (chapter 3, section 3.3.1.3, **Figure 3.7**). Over time, the concentration of phenol will decrease, consequently reducing the rate of the reaction. Thus, selectivity to cyclohexanone decreased over time, while an inverse relationship was observed for selectivity to cyclohexanol and phenol conversion, which increased. The addition of Ru effectively doubled the catalyst's activity for phenol hydrogenation compared to the other bimetallic catalysts. It resulted in good activity for deep hydrogenation of phenol[43,44]. Given its high activity and selectivity for cyclohexanol, the Pd-Ru catalyst stands out as a promising candidate for further investigation in the current study.

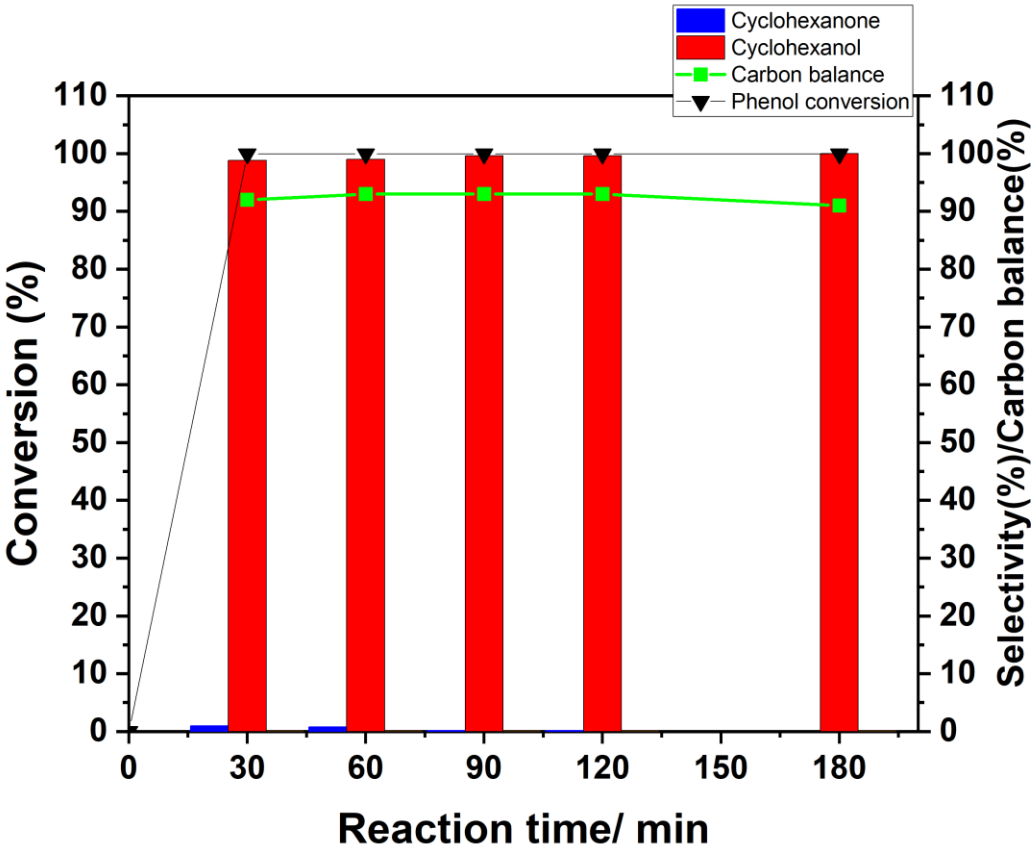

Figure 4.2: Effect of reaction time on conversion and selectivity over 2.5%Pd-2.5%RuH/Al_2O_3 catalyst. **Reaction conditions:** Phenol 0.5 mmol, catalyst 30 mg, isopropanol (IPA) used as a solvent, temperature 50 ºC, 1 bar H_2 gas, all samples analysed by the GC using dodecane as an internal standard.

An analogous behaviour was noticed in the 2.5%Pd-2.5%RuH/Al_2O_3 catalyst and the 2.5%Pd-2.5%NiH/Al_2O_3 catalyst. However, the latter demonstrated a lower activity level in comparison with the former. In **Figure 4.3**, experimental outcomes delineate the impact of reaction duration on the hydrogenation of phenol. Contrary to the Ru-Pd catalyst, there was a minor increase in selectivity for cyclohexanone before the

selectivity curve diminished to 1 % at the 180-minute mark. The conversion of phenol experienced an initial rise, culminating at the conclusion of the reaction time of 180 minutes, resulting in a 48 % conversion and a 99 % selectivity towards cyclohexanol. The phenol conversion and cyclohexanol selectivity in phenol hydrogenation executed over the 2.5%Pd-2.5%NiH/Al_2O_3 catalyst was appreciably inferior to those performed over the 2.5%Pd-2.5%RuH/Al_2O_3 catalyst. As depicted in **Figure 4.3**, the 2.5%Pd-2.5%NiH/Al_2O_3 catalyst's hydrogenation performance was somewhat weaker in terms of phenol conversion compared to the 2.5%Pd-2.5%RuH/Al_2O_3 catalyst, although their product selectivity remained nearly identical[45–47].

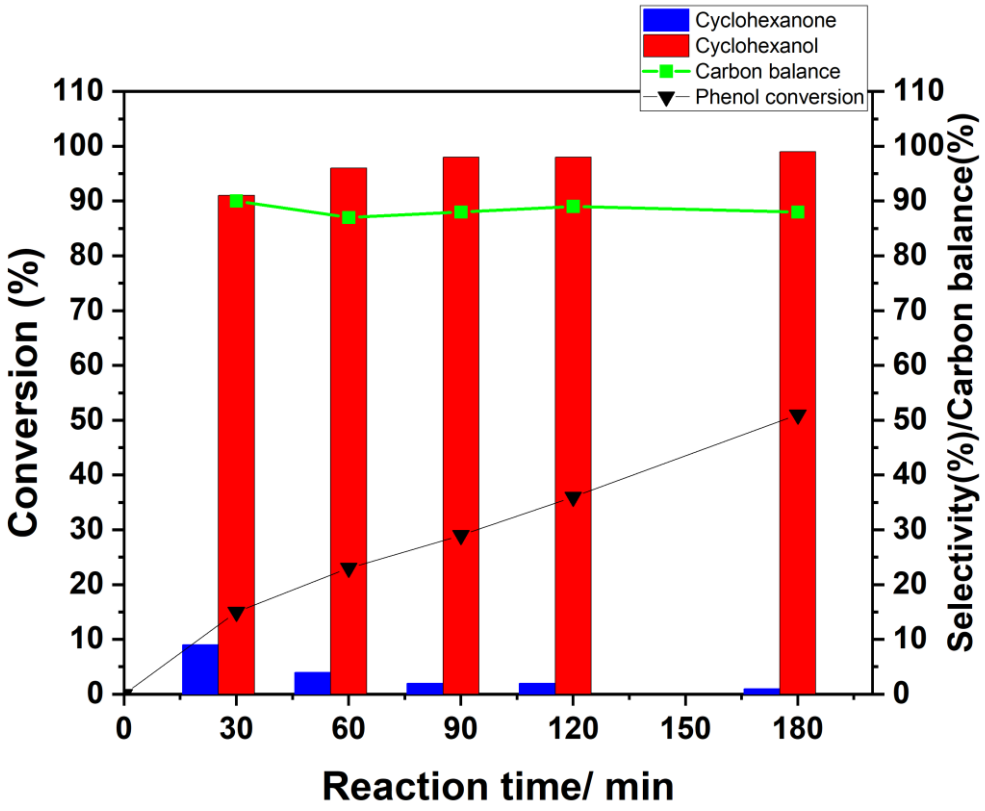

Figure 4.3: Effect of reaction time on conversion and selectivity over 2.5%Pd-2.5%NiH/Al_2O_3 catalyst. **Reaction conditions:** Phenol 0.5 mmol, catalyst 30 mg, isopropanol (IPA) used as a solvent, temperature 50 ºC, 1 bar H_2 gas, all samples analysed by the GC using dodecane as an internal standard.

However, the use of 2.5%Pd-2.5%Ni on alumina did not yield superior results. Both the 2.5%Pd-2.5%CuH/Al_2O_3 (refer to **Figure 4.4**) and 2.5%Pd-2.5%FeH/Al_2O_3 catalysts (refer to **Figure 4.5**) exhibited limited activity. The product selectivity exhibited a difference when the catalyst used was 2.5%Pd-2.5%CuH/Al_2O_3. The proportion of cyclohexanone was high at the onset until the reaction time reached one hour, with a 5 % conversion and 100 % selectivity towards cyclohexanone. Subsequently, cyclohexanol was produced, with the selectivity rising to 43 % at 180

minutes. A mere 12 % phenol conversion was identified at the reaction's conclusion when the 2.5%Pd-2.5%CuH/Al_2O_3 catalyst was employed, indicating its considerably lower activity in comparison to the other catalysts[48].

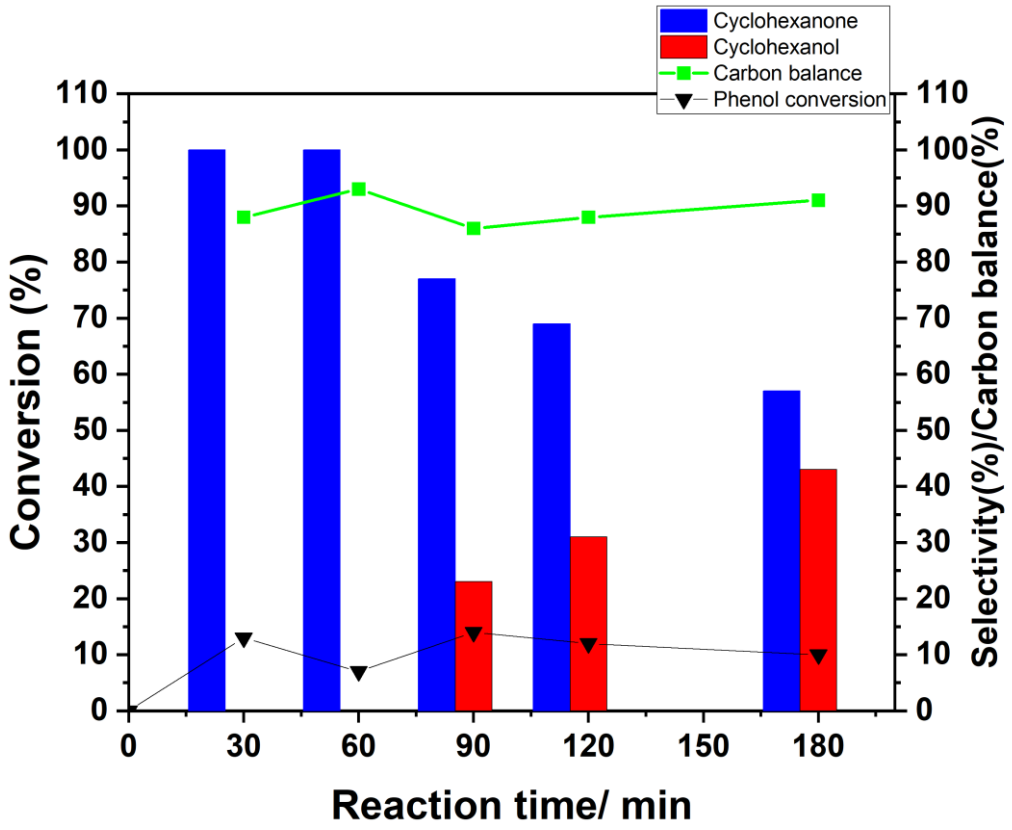

Figure 4.4: Effect of reaction time on conversion and selectivity over 2.5%Pd-2.5%CuH/Al_2O_3 catalyst. **Reaction conditions:** Phenol 0.5 mmol, catalyst 30 mg, isopropanol (IPA) used as a solvent, temperature 50 ºC, 1 bar H_2 gas, all samples analysed by the GC using dodecane as an internal standard.

Although the non-precious 2.5%Pd-2.5%FeH/Al_2O_3 catalyst achieves limited phenol conversion, it exhibits commendable selectivity for cyclohexanone, potentially due to its electronic structure and lower conversion levels. As the reaction time extends from 30 to 180 minutes (refer to **Figure 4.5**), a notable quantity of cyclohexanone is generated, while its selectivity declines in line with the phenol conversion nearing 10 %. Notably, secondary cyclohexanol reactions commence after 90 minutes, with selectivity escalating to 43 %, with no significant alteration in phenol conversion. Consequently, it is postulated that most of the aromatic ring saturation (transforming into cyclohexanol) likely occurs via the hydrogenation of the tautomerisation reaction pathway (converting into cyclohexanone) over the Pd/Fe bimetallic catalysts[49]. Xiaowa et al.[50] discovered that the direct hydrogenation of the aromatic ring

constituted the kinetically favoured pathway for phenol conversion on Pd doped Fe(110) and Fe(111) surfaces.

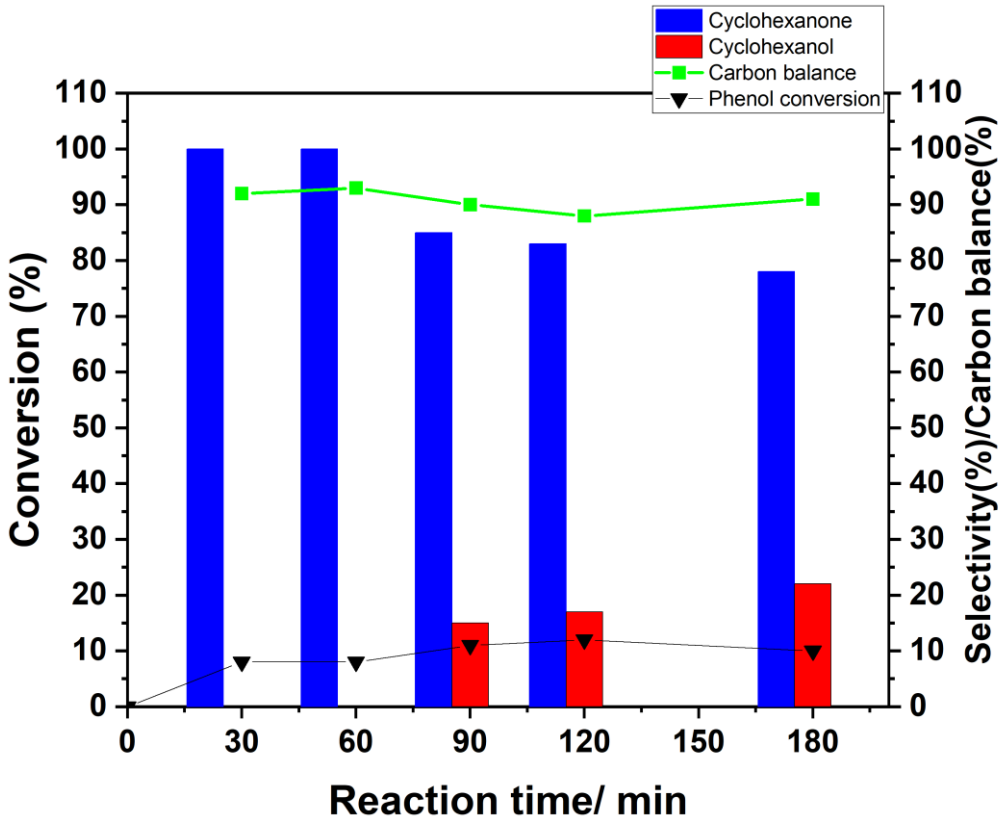

Figure 4.5: Effect of reaction time on conversion and selectivity over 2.5%Pd-2.5%FeH/Al_2O_3 catalyst. **Reaction conditions:** Phenol 0.5 mmol, catalyst 30 mg, isopropanol (IPA) used as a solvent, temperature 50 ºC, 1 bar H_2 gas, all samples analysed by the GC using dodecane as an internal standard.

Furthermore, the interaction between Pd and Au in the 2.5%Pd-2.5%AuH/Al_2O_3 bimetallic catalyst (refer to **Figure 4.6**) alters the electronic properties of Pd, thus influencing Pd's catalytic behaviour. From the standpoint of product output, Pd-Au does not augment the conversion of phenol compared to the Pd-Ru and Pd-Ni catalysts, although it performs well in terms of selectivity for cyclohexanone. This suggests that the selection of an appropriate metal is crucial to enhancing the results. The size of a metal's nanoparticles (NPs) establishes their geometric and electronic structures, which, in turn, determines their catalytic performance[51]. Nonetheless, the entanglement of geometric and electronic structures, often dependent on size, frequently leads to a trade-off between activity and selectivity. This poses a limitation on the potential to optimise the overall catalytic performance[52].

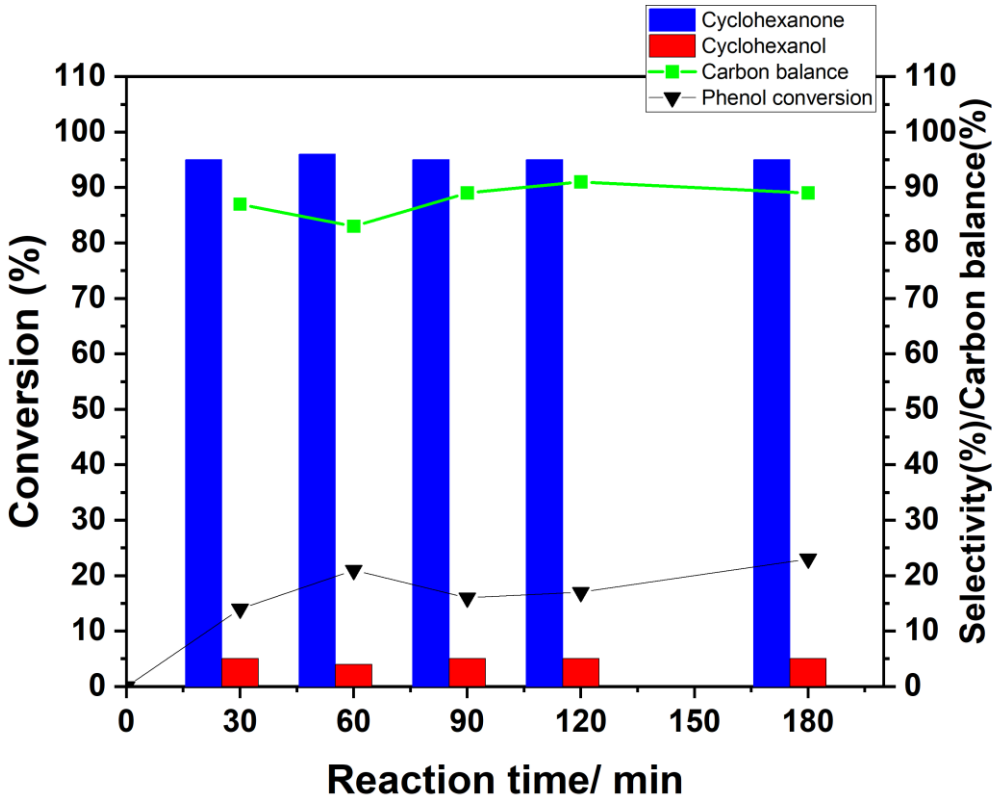

Figure 4.6: Effect of reaction time on conversion and selectivity over 2.5%Pd-2.5%AuH/Al_2O_3 catalyst. **Reaction conditions:** Phenol 0.5 mmol, catalyst 30 mg, isopropanol (IPA) used as a solvent, temperature 50 ºC, 1 bar H_2 gas, all samples analysed by the GC using dodecane as an internal standard.

XPS (X-ray Photoelectron Spectroscopy) examinations were performed to provide additional information regarding monometallic Pd and Ru, the interactions between Pd and X (where X refers to Ru, Au, Ni, Cu, and Fe), and the valence states of the surface metal species for the samples as depicted in **Table 4.2**. From the table, it can be observed that all bimetallic catalysts possess $Pd^{2+}3d+Cl^-$ species, except for the 2.5%Pd-2.5%AuH/Al_2O_3 catalyst. Only the 2.5%Pd-2.5%RuH/Al_2O_3 catalyst is found to have Ru3dOx species. In reference to **Table 4.2**, the highest atomic concentration of Pd^0 is recorded at 0.72 for the 2.5%Pd-2.5%FeH/Al_2O_3 catalyst. However, the high concentration of non-noble metals paired with palladium in the catalyst could have been the primary reason for the catalysts' relative ineffectiveness when compared to noble metal catalysts.

Table 4.2: XPS data for bimetallic Pd-X (X= Ru, Au, Ni, Fe and Cu) catalysts

Compound	Pd^0 Position/ %At Conc.	$Pd^{2+}3d$ Position/ %At Conc.	$Pd^{2+}3d+Cl^-$ Position/ %At Conc.	Cl^-2p Position/ %At Conc.	X=(Ru, Au, Ni, Cu and Fe) Position/ %At Conc.	Ru3d O_x Position/ %At Conc.	C1s Position/ %At Conc.	Pd^{2+}/Pd^0 Molar ratio
2.5%Pd-2.5%Ru	335.64/0.29	337.19/0.27	338.72/0.16	199.64/0.52	**$Ru^0$3d** (280.82/0.2)	281.9/0.37	285.03/11.23	0.9
2.5%Pd-2.5%Au	335.21/0.31	336.62/0.05	------	198.75/0.56	**$Au^0$4f** (83.75/0.18)	------	------	0.16
2.5%Pd-2.5%Ni	335.31/0.55	336.34/0.33	337.68/0.12	198.99/0.7	**Ni2p** (856.49/0.83)	------	------	0.6
2.5%Pd-2.5%Cu	335.45/0.49	336.93/0.25	338.42/0.05	199.22/0.84	**$Cu2p_{3/2}$ (**933.22/1.44)	------	------	0.5
2.5%Pd-2.5%Fe	335.36/0.72	336.24/0.15	337.72/0.05	198.38/0.63	**Fe2p** (710.98/1.33)	------	------	0.2

4.3.3. Comparing the Pd-Ru bimetallic catalyst with Pd and Ru monometallic catalysts

In an earlier study, Liao et al.[28] found that the Pd-Ru/MSN (mesoporous silica nanoparticles) catalyst demonstrated an activity five times greater than that of Pd/MSN towards the liquid-phase hydrogenation of phenol under mild conditions (50 °C, 1.0 MPa PH_2, m(Pd) / m(phenol) = 1:500, reaction for 60 min). Here, the conversion was 72 % and the selectivity for all products was as follows: Cyclohexanone 63 %, Cyclohexanol 26 %, Cyclohexane 11 %.

Monometallic Ru, Pd and bimetallic Pd-Ru (in a 1:1 weight ratio) with a metal loading of 5 % wt. were prepared using the M_{im} methods, with reduction by $NaBH_4$. These catalysts were evaluated for phenol hydrogenation under mild conditions to investigate the catalytic performance of the bimetallic Pd-Ru catalyst supported on Al_2O_3. The performance results are presented in terms of the activity of the reaction and the selectivity for cyclohexanone and cyclohexanol, the two products and catalytic activity, as delineated in **Table 4.3.** The monometallic Pd catalyst displays a lower conversion of 26 % compared to both the monometallic Ru and the bimetallic Pd-Ru catalysts, which achieved 100 % conversion.

Table 4.3: Comparing mono and bimetallic Ru and Pd catalysts on phenol hydrogenation conversion and selectivity:

Catalysts	Conv. (%) Phenol	Sel. (%)		Mass balance (%)
		Cyclohexanone	Cyclohexanol	
2.5%Pd-2.5%RuH/Al_2O_3	**100**	**0**	**99**	**98**
5%PdH/Al_2O_3	**26**	**95**	**5**	**95**
5%RuH/ Al_2O_3	**100**	**0**	**100**	**100**

Reaction conditions: Phenol 0.5 mmol, catalyst 30 mg, isopropanol (IPA) used as a solvent, temperature 50 ºC, 3 hours, 1 bar H_2 gas, all samples analysed by the GC using dodecane as an internal standard.

For extended reaction times, both the monometallic Ru catalyst (as seen in **Figure 4.7**) and the bimetallic Pd-Ru catalyst (discussed in section 4.3.2, see **Figure 4.2**) demonstrate high selectivity towards cyclohexanol alongside complete conversion. Utilizing a 5%RuH/Al_2O_3 catalyst, the formation of cyclohexanol was detected with 100 % conversion of phenol[53]. The bimetallic Pd-Ru catalyst achieved 100 % phenol conversion in 30 minutes, whereas the monometallic Ru catalyst only attained a 5 % conversion at the same time. The Ru catalyst required quadruple the time, reaching 100 % phenol conversion after 120 minutes. The intermediate product, cyclohexanone, initially held 45 % selectivity, which then diminished to 0 % by 120 minutes. With the monometallic Ru catalyst (refer to **Figure 4.7**), we noticed an increase in conversion (100 %) paired with a surge in the formation of cyclohexanol (over 99 %). However, these findings show that the monometallic Ru's activity is inferior to that of the bimetallic Pd-Ru for phenol hydrogenation under the same conditions. Also, cyclohexane was identified as another product with 1 % selectivity when employing the bimetallic Pd-Ru catalyst. The enhanced hydrogenation performance of the 2.5%Pd-2.5%RuH/Al_2O_3 catalyst can be attributed to the superior activity and dispersion of the Pd-Ru phase. On the other hand, the monometallic Pd catalyst (refer to **Figure 4.8**) displays a similar selectivity ratio towards cyclohexanone and cyclohexanol throughout the reaction's duration. Nevertheless, the conversion remained low, reaching only 26 % by the end of the reaction.

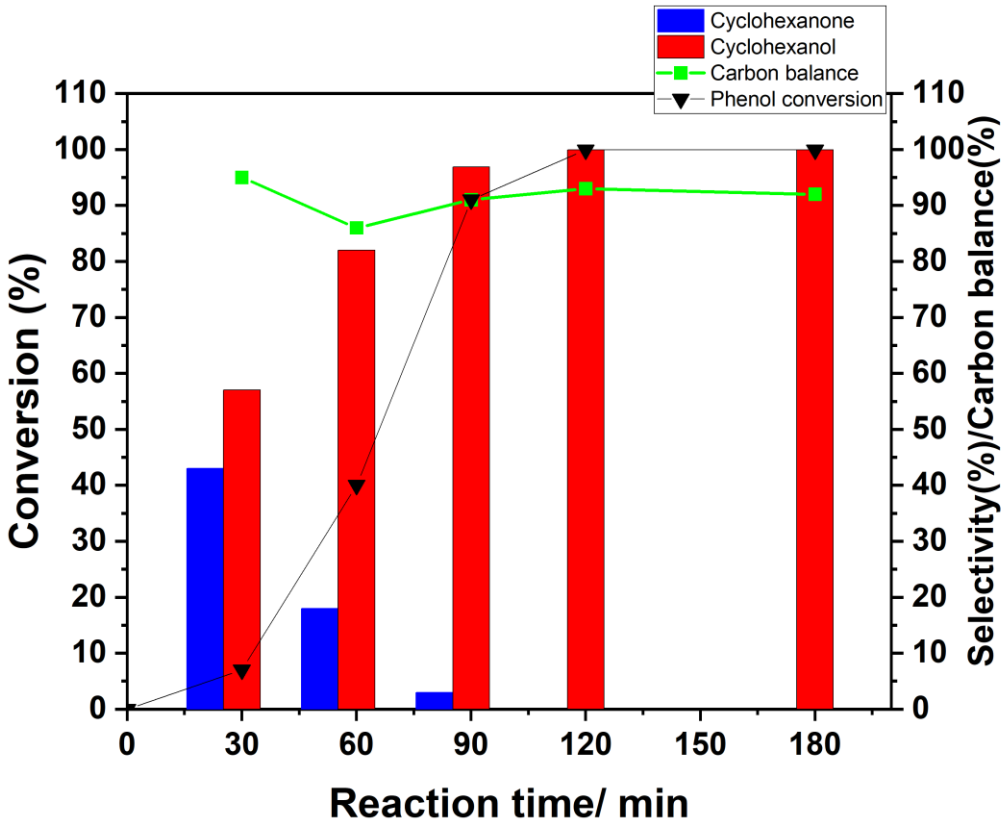

Figure 4.7: Effect of reaction time on conversion and selectivity over monometallic Ru catalyst. **Reaction conditions:** Phenol 0.5 mmol, catalyst 30 mg, isopropanol (IPA) used as a solvent, temperature 50 ºC, 1 bar H_2 gas, all samples analysed by the GC using dodecane as an internal standard.

Phenol adsorption behaviour on the catalyst support can play a significant role in determining the reaction's end products. When phenol is adsorbed on the support's acidic sites in a co-planar manner, it tends to form cyclohexanol due to the strong interaction between the aromatic ring and the support Conversely, when phenol is adsorbed on the base sites in a non-planar configuration, it favours the formation of cyclohexanone. The catalyst support utilized in this study, Al_2O_3, possesses both acidic and basic sites. However, the 5%PdH/Al_2O_3 catalyst (**Figure 4.8)** shows high selectivity for cyclohexanone, reaching 95 %, making it an industrially significant catalyst. Despite the evidence suggesting the role of acidic sites in favouring the formation of cyclohexanone, Chen and Sun[54] have demonstrated that acidic sites are not entirely detrimental to cyclohexanone production. Additionally, Liu et al.[55] conducted a study to understand the effects of Lewis acid on the selective hydrogenation of phenol. They proposed that weak adsorption due to reduced acidity and lower Pd availability could lead to improved selectivity. However, they also noted that if too many acid sites disappear, the selectivity of cyclohexanone would increase. These studies suggest that both the acid-base properties of the catalyst support and

the nature of the metal particles play crucial roles in the hydrogenation of phenol to either cyclohexanol or cyclohexanone. Therefore, a balanced consideration of these factors is crucial when designing efficient catalysts for this reaction.

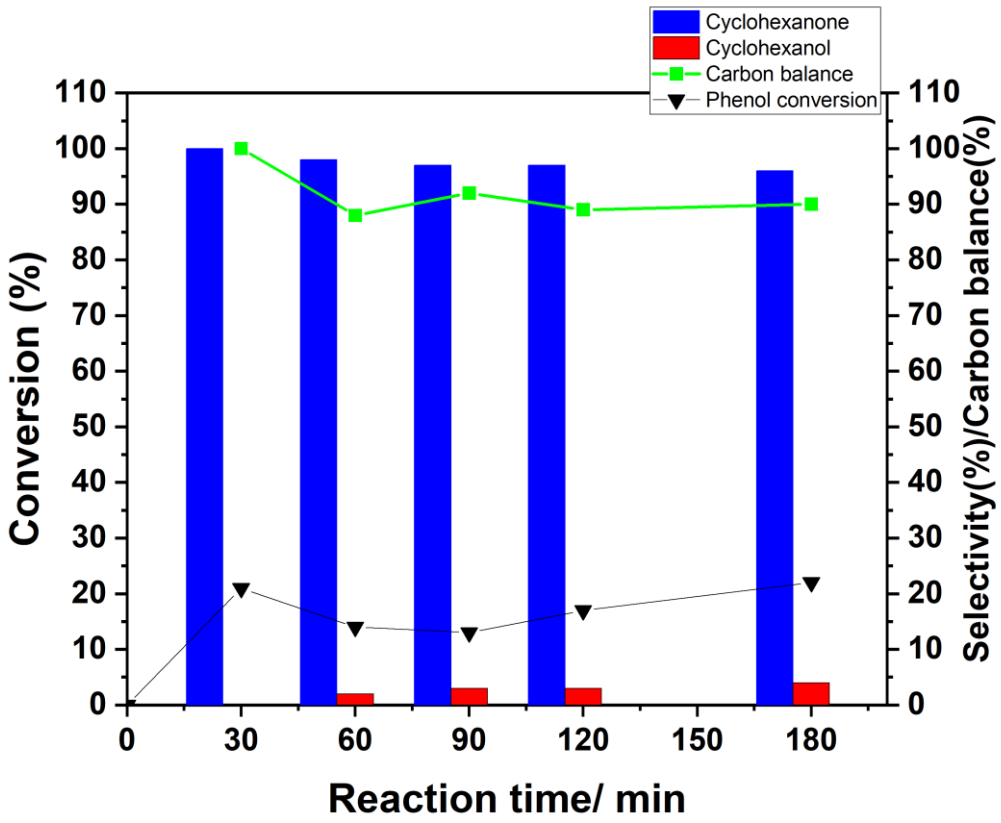

Figure 4.8: Effect of reaction time on conversion and selectivity over monometallic Pd catalyst. **Reaction conditions:** Phenol 0.5 mmol, catalyst 30 mg, isopropanol (IPA) used as a solvent, temperature 50 ºC, 1 bar H_2 gas, all samples analysed by the GC using dodecane as an internal standard.

The experimental setup using time online studies for the 2.5%Pd-2.5%RuH/Al_2O_3 catalyst at a lower temperature (30 °C) provided more nuanced information about the catalyst's behaviour during the phenol hydrogenation process. As indicated by the data obtained (**Figure 4.9**), a clear transformation in selectivity occurs early in the reaction.

As the reaction time was increased, the phenol conversion experienced a significant boost, starting from 5 % at the 5-minute mark to 100 % by 40 minutes. Both cyclohexanone and cyclohexanol were the primary products at the beginning of the reaction. However, as the reaction time progressed, a noticeable decrease in cyclohexanone selectivity was observed, which corresponded with a steady rise in cyclohexanol selectivity. By 40 minutes, the selectivity for cyclohexanol had reached its peak at the 100 % conversion point. After this, the selectivity for cyclohexanol remained consistently high (100 %) after 90 minutes, while cyclohexanone selectivity

dropped to zero. This shift in selectivity patterns could be due to a strong interaction between phenol and the catalyst, leading to complete hydrogenation to produce cyclohexanol. The synergetic effect between Pd and Ru metals might also play a role in this change.

Under the conditions of 30 °C and 1 bar hydrogen pressure, the 2.5%Pd-2.5%RuH/Al_2O_3 catalyst effectively hydrogenated phenol (100 % conversion) with 100 % selectivity to cyclohexanol within an hour. As the reaction time increased, the conversion of phenol also increased. However, an initial drop in selectivity to cyclohexanone was observed. As cyclohexanone was produced, it was further hydrogenated to cyclohexanol.

The presence of Ru in the catalysts may have caused a decrease in the number of small Pd particles, thereby reducing the selectivity of cyclohexanone. This effect might have also contributed to the more pronounced agglomeration and larger average particle sizes66. Further studies involving changes in reaction time at constant temperature (30 °C) and pressure (1 bar) also reflected this trend. The selectivity towards cyclohexanone showed a sharp decline in the first 30 minutes, reaching zero after 60 minutes. The high initial rate of phenol conversion eventually slowed down due to the ongoing hydrogenation of cyclohexanone to cyclohexanol. This dynamic resulted in a corresponding decrease in selectivity towards cyclohexanone and an increase in selectivity towards cyclohexanol [53].

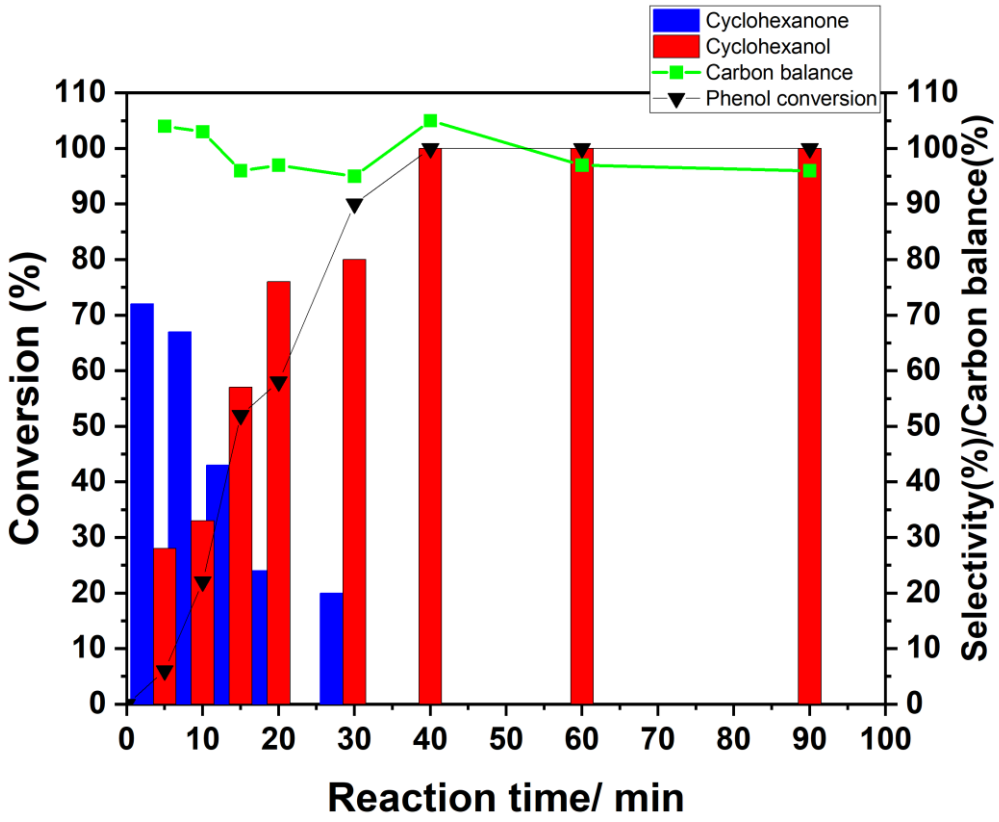

Figure 4.9: Effect of reaction time on conversion and selectivity over 2.5%Pd-2.5%RuH/Al_2O_3 catalyst. **Reaction conditions:** Phenol 0.5 mmol, catalyst 30 mg, water use as a solvent 5ml, temperature 30 ºC, 1 bar H_2 gas, all samples analysed by the GC using dodecane as an internal standard.

The core-level binding energies in the Pd $3d_{5/2}$ and Ru $3d_{5/2}$ spectra of the 2.5%Pd-2.5%RuH/Al_2O_3 catalyst was examined and compared with monometallic Pd and Ru (chapter 3, section 3.6, **Figures 3.19 A & B**). In the case of the Pd core-level binding energy, it could be separated into two pairs of peaks: the higher Pd $3d_{5/2}$ energy value of PdO (approximately 336.18 eV) and the lower energy value of metallic PdO (around 334.9 eV). On observing the 2.5%Pd-2.5%RuH/Al_2O_3 catalyst (**Figure 3.19 D**), it's seen that the Pd^0 and Pd^{2+} fitting peaks are slightly shifted, having corresponding positions of 335.64 eV (a positive shift of 0.74–0.79 eV) and 337.19 eV. This shift in the Pd 3d binding energy for the Pd-Ru bimetallic catalysts indicates a change in the electronic properties of the Pd atom upon alloying with Ru, a modification also detectable by the binding energy shift of Ru. The Ru Pd $3d_{3/2}$ and Ru $3d_{5/2}$ peaks overlap with the C 1s peak. The Ru Pd $3d_{5/2}$ XPS signal was examined in **Figure 3.19 C** for the 2.5%Pd-2.5%RuH/Al_2O_3 catalyst, intending to investigate the chemical state of Ru. The Ru 3d XPS spectra of the 2.5%Pd-2.5%RuH/Al_2O_3 catalyst shown in **Figure 3.19 C** reveals the binding energies of Ru $3d_{5/2}$ in the catalyst at 280.82 eV, which is attributed to Ru^0. There is also a 0.82- eV shift in the Ru peaks. Notably, for the 2.5%Pd-2.5%RuH/Al_2O_3 catalyst, only one pair of fitting peaks of Ru are present,

predominantly existing in the Ru^0 state. This observation further indicates a strong charge-transfer interaction between Ru and Pd atoms in the bimetallic catalyst. Lastly, additional information regarding the species present in all comparison catalysts is provided in **Table 4.4**.

Table 4.4: XPS data for monometallic Pd and Ru compared with bimetallic Pd-Ru catalyst:

Compound	Pd^0 Position/ %At Conc.	$Pd^{2+}3d$ Position/ %At Conc.	$Pd^{2+}3d+Cl^-$ Position/ %At Conc.	Cl^-2p Position/ %At Conc.	$Ru^0 3d$ Position/ %At Conc.	Ru3d O_x Position/ %At Conc.	C1s Position/ %At Conc.
5%Pd	335.22/0.73	336.44/0.18	337.67/0.07	198.73/0.64	------	------	------
5%Ru	------	------	------	198.92/1.71	281.31/0.08	281.85/0.26	284.66/15.04
2.5%Pd-2.5%Ru	335.64/0.29	337.19/0.27	338.72/0.16	199.64/0.52	280.82/0.2	281.9/0.37	285.03/11.23

4.3.3.1. Effect of support for Pd-Ru system

The product formation in the hydrogenation of phenol is influenced by the ability of the phenol to adsorb to and activate the support As reported by Taylor and colleagues in 1972, polyphenols were found to chemisorb strongly to the Al_2O_3 surface with the orientation of the phenoxide surface species being coplanar to the surface[56]. In contrast, Neri et al.[23] demonstrated that using Pd/MgO instead of Pd/A_2O_3 in the phenol hydrogenation resulted in higher selectivity for cyclohexanone, with two different types of adsorbed phenol molecules being observed. Both coplanar and nonplanar modes of phenol adsorption to the support, determined by the acid-base characteristics of a catalyst, play a role in product formation (**Figure 4.10**). It was found that non-planar adsorption of phenols favours the production of cyclohexanone, while coplanar adsorption favours the saturation hydrogenation of cyclohexanone to cyclohexanol[57].

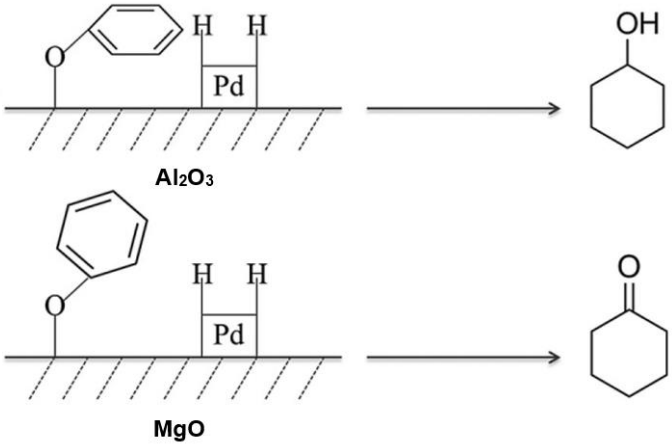

Figure 4.10: Non-planar and coplanar adsorption mode of phenol on the supports. Reproduced from ref.[23].

The bimetallic Pd-Ru nanoparticles (NPs) can be seen as highly active catalysts for the hydrogenation of phenol to cyclohexanol under mild conditions. These NPs function as a tandem catalytic system, with the affinity of the ketone for the metal surface favouring the cyclohexanol formation step and inhibiting the dehydration process[44]. This efficient catalytic activity can be attributed to the electronic synergism between the two metals, which adjusts the electron density of one metal relative to the other. In the case of Pd-Ru NPs, the electron-deficient surface contributes to the catalytic activity, as the electrophilic surface promotes the coordination of unsaturated substrates[58,59]. When Pd-Ru (1 wt. %, ratio 1:1) loading is used, as shown in **Table 4.5**, the type of support used significantly impacts product selectivity. For instance, using TiO_2 as a support, an 80 % conversion of phenol to cyclohexanol was observed, whereas using Al_2O_3 as a support resulted in an increase in conversion from 48 % to 76 %, but with a slight decrease in cyclohexanol formation (78 %). The use of zeolite as a support for phenol hydrogenation is relatively underexplored, mainly due to the predominantly microporous nature of zeolite which is not conducive for aromatic compound mass transfer[60]. However, a 24 % conversion of phenol with 90 % selectivity for cyclohexanone was achieved with zeolite. This was attributed to the effective cooperation of 'electron-deficient' Pd-Ru and the Pd-Ru peripheral zeolite skeleton.

A 0.5%Pd-0.5%RuH/CeO_2 catalyst demonstrated no activity for phenol hydrogenation, potentially due to weak interaction between the support and metals, leading to poor metal NP dispersion and particle agglomeration[61]. However, the 0.5%Pd-0.5%RuH/Al_2O_3 catalyst proved to be the optimal choice for phenol hydrogenation, as it increases selectivity and promotes complete transformation. The performance increase of the 0.5%Pd-0.5%RuH/Al_2O_3 catalyst is attributed to the

support's adjustable pore structure, strong shape-selective catalytic property, and acid-base performance, as well as the reduction method.

Table 4.5: Comparing bimetallic Ru and Pd catalysts supported on deferent metal oxide on phenol hydrogenation conversion and selectivity:

Catalyst	Phenol conv. %	C=O Sel. %	C-OH Sel. %	Carbon balance %
0.5%Pd-0.5%RuH/Al_2O_3	**76**	**22**	**78**	**99**
0.5%Pd-0.5%RuH/TiO_2	**48**	**20**	**80**	**98**
0.5%Pd-0.5%RuH/Zeolite Y hydrogen	**24**	**90**	**10**	**96**
0.5%Pd-0.5%RuH/CeO_2	**0**	**0**	**0**	**96**

Reaction conditions: phenol 0.2 mmol, catalyst 30 mg, water used as a solvent, temperature 30 ºC, 1 hour, 1 bar H_2 gas, all samples analysed by the GC.

To delve further into this matter, the 0.5%Pd-0.5%RuH/Al_2O_3, 0.5%Pd-0.5%RuH/CeO_2, 0.5%Pd-0.5%RuH/TiO_2 and 0.5%Pd-0.5%RuH/zeolite Y hydrogen catalysts were characterised using XPS, and the outcomes are displayed in **Table 4.6**. According to the table, only the 0.5%Pd-0.5%RuH/zeolite Y hydrogen catalyst exhibits both Pd and Ru metals, along with their oxide states, in the presence of Cl^-. Conversely, 0.5%Pd-0.5%RuH/TiO_2 features Pd and Ru metals and their oxide states, but without the presence of Cl^-. For the 0.5%Pd-0.5%RuH/CeO_2 catalyst, no peaks were observed for Pd metal and Cl^-. Finally, the results for the 0.5%Pd-0.5%RuH/Al_2O_3 catalyst showed no peak for the RuOx state alone.

Table 4.6: XPS data for bimetallic 0.5%Pd-0.5%Ru catalyst supported on deferent metal oxide:

Compound	Pd^0 Position/ %At Conc.	$Pd^{2+}3d$ Position/ %At Conc.	Cl^-2p Position/ %At Conc.	$Ru^0 3d$ Position/ %At Conc.	Ru3d O_x Position/ %At Conc.	C1s Position/ %At Conc.
0.5%Pd-0.5%RuH/ Zeolite Y hydrogen	334.94/0.45	336.98/0.13	198.05/0.21	279.91/0.22	280.76/0.35	284.8/11.78
0.5%Pd-0.5%RuH/TiO_2	335.18/0.27	337.36/0.2	------	280.61/0.32	281.38/0.17	284.8/18.77
0.5%Pd-0.5%RuH/CeO_2	------	337.83/0.73	------	281.23/0.55	281.93/0.28	284.8/21
0.5%Pd-0.5%RuH/Al_2O_3	335.31/0.55	336.34/0.33	198.99/0.7	279.91/0.22	------	284.96/22.98

4.3.3.2. Effect of solvent on conversion and selectivity of phenol hydrogenation

The hydrogenation of phenol was examined using Al_2O_3 supported catalysts, specifically 0.5%Pd-0.5%Ru and 0.5%Pd-0.5%Au, within a range of solvents [62]. . Observations highlighted in **Figure 4.11** revealed that the Pd-Ru catalyst achieved conversion and cyclohexanol selectivity of just below 97 % in both water and isopropanol. Interestingly, cyclohexanone was not detected until ethanol was introduced as the solvent. Moreover, cyclohexane emerged exclusively for the Pd-Ru catalyst in all solvents except water. Toluene was also employed as a solvent, with results detailed in **Figure 4.11**, and yielded methylcyclohexane as a by-product from the hydrogenation of toluene in the presence of the 0.5%Pd-0.5%Ru catalyst. Consequently, despite the 54 % cyclohexane selectivity making it an attractive solvent, the catalyst's efficacy could be compromised.

On the other hand, the 0.5%Pd-0.5%Au catalyst demonstrated the least conversion in both alcohol-based solvents. However, this catalyst showcased a high conversion rate and 95 % cyclohexanone selectivity when water was used as the solvent, as shown in **Figure 4.12**. When toluene was utilized, the phenol conversion was 45 % with selectivity of 78 %, 5 %, and 17 % for cyclohexanone, cyclohexanol, and cyclohexane, respectively. Despite evidence of toluene hydrogenation, the conversion rate was lower than when water was the solvent, thus deeming it less ideal for selectivity[33]. The marked improvement in the selectivity of the Pd-Ru catalyst

towards cyclohexanol in a water-based solvent is noteworthy. Also, it's important to highlight that the Pd-Au catalyst's activity was enhanced when water was used as a solvent. Further observations revealed a 54 % selectivity for cyclohexane in a toluene solvent.

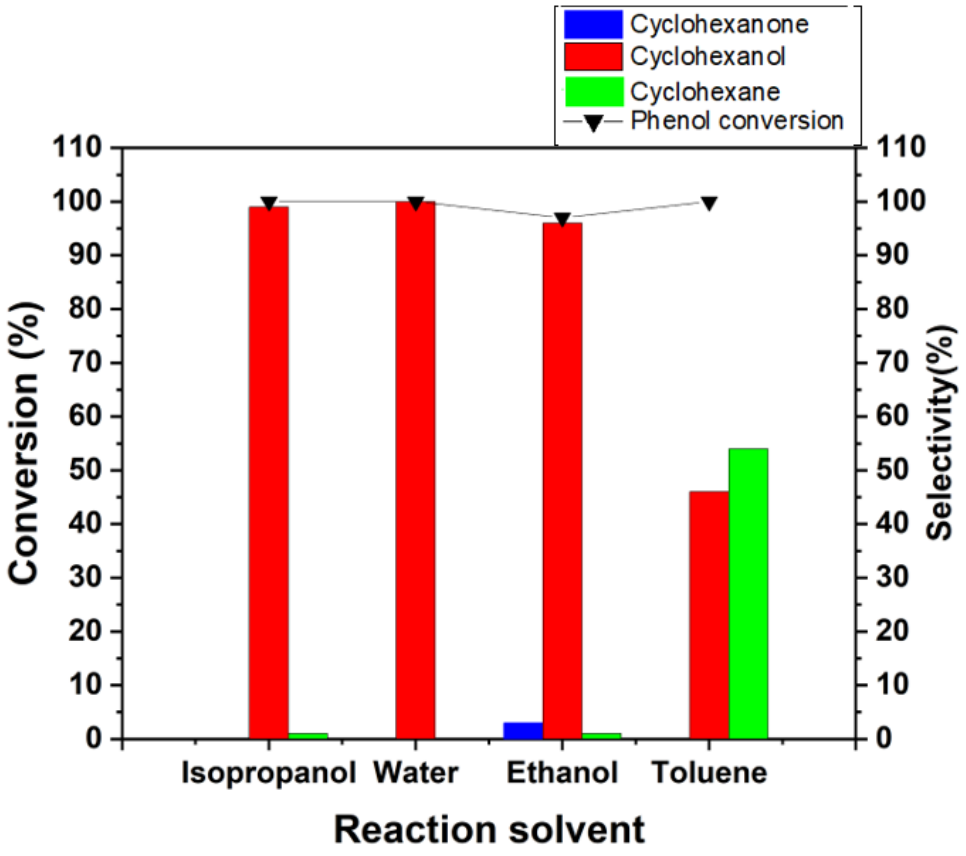

Figure 4.11: Effect of reaction solvent on conversion and selectivity over 0.5%Pd-0.5%RuH/Al_2O_3 catalyst. **Reaction conditions:** phenol (0.5 mmol), catalyst (30 mg), solvent 5 ml, 50 ºC, 1 bar H2. b conversion and selectivity determined by GC after 3 hours of reaction.

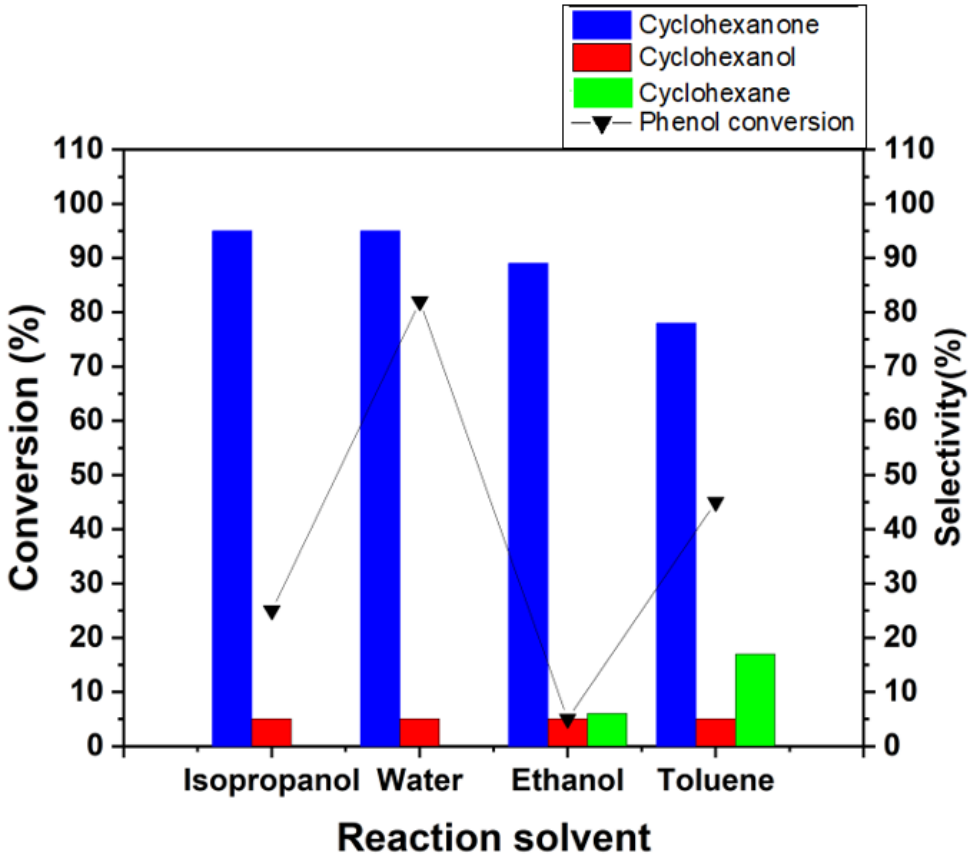

Figure 4.12: Effect of reaction solvent on conversion and selectivity over 0.5%Pd-0.5%AuH/Al_2O_3 catalyst. **Reaction conditions:** phenol (0.5 mmol), catalyst (30 mg), solvent 5 ml, 50 ºC, 1 bar H2. b conversion and selectivity determined by GC after 3 hours of reaction.

However, The selectivity of cyclohexanol using the Pd-Ru catalyst in all solvents is remarkably high, however, it results in a mix of products, except in the case of water[62]. Phenol hydrogenation in ethanol is suboptimal due to the inhibitory impact of ethanol on the hydrogenation of aromatic compounds, a phenomenon that escalates with declining catalytic activity[34]. These findings suggest that the Pd-Ru catalyst's initial catalytic activity in water is notably superior compared to other solvents, a difference likely attributed to solvent inhibition. To elucidate the effect of water on conversion and selectivity of phenol hydrogenation over the 0.5%Pd-0.5%RuH/Al_2O_3 catalyst, a time-dependent study was carried out. This involved using water as a solvent at 30 ºC under a 1 bar H_2 gas pressure for a duration of 90 minutes. Details of this procedure are further elaborated in section 4.3.3, **Figure 4.9**.

In a scenario where water replaces organic solvents, there is continuous adsorption of phenol on the Pd-Ru catalyst. This helps maintain the dispersion of Pd-Ru nanoparticles and aids in the reduction of Pd (2+) and Ru (3+). In essence, water emerges as a suitable solvent for producing cyclohexanol and cyclohexanone through

selective phenol hydrogenation over the 0.5%Pd-0.5%RuH/Al_2O_3 and 0.5%Pd-0.5%AuH/Al_2O_3 catalysts, respectively[63].

4.3.3.3. Temperature dependency study

The effect of temperature on phenol conversion over time using the 0.5%Pd-0.5%AuH/Al_2O_3 bimetallic catalyst is of particular interest. As one might anticipate, a temperature rises from 30 °C to 50 °C markedly enhances phenol hydrogenation65. At 30 °C, a remarkable 90 % phenol conversion was observed, with product distribution consisting of 80 % cyclohexanol and 20 % cyclohexanone – a performance that stands out as exceptional. Meanwhile, at the elevated temperature of 50 °C, the conversion reached a full 100 %, with cyclohexanol demonstrating an impressive 100 % selectivity (using water as a solvent). This raises the question of whether a boost in reaction temperature contributes to an increase in the catalyst's activity. Intriguingly, across both reaction temperatures, the same pattern in catalytic activity towards cyclohexanol formation was observed (see **Figure 4.13**). In the presence of water, total phenol conversion was achieved within a 60-minute span, yielding 100 % cyclohexanol. This indicates that as reaction temperature rises, the substrate's interaction with the active catalyst site intensifies. Phenol hydrogenation has been explored at lower reaction temperatures but has garnered substantial interest at higher ones. Conversely, the phenol hydrogenation reaction picks up speed at elevated temperatures due to the accelerated rate of complete conversion[48].

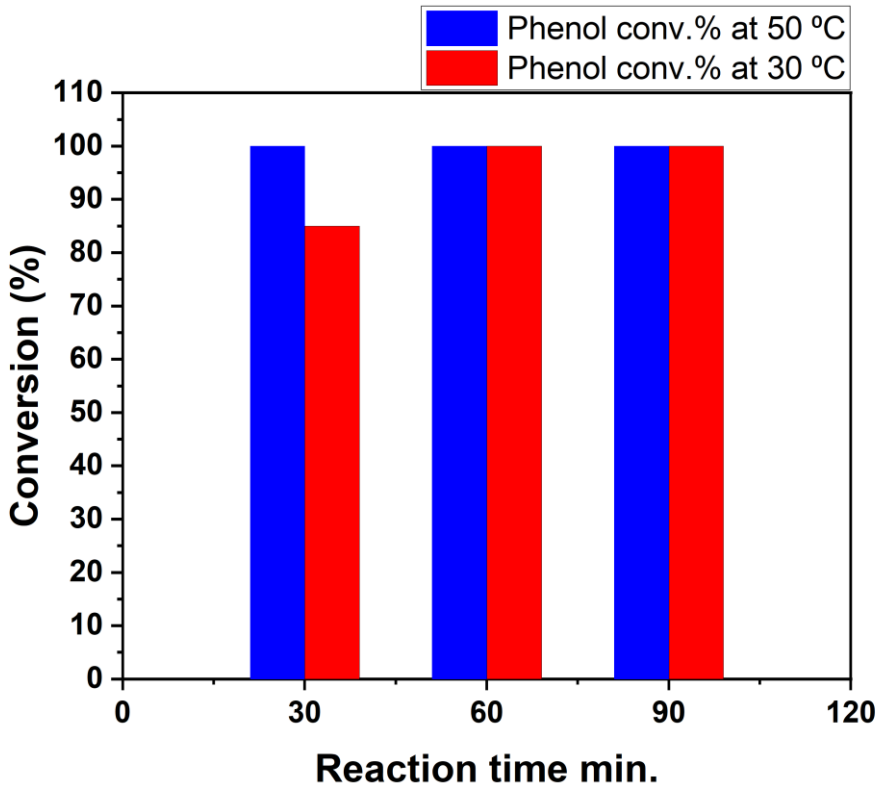

Figure 4.13: Effect of temperature on the hydrogenation of phenol over Pd-Ru bimetallic catalysts. **Reaction conditions:** Phenol 0.5 mmol, catalyst 30 mg, isopropanol (IPA) used as a solvent, temperature 30 and 50 ºC, 1 bar H_2 gas, all samples analysed by the GC using dodecane as an internal standard.

4.3.3.4. Effect of metal loading and metal ratio

After the exploration of phenol hydrogenation over the 0.5%Pd-0.5%RuH/Al_2O_3catalyst, supplementary tests were conducted using Pd-Ru bimetallic catalysts supported on different materials. Gamma alumina was selected as the preliminary support material, inspired by empirical studies that validate Al_2O_3 as a potent catalyst in phenol hydrogenation, achieving full conversion[53,64]. To amalgamate active catalysts for hydrogenation, two Pd-RuH/Al_2O_3 catalysts – with metal loadings of 5% and 1% (expressed as a weight percentage of the metal to the support) – were evaluated for their activity in phenol hydrogenation. The conversion of phenol and the selectivity towards cyclohexanol, as determined by gas chromatography, are presented in **Table 4.7.**

Table 4.7: Effect of the metal loading for Pd-Ru system:

Entry	Catalyst	Phenol conv. %	C=O Sel. %	C-OH Sel. %	Carbon balance %
1	0.5%Pd-0.5%RuH/Al_2O_3	66	34	66	98
2	2.5%Pd-2.5%RuH/Al_2O_3	100	0	100	100
3	0.5%Pd-0.5%RuH/Al_2O_3*	100	0	100	96

Reaction conditions: phenol 0.04 mmol, catalyst 15 mg, water used as a solvent, temperature 30 ºC, 1 hours, 1 bar H_2 gas, all samples analysed by the GC. * Time increased to 3 hours.

As is evident, the loading of Pd-Ru notably impacts the catalyst's properties. The conversion of phenol substantially increased as the metal loading escalated, and the selectivity in both cases was remarkably high. As per **Table 4.7**, the selectivity of cyclohexanol was 66 % and 100 % for 0.5%Pd-0.5%RuH/Al_2O_3 and 2.5%Pd-2.5%RuH/Al_2O_3 respectively under identical conditions. Conversely, extending the reaction time from 1 to 3 hours for 0.5%Pd-0.5%RuH/Al_2O_3 (Entry 3, **Table 4.7**) resulted in the selectivity rising to 100 %. The highest yield of cyclohexanol was achieved at 2.5%Pd-2.5%RuH/Al_2O_3 under the same conditions. Enhanced metal loading resulted in increased activity, possibly due to variations in the size of the catalyst particles and their dispersion during catalyst reduction, leading to an increase in active sites. Given its selectivity for phenol hydrogenation, 0.5%Pd-0.5%RuH/Al_2O_3 was chosen for additional investigation. The effect of the metal ratio was also studied, with 0.5%Pd-0.5%RuH/Al_2O_3 scrutinized for the selective hydrogenation of phenol. The well-defined Ru catalyst demonstrates superior catalytic performance for the selective hydrogenation of phenol, on par with palladium catalysts, leading to the selection of bimetallic Pd-Ru to develop a catalyst encompassing the attributes of both metals. This work observed that the activity of Pd-Ru nanoparticles (NPs) was contingent upon the particle composition for phenol hydrogenation. Although the use of water as a solvent was aimed at tuning the selectivity of the products, there was a formation of cyclohexanol (75 %) and the intermediate cyclohexanone (25 %) during phenol hydrogenation using Pd:Ru in a 1:1 ratio, with a conversion of 24 %. However, the addition of a small amount of Pd (Pd:Ru, 1.5:1) led to a decreased conversion to 22 % under the same reaction conditions. This result suggests that the presence of Pd dampens catalyst activity and the bimetallic material (Pd:Ru, 1:1) behaves more

akin to monometallic Ru, indicating selective hydrogenation of phenol to cyclohexanol. Moreover, an equimolar ratio of Pd:Ru (1:1.5) engenders particles with high activity (35 % conversion) and selectivity (57 %) for the hydrogenation of phenol to cyclohexanol (refer **Table 4.8**). Indeed, the bimetallic Pd-Ru NPs (1:1) fostered the hydrogenation of phenol in water, exclusively resulting in the formation of cyclohexanol. It is posited that cyclohexanone is formed in the first step, which is then rapidly hydrogenated to form cyclohexanol[44].

Table 4.8: Comparing the metal ratio of Ru and Pd on phenol hydrogenation conversion and selectivity:

Metal ratio Pd: Ru	Phenol conv. %	C=O Sel. %	C-OH Sel. %	Carbon balance %
1:1	**24**	**25**	**75**	**94**
1.5:1	**22**	**57**	**43**	**104**
1:1.5	**35**	**43**	**57**	**105**

Reaction conditions: phenol 0.2 mmol, catalyst 30 mg, water used as a solvent, temperature 30 ºC, 0.5 hours, 1 bar H_2 gas, all samples analysed by the GC.

4.3.3.5. Catalyst stability, the effect of leaching

To assess the reusability of the experiment, the catalyst was separated from the reaction mixture and dried under vacuum prior to its reuse. The reaction conditions for this study were set at 30 °C and 1 bar with 15 mg of catalyst. The activity of the 0.5%Pd-0.5%RuH/Al_2O_3 catalyst was observed to decrease slightly during the first run due to minor catalyst deactivation. As demonstrated in **Figure 4.14**, the phenol conversion experienced a minor reduction in the first run with no substantial change in subsequent runs, and the selectivity of cyclohexanol remained almost constant. Consequently, under the given reaction conditions, the catalyst could be recycled without experiencing significant loss in activity.

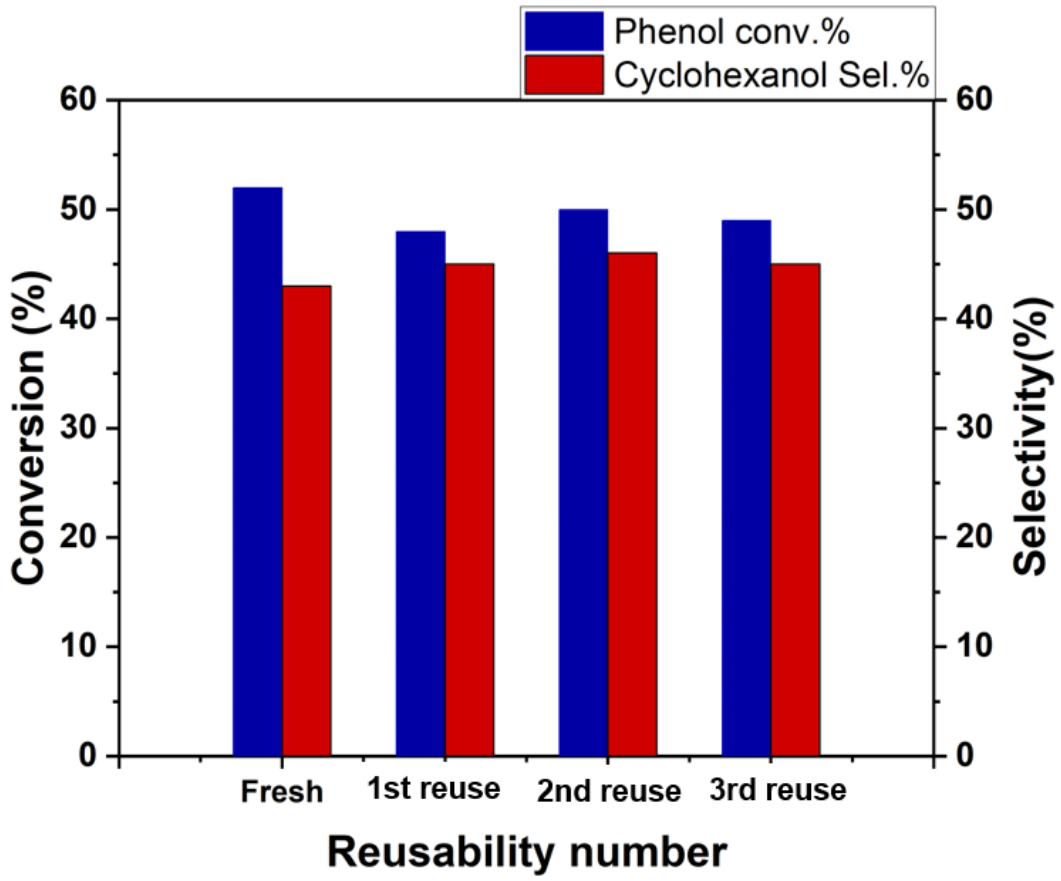

Figure 4.14: Effect of recycling the 0.5%Pd-0.5%RuH/Al_2O_3 catalyst for hydrogenation of phenol. **Reaction conditions:** phenol 0.5 mmol, catalyst 15 mg, water use as a solvent, temperature 30 ºC, time 15 minutes, 1 bar H_2 gas, all samples analysed by the GC using isopropanol as an internal standard.

While the 0.5%Pd-0.5%RuH/Al_2O_3 catalyst demonstrated comparatively high activity, the leaching of the active component into the solution poses a significant challenge for heterogeneous catalysts, especially in the liquid phase. Regarding the 0.5%Pd-0.5%RuH/Al_2O_3 catalyst, the ICP analysis revealed Pd-Ru leaching (Refer to **Table 4.9**), which corresponds to the Pd-Ru present in the reaction mixture across three reuse cycles. The quantities of Ru and Pd in the 1st, 2nd, and 3rd cycles, respectively, are displayed in **Table 4.9** (these represent the original amounts used in the reaction).

Table 4.9: ICP analysis data for Pd and Ru leaching of 0.5%Pd-0.5%RuH/Al_2O_3 catalyst:

Reusability number	Pd leaching %	Ru leaching %
1st	**2.4**	**2.5**
2nd	**2.2**	**5.7**
3rd	**3.5**	**4.3**

Leaching during liquid-phase hydrogenation is often due to Al_2O_3 deactivation, and the catalyst reduction method used in this study was specifically chosen to mitigate this issue. To explore the influence of metal loading on the synthesis of the Pd-Ru bimetallic catalyst, the electronic structure of the low loading 0.5%Pd-0.5%RuH/Al_2O_3 catalyst and its reused samples were examined using XPS. This analysis offers insights into surface elemental composition and oxidation state (refer to **Table 4.10**). The XPS data reveal a notable peak associated with the Pd metal and Pd^{2+}, with the molar ratio of Pd^{2+}/Pd^0 stated for both the 0.5%Pd-0.5%RuH/Al_2O_3 and 0.5%Pd-0.5%RuH/Al_2O_3 reused catalyst. Furthermore, the only identifiable peak pertains to Ru^0, with respective positions of 279.91 and 280.75 for the 0.5%Pd-0.5%RuH/Al_2O_3 and reused samples[56,57]. The absence of Pd peaks suggests small catalyst particle sizes, corroborated by the previously discussed TEM data. The average particle sizes were 2.17 nm for the 0.5%Pd-0.5%RuH/Al_2O_3 catalyst and 3 nm for its reused counterpart. The mean particle sizes for both catalysts are less than 5nm, below the detection limit of the XPS region of the spectra, which can measure approximately 5nm from the sample surface.

Table 4.10: XPS data of 0.5%Pd-0.5%RuH/Al_2O_3 and reused 0.5%Pd-0.5%RuH/Al_2O_3 catalysts

Compound	Pd^0 Position/ %At Conc.	Pd^{2+}3d Position/ %At Conc.	Cl^-2p Position/ %At Conc.	$Ru^0$3d Position/ %At Conc.	C1s Position/ %At Conc.	Pd^{2+}/Pd^0 Molar ratio
0.5%Pd-0.5%Ru/Al_2O_3	335.31/0.55	336.34/0.33	198.99/0.7	279.91/0.22	284.96/22.98	0.6
0.5%Pd-0.5%Ru/Al_2O_3 Reused	335.41/0.06	337.62/0.02	199.4/0.35	280.75/0.05	284.84/31.92	0.3

4.4. Conclusion

The 5%RuH/Al_2O_3 and 2.5%Pd-2.5%RuH/Al_2O_3 catalysts have proven to be effective heterogeneous catalysts for the selective hydrogenation of phenol to cyclohexanol under mild conditions. Intriguingly, the Pd catalyst shows efficient catalysis in the hydrogenation of phenol—a process that typically proves challenging to achieve with high selectivity to cyclohexanone under moderate conditions[42]. The 2.5%Pd-2.5%RuH/Al_2O_3 catalyst stands out due to its ease of recovery from the product by simple filtration. In addition, recycling experiments reveal that the catalyst retains much of its activity and selectivity to cyclohexanol even after four consecutive runs. These preliminary findings hint at the potential application of the Pd mono catalyst in the hydrogenation of phenol to cyclohexanone, and the Pd-Ru catalyst in the conversion to cyclohexanol.

In terms of hydrogenation activities and yield of cyclohexanol product, Pd-Ru supported on alumina outperforms the other options. The high-activity Pd-RuH/Al_2O_3 bimetallic catalyst, synthesized via a modified impregnation technique and reduced with $NaBH_4$, showed superiority to PdH/Al_2O_3 catalyst in terms of activity and deep hydrogenation capabilities. These enhanced properties can be attributed to the reduced metal particle size, which yields more active sites, and the modulation of electrical characteristics leading to intensified electronic interaction.

Given its high activity and selectivity for cyclohexanol, the Pd-RuH/Al_2O_3 catalyst holds significant promise for both fundamental research and practical applications in this field.

4.5. References

1 X. Kong, Y. Gong, S. Mao and Y. Wang, *ChemNanoMat*, 2018, **4**, 432–450.

2 E. J. Shin and M. A. Keane, *Ind. Eng. Chem. Res.*, 2000, **39**, 883–892.

3 Y. Xiang, L. Ma, C. Lu, Q. Zhang and X. Li, *Green Chem.*, 2008, **10**, 939–943.

4 H. Xia, H. Tan, H. Cui, F. Song, Y. Zhang, R. Zhao, Z. N. Chen, W. Yi and Z. Li, *Catal. Sci. Technol.*, 2021, **11**, 1881–1887.

5 S. S. Wong, R. Shu, J. Zhang, H. Liu and N. Yan, *Chem. Soc. Rev.*, 2020, **49**, 5510–5560.

6 J. Zhong, J. Chen and L. Chen, *Catal. Sci. Technol.*, 2014, **4**, 3555–3569.

7 S. Dai, Z. Hou, M. Chen, Y. Cui, W. Qian, Q. Peng, J. Wang, H. Gong and J. Fang, *Langmuir*, 2020, **36**, 11589–11599.

8 I. E. Ertas, M. Gulcan, A. Bulut, M. Yurderi and M. Zahmakiran, *Microporous Mesoporous Mater.*, 2016, **226**, 94–103.

9 J. Chen, W. Zhang, L. Chen, L. Ma, H. Gao and T. Wang, *Chempluschem*, 2013, **78**, 142–148.

10 H. Chen and J. Sun, *J. Ind. Eng. Chem.*, 2021, **94**, 78–91.

11 L. Wang, J. Zhang, X. Yi, A. Zheng, F. Deng, C. Chen, Y. Ji, F. Liu, X. Meng and F. S. Xiao, *ACS Catal.*, 2015, **5**, 2727–2734.

12 D. Liu, G. Li, F. Yang, H. Wang, J. Han, X. Zhu and Q. Ge, *J. Phys. Chem. C*, 2017, **121**, 12249–12260.

13 W. Zhang, J. Chen, R. Liu, S. Wang, L. Chen and K. Li, *ACS Sustain. Chem. Eng.*, 2014, **2**, 683–691.

14 A. Li, K. Shen, J. Chen, Z. Li and Y. Li, *Chem. Eng. Sci.*, 2017, **166**, 66–76.

15 J. Long, S. Shu, Q. Wu, Z. Yuan, T. Wang, Y. Xu, X. Zhang, Q. Zhang and L. Ma, *Energy Convers. Manag.*, 2015, **105**, 570–577.

16 J. Yi, Y. Luo, T. He, Z. Jiang, J. Li and C. Hu, *Catal. 2016, Vol. 6, Page 12*, 2016, **6**, 12.

17 C. R. Lee, J. S. Yoon, Y. W. Suh, J. W. Choi, J. M. Ha, D. J. Suh and Y. K. Park, *Catal. Commun.*, 2012, **17**, 54–58.

18 Y. Jing, Y. Wang, S. Furukawa, J. Xia, C. Sun, M. J. Hülsey, H. Wang, Y. Guo, X. Liu and N. Yan, *Angew. Chemie Int. Ed.*, 2021, **60**, 5527–5535.

19 V. Vinokurov, A. Glotov, Y. Chudakov, A. Stavitskaya, E. Ivanov, P. Gushchin, A. Zolotukhina, A. Maximov, E. Karakhanov and Y. Lvov, *Ind. Eng. Chem. Res.*, 2017, **56**, 14043–14052.

20 H. Li, J. Liu, S. Xie, M. Qiao, W. Dai, Y. Lu and H. Li, *Adv. Funct. Mater.*, 2008, **18**, 3235–3241.

21 Y. Wang, J. Yao, H. Li, D. Su and M. Antonietti, *J. Am. Chem. Soc.*, 2011, **133**, 2362–2365.

22 W. Luo, W. Cao, P. C. A. Bruijnincx, L. Lin, A. Wang and T. Zhang, *Green Chem.*, 2019, **21**, 3744–3768.

23 G. Neri, A. M. Visco, A. Donato, C. Milone, M. Malentacchi and G. Gubitosa, *Appl. Catal. A Gen.*, 1994, **110**, 49–59.

24 J. Zhong, J. Chen and L. Chen, *Catal. Sci. Technol.*, 2014, **4**, 3555–3569.

25 Y. Xiang, L. Kong, P. Xie, T. Xu, J. Wang and X. Li, *Ind. Eng. Chem. Res.*, 2014, **53**, 2197–2203.

26 W. Schutyser, S. Van Den Bosch, J. Dijkmans, S. Turner, M. Meledina, G. Van Tendeloo, D. P. Debecker and B. F. Sels, *ChemSusChem*, 2015, **8**, 1805–1818.

27 W. Schutyser, G. Van Den Bossche, A. Raaffels, S. Van Den Bosch, S. F. Koelewijn, T. Renders and B. F. Sels, *ACS Sustain. Chem. Eng.*, 2016, **4**, 5336–5346.

28 C. Huang, X. Yang, H. Yang, P. Huang, H. Song and S. Liao, *Appl. Surf. Sci.*, 2014, **315**, 138–143.

29 H. Ogihara, N. Imai and H. Kurokawa, *Int. J. Hydrogen Energy*, 2020, **45**, 33612–33622.

30 M. Li, Y. Li, L. Jia and Y. Wang, *Catal. Commun.*, 2018, **103**, 88–91.

31 Y. Cheng, H. Pham, J. Huo, R. Johnson, A. K. Datye and B. Shanks, *Mol. Catal.*, 2019, **477**, 110546.

32 L. Giraldo, M. Bastidas-Barranco and J. C. Moreno-Piraján, *Molecules*, 2014, **19**, 20594–20612.

33 F. Alshehri, C. Feral, K. Kirkwood and S. D. Jackson, *React. Kinet. Mech. Catal.*, 2019, **128**, 23–40.

34 X. Wang and R. Rinaldi, *ChemSusChem*, 2012, **5**, 1455–1466.

35 A. N. Raut, S. U. Nandanwar, Y. R. Suryawanshi, M. Chakraborty, S. Jauhari, S. Mukhopadhyay, K. T. Shenoy and H. C. Bajaj, *Кинетика И Катализ*, 2016, **57**, 42–48.

36 S. Velu, M. P. Kapoor, S. Inagaki and K. Suzuki, *Appl. Catal. A Gen.*, 2003, **245**, 317–331.

37 G. Feng, Z. Liu, P. Chen and H. Lou, *RSC Adv.*, 2014, **4**, 49924–49929.

38 F. Zhang, S. Chen, H. Li, X. M. Zhang and H. Yang, *RSC Adv.*, 2015, **5**, 102811–102817.

39 M. M. Najafpour, G. Renger, M. Hołyńska, A. N. Moghaddam, E. M. Aro, R. Carpentier, H. Nishihara, J. J. Eaton-Rye, J. R. Shen and S. I. Allakhverdiev, *Chem. Rev.*, 2016, **116**, 2886–2936.

40 K. R. Reddy, K. V. Karthik, S. B. B. Prasad, S. K. Soni, H. M. Jeong and A. V. Raghu, *Polyhedron*, 2016, **120**, 169–174.

41 K. A. Resende, C. E. Hori, F. B. Noronha, H. Shi, O. Y. Gutierrez, D. M. Camaioni and J. A. Lercher, *Appl. Catal. A Gen.*, 2017, **548**, 128–135.

42 L. Cheng, Q. Dai, H. Li and X. Wang, *Catal. Commun.*, 2014, **57**, 23–28.

43 L. L. R. Vono, C. Broicher, K. Philippot and L. M. Rossi, *Catal. Today*, 2021, **381**, 126–132.

44 G. Abarca, W. D. G. Goncalves, B. L. Albuquerque, J. Dupont, M. H. G. Prechtl and J. D. Scholten, *New J. Chem.*, 2021, **45**, 98–103.

45 C. Chen, P. Liu, M. Zhou, B. K. Sharma and J. Jiang, *Energies 2020, Vol. 13, Page 846*, 2020, **13**, 846.

46 M. M. Ambursa, J. C. Juan, Y. Yahaya, Y. H. Taufiq-Yap, Y. C. Lin and H. V. Lee, *Renew. Sustain. Energy Rev.*, 2021, **138**, 110667.

47 Z. Yu, Y. Yao, Y. Wang, Y. Li, Z. Sun, Y. Y. Liu, C. Shi, J. Liu, W. Wang and A. Wang, *J. Catal.*, 2021, **396**, 324–332.

48 A. Bjelić, M. Grilc and B. Likozar, *Chem. Eng. J.*, 2020, **394**, 124914.

49 J. Zhang, J. Sun, B. Sudduth, X. Pereira Hernandez and Y. Wang, *Catal. Today*, 2020, **339**, 305–311.

50 X. Nie, Z. Zhang, H. Wang, X. Guo and C. Song, *Catal. Today*, 2021, **371**, 189–203.

51 T. Mitsudome and K. Kaneda, *Green Chem.*, 2013, **15**, 2636–2654.

52 J. Zhao, L. Ge, H. Yuan, Y. Liu, Y. Gui, B. Zhang, L. Zhou and S. Fang, *Nanoscale*, 2019, **11**, 11429–11436.

53 D. Singh and P. L. Dhepe, *Mol. Catal.*, 2020, **480**, 110525.

54 H. Chen and J. Sun, *J. Ind. Eng. Chem.*, 2021, **94**, 78–91.

55 H. Liu, T. Jiang, B. Han, S. Liang and Y. Zhou, *Science (80-.).*, 2009, **326**, 1250–1252.

56 D. R. Taylor and K. H. Ludlum, *J. Phys. Chem.*, 1972, **76**, 2882–2886.

57 L. L. R. Vono, C. Broicher, K. Philippot and L. M. Rossi, *Catal. Today*, 2021, **381**, 126–132.

58 J. A. Rodriguez and D. W. Goodman, *Science*, 1992, **257**, 897–903.

59 N. Toshima and T. Yonezawa, *New J. Chem.*, 1998, **22**, 1179–1201.

60 Z. Zhang, L. Ding, J. Gu, Y. Li, N. Xue, L. Peng, Y. Zhu and W. Ding, *Catal. Sci. Technol.*, 2017, **7**, 5953–5963.

61 C. Liu, J. Wang, P. Zhu, H. Liu and X. Zhang, *Chem. Eng. J.*, 2022, **430**, 1385–8947.

62 G. Feng, Z. Liu, P. Chen and H. Lou, *RSC Adv.*, 2014, **4**, 49924–49929.

63 X. Zhang, Y. Du, H. Jiang, Y. Liu and · Rizhi Chen, *Catal. Letters*, 2019, **3**, 3087–3096.

64 P. Yan, J. Mensah, M. Drewery, E. Kennedy, T. Maschmeyer and M. Stockenhuber, *Appl. Catal. B Environ.*, 2021, **281**, 119470.

Chapter 5: N-alkylation of ρ-toluidine with phenol over highly active heterogeneous palladium catalysts

5.1. Introduction

Biomass, an abundant renewable energy resource, possesses a multifaceted mixture of carbon, aiding in fulfilling global energy demands. As it stands, biomass energy contributes roughly 14 % to the worldwide energy consumption, constituting approximately one-third of the overall final energy consumption and nearly 75 % of the household energy consumption[1]. Producing chemicals from renewable sources possesses several technical merits. Compounds obtained from bio-based resources are pre-functionalised, implying a potentially simpler chemical synthesis process than that from alkane, thus mitigating waste production[2]. Furthermore, products derived from bio-based resources may surpass their hydrocarbon-derived counterparts in terms of biodegradability and biocompatibility. However, the industrial-scale production of biomass introduces serious environmental and ethical issues. The transformation of biomass into biofuels and bioproducts presents multiple challenges, such as the need for novel catalytic routes and processes apt for oxygenated molecules, to supplant the current hydrocarbon-centric value chains. The two chief methods for biomass-to-energy conversion are thermochemical and biochemical processes. The chosen conversion technology is contingent upon the form of energy demanded, such as heat, mechanical, or electrical energy[3].

In the coming years, lignocellulosic biomass or waste biomass could serve as renewable raw materials to produce fuels, chemicals, and energy. This composite substance primarily consists of crop waste or organic residues[2]. However, the presence of lignin (a major constituent of lignocellulose) engenders the creation of a complex three-dimensional amorphous polymer made up of substituted phenols. Chemically, lignocellulosic biomass exhibits a substantially higher oxygen content than traditional petroleum-based raw materials. A process known as hydrodeoxygenation, which involves the removal of oxygen using hydrogen, is necessary to transform biomass feedstock into hydrocarbons. To circumvent this costly phase, innovative reaction procedures are essential. Frequently, in a host of chemical investigations, lignin is replaced with model compounds like phenol, guaiacol, 4-propylphenol, diphenyl ether, vanillin, guaiacylpropane, syringol, or syringylpropane due to its structural complexity and irregularity. Significant advancements have been made in the past regarding the catalytic conversion of lignin model compounds to fabricate beneficial chemicals through oxidation, reduction, redox-neutral processes, among others[4].

Amines and their derivatives, vital organonitrogen compounds, serve as intermediates for the synthesis of fine chemicals, pharmaceuticals, agrochemicals, and natural products[4,5]

Phenol, a valuable intermediate, is integral in synthesizing chemical drugs, petrochemicals, agrochemicals, and synthetic resin. Phenol's production in the chemical industry currently relies on the multistep cumene process, which unfortunately has its pitfalls - high energy consumption, low atom utilization, explosive intermediate safety issues, and a costly downstream separation of the significant amount of acetone by-product[6]. A one-step hydroxylation of benzene to phenol has been proposed as a preferable alternative, motivated by economic and environmental concerns. Direct production of phenol from benzene, with oxygen being used, carries significant economic advantages. Several studies have documented phenol production with gaseous hydrogen and oxygen as reactants[6]. Active oxygen species can convert benzene directly to phenol by reacting with hydrogen on the catalyst.

Catalytic techniques have increasingly been applied in recent years to produce and synthesize complex fine and specialty chemicals such as agrochemicals and pharmaceuticals. Palladium (Pd) is the most versatile and widely utilized catalytic metal[7]. Homogeneous Pd catalysts provide several advantages: (i) an abundance of metal precursors are known and accessible; (ii) Pd forms complexes with a variety of organic ligands with P, N, and O atoms; (iii) many of these complexes are relatively simple to prepare and manage; (iv) Pd-catalysed reactions often yield dependable results and can be conducted with standard equipment; (v) functional group tolerance is generally excellent[7].

Furthermore, heterogeneous catalysts, either in the metallic state or as oxides, are also utilized in industrial applications. To this day, the application of heterogeneous Pd in fine chemical synthesis has been limited and was traditionally confined to hydrogenation and dehydrogenation reactions. However, several studies have utilized heterogeneous Pd for model substrates under non-optimized conditions.

The selection of heterogeneous catalysts typically involves an experimental trial-and-error process, and the reasons why certain catalysts outperform others remain elusive. Various factors influence a catalyst's properties, including the catalyst type and the metal loading; the concentration of the metal, often stated in the catalyst's description, and the metal content (standardly 5 % for most Pd catalysts)[7]. For instance, 5%Pd on an active carbon support is denoted as 5%Pd/C, and charcoal or active carbon support is popular because it can adsorb large amounts of water. For safety reasons, Pd/C catalysts are generally sold with a water content of

approximately 50 %. Other materials, such as alumina, silicas, $CaCO_3$ and $BaSO_4$, are also used for special applications.

The preparation methods for catalysts and the types of carbon used are crucial factors. Two commercial catalysts with the same classification, such as 5%Pd/C, can exhibit divergent performance due to differing preparation methods.

One of the most environmentally sound transformations is the hydrogenation of the amine-carbonyl compound mixture through a heterogeneous transition metal catalyst. The reaction is typically carried out in water or another green solvent using gaseous H_2 as a hydrogen source. A significant advancement is the generation of the carbonyl compound from alcohols under suitable conditions through reductive amination.

Monometallic and bimetallic catalysts are instrumental in producing fuels and chemicals from conventional crude oil-based feedstocks and bio-renewable feedstocks. There's a noteworthy difference between the properties of bimetallic catalysts and monometallic catalysts, often attributed to the 'synergistic' effects between the two metal analogues[8]. Several methods are used to prepare bimetallic materials. Among these methods is chemical reduction, the inaugural method used to synthesize monometallic nanostructures. In this method, a metal precursor solution in a suitable solvent is reduced by a reducing agent (normally $NaBH_4$ or N_2H_4 or H_2 gas) in the presence of stabilizing molecules such as surfactant ligands or polymeric ligand, polyvinyl alcohol (PVA), which serves to passivate the nanoparticle surfaces and prevent aggregation[8]. To synthesize bimetallic nanoalloys, the same process is used, but the precursor solution contains both metal ions instead of a single metal ion as in monometallic preparation.

Li and colleagues have documented a Pd-catalysed reductive coupling of phenols with anilines in toluene at 100 °C[4].

Shortly after Li's report, Taddiei and his team reported that microwave (MW) heating was more beneficial to the reductive amination of phenols[9]. In the above studies, sodium formate was utilized as a hydrogen source to reduce phenols through a catalytic hydrogen transfer reaction. This strategy was examined in this study over Pd catalysts and is detailed in (Section 5.4). The process is referred to as catalytic transfer hydrogenation (CTH). Fu et.al.[10] developed an efficient, highly active PdHx/ Al_2O_3 catalyst for the reductive coupling of lignin-derived phenols with amines, achieving high yield and good stereoselectivity under mild conditions.

In this research, we have developed a highly active 5%PdH/Al_2O_3 catalyst intended for the reductive coupling of lignin-derived phenols with amines. The effectiveness of the 5%PdH/Al_2O_3 catalyst is scrutinized by implementing various preparation techniques.

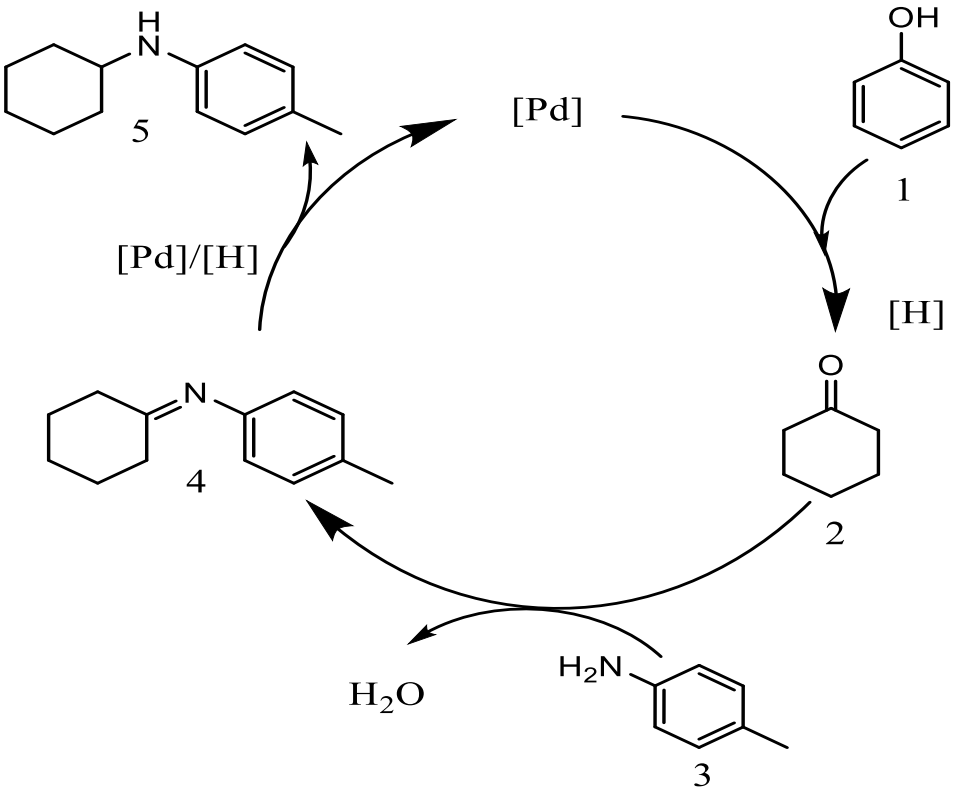

Scheme 5.1: represents a tentative mechanism for the reaction involving phenol and aniline, where Phenol (1), cyclohexanone (2), ρ-toluidine (3), imine (4), and N-cyclohexyl-4-methylaniline (5) are involved.

The proposed mechanism of the reaction, as outlined in **Scheme 5.1**, initiates with the reduction of phenol (1) into cyclohexanone (2) under the influence of the [Pd]/[H]-catalysed reductive conditions. Subsequently, the imine (4) intermediate is produced through the standard condensation process involving ρ-toluidine (3) and cyclohexanone. The final step entails the reduction of the imine intermediate under [Pd]/[H] conditions, which produces the N-cyclohexyl-4-methylaniline (5) derivative and concurrently rejuvenates the active palladium catalyst[11].

5.2. Experimental work

5.2.1. Catalyst preparation

In this study, the catalysts were prepared using two distinct methods: the Modified Impregnation Method (M_{im}) and the Sol-Immobilisation Method (S_{im}), as described in Chapter 2 (for more information, see Sections 2.2.2 and 2.2.1, respectively).

For the monometallic catalysts, 5%Pd/Al_2O_3, the Modified Impregnation Method (M_{im}) was employed. The detailed synthesis process for 5%Pd/Al_2O_3 can be found in Chapter 2, specifically in Sections 2.2.3.1 and 2.2.3.2, which provide a comprehensive outline of the catalyst preparation procedure.

Regarding the bimetallic catalyst, 2.5%Pd-2.5%Au/Al_2O_3, the Sol-Immobilisation Method (S_{im}) was utilized. The study presents a detailed account of the synthesis process for 2.5%Pd-2.5%Au/Al_2O_3 in Chapter 2, specifically in Sections 2.2.3.3 and 2.2.3.4, offering a thorough description of how the bimetallic catalyst was prepared.

By employing both the Modified Impregnation Method (M_{im}) and the Sol-Immobilisation Method (S_{im}) for catalyst preparation, the research aims to investigate the influence of different preparation techniques on the catalytic performance and properties of the resulting monometallic and bimetallic catalysts. These methods offer unique advantages and can impact the catalyst's composition, structure, and activity, providing valuable insights into catalyst design and optimization for specific hydrogenation reactions.

The utilization of specific metal loadings, such as 5%Pd for the monometallic catalyst and 2.5%Pd-2.5%Au for the bimetallic catalyst, allows researchers to carefully control the catalyst's active sites and tailor its reactivity for the hydrogenation of phenol, as well as potentially other reactions. Such systematic investigation of catalyst preparation techniques and metal combinations is crucial for advancing the field of catalysis and enabling the development of efficient and selective catalysts for various industrial applications.

5.2.2. Catalyst testing using N-alkylation of ρ-toluidine with phenol reaction

In Chapter 2 of the study, the performance of two types of catalysts was evaluated using the N-Alkylation of ρ-toluidine with phenol as the model reaction. The catalysts under investigation were monometallic 5%Pd/Al_2O_3 and bimetallic 2.5%Pd-2.5%Au/Al_2O_3, both of which were prepared using different methods: the Modified Impregnation Method (M_{im}) and the Sol-immobilisation method (S_{im}).

The N-Alkylation of ρ-toluidine with phenol serves as the model reaction in this study, providing a well-defined and commonly used benchmark to assess the catalytic activity and selectivity of the tested catalysts. This reaction involves the addition of an

alkyl group to the nitrogen atom of ρ-toluidine using phenol as the alkylating agent in the presence of the catalyst.

The monometallic 5%Pd/Al_2O_3 catalyst was prepared using the Modified Impregnation Method (M_{im}), while the bimetallic 2.5%Pd-2.5%Au/Al_2O_3 catalyst was synthesized using the Sol-immobilisation method (S_{im}). These different preparation techniques may result in variations in the catalyst's active sites, composition, and structure, potentially influencing their catalytic performance.

By investigating the performance of both monometallic and bimetallic catalysts prepared via different methods, the study aims to gain insights into the influence of catalyst composition and preparation technique on the N-Alkylation reaction. The results obtained from this investigation will aid in understanding the catalytic behaviour of these catalysts and identifying the most efficient catalyst for this specific reaction.

The N-Alkylation of ρ-toluidine with phenol is of significant interest due to its relevance in various industrial processes and the potential application of the catalysts in the synthesis of valuable products. The findings from this study can contribute to the development and optimization of catalysts for N-Alkylation reactions and pave the way for their broader utilization in other important catalytic processes.

5.2.3. Catalyst characterisation

In Chapter 3 of the study, the monometallic 5%Pd/Al_2O_3 and bimetallic 2.5%Pd-2.5%Au/Al_2O_3 catalysts were subjected to thorough characterization using various analytical techniques. The characterization methods employed include Scanning Electron Microscopy (SEM), Transmission Electron Microscopy (TEM), X-ray Diffraction (XRD), and X-ray Photoelectron Spectroscopy (XPS).

For the monometallic 5%Pd/Al_2O_3 catalyst, the details of its characterization can be found in Section 3.3.1 of Chapter 3. This section provides a comprehensive description of the SEM, TEM, XRD, and XPS analyses carried out to investigate the morphology, structure, crystallography, and surface chemical composition of the 5%Pd/Al_2O_3 catalyst.

Similarly, for the bimetallic 2.5%Pd-2.5%Au/Al_2O_3 catalyst, the characterization results are elaborated in Section 3.4.1 of Chapter 3. This section presents detailed information on the SEM, TEM, XRD, and XPS data, offering insights into the catalyst's physical and chemical properties, including particle size, distribution, and the presence of different metallic components.

These characterization techniques play a vital role in understanding the structure-activity relationship of the catalysts. SEM and TEM allow researchers to visualize the morphology and size distribution of catalyst particles at the micro and nanoscale

levels, respectively. XRD provides valuable information about the catalyst's crystallography and phase composition, while XPS offers insights into the chemical states and surface composition of the catalyst.

The results obtained from these characterizations will be essential for drawing correlations between the catalysts' structural features and their catalytic performance in the N-Alkylation of ρ-toluidine with phenol, as investigated in Chapter 2. The interpretations and explanations of the data obtained from these characterizations will further enrich the understanding of the catalysts' behaviour and their potential applicability in various hydrogenation reactions.

By combining the findings from the catalyst characterization with the catalytic performance data, the study aims to establish a comprehensive understanding of the catalytic systems and facilitate the rational design and optimization of efficient catalysts for important chemical transformations.

5.3. Results and discussion

5.3.1. N-alkylation of ρ-toluidine with phenol over highly active heterogeneous palladium catalysts

The model reaction applied in this process was the N-Alkylation of ρ-toluidine with phenol. Different Pd catalysts were synthesised and evaluated in the reductive amination reaction to determine the most effective one. The primary objective of this study was to investigate the influence of different Pd particle species and supports on the reaction. The activities of Pd catalysts being studied for the cyclohexylamine of ρ-toluidine with phenol were selected to accomplish this goal. The results of these tests are presented in **Table 5.1**. According to the table, except for the Al_2O_3 and TiO_2 catalysts, most of the monometallic Pd metal supports achieved low catalytic activity for this conversion[10].

Table 5.1: Monometallic Pd catalyst screening for reductive amination with different supports:

Entry	Catalyst	Conversion (Phenol) (%)	Yield (N-cyclohexyl-4-methylaniline) (%)
1	5%Pd/TiO_2	23	18
2	5%Pd/MgO	8	7
3	5%Pd/C	2	2
4	5%Pd/CeO_2	6	5
5	5% Pd/Al_2O_3	22	20
6	5%PdH/ Al_2O_3	45	46
7	5%PdH/ TiO_2	32	33
8	Al_2O_3	0	0
9	TiO_2	0	0

Reaction conditions: 0.2 mmol phenol and 0.4 mmol p-toluidine were added to 2 mL toluene with 30 mg catalyst under 1 bar H_2 atmosphere at 50 ºC for 3 hours. The yield was calculated by GC with mesitylene as the internal standard.

The heightened activity can be attributed to the Pd support. By contrast, the yield of N-cyclohexyl-4-methylaniline was merely 6 %, 8 %, and 9 % when 5%Pd/MgO, 5%Pd/C and 5%Pd/CeO_2 were deployed in the reaction (entries 2, 3, and 4 in **Table 5.1**), respectively. This suggests a substantial influence of the support on catalytic activity. Furthermore, the type of Pd particles also plays a crucial role in catalytic activity. PdH species (palladium hydride) (Entries 6 and 7 in **Table 5.1**) exhibited a higher conversion rate and selectivity than other Pd species. **Table 5.1** reveals that when only Al_2O_3 or TiO_2 supports are present in the reaction solution (Entries 8 and 9 in **Table 5.1**), no conversion of phenol occurs. Therefore, it seems that without a catalyst in the reaction solution, the amination of phenol is hindered. Initially, various Pd catalysts were created and tested in the reductive amination reaction to determine the most effective. 5%Pd/Al_2O_3, 5%Pd/C and 5%Pd/TiO_2 were selected from the tested catalysts (**Table 5.1**) for studying the real-time progression of products (refer to **Figure 5.1**). The real-time effect for all catalysts was examined with Pd species. Catalyst activity is notably influenced by supports, as previously established[12,13] . Metal oxides are often used as supports in heterogeneous catalysts due to their substantial impact on catalyst activity. The adsorption characteristics of these supports have been found to significantly influence the adherence of palladium

nanoparticles[10,14], subsequently affecting catalytic activity. Two distinct metal oxides have been examined for phenol amination in the current study: TiO_2 and Al_2O_3.

The results demonstrated that 5%Pd supported on TiO_2 achieved the highest conversion, reaching 42% after 8 hours. Based on the XRD for both 5%PdH/Al_2O_3 and 5%PdH/TiO_2 catalysts (refer to **Figure 3.2** and **Figure 3.7**, Chapter Three, respectively), PdH formation was observed. According to **Figure 3.2**, a broad peak of metallic palladium shifted from Pd^0at 2θ= 40.0° to the left at 39.5° due to peak convolution with the (101) palladium hydride peak[10]. The diffraction peaks at 2θ = 32.5°, 39.5°, and 78.5° corresponded to the (100), (101), and (121) planes of the tetragonal phase of PdH (JCPDS No. 01-073-0004) respectively. In contrast, **Figure 3.7** showcased three additional peaks at 2θ = 42.27°, 44.17°, and 64.35°, corresponding to the (101), (110), and (112) crystal planes of metal PdH (JCPDS No. 01-073-0004), respectively. These peaks not only confirm the palladium hydride state of the loaded PdH particles but also demonstrate their stable PdH crystalline condition, which may suggest potential improvements in catalyst performance.

Meanwhile, when PdH species were supported on the same metal oxides (Al_2O_3 and TiO_2), the conversion rates varied (refer to **Figures 5.2 and 5.3**). The Al_2O_3 support achieved the highest conversion rate, reaching 62 % after 8 hours, while the TiO_2 support attained almost 52 % conversion in the same duration. In an earlier study, Yan et al.[10] reported a higher catalytic activity for the fresh 5%PdH/Al_2O_3 catalyst than Pd/Al_2O_3 in the reductive amination reaction, aligning with our expectations. The increased activity could be ascribed to the PdH species.

In contrast, the yield of N-cyclohexyl-4-methylaniline was only 6 % when PdH/C was utilized in the reaction after 8 hours (refer to **Figure 5.1**), emphasizing the importance of the support in catalytic activity. The highest yield of N-cyclohexyl-4-methylaniline was obtained with the 5%PdH/Al_2O_3 and 5%PdH/TiO_2 catalysts (Entry 6 and 7, respectively).

Following the proposed reaction mechanism for HDO of phenol[15], phenol gets adsorbed as phenoxy species on the support Lewis acid sites, leading to the formation of cyclohexanone (2) (refer to **Scheme 5.1**). Then, N-cyclohexyl-4-methylaniline likely results from the N-alkylation process through the reaction of p-toluidine with cyclohexanone over Lewis's acid sites. Compared to Pd supported on Al_2O_3, Pd deposited on TiO_2 (**Table 5.1**, Entry 6 and 7, respectively), the highest yield of 46 % for N-cyclohexyl-4-methylaniline was detected at the end of the reaction when 5%PdH/Al_2O_3 (Entry 6) was used as the catalyst, compared to others including 5%PdH/TiO_2. This could be due to the presence of strong acidic sites on the surface of the 5%PdH/Al_2O_3 catalyst compared with other support catalysts[15,16].

In many previous studies, carbon has been extensively used as a support for palladium catalysts prepared through various methods and demonstrated impressive conversion rates [9,17,18]. In the current study, with the real-time study, the conversions and selectivity of N-cyclohexyl-4-methylaniline progressively increased.

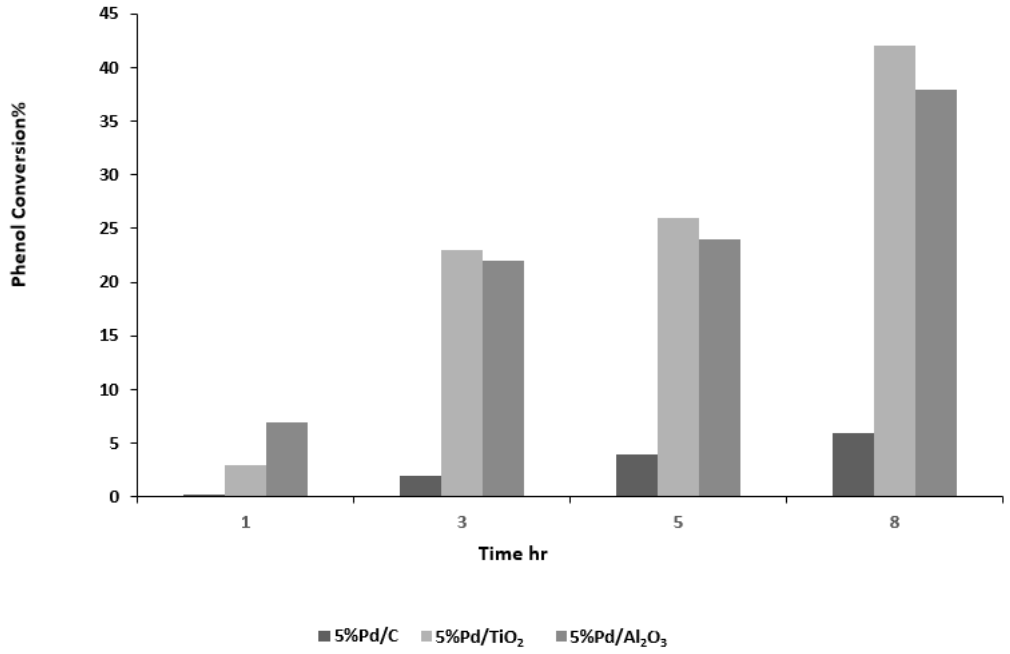

Figure 5.1: Time online study for amination of phenol using 5%Pd supported on C, TiO_2 and Al_2O_3: Reaction conditions: 0.2 mmol phenol and 0.4 mmol p-toluidine were added to 2 mL toluene with 30 mg catalyst under 1 bar H_2 atmosphere at 50 ºC. The yield was converted by GC with mesitylene as the internal standard**.**

The corresponding conversion rates and selectivity are depicted in **Figures 5.2** and **5.3.** Using 5%PdH catalysts under these prescribed conditions, phenol conversion rates ranging from 86 to 96 % can be easily achieved within the allocated time frame and at a 1 bar hydrogen atmospheric pressure. Pd catalysts showcase elevated activity contingent on the Pd species.

If phenol does not undergo full conversion, the formation of cyclohexanone is rarely observed. The highest activity was noted over the 5%PdH/Al_2O_3 catalyst. The high selectivity of N-cyclohexyl-4-methylaniline was achieved, reaching a minimum of 95% (refer to **Figure 5.2**).

5.3.1.1. Time online study for amination of phenol over 5%PdH/Al_2O_3 and 5%PdH/TiO_2

The process of phenol amination was conducted using supported catalysts 5%PdH/Al_2O_3 and 5%PdH/TiO_2. In a study monitoring the reaction over time, the influence of hydrogen atmospheric pressure on the amination mechanism was assessed. The resultant data is illustrated in **Figures 5.2 and 5.3**, respectively. It was discerned that the conversion elevated to 95 % post 24 hours when employing 5%PdH/Al_2O_3 as the catalyst, whereas it was 79 % when 5%PdH/TiO_2 was utilized under identical conditions. Additionally, as depicted in **Figures 5.2 and 5.3**, similar outcomes were observed for both catalysts, where the selectivity for N-cyclohexyl-4-methylaniline escalated to roughly 90%. These findings align with those from Yao Fu's prior research [10], which examined the N-Alkylation of amines with phenols over highly active heterogeneous palladium hydride catalysts.

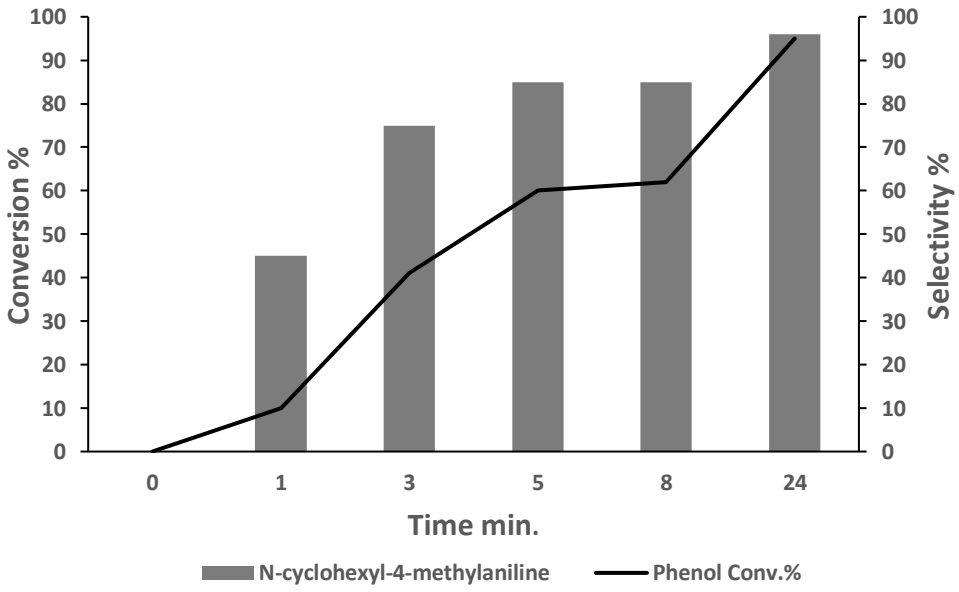

Figure 5.2: N-Alkylation of amine with phenol over 5%PdH/Al_2O_3 catalyst. **Reaction conditions**: 0.2 mmol phenol and 0.4 mmol p-toluidine were added to 2 mL toluene with a 30 mg catalyst under 1 bar H_2 atmosphere at 50 ºC. The yield was converted by GC with mesitylene as the internal standard.

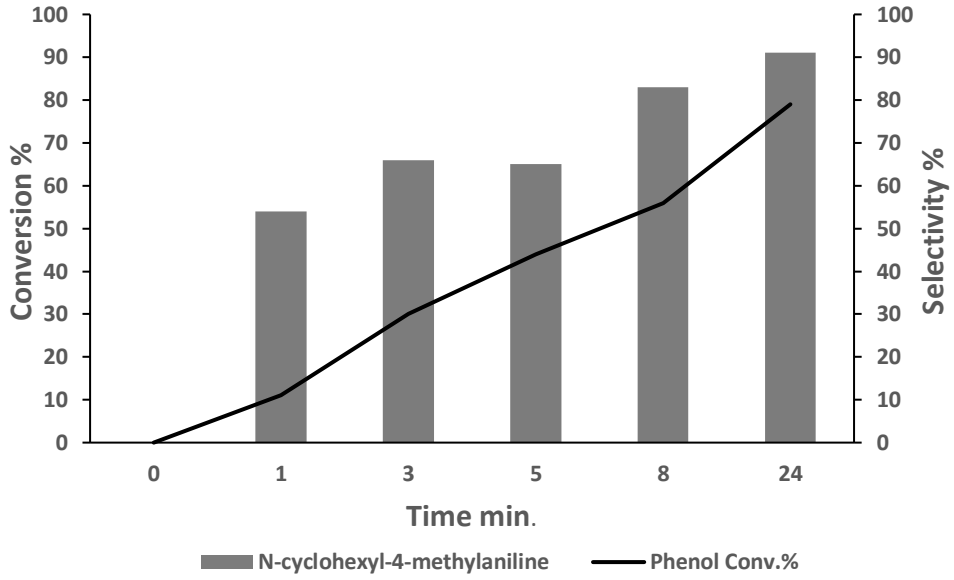

Figure 5.3: N-Alkylation of amine with phenol over 5%PdH/TiO_2 catalyst. **Reaction conditions**: 0.2 mmol phenol and 0.4 mmol p-toluidine were added to 2 mL toluene with a 30 mg catalyst under 1 bar H_2 atmosphere at 50 ºC. The yield was converted by GC with mesitylene as the internal standard.

5.3.1.2. Potential Routes for the Reductive Amines Reaction (N-Alkylation of Amine with Phenol)

Echoing the findings in Slowing's research[19], phenols were initially adsorbed, taking the place of the absorbed water molecules on the Al_2O_3. surface. Following adsorption, the absorbed phenol was hydrogenated to cyclohexanone using the 5%PdH/Al_2O_3 catalyst (refer to **Scheme 5.1**). The adsorbed phenol and cyclohexanone obstructed the adsorption of soluble p-toluidine on the catalyst surface, thereby protecting the catalyst from poisoning. Two potential reaction pathways, as proposed in **Scheme 5.2**[10]. In the principal pathway (A), phenol underwent conversion to cyclohexanone, subsequently coupling with p-toluidine over the acid sites of Al_2O_3. The resulting imine was then reduced to generate N-Cyclohexyl-4-methylaniline using the 5%PdH/Al_2O_3 catalyst. In the secondary pathway (B), p-toluidine was hydrogenated into an enamine intermediate. The unstable enamine intermediate then yielded p-methylcyclohexanone via hydrolysis [20]. The resultant imine was reduced to yield 4-Methyl-N-(4-methylcyclohexyl) aniline, with the conversion mirroring the main pathway. This process aligns closely with descriptions in previous literature [21].

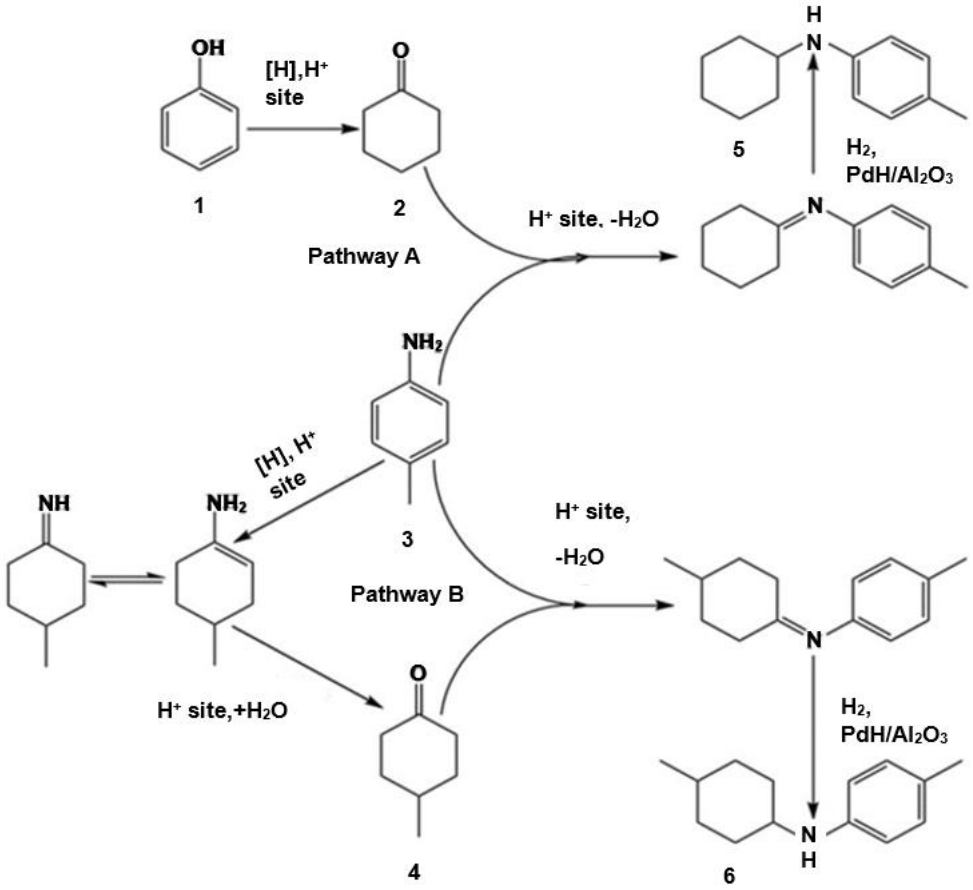

Scheme 5.2: Two possible pathways for the reductive amine reaction[10].

The product (5) (N-Cyclohexyl-4-methylaniline) can be identified via NMR and GC-MS analysis (see Appendix A and B(a) respectively), while (6) (4-Methyl-N-(4-methylcyclohexyl) aniline), due to its smaller quantity in this study, can be detected through GC-MS (see Appendix B (b)).

5.3.1.3. Effect of the catalyst mass of the 5%PdH/Al_2O_3

The impact of the quantity of 5%PdH/Al_2O_3 catalyst utilized in the N-Alkylation of amine with phenol was investigated at a temperature of 50 °C, utilizing toluene as a solvent, over a 24-hour period under a 1bar H_2 gas atmosphere. The phenol quantity was 0.2 mmol. **Figure 5.4** reveals that the phenol conversion slightly augments with an increase in the catalyst amount, mirroring the selectivity increase for N-Cyclohexyl-4-methylaniline. Doubling the mass of the 5%PdH/Al_2O_3 catalyst from 20 mg to 40 mg resulted in a conversion increase from 24 % to 34 %. However, for catalysts, the rise in mol % (metal quantity relative to phenol quantity) led to a conversion increase for 5%PdH/Al_2O_3, potentially indicating a mass transport limitation within this range. Additionally, the influence of catalyst mass on the amination of phenol using 5%PdH/Al_2O_3 was scrutinized. The quantity of 5%PdH/Al_2O_3 ranged between 20-55

mg. As seen in **Figure 5.4**, the phenol conversion rose from 24 % to 37 % with an increase in the catalyst mass from 20 mg to 55 mg, while the selectivity for N-Cyclohexyl-4-methylaniline grew from 56 % to 76 %. This emphasizes the significance of the Pd surface for directing selectivity towards cyclohexanone and 4-methyl cyclohexanone. Raising the catalyst mass from 40 mg to 55 mg resulted in an increase in conversion from 34 % to 37 %. However, increasing the mass from 40 mg to 55 mg led to only a 3 % increase in conversion, which might indicate mass transport limitation within this range. When the rate of mass transport is equal to or lower than the interaction association rate constant, the binding kinetics will be mass transport limited. This may result in inaccurate data, leading to slower apparent association rate constants. Therefore, under these conditions (at 50 °C using toluene as a solvent under 1 bar H_2 gas), 40 mg (0.02 mmol %, Pd amount relative to the phenol) is the optimal quantity of 5%PdH/Al_2O_3 catalyst for the amination of phenol. The initial concentration of phenol was set to 0.2 mmol, which is used for standard reaction conditions.

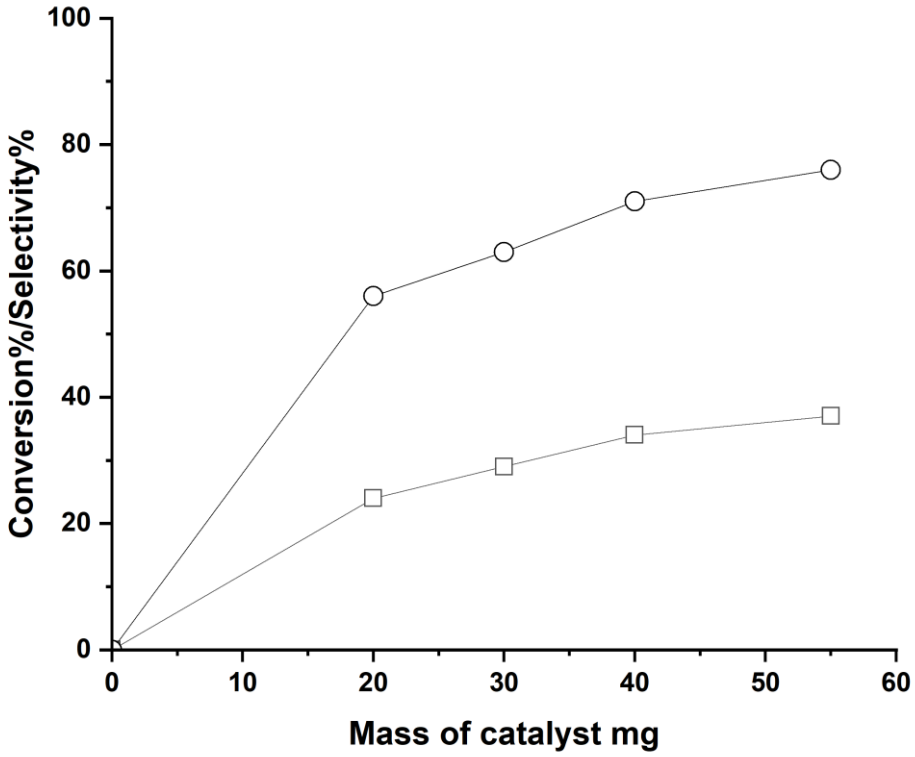

Figure 5.4: Conversion as a function of varying the mass of 5%PdH/Al_2O_3 catalyst for N-Alkylation of amine with phenol. **Reaction conditions:** 50 °C, 1 bar H_2, 24 hours, 0.2 mmol phenol and 0.4 mmol p-toluidine were added to 2 mL toluene at 1000 rpm. (□ Conversion, ○ Selectivity)

Based on nitrogen physisorption (BET) analysis, the surface area of fresh and reduced supported palladium and palladium-gold catalysts is presented in **Table 5.2.** An increased surface area of the reduced catalyst was noticed compared to the fresh catalyst, possibly indicating efficient dispersion of Pd and Au NPs within the support pores. Furthermore, the surface area of the monometallic catalyst was higher by 122 m^2g^{-1} compared to the bimetallic. The analysis was conducted twice, revealing that the margin of error in the analysis did not exceed 1 m^2g^{-1}.

Table 5.2: Surface area of 5%Pd/Al_2O_3 and 5%Pd-Au/Al_2O_3 fresh and reduced with $NaBH_4$ nanoparticles:

Catalyst	**Surface area m^2 g^{-1}**
5%Pd/ Al_2O_3 fresh	53
5%PdH/ Al_2O_3 reduced	122
2.5%Pd-2.5%Au/Al_2O_3 fresh	94
2.5%Pd-2.5%AuH/Al_2O_3 reduced	120

5.3.2. Effect of solvent on reductive amination of phenol to synthesis N-cyclohexyl-4-methylaniline over 5%PdH/Al_2O_3 and 2.5%Pd-2.5%AuH/Al_2O_3

The effect of different solvents on the reductive amination of phenol to synthesize N-Cyclohexyl-4-methylaniline using 5%PdH/Al_2O_3 and 2.5%Pd-2.5%AuH/Al_2O_3 catalysts was assessed. The catalysts were evaluated under standard conditions (50 °C and 1 bar H_2), with the time online results depicted in **Figures 5.5 and 5.6**. In the presence of hexane, a remarkable conversion of 99% was achieved for both catalysts (see **Figure 5.5**). In contrast, toluene was less effective, yielding conversions of 56 % and 84 % for the 5%PdH/Al_2O_3 and 2.5%Pd-2.5%AuH/Al_2O_3 catalysts, respectively. For the solvents toluene and hexane, high conversion rates were noted in the reductive amination of phenol, as shown in **Figures 5.5 and 5.6**[10]. The catalytic activity of the 5%PdH/Al_2O_3 and 2.5%Pd-2.5%AuH/Al_2O_3 catalysts was investigated in the context of the two solvents (toluene and hexane) over time. From **Figure 5.6**, it was observed that the selectivity of N-Cyclohexyl-4-methylaniline followed a similar trend to the conversion in both solvents. While Li and colleagues reported toluene as the superior solvent for this reaction compared to others[4], this study found that hexane exhibited impressive conversion and selectivity relative to toluene.

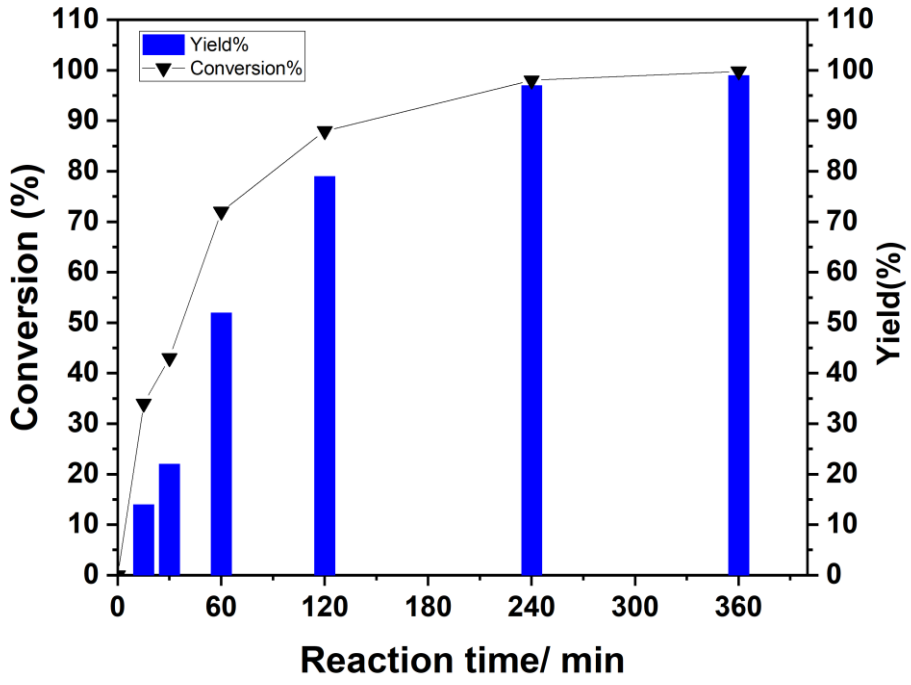

Figure 5.5. Effect of Hexane solvent on phenol conversion over 5%PdH/Al_2O_3 and N-Cyclohexyl-4-methylaniline yield**. Reaction conditions:** Phenol 0.2 mmol, ρ- Toluidine 0.4 mmol, using hexane as solvent 2 ml, 40 mg 5%PdH/Al_2O_3 catalyst, under 1 bar H_2, 50 ºC, 1000 rpm.

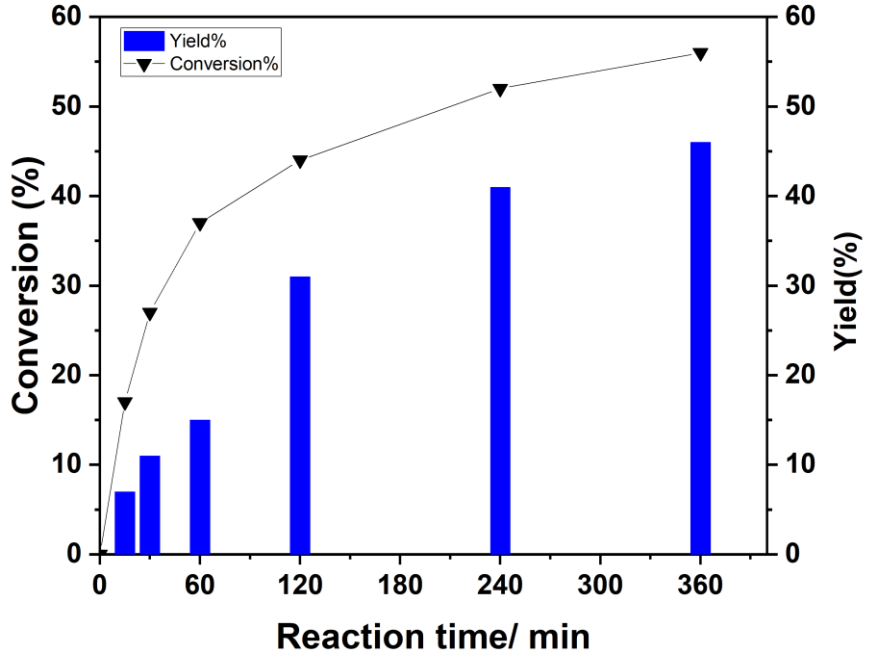

Figure 5.6. Effect of Toluene solvent on phenol conversion over 5%PdH/Al_2O_3 and N-Cyclohexyl-4-methylaniline yield**. Reaction conditions:** Phenol 0.2 mmol, ρ- Toluidine 0.4 mmol, using Toluene as solvent 2 ml, 40 mg 5%PdH/Al_2O_3 catalyst, under 1 bar H_2, 50 ºC, 1000 rpm.

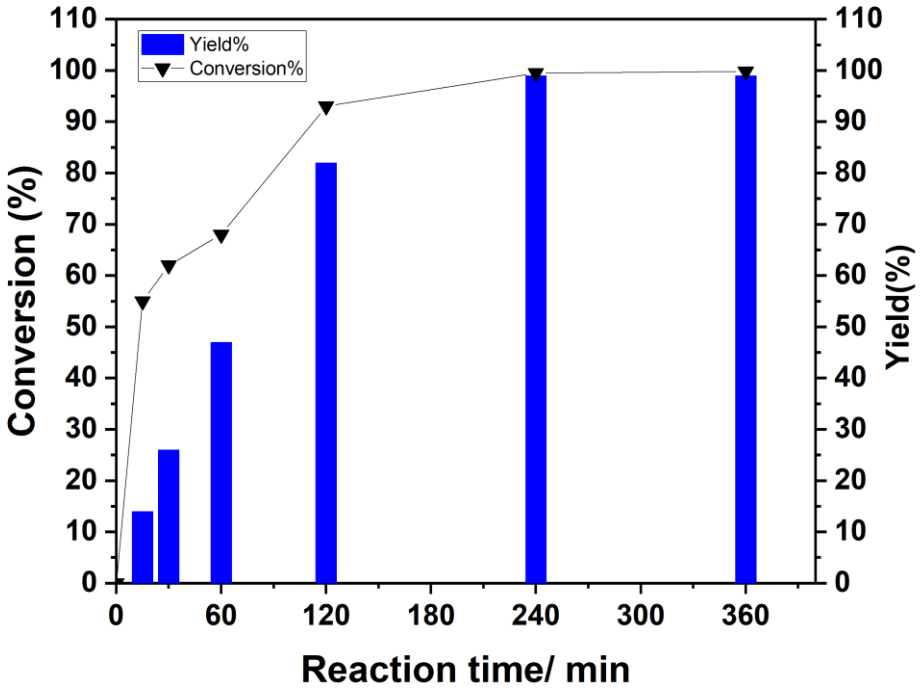

Figure 5.7. Effect of Hexane solvent on phenol conversion over 2.5%Pd-2.5%AuH/Al_2O_3 and N-Cyclohexyl-4-methylaniline yield**. Reaction conditions:** Phenol 0.2 mmol, ρ- Toluidine 0.4 mmol, using hexane as solvent 2 ml, 40 mg 2.5%Pd-2.5%AuH/Al_2O_3 catalyst, under 1 bar H_2, 50 ºC, 1000 rpm.

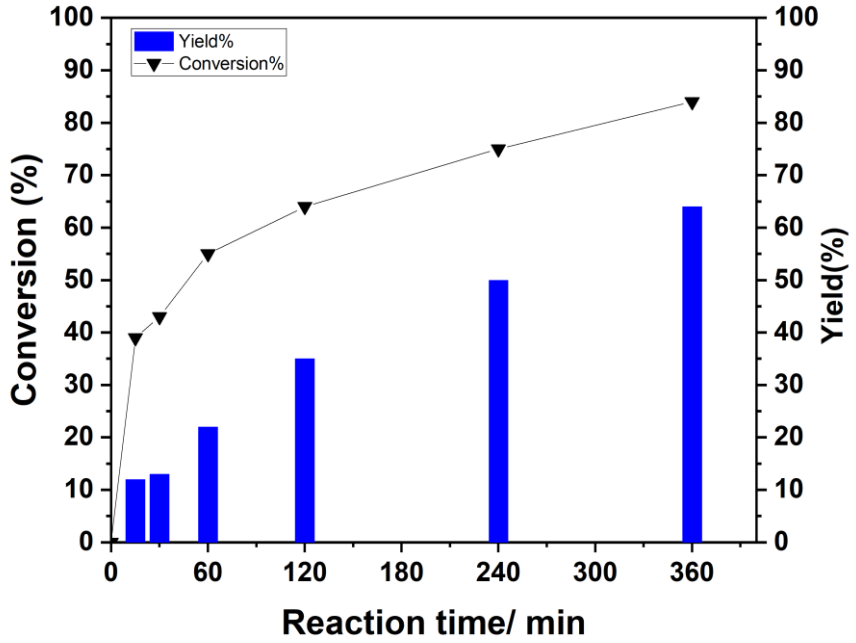

Figure 5.8. Effect of Toluene solvent on phenol conversion over 2.5%Pd-2.5%AuH/Al_2O_3 and N-Cyclohexyl-4-methylaniline yield**. Reaction conditions:** Phenol 0.2 mmol, ρ- Toluidine 0.4 mmol, using Toluene as solvent 2 ml, 40 mg 2.5%Pd-2.5%AuH/Al_2O_3 catalyst, under 1 bar H_2, 50 ºC, 1000 rpm.

5.3.2.1. Effect of the catalyst preparation methods and catalysts following different treatments of monometallic 5%Pd and bimetallic 5%Au-Pd supported on Al_2O_3 and TiO_2

An influential factor that can impact the catalytic activity is the method of catalyst preparation. Initial investigations on the N-alkylation of amine with phenol (using 40 mg catalysts, 50 °C, toluene as a solvent, atmospheric pressure of 1 bar H_2, and a 24-hour reaction time) indicated that 2.5%Pd-2.5%AuH/Al_2O_3 prepared through modified impregnation reduction by $NaBH_4$ is an effective catalyst for this reaction. Two preparation methods were studied for all catalysts: sol-immobilization and modified impregnation (as described in Sections 2.2.1 and 2.)[22]. The results presented in **Figures 5.7, 5.8, 5.9, and 5.10** demonstrate that 2.5%Pd-2.5%AuH/Al_2O_3 prepared through modified impregnation reduction by $NaBH_4$ yielded the highest N-cyclohexyl-4-methylaniline yield (as determined by GC analysis). The conversion and selectivity for N-cyclohexyl-4-methylaniline were 99.9 % each. The observed activity and selectivity were superior to those of the other catalysts prepared using the same method. These findings support previous observations regarding the N-alkylation of amine with phenol[10]. It was discovered that the preparation of gold-palladium catalysts supported on alumina through the modified impregnation reduction by $NaBH_4$ method significantly enhanced the catalyst's activity in the N-alkylation of amine with phenol. On the other hand, lower activity was observed when applying the modified impregnation method with heat treatment in 5% H_2/Ar at 450 °C at a heating rate of 2 K/min for gold-palladium catalysts supported on alumina, as mentioned earlier in Section 5.4.2. To comprehend the effect of different Pd oxidation states in this reaction, additional experiments were conducted. Consequently, different catalysts, including 5wt.%Pd and bimetallic 5%Au-Pd supported on Al_2O_3 and TiO_2, were prepared and subjected to all of the methods and treatments explained above. All catalysts were tested under standard reaction conditions. The data for 5%Pd/TiO_2, 5%Pd/Al_2O_3, 2.5%Au-2.5%Pd/TiO_2 and 2.5%Au-2.5%Pd/Al_2O_3 are presented in **Figures 5.7, 5.8, 5.9, and 5.10**, respectively. The catalysts prepared using the modified impregnation method underwent three types of treatment. The first treatment involved a heat treatment in 5% H_2/Ar at 450 °C with a heating rate of 2 K/min (M_{im}/Red). The second treatment was reduction by $NaBH_4$ (M_{im} (Hx)), while the third treatment involved calcination at 450 °C in air with a ramp rate of 20 °C/min. The reason for this pre-treatment is that during the catalyst preparation step through sol-immobilization, a drying step of the catalyst under air is conducted at 110 °C (Sim/PVA).

5.3.2.2. 5%Pd/TiO_2 Catalyst

The results of the experiments for 5%Pd/TiO_2 are depicted in **Figure 5.7.** It can be observed that when the catalyst is calcined in air for 24 hours, the conversion of phenol reaches 49 %, which is nearly the same as that observed when using a catalyst prepared through sol-immobilization (43 %). Additionally, when the catalyst undergoes heat treatment in 5% H_2/Ar at 450 °C and is tested, the conversion of phenol is the lowest (6 %). Furthermore, the highest conversion of phenol (86 %) is achieved when using the catalyst reduced by $NaBH_4$. These results indicate an enhanced phenol conversion for the catalyst reduced by $NaBH_4$, with the selectivity for N-Cyclohexyl-4-methylaniline reaching its peak at 54 %.

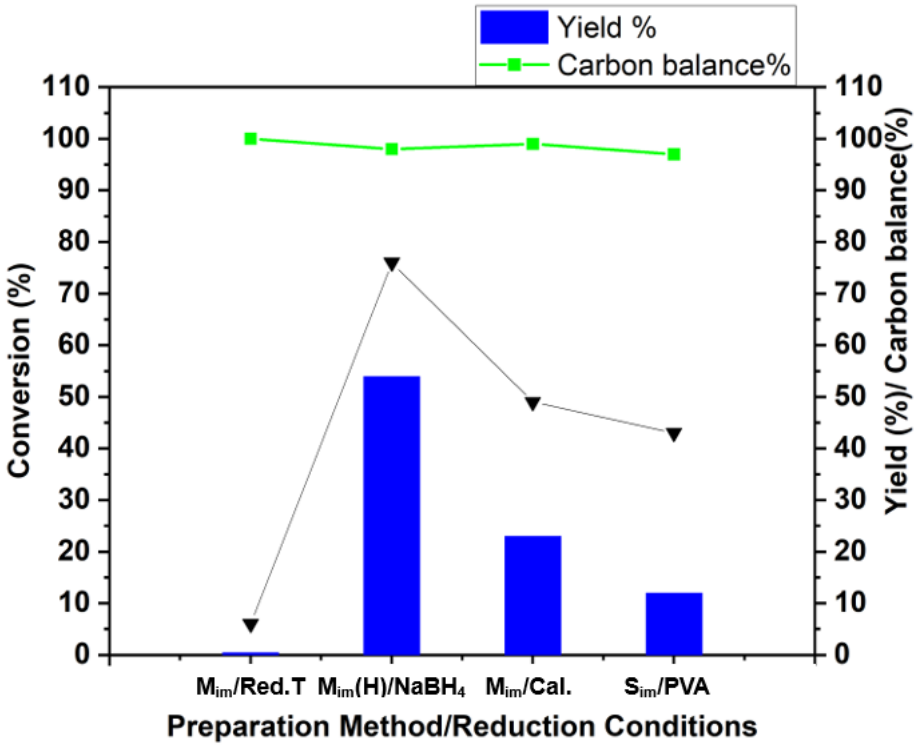

Figure 5.7: Effect of preparation methods and reduction conditions of 5%Pd/TiO_2 catalyst. **Reaction conditions:** Phenol 0.2 mmol, ρ-toluidine 0.4 mmol, using toluene as the solvent 2 ml ,40 mg 5%Pd/TiO_2 catalyst, under 1 bar H_2, 50 ºC, 24 hour, 1000 rpm. Catalysts prepared using the modified impregnation method (M_{im}/Red.T = catalyst reduced at 450 °C in 5% H_2/Ar at a heating rate of 2 K/min.) (M_{im}(H)/$NaBH_4$ = catalyst reduced By $NaBH_4$) and (M_{im}/Cal.= catalyst calcination at 450 °C in air at a heating rate of 2 K/min.). S_{im}/PVA = catalyst preparation by sol-immobilisation using a PVA stabiliser.

5.3.2.3. 5%Pd/Al_2O_3 Catalyst

Figure 5.8: demonstrates the outcomes of experiments conducted with 5%Pd/Al_2O_3. The figure reveals that when the catalyst was calcined in air for 24 hours, the conversion of phenol reached 52 %. Additionally, when the catalyst underwent heat treatment in 5% H_2/Ar at 450 °C and was examined, the conversion of phenol was only 34 %, which was identical to the conversion achieved when using the catalyst prepared through sol-immobilization. Furthermore, the maximum conversion of phenol (99.8 %) was achieved when $NaBH_4$ was utilized for catalyst reduction. It is evident that there is an increase in phenol conversion with $NaBH_4$ catalyst reduction, accompanied by the highest selectivity for N-cyclohexyl-4-methylaniline (85 %).

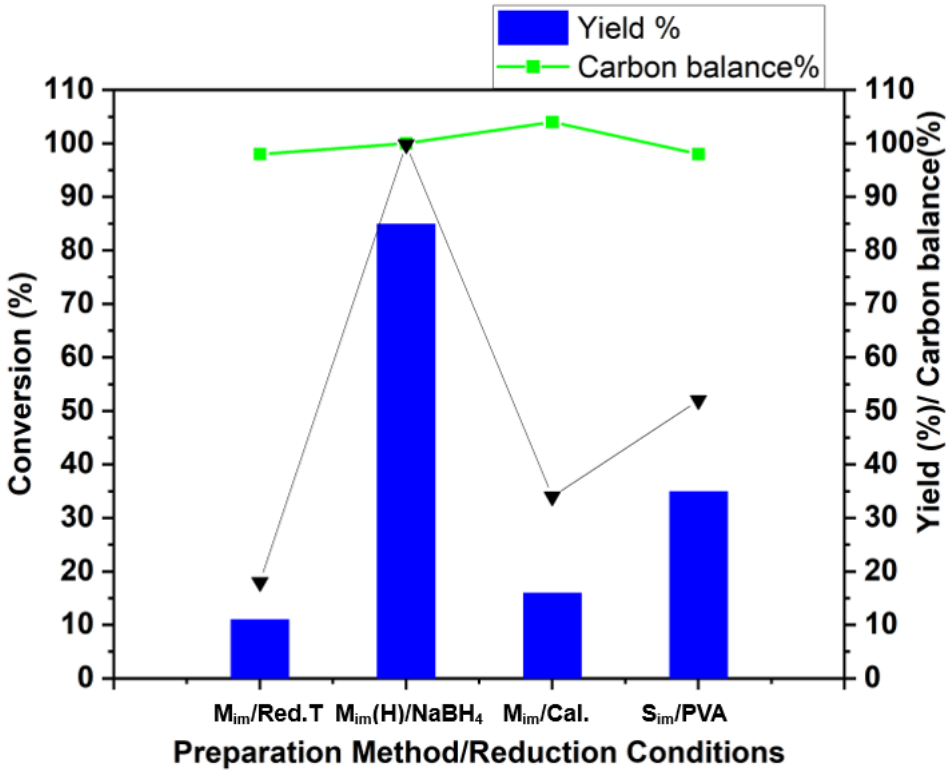

Figure 5.8: Effect of preparation methods and reduction conditions of 5%Pd/Al_2O_3 catalyst. **Reaction conditions:** Phenol 0.2 mmol, ρ-toluidine 0.4 mmol, using toluene as the solvent 2 ml ,40 mg 5%Pd/Al_2O_3 catalyst, under 1 bar H_2, 50 ºC, 24-hour, 1000 rpm. Catalysts prepared using the modified impregnation method (M_{im}/Red.T = catalyst reduced at 450 °C in 5% H_2/Ar at a heating rate of 2 K/min.) (M_{im}(H)/$NaBH_4$ = catalyst reduced By $NaBH_4$) and (M_{im}/Cal. = catalyst calcination at 450 °C in air at a heating rate of 2 K/min.). S_{im}/PVA = catalyst preparation by sol-immobilisation using a PVA stabiliser.

5.3.2.4. 2.5%Au-2.5%Pd/TiO_2 Catalyst

The outcomes of the experiments conducted with 2.5%Au-2.5%Pd/TiO_2 are presented in **Figure 5.9.** The figure indicates that both reduction methods, $NaBH_4$ and heat treatment at 450 °C in 5%H_2/Ar, resulted in the lowest conversions of 17 % and 8 %, respectively. On the other hand, the calcined catalyst exhibited a conversion of phenol at 44 %. Notably, the catalyst prepared via Sol-immobilization recorded the highest conversion of phenol at 85 %. Additionally, the selectivity for N-cyclohexyl-4-methylaniline was highest at 43 %.

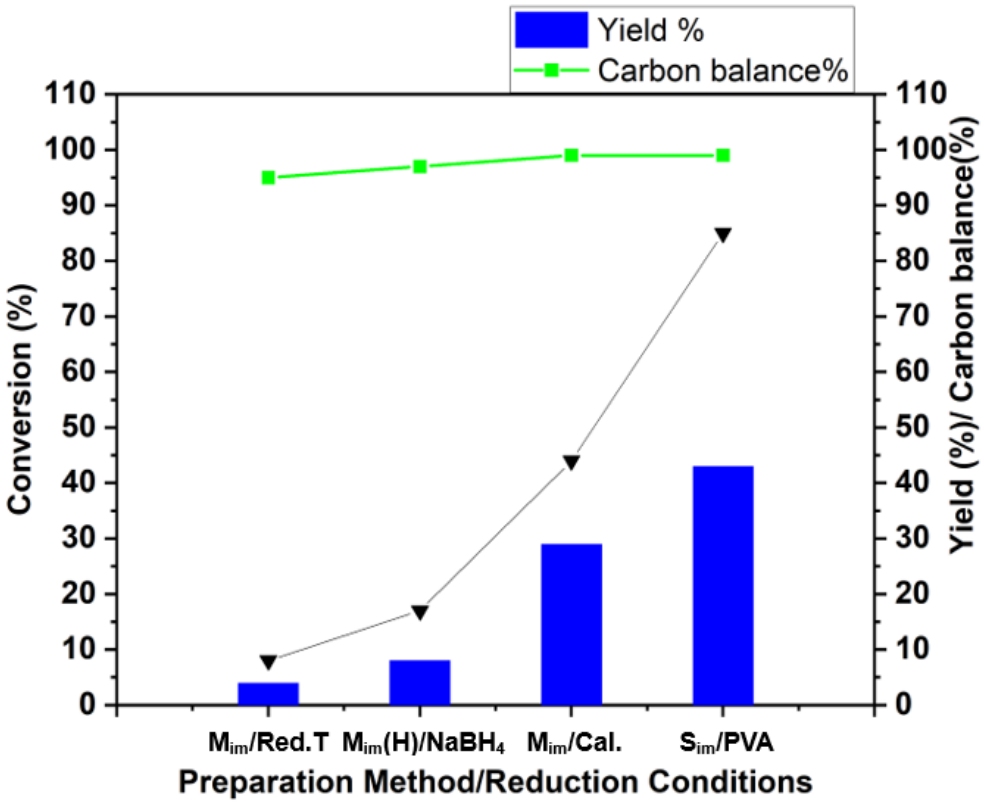

Figure 5.9: Effect of preparation methods and reduction conditions of 2.5%Pd-2.5%Au/TiO_2 catalyst**. Reaction conditions:** Phenol 0.2 mmol, ρ-toluidine 0.4 mmol, using toluene as the solvent 2 ml ,40 mg 2.5%Pd-2.5%Au/TiO_2 catalyst, under 1 bar H_2, 50 ºC, 24 hour, 1000 rpm. Catalysts prepared using the modified impregnation method (M_{im}/Red.T = catalyst reduced at 450 °C in 5% H_2 /Ar at a heating rate of 2 K/min.) (M_{im}(H)/$NaBH_4$ = catalyst reduced By $NaBH_4$) and (M_{im}/Cal. = catalyst calcination at 450 °C in air at a heating rate of 2 K/min.). S_{im}/PVA = catalyst preparation by sol-immobilisation using a PVA stabiliser.

5.3.2.5. 2.5%Au-2.5%Pd/ Al_2O_3 Catalyst

Figure 5.10 illustrates the results obtained with 2.5%Au-2.5%Pd/Al_2O_3, showing that both reduction methods, $NaBH_4$ and heat treatment at 450 °C in 5% H_2/Ar, via modified impregnation, achieved the highest conversions at 99.9 % and 99 %, respectively. Moreover, these catalysts exhibited high selectivity, with 99.9 % and 76 % selectivity, respectively. On the other hand, the catalyst prepared via Sol-immobilization achieved a high conversion of 93 %, while the calcined catalyst displayed low catalytic activity with only 3 % conversion of phenol. It is evident that 2.5%Au-2.5%Pd/Al_2O_3prepared via modified impregnation reduction with $NaBH_4$ exhibits the highest catalytic activity for the N-alkylation of amine with phenol.

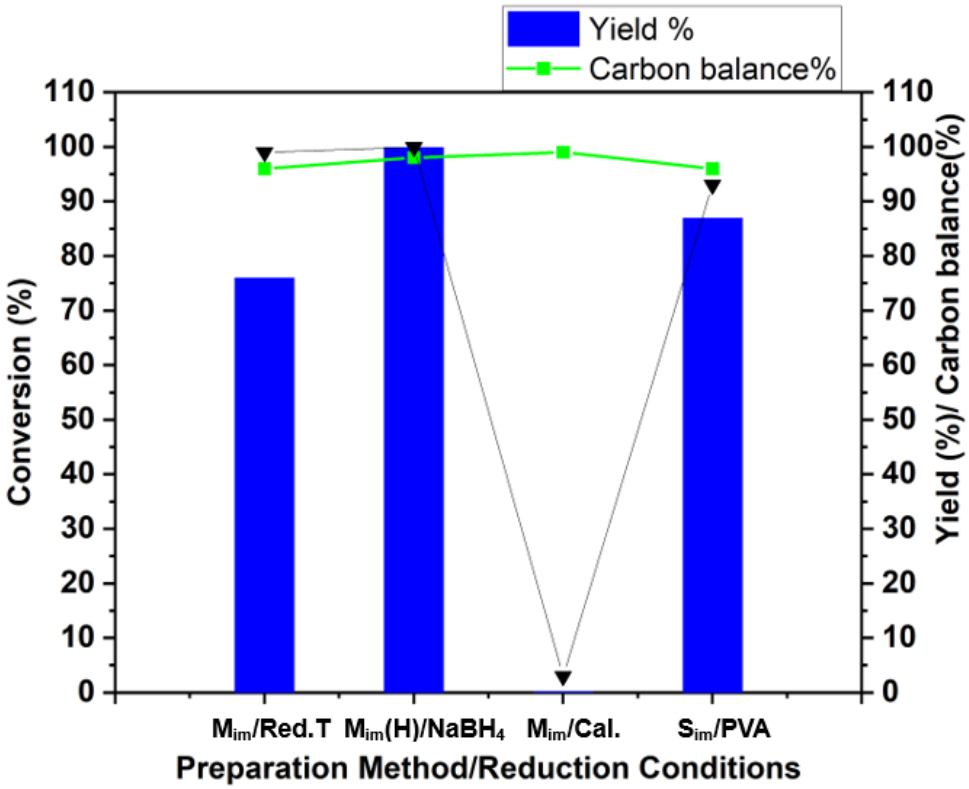

Figure 5.10: Effect of preparation methods and reduction conditions of 2.5%Pd-2.5%Au/Al_2O_3 catalyst. Reaction conditions**:** Phenol 0.2mmol, ρ-toluidine 0.4 mmol, using toluene as the solvent 2 ml ,40 mg 5%Pd-Au/Al_2O_3 catalyst, under 1 bar H_2, 50 ºC, 24 hour, 1000 rpm. Catalysts prepared using the modified impregnation method (M_{im}/Red.T = catalyst reduced at 450 °C in 5%H_2 /Ar at a heating rate of 2 K/min.) (M_{im}(H)/$NaBH_4$ = catalyst reduced By $NaBH_4$) and (M_{im}/Cal. = catalyst calcination at 450 °C in air at a heating rate of 2 K/min.). S_{im}/PVA = catalyst preparation by sol-immobilisation using a PVA stabiliser.

Based on the data presented in **Figures 5.7 to 5.10**, it can be concluded that the bimetallic 2.5%Pd-2.5%Au support on Al_2O_3 , prepared via the modified impregnation method and reduced with $NaBH_4$ (2.5%Pd-2.5%AuH/Al_2O_3) , exhibited the best catalytic performance for the N-alkylation of amine with phenol. Similarly, the monometallic 5%PdH/Al_2O_3 prepared using the same method demonstrated high activity for the reaction. However, the 2.5%Pd-2.5%AuH/Al_2O_3 catalyst exhibited greater effectiveness than 5%PdH/Al_2O_3. The XPS data for both catalysts (5%PdH/Al_2O_3 section 3.3.1. **Figure 3.4** and 2.5%Pd-2.5%AuH/Al_2O_3section 3.4.1. **Figure 3.16(a&b**), Chapter three) indicates the presence of both Pd^0 and Pd^{2+} species in 5%PdH/Al_2O_3, whereas Pd^{2+} species were absent in 2.5%Pd-2.5%AuH/Al_2O_3. This reduction in the presence of Pd^0 in 5%PdH/Al_2O_3 catalyst, where Pd^0 is the active species for the tested reactions, may contribute to the enhanced efficacy of the 2.5%Pd-2.5%AuH/Al_2O_3 catalyst.

5.3.2.6. Time online to compare activity of 2.5%Pd-2.5%AuH/Al_2O_3 M_{im} and 2.5%Pd-2.5%Au/Al_2O_3 S_{im} catalysts for N-alkylation of ρ-toluidine with phenol

To demonstrate the effectiveness of the M_{Im} preparation method with $NaBH_4$ reduction, catalysts M_{Im} and S_{Im} were tested for the N-alkylation of amine with phenol at 50 °C under 1 bar H_2. It has been previously established (see Section 5.4.4) that supported gold-palladium nanoparticles, 2.5%Pd-2.5%AuH/ Al_2O_3, are highly active catalysts for this reaction. For a fair comparison, the catalysts were prepared with the same metal content (2.5wt.% Au and 2.5wt.% Pd) on the same support of Al_2O_3. The results are presented in **Figure 5.11**, where the molar conversions for these reactions are displayed along with the corresponding selectivity for N-Cyclohexyl-4-methylaniline (the main product) and cyclohexanone (the by-product). Slight differences in the catalytic activities of the catalysts prepared using the two different methodologies were observed, with the order being M_{Im} > S_{Im}. The M_{Im} catalyst exhibited slightly higher activity compared to the S_{Im} catalyst, but both catalysts were equally active within the experimental error limits. This comparability of activity highlights the superiority of the current modified impregnation methodology over other methodologies, especially the S_{Im} method, which has been reported to be exceptionally active. The enhanced catalytic activity of the M_{Im} catalyst may be attributed to an optimized nanostructure compared to the corresponding S_{Im} catalyst, which is discussed in detail in Chapter Three. A comparison of the activity data reveals a general increase in activity for both catalysts. However, the catalysts prepared using

the M_{Im} method demonstrated better catalytic performance than the S_{Im} method at all reaction times.

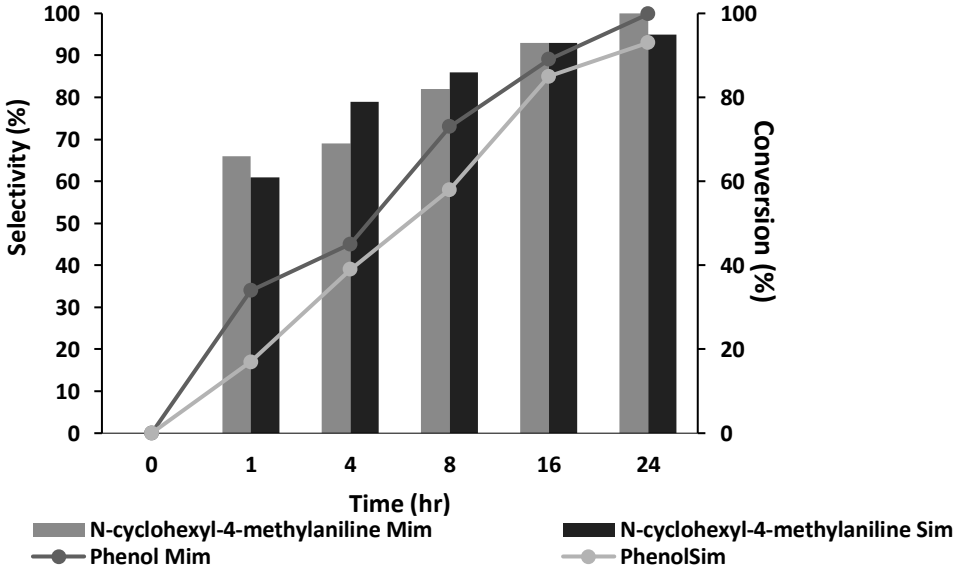

Figure 5.11. Time online of 2.5%Pd-2.5%AuH/Al_2O_3 M_{im} and 2.5%Pd-2.5%Au/Al_2O_3 S_{im} catalysts for N-alkylation of ρ-toluidine with phenol**. Reaction conditions:** Phenol 0.2 mmol, ρ-toluidine 0.4 mmol, using toluene as a solvent 2 ml, 40 mg catalyst, under 1 bar H_2, 50 ºC. (●) Phenol conversion% and (column) N-cyclohexyl-4-methylaniline selectivity%.

5.3.2.7. Reusability comparison of 2.5%Pd-2.5%AuH/Al_2O_3 M_{im} and 2.5%Pd-2.5%Au/Al_2O_3 S_{im} catalysts for N-alkylation of ρ-toluidine with phenol

The reusability of 2.5%Pd-2.5%AuH/Al_2O_3 M_{im} and 2.5%Pd-2.5%Au/Al_2O_3 S_{im} catalysts was evaluated by testing their stability, recovering them, and retesting them under standard conditions (50 °C, 4 hours, and 1 bar H_2). The results are presented in **Figure 5.12.** The reusability studies show the conversion of phenol and the selectivity towards N-Cyclohexyl-4-methylaniline. In each cycle, the solid catalyst was recovered through filtration, followed by rinsing with toluene once and acetone three times, and then drying at room temperature. Both recovered catalysts were reused in the subsequent reactions, and the results are summarized in **Figure 5.12.** After the first cycle, a significant reduction in conversion was observed for both reused catalysts. The conversion decreased from 54 % for the fresh 2.5%Pd-2.5%AuH/Al_2O_3 M_{im} catalyst and 49 % for the fresh 2.5%Pd-2.5%Au/Al_2O_3 S_{im} catalyst to 45 % and 39 % for the reused catalysts, respectively. However, there was no significant impact on

the selectivity towards N-Cyclohexyl-4-methylaniline, which remained similar at 72-76 % for 2.5%Pd-2.5%AuH/Al_2O_3 M_{im} and 75-77 % for 2.5%Pd-2.5%Au/Al_2O_3 S_{im}. In the second cycle, the conversion of phenol further decreased to 36 % for 2.5%Pd-2.5%AuH/Al_2O_3 M_{im} and 28 % for 2.5%Pd-2.5%Au/Al_2O_3 S_{im}, along with a decrease in selectivity. The third and fourth cycles showed a slight reduction in phenol conversion, reaching 28 % and 24 % by the end. The selectivity towards cyclohexyl-4-methylaniline also experienced a slight decrease, reaching approximately 60 % and 63 % for the respective catalysts. As Pd^0 is being the active species for the tested reactions and Based on the XPS data illustrated in (**Table 3.3**, Chapter three), the composition of Pd-Au alloys was evaluated and found that the Pd/Au molar ratio for fresh 2.5%Pd-2.5%Au/Al_2O_3 S_{im} catalyst was 1.7. While the Pd/Au molar ratio for the fresh 2.5%Pd-2.5%AuH/Al_2O_3 M_{im} catalyst was 2.1. This indicates that the percentage of Pd^0 in 2.5%Pd-2.5%AuH/Al_2O_3 M_{im} is more than in 2.5%Pd-2.5%Au/Al_2O_3 $S_{im.}$ In addition, the present of Cl^- 2p at 198.6 eV with At%Conc. 0.14 only in 2.5%Pd-2.5%AuH/Al_2O_3 M_{im} catalyst, whether this Cl is adsorbed on the Pd itself or neighbouring sites. This latter point supports the findings of Shen et. al.[23], who reported similar Pd binding energies for Cl^- containing catalysts and suggests that Pd has a more positive valency, resulting in a more stable Pd surface structure than the corresponding halide free system. While, the reduction in activity observed for both reused 2.5%Pd-2.5%AuH/Al_2O_3 M_{im} and 2.5%Pd-2.5%Au/Al_2O_3 S_{im} catalysts may be attributed to the surface poisoning caused by reactants, as indicated by the XPS data (**Table 3.4**, Chapter three), , which shows the presence of new peaks corresponding to O 1s (OH/Organic) at 532.18 eV for reused 2.5%Pd-2.5%AuH/Al_2O_3 M_{im} and 532.21 eV for reused 2.5%Pd-2.5%Au/Al_2O_3 S_{im}.

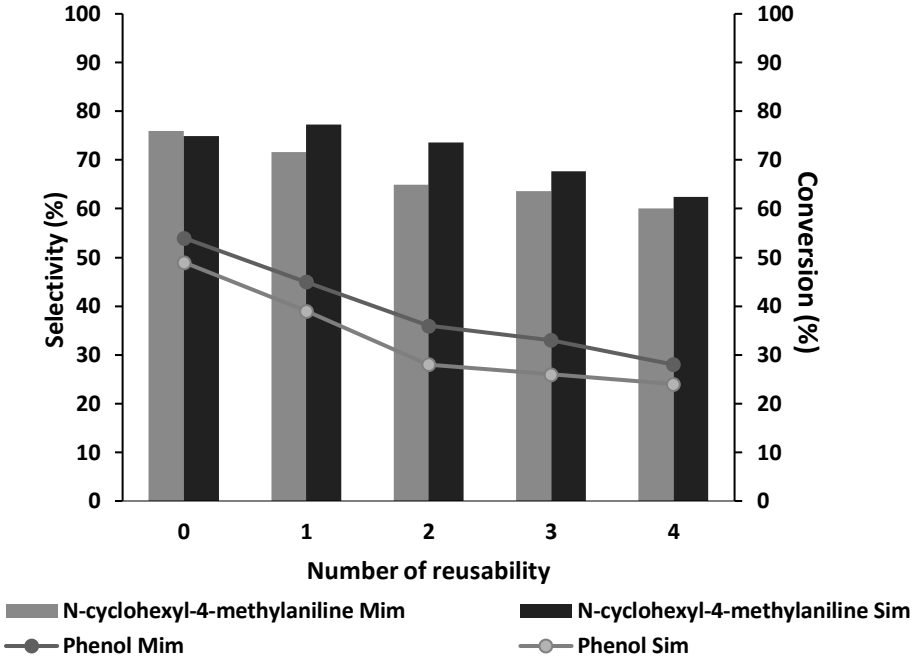

Figure 5.12: Reusability of 2.5%Pd-2.5%AuH/Al_2O_3 M_{im} and 2.5%Pd-2.5%Au/Al_2O_3 S_{im} catalysts for N-alkylation of ρ-toluidine with phenol**. Reaction conditions:** Phenol 0.2 mmol, ρ-toluidine 0.4 mmol, using toluene as a solvent 2 ml, 40 mg catalyst, under 1 bar H_2, 50 ºC, 4 hours. (●) Phenol conversion% and (column) N-cyclohexyl-4-methylaniline selectivity%.

5.4. The reductive coupling of phenol with ρ-toluidine over palladium catalysts through catalytic transfer hydrogenation pathway

The catalytic transfer hydrogenation (CTH) process allows organic compounds, such as alcohols, acids, and acid salts, to act as hydrogen donors during hydrogenation reactions in the presence of catalysts. This technique eliminates the need for high-pressure hydrogen gas and enhances the solubility of hydrogen donors. Moreover, when targeting partially hydrogenated compounds, the reduced hydrogenating capacity of most organic hydrogen donors can influence product selectivity effectively. Initial studies focused on synthesizing several Pd catalysts using the M_{im} method, which involves heat treatment for reduction, and evaluating the reductive amination reaction using sodium formate as the hydrogen donor (refer to **Table 5.3**)[18].

The cross-coupling of phenol and p-toluidine was extensively investigated to determine the feasibility of achieving the desired coupling products using conventional metal catalysts. Transition metal complexes, including Au and Pd, were tested, but failed to generate the desired coupling products[24–27]. Various palladium catalysts were also examined, and the results are presented in **Table 5.3.** Among the supported Pd catalysts, only 5%Pd/Al_2O_3, 2.5%Pd-2.5%Au/TiO_2 and 2.5%Pd-2.5%Au/Al_2O_3

catalysts. exhibited significant catalytic activity for this conversion. Notably, 5%Pd/Al_2O_3 yielded the best results (entry 10) with a conversion of 31% and a selectivity of 74%. Furthermore, 5%Pd/Al_2O_3 effectively catalysed the reaction to produce N-cyclohexyl-4-methylaniline with a yield of 23 % after eliminating the water molecule from the reactants. While 5%Pd/Al_2O_3 reported that the most effective reaction occurred with 10mol% of Pd/C, yielding optimal catalytic activity[18]. However, in this study, it was found that the best catalysts are 5%Pd/Al_2O_3 and 2.5%Pd-2.5%Au/Al_2O_3. Product conversions and yields were obtained using a gas chromatograph (GC).

Table 5.3: Catalyst screening for N-alkylation of ρ- toluidine with phenol

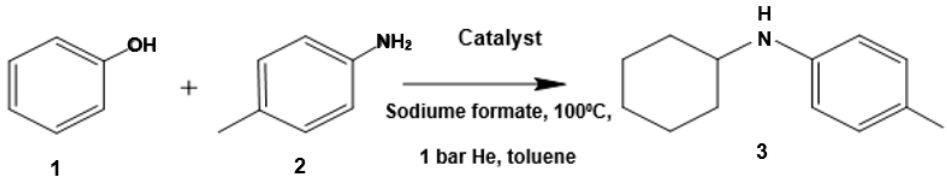

(1) Phenol, (2) ρ-toluidine, (3) N-cyclohexyl-4-methylaniline.

The (3) (N-Cyclohexyl-4-methylaniline) product can be identified by NMR and GC-MS (see Appendix A)

Entry	Catalyst	Conv. % (Phenol)	Sel. % (N-cyclohexyl-4-methylaniline)	Yield % (N-cyclohexyl-4-methylaniline)
1	Blank reaction (non)	0	0	0
2	0.5% Pd-0.5%Au/TiO_2	0	0	0
3	2.5% Pd-2.5%Au/TiO_2	24	97	23
4	2.5% Pd-2.5%Au/C	1	100	1
5	5% Pd/TiO_2	13	26	3
6	5% Au/TiO_2	0	0	0
7	5% Pd/C	2	100	2
8	5%Pd/MgO	3	0	0
9	5%Pd/CeO_2	1	17	0.1
10	5%Pd/ Al_2O_3	31	74	23
11	10%Pd/C	5	76	4

Reaction conditions: phenol (0.2 mmol, 19 mg), p-toluidine (0.2 mmol, 21 mg), catalyst (40 mg), sodium formate (6 equiv., 82 mg) and toluene as a solvent (0.8 mL) under 1 bar He atmosphere, 24 hours, 100 ºC. Yields were determined by GC analysis with mesitylene as the internal standard.

5.5. Conclusion

In conclusion, we have successfully developed a highly active catalyst, 5%PdH/Al_2O_3 , for the reductive coupling of lignin-derived phenols with amines. This catalyst demonstrated excellent performance, achieving high yields and good stereoselectivity under mild reaction conditions. The exceptional activity of the 5%PdH/Al_2O_3 catalyst can be attributed to the high reactivity of the PdH species and the activation of phenol by the Al_2O_3 support. These promising results open new possibilities for the utilization of lignin as a renewable reagent in future chemical synthesis. Additionally, the reusability study indicated that the 2.5%Pd-

2.5%AuH/Al_2O_3 bimetallic catalyst, prepared via modified impregnation and reduced with $NaBH_4$, exhibited higher activity compared to the 2.5%Pd-2.5%Au/Al_2O_3 bimetallic catalyst prepared by sol-immobilisation for the N-alkylation of ρ-toluidine with phenol.

5.6. References

1 International Energy Agency, *World Energy Outlook* **1998**.

2 P. Gallezot, *ChemSusChem*, 2008, **1**, 734–737.

3 A. Kumar, N. Kumar, P. Baredar and A. Shukla, *Renew. Sustain. Energy Rev.*, 2015, **45**, 530–539.

4 Z. Chen, H. Zeng, H. Gong, H. Wang and C. J. Li, *Chem. Sci.*, 2015, **6**, 4174–4178.

5 X. Ma, C. Su and Q. Xu, *Hydrogen Transfer Reactions*, 2016, 291–364.

6 X. Wang, B. Meng, X. Tan, X. Zhang, S. Zhuang and L. Liu, *Ind. Eng. Chem. Res.*, 2014, **53**, 5636–5645.

7 H.-U. Blaser, A. Indolese, A. Schnyder, H. Steiner and M. Studer, *J. Mol. Catal. A Chem.*, 2001, **173**, 3–18.

8 M. Sankar, N. Dimitratos, P. J. Miedziak, P. P. Wells, C. J. Kiely and G. J. Hutchings, *Chem. Soc. Rev.*, 2012, **41**, 8099–8139.

9 V. R. Jumde, E. Petricci, C. Petrucci, N. Santillo, M. Taddei and L. Vaccaro, *Org. Lett.*, 2015, **17**, 3990–3993.

10 L. Yan, X. X. Liu and Y. Fu, *RSC Adv.*, 2016, **6**, 109702–109705.

11 Z. Chen, H. Zeng, H. Gong, H. Wang and C. J. Li, *Chem. Sci.*, 2015, **6**, 4174–4178.

12 P. Paul, P. Bhanja, N. Salam, U. Mandi, A. Bhaumik, S. M. Alam and S. M. Islam, *J. Colloid Interface Sci.*, 2017, **493**, 206–217.

13 C. C. Torres, V. A. Jiménez, C. H. Campos, J. B. Alderete, R. Dinamarca, T. M. Bustamente and B. Pawelec, *Mol. Catal.*, 2018, **447**, 21–27.

14 S. Jadhav, A. Jagdale, S. Kamble, A. Kumbhar and R. Salunkhe, *RSC Adv.*, 2016, **6**, 3406–3420.

15 P. M. De Souza, R. C. Rabelo-Neto, L. E. P. Borges, G. Jacobs, B. H. Davis, T. Sooknoi, D. E. Resasco and F. B. Noronha, *ACS Catal.*, 2015, **5**, 1318–1329.

16 A. Bjelić, M. Grilc and B. Likozar, *Chem. Eng. J.*, 2020, **394**, 124914.

17 Z. Chen, H. Zeng, H. Gong, H. Wang and C. J. Li, *Chem. Sci.*, 2015, **6**, 4174–4178.

18 Z. Chen, H. Zeng, S. A. Girard, F. Wang, N. Chen and C. J. Li, *Angew. Chemie - Int. Ed.*, 2015, **54**, 14487–14491.

19 N. C. Nelson, J. S. Manzano, A. D. Sadow, S. H. Overbury and I. I. Slowing, *ACS Catal.*, 2015, 5, 2051–2061.

20 K. Maeda, R. Matsubara and M. Hayashi, *Org. Lett.*, 2021, **23**, 1530–1534.

21 A. H. Pizarro, C. B. Molina, J. A. Casas and J. J. Rodriguez, *Appl. Catal. B Environ.*, 2014, **158**–**159**, 175–181.

22 M. Sankar, Q. He, M. Morad, J. Pritchard, S. J. Freakley, J. K. Edwards, S. H. Taylor, D. J. Morgan, A. F. Carley, D. W. Knight, C. J. Kiely and G. J. Hutchings, *ACS Nano*, 2012, **6**, 6600–6613.

23 Y. Shen, S. Wang and K. Huang, *Appl. Catal.*, 1990, **57**, 55–70.

24 C. Liu, J. Wang, P. Zhu, H. Liu and X. Zhang, *Chem. Eng. J.*, 2022, **430**, 1385–8947.

25 G. Xue, L. Yin, S. Shao and G. Li, *Nanotechnology*, 2022, **33**, 072003.

26 Z. Zhang and H. Li, *Fuel*, 2022, 310.

27 D. V. Kurandina, E. V. Eliseenkov, T. S. Khaibulova, A. A. Petrov and V. P. Boyarskiy, *Tetrahedron*, 2015, **71**, 7931–7937.

Chapter 6: Synthesis of imines and secondary amines from nitrobenzene and benzyl alcohol using supported Ru-Pd bimetallic catalyst

6.1. Introduction

The method of hydrodeoxygenation, which involves the removal of oxygen using hydrogen, is a commonly employed strategy for transforming oxygen-rich biomass feedstock into hydrocarbons. Yet, hydrogen's high cost, coupled with its frequent derivation from petroleum feedstock, presents a challenge. As a result, there's a growing necessity for the creation of new reaction techniques that circumvent the need for external hydrogen. Considering this, the hydrogen auto-transfer (HAT) process, also referred to as "borrowing hydrogen," offers a promising alternative. This approach utilizes hydrogen from a dehydrogenation reaction for in situ hydrogenation or hydrodeoxygenation reactions[1,2]

The HAT reaction examined in this study proceeds as follows. The initial step entails the dehydrogenation of benzyl alcohol, resulting in benzaldehyde. In this mechanism, the redundant hydrogen produced is subsequently hydrogenated into by-products, such as water. This process is known as oxidative dehydrogenation[3]. Moreover, limiting the dehydrogenation of BOH is crucial to curtail the generation of toluene, a product of the hydrogenolysis of BOH, as outlined in **Scheme 6.1**[4].

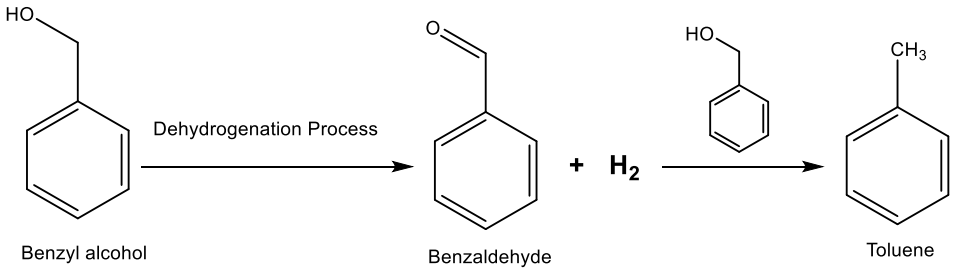

Scheme 6.1: Conversion of Benzyl Alcohol to Benzaldehyde via Dehydrogenation Processes[4].

Secondly, the subsequent step involves the hydrogenation of nitrobenzene to yield aniline, a vital intermediate used in the production of plastics and secondary amines. In the liquid phase, primary catalysts used for the conversion of nitrobenzene (NB) to

aniline are typically based on noble metals, such as Palladium[5], Platinum[6], and Ruthenium[7]. The final stages of the process include the coupling of aniline with benzaldehyde to yield imine, followed by the hydrogenation of the imine to generate secondary amine.

An illustration of this HAT reaction involves the direct production of imines, secondary amines, and tertiary amines from benzyl alcohol and nitrobenzene, without the necessity for external hydrogen. The HAT reaction offers environmental advantages and is also beneficial in terms of atom economy. Alongside the formation of C-N bonds, this HAT strategy is employed to create C-C bonds as well[8]. In the HAT reaction, supported metal catalysts prove particularly efficient for the dehydrogenation of benzyl alcohol (as referred to in HAT) to benzaldehyde. The generated hydrogen is then used for reducing nitrobenzene to aniline. Both benzaldehyde and aniline can be readily coupled to yield imine, and if excess hydrogen is produced from the dehydrogenation of surplus benzyl alcohol, the imine undergoes further reduction to form a secondary amine (**Scheme 6.2**).

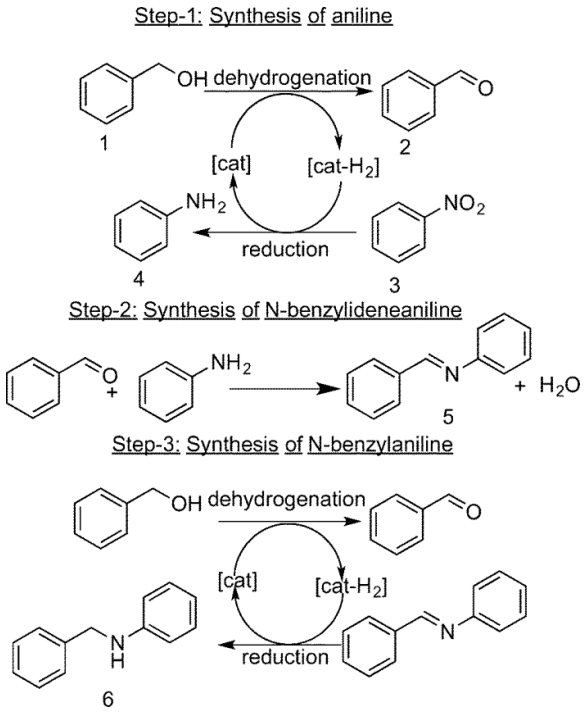

Scheme 6.2: HAT reaction steps to produce (5) N-benzylideneaniline and (6)N-benzylaniline from (1) Benzyl Alcohol and (3) Nitrobenzene. (2) is Benzaldehyde and (4) is Aniline[9].

HAT reactions typically utilize homogeneous catalysts, although some heterogeneous catalysts have been reported as well. For instance, the $Ru(NHC)_2$ homogeneous catalyst has been used for α-alkylation of a wide array of methylene ketones to yield branched products[10]. Additionally, the heterogeneous Pt-Sn/γ-Al_2O_3 bimetallic

catalyst has been employed to catalyse the direct synthesis of diamines from the N-alkylation of amines with diols[11].

Both monometallic and bimetallic nanoparticle-based materials have been reported as heterogeneous catalysts for this reaction[12].

The focus of this study is to engineer heterogeneous catalysts for the HAT reaction using Benzyl Alcohol and Nitrobenzene as the model reaction. This will lay the groundwork for the future HAT of bio renewable feedstock.

This specifically involves the creation of supported bimetallic catalysts (Palladium and Ruthenium) for a basic HAT reaction. Shortlisted catalysts will be subjected to complex HAT reaction testing. Up until now, selected promising bimetallic catalysts have been utilized in the BAO reaction and in a simple HAT reaction between Benzyl Alcohol and Nitrobenzene to generate imines and amines[9,13]. In this study, the bimetallic Ru-Pd nanoparticles are supported on diverse supports (Al_2O_3, TiO_2, Zeolite and CeO_2). All these catalysts were created using the recently reported modified impregnation method (M_{im})[14] and reduced with borohydride $NaBH_4$.

6.2. Experimental work

6.2.1. Catalyst preparation

The catalysts used in the study were prepared using the Modified Impregnation Method (M_{im}) as outlined in Chapter 2, specifically in Section 2.2.2. Following the preparation process, the catalysts underwent a reduction step using borohydride $NaBH_4$, resulting in the formation of the bimetallic catalyst 0.5%Pd-0.5%RuH/Al_2O_3.

The detailed instructions for synthesizing the 0.5%Pd-0.5%RuH/Al_2O_3 bimetallic catalyst can be found in Chapter 2, specifically in Section 2.2.3.4. This section provides comprehensive guidance on the precise procedure used to obtain the desired catalyst.

In this study, the metal loading on the support is expressed as the weight percentage of the metal relative to the support material, which is Al_2O_3 in this case. For the 0.5%Pd-0.5%RuH/Al_2O_3 bimetallic catalyst, the weight percentage of both Pd and RuH is 0.5% each with respect to the total weight of the Al_2O_3 support.

By controlling the metal loading on the support, researchers can tailor the catalyst's composition and active sites, which significantly influences its catalytic performance. In the case of bimetallic catalysts, the presence of multiple metals can lead to synergistic effects, enhancing the catalyst's activity, selectivity, and stability in various hydrogenation reactions.

The utilization of the Modified Impregnation Method (M_{im}) and the subsequent reduction step with borohydride NaBH4 allows for the precise preparation of the

0.5%Pd-0.5%RuH/Al_2O_3 bimetallic catalyst and facilitates the comparison of its performance with other monometallic and bimetallic catalysts in the study.

Overall, the details provided on the catalyst formulation, preparation, and metal loading are essential for ensuring reproducibility and accurate interpretation of the results. This systematic approach to catalyst synthesis and characterization contributes to the reliability and significance of the study's findings and insights into the design and optimization of bimetallic catalysts for hydrogenation reactions.

6.2.2. Catalyst testing

In this current investigation, the focus was on examining the performance of the bimetallic catalyst 0.5%Pd-0.5%RuH/Al_2O_3, which is supported on gamma-alumina. The catalyst was evaluated in the synthesis of imines and secondary amines from Benzyl Alcohol and Nitrobenzene.

The detailed methodology for this investigation can be found in Chapter 2, specifically in Section 2.3.3. The reaction process employed for the synthesis of amines and imines involved the direct conversion of nitrobenzene and benzyl alcohol through a hydrogen auto-transfer reaction technique.

In this process, the catalyst played a crucial role as a mediator for the transfer of hydrogen between nitrobenzene and benzyl alcohol, facilitating the formation of both imines and secondary amines. The hydrogen auto-transfer reaction technique is a unique and valuable approach in catalysis, enabling the simultaneous conversion of multiple reactants in a single reaction system, leading to the synthesis of amines and imines.

The investigation of this reaction system using the bimetallic Pd and Ru supported gamma-alumina catalyst, 0.5%Pd-0.5%RuH/Al_2O_3, offers insights into the catalytic activity and selectivity of this specific catalyst for the targeted synthesis of amines and imines. The choice of bimetallic catalyst is particularly interesting, as it allows for the exploration of potential synergistic effects between Pd and Ru in the hydrogenation and condensation reactions.

Understanding the catalytic performance of this bimetallic catalyst in the hydrogen auto-transfer reaction is of significant interest due to the importance of imines and secondary amines in various chemical and pharmaceutical applications. The findings from this study can contribute to the development of efficient catalytic systems for the direct synthesis of valuable compounds from readily available starting materials, potentially offering greener and more sustainable pathways to produce amines and imines in the future.

6.2.3. Catalyst characterisation

In Chapter 3 of the study, the catalysts underwent thorough characterization using X-ray Photoelectron Spectroscopy (XPS) and Transmission Electron Microscopy (TEM) techniques. These investigations aimed to gain insights into the catalysts' stability and activity, with a specific focus on the bimetallic Pd and Ru supported gamma-alumina catalyst, 0.5%Pd-0.5%RuH/Al_2O_3.

In Section 3.6 of Chapter 3, the detailed results, and observations from the XPS and TEM characterizations are presented. XPS is a powerful tool that provides valuable information about the surface chemical composition and electronic states of the catalyst, which are crucial for understanding the catalyst's active sites and interactions between Pd and Ru.

On the other hand, TEM offers high-resolution imaging of the catalyst at the nanoscale, allowing researchers to visualize the distribution, size, and morphology of the metal particles. By examining the catalyst at this level, the researchers can gain valuable insights into the physical properties of the Pd and Ru particles, which are directly linked to the catalyst's stability and activity.

The observations from the characterization data suggest the presence of a geometric effect between Pd and Ru, indicating that the arrangement and spatial distribution of the two metals influence the catalyst's behaviour. This geometric effect can play a crucial role in enhancing the catalyst's efficiency in the desired hydrogenation and condensation reactions.

Furthermore, the data also indicate that excessive Ru loading on the catalyst may lead to metal particle aggregation. This finding is essential as it highlights the importance of optimizing the metal loading to avoid potential detrimental effects on the catalyst's performance. By maintaining an appropriate Pd-Ru ratio, researchers can maximize the synergistic interactions between the two metals and improve the overall catalytic performance.

Overall, the characterization data obtained through XPS and TEM provide valuable information about the catalyst's properties and behaviour, shedding light on the mechanisms that govern its stability and activity in the studied reactions. These insights are crucial for guiding the design and development of highly efficient and stable bimetallic catalysts for various hydrogenation and condensation processes in the field of catalysis.

6.3. Results and discussion

6.3.1. Catalytic data for the HAT reactions

Preliminarily, the HAT reaction outcomes with mono and bimetallic catalysts were unsatisfactory, mainly attributable to the inaccurate area ratio readings from the GC, which yielded varied quantification values for identical samples. The catalytic reactions were conducted under the following conditions: 120 °C, 3 h, 1 bar N_2, 1000 rpm stirring speed. Consequently, a different GC was utilized for calibrating the same samples (refer to **Table 6.1**). From **Table 6.1**, it is evident that the maximum conversion rate of Nitrobenzene reached 20 %, with a selectivity of 89 % for N-benzylaniline production, using 0.5%Pd-0.5%RuH/Al_2O_3 at 120 °C after 3 hours under 1 bar N_2. Additionally, the catalyst demonstrating the highest selectivity for both products (N-benzylideneaniline and N-benzylaniline) was 0.5%Pd-0.5%RuH/CeO_2, with an 18 % conversion rate of nitrobenzene. Nonetheless, the selectivity percentage varied upon alteration of the metal oxide support. To observe the impact of the support on the catalyst's activity, another experiment was performed using the 0.5%Pd-0.5%RuH/Al_2O_3 catalyst, with an online analysis of the reaction time. The products were identified based on gas chromatography (GC) and GC-MS results (refer to Appendix C (a, b) for N-benzylideneaniline, and Appendix D (a, d) for N-benzylaniline).

6.3.2. Metal oxides as supports on bimetallic palladium and ruthenium for the synthesis of imines and secondary amines from nitrobenzene and benzyl alcohol

Supports are well-recognized for their substantial impact on catalyst activity. In the realm of heterogeneous catalysts, metal oxides are predominantly employed as supports, significantly determining the catalyst's activity. The fusion of two active noble metals has been proven effective in generating high-performing oxide-supported catalysts. Sankar et al.[9] examined the alloy impact of Pd-Ru/TiO_2 for the direct synthesis of imine and amine. The properties inherent in these supports are reported to play a crucial role in the adsorption of bimetallic palladium and ruthenium nanoparticles[9,15], which subsequently affect the catalytic activity. As metal oxides have demonstrated appreciable activity in the reductive imination of alcohols with nitrobenzenes[9,16,17] four distinct metal oxides have been scrutinized for synthesizing imines and secondary amines from Benzyl Alcohol and Nitrobenzene. Commercial supports (Al_2O_3, TiO_2, zeolite and CeO_2) were utilized for this purpose. From **Table 6.1**, it is evident that TiO_2 exhibited significantly reduced activity (17 % conversion)

and amine selectivity compared to the Al_2O_3-supported catalyst (20 % conversion). The zeolite Y hydrogen and CeO_2-supported Ru–Pd catalysts also displayed diminished activity (11 % conversion and 18 % conversion, respectively) (see **Table 6.1**). The catalytic outcomes convincingly demonstrate that the Al_2O_3 supported Pd-Ru catalyst surpassed in terms of activity and amine selectivity compared to the other supported catalysts. Prior studies have indicated that when TiO_2 is employed as a support, 0.5%Pd-0.5%Ru/TiO_2 achieves a superior conversion (99 %) of Nitrobenzene relative to 0.5%Pd-0.5%Ru/MgO (26 %) prepared under identical conditions[9]. This study further uncovered that the primary contribution of the bimetallic catalysts is to augment the rate of the initial dehydrogenation step, which has substantial advantages for the subsequent production of N-benzylideneaniline and the secondary amine N-benzylaniline.

The TEM characterization of the most active 0.5%Pd-0.5%RuH/Al_2O_3 catalyst revealed that the catalyst is comprised of extremely minute nanoparticles (2.17 nm) with a narrow particle size distribution.

Table 6.1: Direct synthesis of N-benzylideneaniline (Imin) (5) and N-benzylaniline (Amin) (6) from Benzyl Alcohol (1) and Nitrobenzene (3) using metal oxide as a support on Pd-Ru metals:

Catalyst	Conversion (%)	Selectivity (%)		Yield (%)		Carbon mass balance
	Nitrobenzene (NB)	Imin	Amin	Imin	Amin	mol%
0.5%Pd-0.5%RuH/Al_2O_3	20	11	89	2	18	92
0.5%Pd-0.5%RuH/CeO_2	18	56	44	10	8	95
0.5%Pd-0.5%RuH/Zeolite Y hydrogen	11	12	88	1	9	97
0.5%Pd-0.5%RuH/TiO_2	17	35	65	6	11	92

Reaction conditions: catalyst: 0.02 g; Nitrobenzene: 0.9 mmol; Benzyl Alcohol: 9 mmol; N_2: 1 bar; mesitylene (solvent): 1 ml, 120 °C, 3 h; stirring speed: 1000 rpm.

The product (Imin) (N-benzylideneaniline) can be identified via GC-MS analysis (see Appendix C(a) and C(b) respectively), while (6) (Amin) (N-benzylaniline) can be detected through GC-MS (see Appendix D(a) and D(b) respectively).

The XRD diffraction profiles for all supported catalysts have been gathered and can be found in Chapter 3 (refer to **Figure 3.27**). There is no significant discernible differentiation in the reflections of the XRD patterns across all the supported catalysts. This could be attributed to the overlap between the phases of the support and the reflections of Pd-Ru, or to the metal loadings being less than the XRD differentiation region. The minute crystallite sizes and the 1% loading suggest that these metal sites are likely below the detection threshold of X-ray diffraction analysis. As seen in **Table 6.1**, when Al_2O_3 was used as a support, it exhibited higher activity compared to other supports. Consequently, the support role in the Pd-Ru bimetallic catalyst significantly influences the selectivity of HAT reaction products.

Based on XPS data (refer to Chapter 3, Section 3.4.3. **Table 3.8** for more details), the 0.5%Pd-0.5%RuH/Al_2O_3, 0.5%Pd-0.5%RuH/CeO_2, 0.5%Pd-0.5%RuH/TiO_2 and 0.5%Pd-0.5%RuH/zeolite Y hydrogen catalysts were characterized, with the results displayed in **Table 6.2.** According to the table, only the 0.5%Pd-0.5%RuH/zeolite Y hydrogen catalyst contains Pd and Ru metals and their oxide states in the presence of Cl^-. The 0.5%Pd-0.5%RuH/TiO_2 has Pd and Ru metals and their oxide states but with no presence of Cl^-. In the case of 0.5%Pd-0.5%RuH/CeO_2 catalyst, no peak for Pd metal and Cl^- is observed. For the 0.5%Pd-0.5%RuH/Al_2O_3, results indicate no peak for RuOx state only catalyst.

Table 6.2: XPS data for bimetallic 0.5%Pd-0.5%RuH catalyst supported on deferent metal oxide:

Compound	**Pd^0** **Position/ %At Conc.**	**Pd^{2+}3d** **Position/ %At Conc.**	**Cl^-2p** **Position/ %At Conc.**	**$Ru^0$3d** **Position/ %At Conc.**	**Ru3d O_x** **Position/ %At Conc.**	**C1s** **Position/ %At Conc.**	**Pd^{2+}/ Pd^0** Molar ratio (%)
0.5%Pd-0.5%RuH/Zeolite Y hydrogen	334.94/0.45	336.98/0.13	198.05/0.21	279.91/0.22	280.76/0.35	284.8/11.78	0.29
0.5%Pd-0.5%RuH/TiO_2	335.18/0.27	337.36/0.2	------	280.61/0.32	281.38/0.17	284.8/18.77	0.74
0.5%Pd-0.5%RuH/CeO_2	------	337.83/0.73	------	281.23/0.55	281.93/0.28	284.8/21	0
0.5%Pd-0.5%RuH/Al_2O_3	335.31/0.55	336.34/0.33	198.99/0.7	279.91/0.22	------	284.96/22.98	0.6

Zhang and Su et al.[18] have recently demonstrated the influential role of Pt and Pd nanoparticles (NPs) in directing selectivity in photocatalytic primary amine reactions. When Pt/C_3N_4 serves as the photocatalyst, imines are produced through the dehydrogenative homocoupling of primary amines, attributed to the weak adsorption of photogenerated imines and hydrogen atoms on Pt NPs. Conversely, Pd/C_3N_4 encourages the subsequent hydrogenation of photogenerated imines into secondary amines, resulting from a strong affinity of both imine and hydrogen atoms for the surface of Pd NPs. The usage of 0.5%Pd-0.5%RuH/Al_2O_3 may facilitate the transformation of hydrogenated imines into secondary amines due to the pronounced affinity of both imine and hydrogen atom for the Pd NP surface. An XPS analysis, as shown in **Table 6.2**, reveals that the 0.5%Pd-0.5%RuH/Al_2O_3 catalyst contains a higher proportion of Pd metal relative to Ru metal compared to other catalysts listed in **Table 6.1**.

6.3.3. Effect of the reaction temperature on the reactivity of 0.5%Pd-0.5%RuH/Al_2O_3 catalyst using (Buchi) reactor

To examine the effect of temperature on the reaction, the 0.5%Pd-0.5%RuH/Al_2O_3 catalyst was subjected to varying temperatures under standard reaction conditions, and the corresponding activity data are depicted in **Figure 6.1**

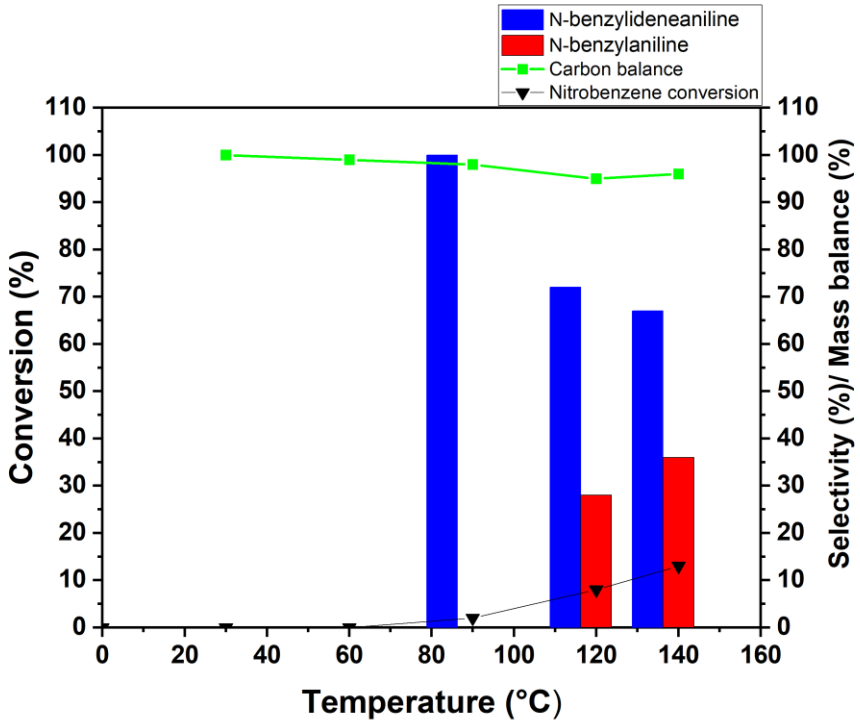

Figure 6.1: Response to Differing Reaction Temperatures. Reaction conditions: catalyst: 0.02 g; Nitrobenzene: 0.9 mmol; Benzyl Alcohol: 9 mmol; N_2: 1 bar; mesitylene (solvent): 1 ml; duration: 160 min; 1000 rpm.

In **Figure 6.1**, we observe no activity in the range from 30 °C to 60 °C. Beyond 80 °C, the HAT reaction is apparent, likely because the crucial dehydrogenation step in this HAT reaction of benzyl alcohol occurs only above this temperature. As a result, we see an increase in nitrobenzene conversion and the production of N-benzylideneaniline. Further temperature elevation to 120 °C reveals an 8 % conversion with full selectivity to N-benzylideneaniline and a 28 % selectivity towards N-benzylaniline. A notable rise in conversion to 13 % is observed at 140 °C, with selectivity towards N-benzylideneaniline and N-benzylaniline at 67 % and 36 %, respectively, and a mass balance of 96 %. Between 120 °C and 140 °C, we see an increase in nitrobenzene conversion and a shift in selectivity for N-benzylideneaniline and N-benzylaniline.

6.3.4. Time online

To evaluate the effect of time on the catalyst's activity, an additional experiment was conducted using the 0.5%Pd-0.5%RuH/Al_2O_3 catalyst, and the reaction time was extended to 8 hours, as represented in **Figure 6.2**. It becomes clear that extending the reaction time results in a substantial increase in nitrobenzene conversion from 13 % at 30 minutes to 58 % at 480 minutes. Moreover, the most stable product, N-benzylideneaniline, was most abundantly produced at the reaction's outset. A further prolongation in reaction time from 30 minutes to 60 minutes leads to a decrease in this product's selectivity, while there is a gradual increase in N-benzylaniline selectivity, peaking at 120 minutes with a conversion of 26 %. Notably, extending thereaction time beyond 120 minutes resulted in a consistent decline in N-benzylideneaniline selectivity to 21 % at 480 minutes. On the other hand, the selectivity of N-benzylaniline exhibited a slight rise with the extension of reaction time. This outcome provides insight into the behaviour of the 0.5%Pd-0.5%Ru/Al_2O_3 catalyst over a 480-minute reaction period. Beyond 240 minutes, the conversion of nitrobenzene only modestly increased, and the selectivity towards N-benzylideneaniline and N-benzylaniline steadily decreased and increased, respectively. This trend suggests that no increase in conversion occurs beyond 240 minutes of the reaction.

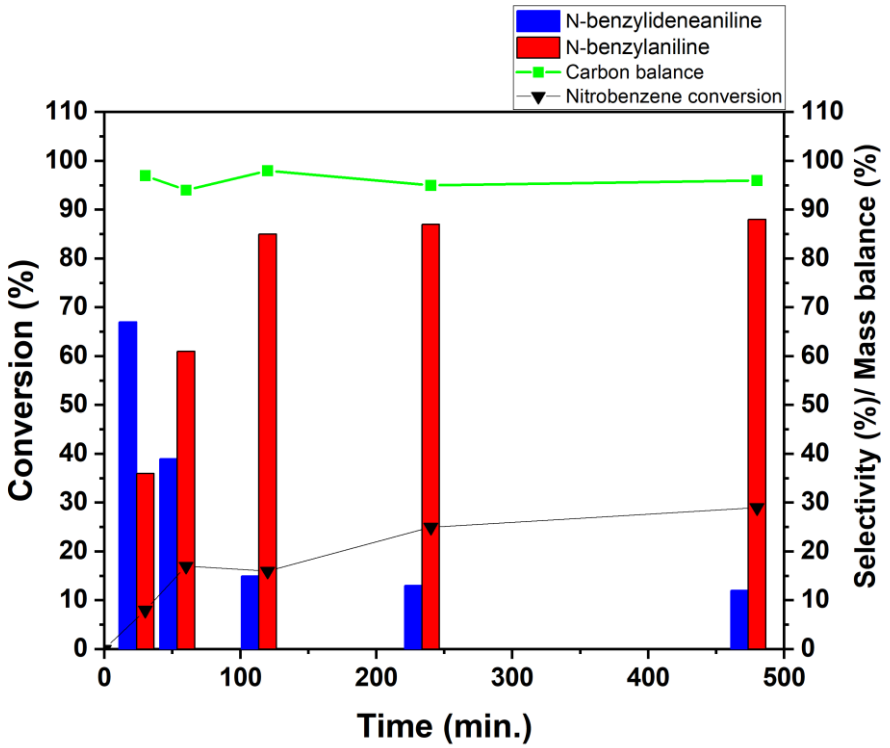

Figure 6.2: Impact of Reaction Time on Conversion and Selectivity over o.5%Pd-0.5%RuH/Al_2O_3 Catalyst. Reaction conditions: catalyst: 0.02 g; Nitrobenzene: 0.9 mmol; Benzyl Alcohol: 9 mmol; N_2: 1 bar; mesitylene (solvent): 1 ml; Temperature: 413 K; 1000 rpm.

6.3.5. Effect of treatment method on the catalytic activity of 0.5%Pd-0.5%RuH/Al_2O_3 catalyst

The crucial phase in the production of catalysts via the M_{im} method is the post-synthesis treatment of the resultant catalysts. Three different treatment techniques were employed on the 0.5%Pd-0.5%RuH/Al_2O_3 prepared via M_{im}: reduction using $NaBH_4$; catalyst heating under 5% H_2/Ar for 4 hours at 450 °C; and calcination of the catalyst under air for 4 hours at 450 °C, followed by heat treatment under 5% H_2/Ar for 4 hours at 450 °C. The synthesis of amine and imine from nitrobenzene and benzyl alcohol was conducted to evaluate the efficiency of the treated catalysts. The results are summarized in **Table 6.3**. Compared to other differently treated catalysts, the catalyst reduced by $NaBH_4$ exhibits superior activity for nitrobenzene reduction and imine selectivity (55 % and 25 %, respectively). Both heat-treated catalysts exhibit nearly identical catalytic activity for both nitrobenzene conversion and the selectivity of both products. This could be attributable to the agglomeration and sintering of catalyst particles during heat treatment, which potentially reduces the number of

active sites. **Table 6.3** indicates that 0.5%Pd-0.5%RuH/Al_2O_3 prepared via M_{im} reduction with $NaBH_4$ was selected for further examination based on the results.

Table 6.3: Effect of reduction method on the catalytic activity of 0.5%Pd-0.5%RuH/Al_2O_3 catalyst

Treatment method	Conversion (%) Nitrobenzene (NB)	Selectivity (%)		Carbon mass balance
		Imin	Amin	Mol (%)
By $NaBH_4$	55	25	75	96
Gas phase reduction @450 ºC	30	20	80	97
Calcination + Reduction @ 450 ˚C	27	15	95	94

Reaction conditions: catalyst: 0.02 g; Nitrobenzene: 0.9 mmol; Benzyl Alcohol: 9 mmol; N_2: 1 bar; mesitylene (solvent): 1 ml; Temperature: 413 K; Stirring Speed: 1000 rpm; Time: 4 hours.

6.3.6. Effect of metal loading

This section highlights the influence of varying bimetallic Pd-Ru loading percentages on Al_2O_3 regarding nitrobenzene conversion and the selectivity of both products. A series of Ru-PdH/Al_2O_3 catalysts with 1wt.%, 0.5wt.%, and 0.2wt.% weight loadings were prepared and tested for the synthesis of amine and imine from nitrobenzene and benzyl alcohol under conditions of 140 °C, 1 bar N_2 for 4 hours. The findings are presented in **Table 6.4.**

Table 6.4: Effect of reduction method on the reactivity of 0.5%Pd-0.5%RuH/Al_2O_3 catalyst

Catalyst loading	Conversion (%) (3)	Selectivity (%)		Carbon mass balance
	Nitrobenzene (NB)	Imin	Amin	Mol (%)
0.5%Pd-0.5%RuH/Al_2O_3	55	13	87	96
0.25%Pd-0.25%RuH/Al_2O_3	38	19	81	94
0.1%Pd-0.1%RuH/Al_2O_3	30	18	82	95

Reaction conditions: catalyst: 0.02 g; Nitrobenzene: 0.9 mmol; Benzyl Alcohol: 9 mmol; N_2: 1 bar; mesitylene (solvent): 1 ml; Temperature: 413 K; Stirring Speed: 1000 rpm; Time: 4 hours.

Data from the table demonstrate that upon employing the same quantity of catalyst (0.2 g) for 4 hours, the Nitrobenzene conversion was improved by increasing the Pd-Ru loading from 0.2wt.% to 1wt.%. For instance, Nitrobenzene conversion was 38 % with a 0.5wt.% catalyst but increased to 55 % when 0.5%Pd-0.5%RuH/Al_2O_3 was used. This aligns with the doubling of metal content. Moreover, raising the Pd-Ru metal loading from 0.5 wt. % to 1 wt. % enhanced the active sites (metallic sites) five-fold. However, conversion increased less than twice, indicating that the 0.2 % catalyst is most active. Higher catalyst loading led to a decrease in N-benzylideneaniline selectivity from 19 % to 13 % and an increase in N-benzylaniline selectivity from 81 % to 87 %. For both the 0.2wt.% and 0.5wt.% Pd-RuH/Al_2O_3 catalysts, significant conversions (30 % and 38 %, respectively) were observed, but selectivity remained constant for both products. Therefore, Pd-Ru loading had a significant impact on the catalytic properties, with Nitrobenzene conversion and N-benzylaniline selectivity increasing significantly as Pd-Ru loading increased.

The XPS data, presented in **Table 6.5**, show a decrease in the number of metal nanoparticles dispersed on the support surface as the metal concentration in the catalyst reduces. This could be the primary reason for a decline in the catalyst's activity in tandem with lower metal loading.

Table 6.5: XPS data of Pd-RuH/Al_2O_3 deferent loading metals

Compound	Pd^0 Position/ %At Conc.	$Pd^{2+}3d$ Position/ %At Conc.	Cl^-2p Position/ %At Conc.	$Ru^0 3d$ Position/ %At Conc.	Ru3d O_x Position/ %At Conc.	C1s Position/ %At Conc.	Pd^{2+}/Pd^0 Molar ratio (%)
0.5%Pd-0.5%RuH/Al_2O_3	335.31/0.55	336.34/0.33	198.99/0.7	279.91/0.22	------	284.96/22.98	0.6
0.25%Pd-0.25%RuH/Al_2O_3	335.72/0.06	337.91/0.02	198.86/0.28	281.02/0.05	------	284.78/27.96	0.33
0.1%Pd-0.1%RuH/Al_2O_3	------	------	198.76/0.36	------	------	------	0

6.3.7. The heterogenous 0.5%Pd-0.5%RuH/Al_2O_3 catalytic test and reusability in Radleys reactor

The heterogeneous character of the 0.5%Pd-0.5%RuH/Al_2O_3 catalyst was demonstrated through three distinct methods: (1) hot filtration, (2) Inductively Coupled Plasma Mass Spectrometry (ICP-MS) analysis of the reaction mixture to determine potential metal leaching, and (3) the reusability assessment of the recovered catalyst. The catalytic assessments were conducted in a 50 mL Radleys glass reactor maintained at 393 K and subjected to 1 bar of N_2 pressure.

Hot filtration experiments were performed to establish whether the active metal species were prone to leaching into the reaction medium. **Figure 6.3** illustrates the outcome of the hot filtration method. Here, the catalyst was filtered off after 30 minutes, at which point an 8 % conversion was achieved, and the reaction mixture was then allowed to continue reacting for an additional 150 minutes under standard reaction conditions. Post-filtration, no significant increase in conversion (10 %) and selectivity was observed (**Figure 6.3**). The figure also reveals that, while the reaction proceeded after catalyst removal, it did so at a much slower rate compared to the same period with the catalyst, witnessing a substantial decrease in nitrobenzene conversion from 20 % to 10 % and N-benzylaniline selectivity from 89 % to 28 %. This experiment assists in concluding that the primary catalytic route is heterogeneous, albeit with a minor contribution from homogeneous catalysis. ICP-MS measurements

indicated that the filtered reaction mixture contained negligible amounts of Ru and Pd (0.3 % for Ru and 0.001 % for Pd of the original amounts employed in the reaction).

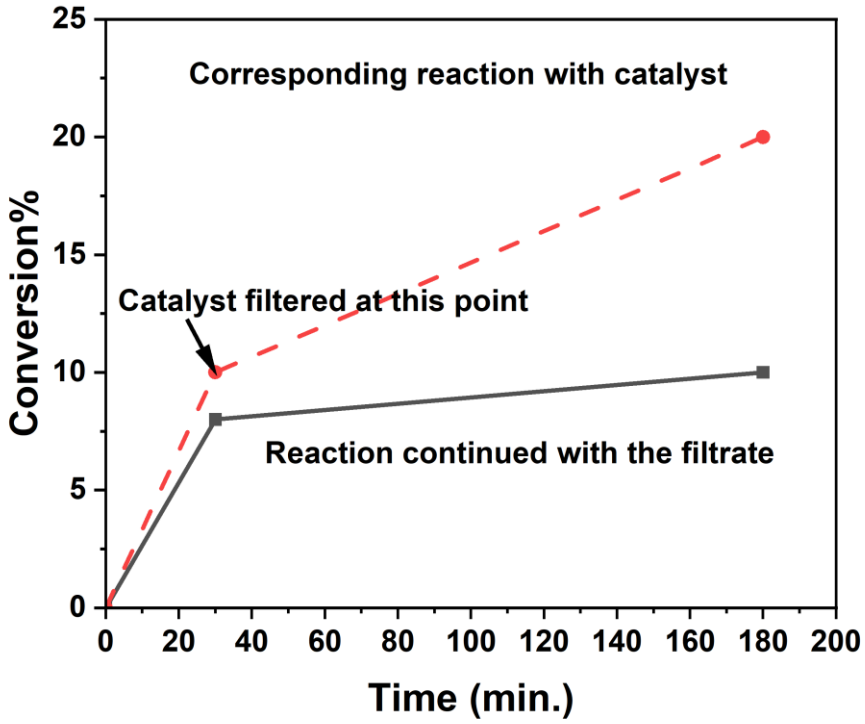

Figure 6.3: Confirming 0.5%Pd-0.5%RuH/Al_2O_3catalyst by hot filtration. **Reaction conditions:** catalyst: 0.02 g; Nitrobenzene: 0.9 mmol; Benzyl Alcohol: 9 mmol; N_2: 1 bar; mesitylene (solvent): 1 ml; Temperature: 393 K; Stirring Speed: 500 rpm.

To investigate the potential for catalyst reusability, a standard reaction was employed. After usage, the 0.5%Pd-0.5%RuH/Al_2O_3catalyst was filtered, washed once each with water and acetone (500 ml), and then dried at room temperature. Interestingly, the catalyst maintained nearly its entire activity (only 2-3 % loss) after three uses. The results are summarized in **Table 6.6**. Notably, the selectivity of N-benzylaniline progressively increased from 34 % with the fresh catalyst to 44 % with the thrice-used catalyst, seemingly at the expense of N-benzylideneaniline for the spent catalysts.

Table 6.6: Reusability study of 0.5%Pd-0.5%RuH/Al_2O_3catalyst:

Catalyst	Conversion (%) Nitrobenzene (NB)	Selectivity (%)		Carbon mass balance
		Imin	Amin	Mol (%)
Fresh	8	66	34	99
1st Reused	11	59	41	93
2nd Reused	8	62	38	96
3ed Reused	10	56	44	93

Reaction conditions: catalyst: 0.02 g; Nitrobenzene: 0.9 mmol; Benzyl Alcohol: 9 mmol; N_2: 1 bar; mesitylene (solvent): 1 ml; Temperature: 393 K; Stirring Speed: 500 rpm; Time:30 min.

The ICP-MS studies of the filtered reaction mixture using the fresh catalyst indicated marginal levels of Ru and Pd (0.2 % for Ru and 0.02 % for Pd, compared to the original amounts used in the reaction). Analysis of Transmission Electron Microscopy (TEM) and Energy-Dispersive X-ray Spectroscopy (EDX) spectra for the fresh and reused 0.5%Pd-0.5%RuH/Al_2O_3catalysts (refer to Chapter 3, Section 3.4.3., **Figures 3.22 and 3.23** respectively), revealed an increase in particle size from 2.17 nm in the fresh catalyst to 3 nm in the reused one. This suggests potential aggregation of the catalyst, even as its catalytic activity remained consistent. The EDX spectra demonstrated an increase in the weight percent of Pd from 0.14 % to 0.32 %, while the Ru weight percent saw a slight decrease from 0.27 % to 0.21 %. These results imply an increased presence of Pd metal on the catalyst's surface, which could influence the catalyst's selectivity in the synthesis of imine and amine. Furthermore, X-ray Photoelectron Spectroscopy (XPS) analysis (refer to Chapter 3, Section 3.4.3. **Table 3.8**), as presented in **Table 6.7**, indicates that the spectrum for the reused catalyst exhibits a slight negative shift, though the Ru metal concentration remains unchanged.

Table 6.7: XPS data of 0.5%Pd-0.5%RuH/$Al_2O_3$and reused 0.5%Pd-0.5%RuH/Al_2O_3catalysts

Compound	Pd^0 Position/ %At Conc.	Pd^{2+}3d Position/ %At Conc.	Cl^-2p Position/ %At Conc.	$Ru^0$3d Position/ %At Conc.	C1s Position/ %At Conc.	Pd^{2+}/ Pd^0 Molar ratio (%)
0.5%Pd-0.5%RuH/Al_2O_3	**335.31/0.55**	**336.34/0.33**	**198.99/0.7**	**279.91/0.22**	**284.96/22.98**	**0.6**
0.5%Pd-0.5%RuH/Al_2O_3 Reused	**335.41/0.06**	**337.62/0.02**	**199.4/0.35**	**280.75/0.05**	**284.84/31.92**	**0.33**

6.4. Conclusion

The bimetallic catalyst 0.5%Pd-0.5%RuH/Al_2O_3exhibited exceptional activity in the direct synthesis of imines and secondary amines from Nitrobenzene and Benzyl Alcohol. Remarkably, it achieved this without the necessity for hydrogen, a sacrificial hydrogen donor, or a base, using a Hydrogen Atom Transfer (HAT) strategy. This approach serves as an alternative to strategies reliant on H_2. Comparatively, the Ruthenium–Palladium bimetallic catalyst supported on Al_2O_3 demonstrated marginally superior activity than the Ruthenium–Palladium catalyst supported on other metal oxides like TiO_2. Consequently, the bimetallic Ru–Pd/Al_2O_3 catalyst exhibited outstanding catalytic activity for both hydrogenation and dehydrogenation reactions.

6.5. REFERENCES

1 G. Guillena, D. J. Ramón and M. Yus, *Chem. Rev.*, 2010, **110**, 1611–1641.

2 E. Podyacheva, O. I. Afanasyev, D. V. Vasilyev and D. Chusov, *ACS Catal.*, 2022, 7142–7198.

3 E. Nowicka, J. P. Hofmann, S. F. Parker, M. Sankar, G. M. Lari, S. A. Kondrat, D. W. Knight, D. Bethell, B. M. Weckhuysen and G. J. Hutchings, *Phys. Chem. Chem. Phys.*, 2013, **15**, 12147–12155.

4 P. Challa, S. S. Enumula, K. Saidulu Reddy, M. Kondeboina, D. R. Burri and S. R. Rao Kamaraju, *Ind. Eng. Chem. Res.*, 2020, **59**, 17720–17728.

5 C. S. Couto, L. M. Madeira, C. P. Nunes and P. Araújo, *Chem. Eng. Technol.*, 2015, **38**, 1625–1636.

6 C. H. Li, Z. X. Yu, K. F. Yao, S. F. Ji and J. Liang, *J. Mol. Catal. A Chem.*, 2005, **226**, 101–105.

7 F. Leng, I. C. Gerber, P. Lecante, S. Moldovan, M. Girleanu, M. R. Axet, P. Serp and M. R. Axet, *ACS Catal.*, 2016, **6**, 6018–6024.

8 M. H. S. A. Hamid, P. A. Slatford and J. M. J. Williams, *Adv. Synth. Catal.*, 2007, **349**, 1555–1575.

9 M. Sankar, Q. He, S. Dawson, E. Nowicka, L. Lu, P. C. A. Bruijnincx, A. M. Beale, C. J. Kiely and B. M. Weckhuysen, *Catal. Sci. Technol.*, 2016, **6**, 5473–5482.

10 C. Schlepphorst, B. Maji and F. Glorius, *ACS Catal.*, 2016, **6**, 4184–4188.

11 L. Wang, W. He, K. Wu, S. He, C. Sun and Z. Yu, *Tetrahedron Lett.*, 2011, **52**, 7103–7107.

12 M. Sankar, N. Dimitratos, P. J. Miedziak, P. P. Wells, C. J. Kiely and G. J. Hutchings, *Chem. Soc. Rev.*, 2012, **41**, 8099.

13 A. J. A. Watson, A. C. Maxwell and J. M. J. Williams, *J. Org. Chem.*, 2011, **76**, 2328–2331.

14 P. Paalanen, B. M. Weckhuysen, M. Sankar, M. Piccinini, J. K. Edwards, A. A. Herzing, A. F. Carley, J. A. Moulijn, C. J. Kiely, G. J. Hutchings, C. J. Kiely, G. J. Hutchings and G. J. Hutchings, *Catal. Sci. Technol.*, 2013, **3**, 2869.

15 M. Sajjadi, M. Nasrollahzadeh, H. Ghafuri, T. Baran, Y. Orooji, N. Y. Baran and M. Shokouhimehr, *Int. J. Biol. Macromol.*, 2022, **209**, 1573–1585.

16 X. Cui, C. Zhang, F. Shi and Y. Deng, *Chem. Commun.*, 2012, **48**, 9391–9393.

17 Q. Peng, Y. Zhang, F. Shi and Y. Deng, *Chem. Commun.*, 2011, **47**, 6476–6478.

18 J. Yu, Q. Liu, W. Qiao, D. Lv, Y. Li, C. Liu, Y. Yu, Y. Li, H. Niemantsverdriet, B. Zhang and R. Su, *ACS Catal.*, 2021, **11**, 6656–6661.

Chapter 7: Conclusion and Future Work

7.1. Conclusions

This thesis aimed to investigate and develop bimetallic catalysts (Pd-Ru and Pd-Au) that exhibit activity, selectivity, and stability in the hydrogenation of phenol, cross-coupling reaction (phenol with p-toluidine), and auto transfer reaction (benzyl alcohol with nitrobenzene)[1]

The advancements in conversion technology have opened numerous possibilities for utilizing biomass resources as renewable carbon sources for fuel and bulk chemicals, making them crucial in the chemical industry. With the increasing concern over petroleum availability and budget constraints, there is a growing need to explore alternative pathways for producing solvents, fuels, and bulk chemicals from biomass. The hydrogenation of phenol using metal catalysts under green chemistry conditions has emerged as an attractive alternative due to phenol's wide availability as a carbon source.

The primary objective of this thesis was to investigate whether catalysts known for their effectiveness in the hydrogenation of phenol could also be applied to other reactions, such as cross-coupling and auto transfer reactions[1]. The aim of this thesis has been met and the outcomes are described as follows: Firstly, as explained in the third chapter, the major goal was to test whether catalysts that have been confirmed to be useful for the hydrogenation of phenol can also be applied to another reaction such as cross coupling reaction and auto transfer reaction. Furthermore, it has been shown that the catalysts are effective under mild conditions using low pressure H_2 as hydrogenate, which represents a significant improvement in the environmental impact of this reaction. Secondly, the thesis aimed to selectively synthesis cyclohexanol while avoiding the cyclohexanone synthesis, as described in the fourth chapter.
Chapter Four demonstrated that the Pd/Al_2O_3 monometallic catalyst exhibited effective hydrogenation of phenol under mild conditions. The ability of the Pd catalyst to efficiently catalyse phenol hydrogenation is significant since phenol is challenging to reduce with high selectivity to cyclohexanone under mild conditions[2]. The 2.5%Pd-2.5%Ru/Al_2O_3 catalyst showed favourable results in the liquid-phase hydrogenation of phenol, achieving high phenol conversions, 100 % cyclohexanol selectivity, and minimal catalyst deactivation after multiple runs. This indicates the potential use of the Pd mono catalyst for phenol hydrogenation to cyclohexanone and Pd-Ru for

cyclohexanol production. Pd-Ru supported on alumina exhibited superior hydrogenation activity and the highest yield of cyclohexanol compared to other alternatives. The Pd-Ru/Al_2O_3 catalyst with a high activity for selective phenol hydrogenation to cyclohexanol was obtained using a modified impregnation technique reduced with $NaBH_4$. The small metal particle size increased active sites, and electronic interaction played a crucial role in enhancing the catalyst's performance. Furthermore, a low loading of 0.5%Pd-0.5%RuH/Al_2O_3 was sufficient to achieve high performance due to its excellent activity and selectivity for cyclohexanol, making it an ideal catalyst for both fundamental research and practical applications.

Chapter Five focused on the N-alkylation reaction of phenol with p-toluidine using a 2.5%Pd-2.5%Au/Al_2O_3 bimetallic catalyst prepared through different methods. The PdH/Al_2O_3 catalyst demonstrated high activity and yielded good stereoselectivity in the reductive coupling of lignin-derived phenols with amines under mild conditions. The performance of the PdH/Al_2O_3 catalyst was attributed to the high reactivity of PdH species and the activation of phenol by the Al_2O_3 support. The results indicated the potential of lignin as a renewable reagent for future chemical synthesis. The influence of a bimetallic catalyst was also studied for the N-alkylation reaction of phenol with p-toluidine.

However, it was shown that the design of the catalysts and control of the reaction conditions could enable a certain degree of control over the reaction products. The influence of a bimetallic catalyst was also tested for N-alkylation reaction of phenol with p-toluidine. From the reusability result 2.5%Pd-2.5%AuH/Al_2O_3 bimetallic catalyst prepared via modified impregnation reduced with $NaBH_4$ shows a high activity compared with 2.5%Pd-2.5%Au/Al_2O_3 bimetallic catalyst prepared by Sol-immobilisation for N-alkylation of phenol with ρ-toluidine.

for the hydrogenation of furfuryl alcohol than graphite supports, particularly TiO_2 and the highest selectivity towards hydrogenation for the desired products was obtained over SiO_2 as the support. In addition, the effect of a solvent was investigated. The highest selectivity for 2-methylfuran was achieved in the presence of a 1,2-dichloroethane solvent, under green conditions.

Chapter Six focused on the liquid-phase auto transfer reaction (HAT) of benzyl alcohol with nitrobenzene under mild conditions. The 0.5%Pd-0.5RuH/Al_2O_3 catalyst showed exceptional activity in the direct synthesis of imines and secondary amines from nitrobenzene and benzyl alcohol without the use of hydrogen, sacrificial hydrogen donors, or bases, employing a HAT strategy as an alternative to traditional hydrogenation methods. The effects of metal oxide support (Al_2O_3 and TiO_2) on the activity of the HAT reaction for the direct synthesis of imines and secondary amines were also investigated. The bimetallic Ru-Pd/ Al_2O_3 catalyst exhibited slightly better

activity than the Ru-Pd catalyst supported on TiO_2. The catalyst showed excellent catalytic activity for both hydrogenation and dehydrogenation reactions.

7.2. Future Work

Several areas in this thesis offer opportunities for further development. The utilisation of bio renewable feedstock using palladium or other metal catalysts on different supports could be studied in more depth. Further investigations are warranted to explore non-noble metals with diverse supports for selective phenol hydrogenation under environmental conditions. The potential improvement in catalytic activity by alloying the catalyst with a second metal, such as Pd, Ni, Ru, Pt, or Rh, should be explored for the N-alkylation of phenol with p-toluidine. Additionally, the impact of solvents on catalyst activity should be further examined by exploring other solvent systems.

Further characterization of the catalysts could provide a deeper understanding of the factors contributing to their improved stability and selective oxidation. Despite the progress made in improving catalyst stability in this thesis, there is room for further enhancement. Future research could focus on developing more stable catalysts by exploring alternative catalyst supports, such as metal oxides (e.g., SnO2 and CeO_2) and carbon supports (e.g., acetylene black and Ketten Black). Understanding the desirable properties of supports with different acidic/basic properties, reducibility, and electronic conductivity could provide insights into improving catalyst performance. Furthermore, exploring the use of non-precious metals (Cu, Co, Ni) as alternatives to Pd could reduce the cost associated with the catalyst and increase its viability.

7.3. References

1 Z. Zhang and H. Li, *Fuel*, 2022, 310.

2 L. Cheng, Q. Dai, H. Li and X. Wang, *Catal. Commun.*, 2014, **57**, 23–28.

Appendix

Appendix A

NMR Spectra

^{1}HNMR characterisation of N-Cyclohexyl-4-methylaniline is shown in **Scheme 5.2.**

1 H NMR (500 MHz, CDCl3): δ = 6.97 (d, J = 7.5 Hz, 2H), 6.53 (d, J = 7.5 Hz, 2H), 3.22 (t, J = 10.0 Hz, 1H), 2.23 (s, 3H), 2.05 (d, J = 12.0 Hz, 2H), 1.75 (d, J = 13.5 Hz, 2H), 1.65 (d, J = 12.5 Hz, 1H), 1.39-1.32 (m, 2H), 1.23 (t, J = 12.5 Hz, 1H), 1.69-1.09 (m, 2H). 13C NMR (125 MHz, CDCl3): δ = 145.0, 129.7, 126.1, 113.5, 52.1, 33.5, 25.9, 25.0, 20.3. MS (EI) m/z: 189, 160, 146, 131, 106, 91, 77, 55.

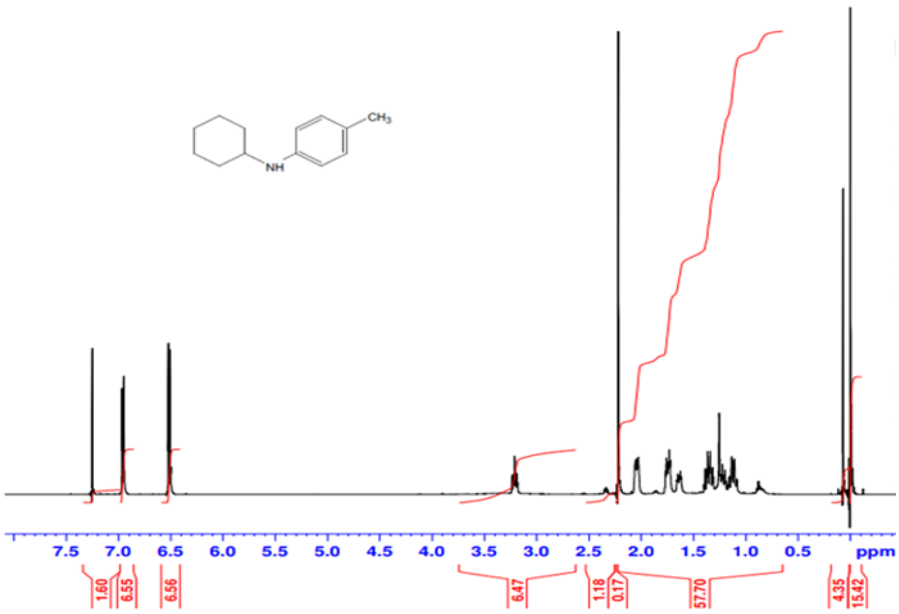

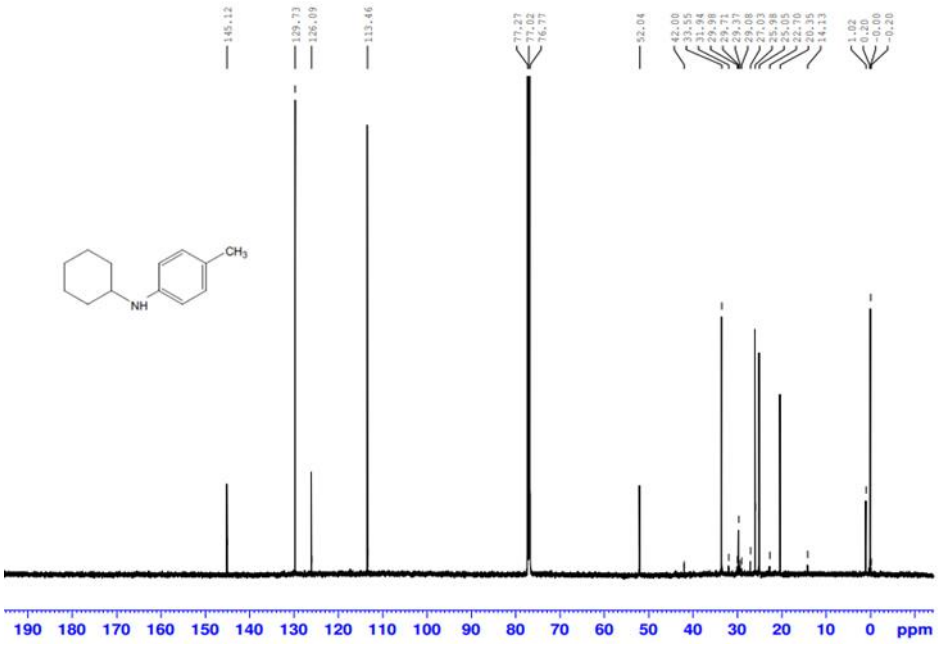

1H NMR and 13C NMR of N-cyclohexyl-4-methylaniline

Appendix B (a)

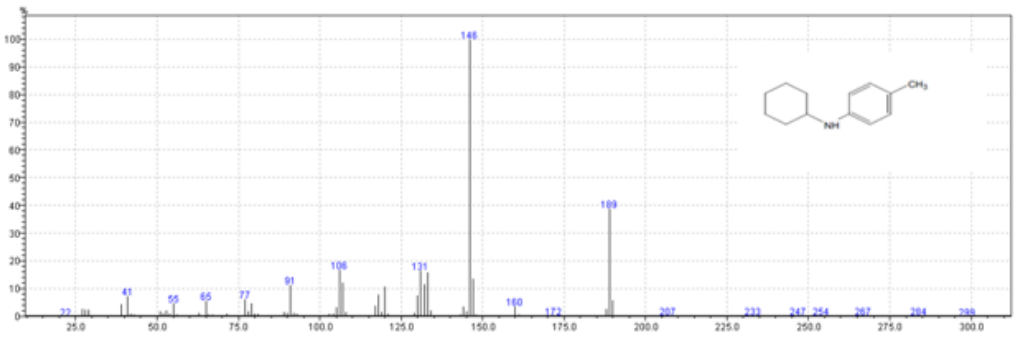

(b)

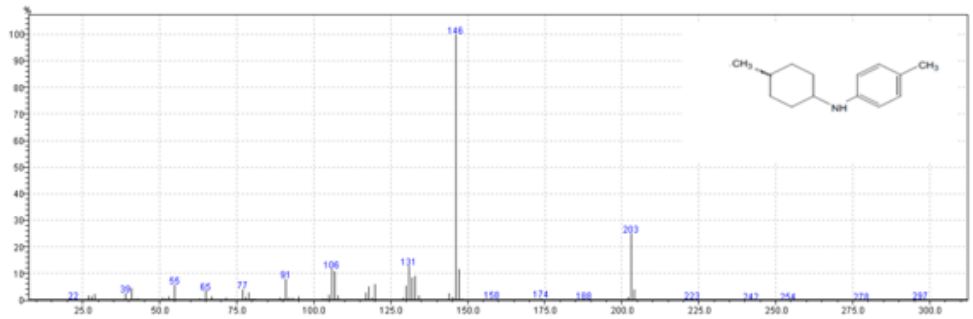

Appendix C(a)

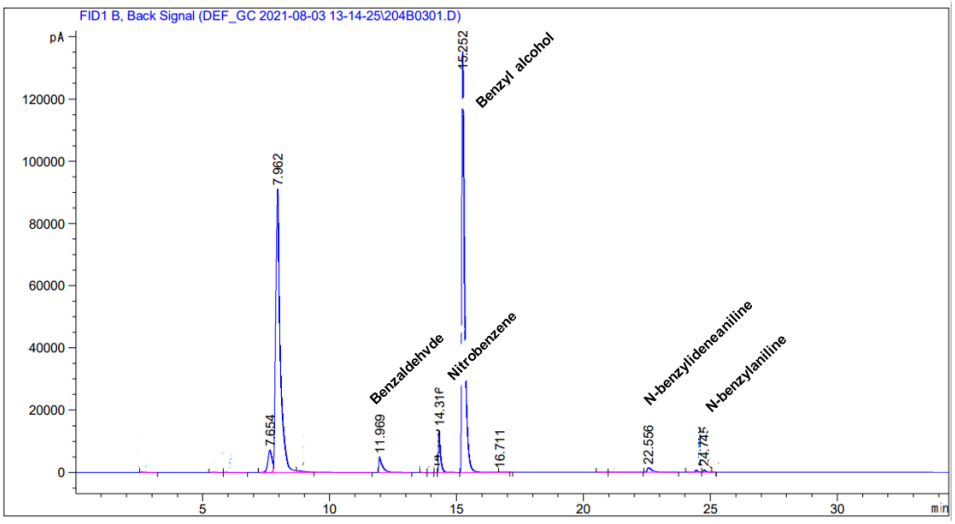

Appendix C(b)

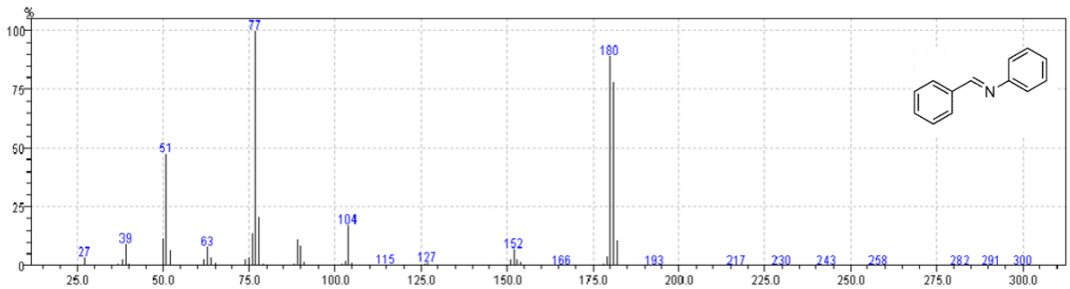

Appendix D(a)

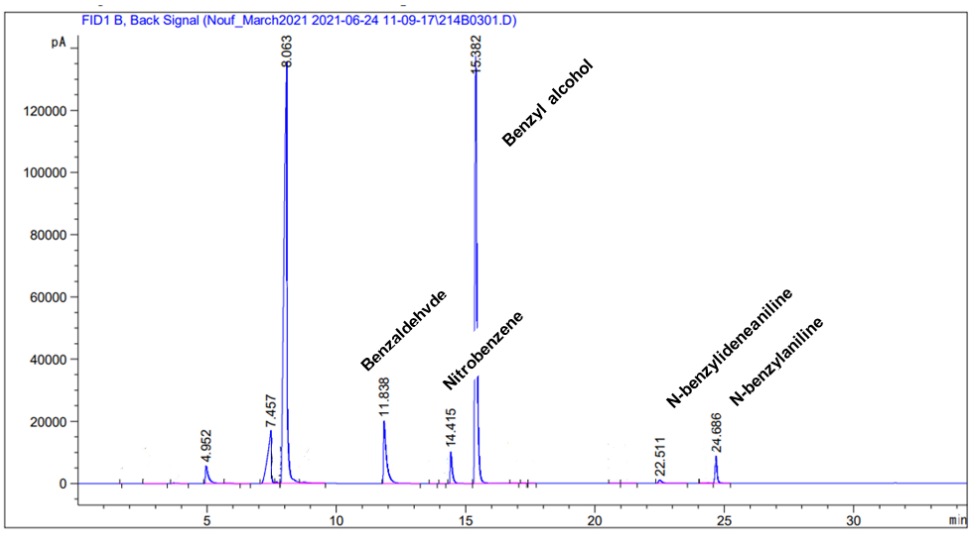

Appendix D(b)